

The association of *SLC6A6* with treatment resistance in glioblastoma

Rhiannon Alice Barrow

Submitted in accordance with the requirements for the degree of
Doctor of Philosophy

The University of Leeds
School of Medicine

Leeds Institute of Medical Research

October 2022

The candidate confirms that the work submitted is her own, except where work which has formed part of jointly-authored publications has been included. The contribution of the candidate and the other authors to this work has been explicitly indicated below. The candidate confirms that appropriate credit has been given within the thesis where reference has been made to the work of others.

This copy has been supplied on the understanding that it is copyright material and that no quotation from the thesis may be published without proper acknowledgement.

Chapter 3 section 3.3.3 contains work from the below:

Rhiannon Barrow, Joseph N. Wilkinson, Yichen He, Martin Callaghan, Anke Brüning-Richardson, Mark Dunning, Lucy F Stead. SpheroidAnalyseR – an online platform for analysing data from 3D spheroids or organoids grown in 96-well plates. bioRxiv. 2022

Chapter 3 clearly states the contribution I had to this paper which is that I was responsible for driving and directing the creation of the app; I led the project and directed the computational scientists with regards to what was needed for the app to be fit for purpose for use by a non-computational expert. I did the testing of the app to ensure it worked and helped with the design and format. I wrote the paper.

Work from chapter 2 and chapter 4 has been included in a paper under submission to Genome Biology:

IDHwt glioblastomas can be stratified by their transcriptional response to standard treatment, with implications for targeted therapy.

Georgette Tanner*, Rhiannon Barrow*, Martina Finetti, Shoaib Ajaib, Nazia Ahmed, Steven Pollock, Nora Rippaus, Alexander F. Bruns, Khaja Syed, James Poulter, Erica Watson, Colin Johnson, Frederick S. Varn, Anke Brüning-Richardson, Catherine Hogg, Alastair Droop, Arief Gusnanto, Matthew A. Care, Luisa Cutillo, David Westhead, Susan C. Short, Michael D. Jenkinson, Andrew Brodbelt, Aruna Chakrabarty, Azzam Ismail, Roel GW Verhaak, Lucy F. Stead.

The right of Rhiannon Alice Barrow to be identified as Author of this work has been asserted by her in accordance with the Copyright, Designs and Patents Act 1988.

Acknowledgements

Firstly, I would like to thank my supervisors as it goes without saying that I would not have got through this PhD without their continued guidance. I would like to thank Lucy Stead for her amazing support over this project. The encouragement and enthusiasm she shows her group is incredible and I feel proud to have a supervisor who is so passionate about making a difference to the lives of those affected by GBM. I also want to thank my co-supervisors James Poulter, Colin Johnson and Erica Watson for their invaluable support, advice, and patience, and for always being there to answer my questions!

Alex, Freya, Tyler, Bronwyn, and Fiona, I could not have got through the last four years without the support of the best group of friends any PhD student could ask for. We have been through the ups and downs of PhD life together and you kept me smiling through it all.

Thank you to the past and current members of the Glioma Genomics group and to past and present members of Level 5, particularly to Ruth, Tom and Anke who trained me when I first started and to Jenny who patiently answered my millions of questions over the last few years!

Thank you to my family for believing in me, especially mum and dad. Thank you to Shaz who has always been there to listen, support and encourage me, but also to buy me takeaways and wine to get me through thesis writing!

Thanks to Nemo, the best dog ever! I think that every PhD student should get a dog because no matter how stressful a day in the lab was, they always cheer you up with their wagging tail when you walk through the door!

Finally, I would like to thank Brain Research UK for funding this project and for all the work they do in making a difference to the lives of those affected by neurological disorders.

Abstract

Glioblastoma (GBM) is an incurable and aggressive form of brain cancer that predominantly affects adults and is the cause of the majority of primary brain tumour related deaths. The prognosis is poor with median survival time of only 12-15 months following diagnosis despite aggressive standardised treatment of debulking surgery and chemoradiotherapy. Almost 100% of GBM tumours recur. This is likely due to inherently treatment resistant cells within the primary tumour that survive and dominate tumour recurrence.

SLC6A6 was deemed a potential for conferring treatment resistance in GBM due to its significantly upregulated expression in recurrent tumours, and previous associations to other cancers. *SLC6A6* encodes a taurine transporter, TauT, that has an important role in embryonic brain development and neurogenesis in the adult brain.

The role of *SLC6A6* in the impact of standard treatment was investigated using shRNA knockdown and TauT inhibitors. This work was performed *in vitro* using 3D spheroid models imaged using a bespoke imaging and analysis platform that I led the development of. Both established and patient derived cell lines cultured in serum free media were used to represent different aspects of GBM biology.

Results showed that TauT inhibitors significantly alter treatment response in different directions in the cell lines. Furthermore the size of the effect implicated an off-target effect: γ -aminobutyric acid (GABA) signalling modulation. RNA sequencing indicated that cells were being transcriptionally reprogrammed in response to standard treatment in different ways, in keeping with a parallel finding from analysis of primary and recurrent patient tissues. The latter suggests that there are two responder subtypes in GBM, with different treatment resistance mechanisms underpinning them.

A possible explanation for my results is, then, that the cell lines fall into different categories of GBM responder subtypes. The varying responses seen after GABA modulation indicate that stratifying treatment based on the response subtype would be beneficial.

Table of Contents

Chapter 1 Introduction	1
1.1 Glioblastoma	1
1.1.1 Diagnosis, classification, and prognosis	1
1.1.2 Primary and secondary GBM.....	2
1.1.3 Recurrent GBM	3
1.2 Heterogeneity within GBM.....	3
1.2.1 Molecular markers.....	4
1.2.2 GBM transcriptional subtypes	7
1.2.3 Cellular states heterogeneity	8
1.3 Cancer stem cells	9
1.3.1 Glioma stem cells.....	10
1.4 Current treatment for GBM	10
1.4.1 Temozolomide.....	11
1.5 RNA sequencing	13
1.5.1 Differential gene expression analysis	14
1.6 SLC6A6 as a gene of interest in GBM	15
1.6.1 Solute Carrier Family 6 Member 6 (<i>SLC6A6</i>).....	17
1.6.2 Taurine transporter (TauT).....	18
1.6.3 Taurine	18
1.7 Current models in GBM research	20
1.7.1 Patient derived cell lines and established cell lines.....	20
1.7.2 3D cell culture	21
1.7.3 Mouse models.....	22
1.8 Aims and Objectives.....	23
Chapter 2 Materials and Methods.....	25
2.1 Preparation of stock solutions.....	25
2.2 Cell culture.....	26
2.2.1 Cell passage	26
2.2.2 Cell freezing and thawing.....	28
2.2.3 Cell counting	28
2.2.4 Coating plates	29
2.3 MTT assay.....	29
2.4 Spheroid culture	29

2.5 Spheroid imaging and growth curves	29
2.5.1 CellTiter-Glo 3D cell viability assay	30
2.6 Treating with temozolomide and irradiation.....	30
2.6.1 In 2D cultures	30
2.6.2 In 3D cultures	30
2.7 Taurine supplementation	31
2.7.1 2D cultures	31
2.7.2 3D cultures	31
2.8 Combined treatment and taurine supplementation.....	31
2.9 Inhibitor treatment on spheroids	31
2.9.1 Inhibitor dose response.....	31
2.9.2 Inhibitor and standard treatment.....	32
2.10 qPCR.....	32
2.10.1 RNA extraction	32
2.10.2 cDNA synthesis.....	33
2.10.3 qPCR.....	33
2.11 Western blotting.....	34
2.11.1 Protein extraction	34
2.11.2 Western blotting	34
2.12 SLC6A6 knockdown using siRNA	34
2.13 SLC6A6 knockdown using GIPZ Lentiviral shRNA	35
2.14 SLC6A6 knockout using CRISPR.....	36
2.14.1 Cloning	36
2.14.2 Sanger Sequencing to confirm insertion of oligo into plasmid.....	38
2.14.3 Transfection of CRISPR plasmids	39
2.15 Immunofluorescence.....	39
2.15.1 Sample preparation – OCT embedded spheroids	39
2.15.2 Immunofluorescent Staining	40
2.16 RNA sequencing	40
2.17 Statistical analysis.....	41
Chapter 3 Optimisation of models.....	42
3.1 Introduction	42
3.1.1 Use of cell line models in GBM	42
3.1.2 3D cell culture and assays	43
3.1.3 Taurine, temozolomide and irradiation doses to be used.....	45

3.1.4 Dose response curves	46
3.2 Aim and Objectives.....	46
3.3 Results	47
3.3.1 Determining suitable cell lines for use	47
3.3.2 Developing an automated imaging and analysis platform for spheroid measurements.	48
3.3.3 Creation of SpheroidAnalyseR.....	53
3.3.4 Determining seeding densities for spheroid models.....	61
3.3.5 Optimising treatment doses and timings of TMZ and irradiation	62
3.3.6 The effect of taurine on spheroid growth	67
3.3.7 Assaying growth effects	72
3.3.8 Assessing proliferation	74
3.4 Discussion	75
3.4.1 The use of cell lines in glioblastoma research	75
3.4.2 Taurine effects on cells in 2D and 3D.....	75
3.4.3 Alternatives to spheroid models.....	77
3.4.4 End point assays.....	80
Chapter 4 SLC6A6 knockdowns and TauT inhibitors.....	83
4.1 Introduction	83
4.1.1 Gene knockdowns and knockouts	83
4.1.2 Small interfering RNA (siRNA).....	83
4.1.3 Short hairpin RNA (shRNA)	85
4.1.4 Delivery of siRNA and shRNA into a cell	87
4.1.5 CRISPR-Cas9.....	89
4.1.6 Validation of knockdowns	91
4.1.7 Inhibitors.....	94
4.2 Aims and objectives	96
4.3 Results	96
4.3.1 <i>SLC6A6</i> siRNA knockdown does not result in differential treatment response.....	96
4.3.2 shRNA knockdown of <i>SLC6A6</i> in A172 and GBM63	98
4.3.3 Knockout of <i>SLC6A6</i> using CRISPR-Cas9 gene editing.....	106
4.3.4 The use of inhibitor to target TauT.....	108
4.4 Discussion	113
4.4.1 siRNA showed no difference in treatment response	113
4.4.2 shRNA showed a difference in treatment response	115
4.4.3 Exploring CRISPR-cas9 attempt.....	116

4.4.4 Inhibitors of TauT and GABA _A Receptor showed differences in response to standard treatment	117
Chapter 5 RNA-sequencing analysis	120
5.1 Introduction	120
5.1.1 GABA and GABA _A receptor	120
5.1.2 Up and Down responder subtypes in glioblastoma	122
5.1.3 Differential gene expression	125
5.2 Aims and Objectives.....	125
5.3 Results	125
5.3.1 Establishing a differential gene expression analysis pipeline.....	125
5.3.2 Number of genes differentially expressed	127
5.3.3 Gene expression direction change between A172 and GBM63 upon standard treatment	129
5.3.4 The effect of standard treatment on A172 and GBM63.....	130
5.3.5 A172 and GBM63 are Up and Down responder cell lines respectively.....	133
5.3.6 Biological similarities in the DEGs and enriched functions through treatment with regards: A172 and U responder patients; GBM63 and D responder patients.....	134
5.3.7 Different responder subtypes for GBM63 and A172 suggest stratified treatments are needed.	139
5.3.8 Differences between the DEGs/enriched functions through treatment with regards: A172 and Up in patient; GBM63 and Down in patients	140
5.4 GAB affects the transcriptional changes observed following treatment... 141	
5.4.1 Transcriptional changes with GAB.....	144
5.5 Discussion	147
5.5.1 Treatment evasion of Up and Down responders	147
5.5.2 Gaboxadol effect on the transcriptome	148
5.5.3 GABA modulation.....	150
Chapter 6 Conclusion and future work.....	152
6.1 Summary of key findings	152
6.2 Discussion	154
6.2.1 Established vs patient derived cell lines	154
6.2.2 Linking back to <i>SLC6A6</i> upregulation.....	155
6.3 Future work.....	155
Abbreviations	157

List of Figures

Figure 1.1. TMZ induces the harmful lesion O ⁶ -methylguanine (O ⁶ -MeG) to DNA.	13
Figure 1.2. <i>SLC6A6</i> expression.	16
Figure 1.3. Genetic manipulations in mice.....	23
Figure 2.1 Plasmid maps.....	38
Figure 3.1. Expression levels of <i>SLC6A6</i>	48
Figure 3.2. The confocal JOB stages and plate spheroid alignment in a well ...	51
Figure 3.3. Determining the threshold level for a spheroid	52
Figure 3.4. A plate of imaged spheroids.	52
Figure 3.5. Heat map of spheroid measurements.	53
Figure 3.6. The Data Input tab.	59
Figure 3.7. The Outlier Removal tab.....	60
Figure 3.8. The Merging tab.	60
Figure 3.9. The Plotting tab.	61
Figure 3.10. Diameter of A172 spheroids	62
Figure 3.11. 2D dose response to TMZ and irradiation in A172.	63
Figure 3.12. Area of A172 spheroids with TMZ or irradiation.....	65
Figure 3.13. Area of A172 spheroids with TMZ and irradiation combined.....	65
Figure 3.15. Area of GBM58 and GBM63 spheroids treated with the chosen treatment.....	67
Figure 3.16. MTT assay in 2D looking at response to taurine.....	70
Figure 3.17. Spheroid size when supplemented with taurine.....	71
Figure 3.18. The effect of taurine and treatment combined on spheroids	73
Figure 3.19. The effect of taurine on treated spheroids.	74
Figure 3.20. Ki67 staining in spheroids supplemented with taurine.....	74
Figure 4.1 siRNA process.....	85
Figure 4.2. shRNA process.	87
Figure 4.3. CRISPR-Cas9 genome editing.....	91

Figure 4.4 qPCR process.....	93
Figure 4.5. Western blot overview.....	94
Figure 4.6 siRNA knockdown of <i>SLC6A6</i>	97
Figure 4.7 Treatment response following siRNA knockdown.....	98
Figure 4.8. EVOS images of puromycin response.	99
Figure 4.9. qPCR validation of four shRNA constructs each used to knockdown the expression of <i>SLC6A6</i> in A172.....	100
Figure 4.10 Decreased TauT protein levels were not observed by western blot following shRNA transfection.....	101
Figure 4.11. Map of <i>SLC6A6</i> isoforms.....	103
Figure 4.12. qPCR validation of <i>SLC6A6</i> shRNA knockdown in GBM63.....	104
Figure 4.13. Percentage area of spheroids compared to untreated..	105
Figure 4.14. Percentage luminescence of spheroids compared to untreated .	105
Figure 4.15. Plasmid maps of px461 and px462.	107
Figure 4.16. Cells expressing GFP.	108
Figure 4.17. Effect of guanidinoethyl sulfonate and gaboxadol on cell lines...	111
Figure 4.18. Standardised effect of Guanidinoethyl sulfonate and Gaboxadol and standard treatment on cell lines.....	112
Figure 4.19. Standardised effect of Guanidinoethyl sulfonate and Gaboxadol and standard treatment on cell lines.....	113
Figure 5.1. RNA-sequencing and Differential gene expression steps.	127
Figure 5.2. Gene expression direction of genes in A172 and GBM63 with standard treatment.	130
Figure 5.3. Gene Ontology in A172.....	131
Figure 5.4. Normalised expression of genes related to proliferation in A172..	131
Figure 5.5 Gene Ontology in GBM63.....	132
Figure 5.6. Normalised expression of genes related to the cell cycle.....	133
Figure 5.7. Responder subtype scatter plot.....	133
Figure 5.8. Normalised expression of genes related to the cell cycle.....	135
Figure 5.9. Normalised expression of genes related to the proliferation/progenitor (PPR) neoplastic GBM cells signature.	136
Figure 5.10. Normalised expression of genes related to proliferation.	139

Figure 5.11. The normalised expression of BTG2 in A172.	139
Figure 5.12. GABA type A receptor associated protein like 1 and 2 (GABARAPL2 and GABARAPL1) normalised expression.....	140
Figure 5.13. Gene ontology enrichment analysis in A172_UnVsT_GAB..	142
Figure 5.14. Normalised expression data for A172 genes.	143
Figure 5.15. Gene ontology enrichment analysis in GBM63_UnVsT_GAB.....	144
Figure 5.16. Venn diagram of genes DE in A172.	145
Figure 5.17. Venn diagram of genes DE in GBM63.	146
Figure 5.18. Gene ontology enrichment analysis in GBM63.....	147

List of Tables

Table 1.1. Summary of the main differences between primary and secondary GBM.....	3
Table 2.1. Reagents prepared for stock solutions	25
Table 2.2. Reagents used in cell culture procedures.	26
Table 2.3. Cell lines used and their required growth medium.....	27
Table 2.4. TaqMan probes.	33
Table 2.5. Sequencing reaction thermocycler conditions.....	39
Table 3.1. Comparison of cell culture methods.	79
Table 4.1 Nucleic acid delivery into a cell.....	88
Table 4.2. The inhibitory effect on TauT and GABA _A receptor.	96
Table 5.1. Biological characteristics of Up and Down Responders	124
Table 5.2. Differentially expressed gene numbers.	128

Chapter 1

Introduction

1.1 Glioblastoma

1.1.1 Diagnosis, classification, and prognosis

Glioblastoma (GBM) is an incurable and aggressive form of brain cancer that predominantly affects adults and results in the majority of primary brain tumour related deaths (1). GBM is a glioma; a tumour of glial cell origin, found mainly in the brain and can occur anywhere in the central nervous system (CNS). The World Health Organisation (WHO) classifies gliomas from grades I to IV according to increased aggressiveness, with GBM assigned grade IV: the most aggressive (2). GBM falls into the category of diffuse glioma that can extensively infiltrate the CNS parenchyma (3). Diffuse gliomas are classified based on the histological and morphological features they share with the glial cells of origin such as astrocytes, oligodendrocytes and mixtures of the two that give rise to astrocytoma, oligodendroglioma and oligoastrocytoma respectively (4). Histologically, GBM is a tumour with neoplastic cells that have astrocytic characteristics and either necrosis and/or endothelial proliferation (5). GBM accounts for 54% of all gliomas and 16% of primary brain tumours making it the most common type of primary brain tumour. It has a median survival rate of 15 months post diagnosis and a five-year survival rate of only 5% (6, 7). The incidence in GBM is 1.6 higher in males than females and has an incidence rate of 5 in 100,000 people, increasing with advanced age at diagnosis. There are around 2,100 new diagnoses in England annually and this appears to be increasing, though annual new diagnoses numbers remain the same in other areas of the world such as the US and Canada (1, 6, 8). The median age of diagnosis for a GBM patient is 65 years and a large majority of all GBM patients have no family history of cancer (9).

Diagnosis of GBM usually follows symptomatic presentation due to the tumour displacing and destroying brain structure and functions through rapid expansion (1). Common clinical presentation includes headaches, seizures, new onset epilepsy, blurred vision, nausea and alterations in mental ability (10). In 21.4% of cases, three or more appointments with a GP were required before patients were referred to a specialist, which slows time to initial treatment and ultimately

contributes to the low median survival time following diagnosis (11). Diagnosis of GBM is typically performed via contrast enhanced magnetic resource imaging (MRI) and confirmed by histological examination and genetic testing following surgical resection (12). This confirms diagnosis as GBM and determines if it is a primary or secondary GBM.

1.1.2 Primary and secondary GBM

The main differences between primary and secondary GBM are summarised in Table 1.1 and described below. Primary GBM develop rapidly de novo, without evidence of development from a lower grade tumour, and usually have a worse prognosis. This is in contrast to secondary GBM where the tumour has developed from a lower grade II or III tumour (13). Primary tumours are most commonly found in older patients (mean age of 62) whereas secondary tumours are more often seen in younger patients (mean age of 45) (14).

Histologically, primary and secondary GBMs are indistinguishable, but their genetic profiles differ. Primary GBM most commonly (90% of cases) do not harbour mutations in the isocitrate dehydrogenase enzyme genes (*IDH1* and *IDH2*). These are called IDH-WT. However, the majority of secondary GBM are IDH-mutant. Furthermore, loss of heterozygosity (LOH) on chromosome 10q is seen in 69% of primary GBM cases. Similarly, secondary GBM also has LOH 10q in around 63% of patients however secondary GBM 65% have tumour protein (*TP53*) mutations, which is only seen in 24-34% of primary GBM (15).

Upon diagnosis of both primary and recurrent GBM, patients have a surgical resection and standard treatment as described in section 1.4. However, due to the highly infiltrative nature of GBM, tumour cells inevitably remain after surgical resection of the tumour and these dominate formation of a recurrent tumour (16).

Table 1.1. Summary of the main differences between primary and secondary GBM.

	Primary GBM	Secondary GBM
Development	Developed de novo	Developed from a lower grade tumour
Mean age of diagnosis	62 years	45 years
IDH status	Usually IDH-WT	Usually IDH-mutant
LOH on chromosome 10q	In 69% of patients	In 63% of patients
Tumour protein (<i>TP53</i>) mutations	In 24-34% of patients	In 65% of patients

1.1.3 Recurrent GBM

Recurrent tumours are a major challenge in GBM as recurrence is inevitable and tumours typically recur after a median interval of around 7 months (17). Recurrent GBM is highly treatment resistant and highly aggressive so patients are encouraged to join clinical trials in the hope of prolonging life whilst finding out which, if any, treatment will extend life expectancy (1, 18). Recurrent GBM can recur at the same site as the original lesion, which is the case in around 80% of patients, or in a different location within the brain (19). However, less than 50% of patients with a GBM recurrence are eligible for a repeated surgery and life expectancy following repeat surgery is only extended by 5-11 months (20-24).

1.2 Heterogeneity within GBM

The challenge with treating GBM tumours comes from their highly heterogeneous nature. This complexity of GBM, including the number of mutations and abnormalities allows treatment resistance and escape, and ultimately tumour cell survival and out-growth (25). GBMs are highly heterogeneous tumours both between patients and also within the same tumour referred to as inter- and intra-tumour heterogeneity respectively. Intratumor heterogeneity (ITH) is the presence of genotypically and/or phenotypically distinct cell populations within a single tumour (26). ITH means that within an individual tumour, there can be cells

with varying phenotypes for example small or large anaplastic cells and of different cell types such as tumour cells, immune cells or cells from blood vessels (25). Furthermore, GBM tumours possess both differentiated tumour cells and stem cells, and individual cancer cells in the tumour may harbour different molecular characteristics to those elsewhere in the tumour. Cancer cells in close proximity to one another tend to share more characteristics than those that are more distant and can give rise to populations of cells within a tumour, referred to as subclones, each harbouring unique mutations (26). Upon treatment, certain subclones can survive and dominate the formation of a recurrent tumour. ITH makes treating GBM challenging as it can be difficult to determine the key driver events responsible for disease progression and recurrence as different drivers and mutations are often seen in different physical areas of the same GBM tumour (27). The high degree of inter-tumour heterogeneity further adds to the problem of finding effective treatments.

GBM tumours can be stratified according to molecular features present in a single section, however this may not be representative of all the subclones present, which may have driven tumour formation or will drive the response to treatment (28).

1.2.1 Molecular markers

GBM has several associated molecular markers specified by the WHO that are used to determine classification.

1.2.1.1 IDH

Over 90% of de novo GBM cases are IDH-WT. These are more aggressive than IDH-mutant tumours, which make up around 70% of secondary GBM cases. IDH status is often used to indicate what is likely a de novo tumour or a secondary tumour (29). In GBM, patient with mutations in IDH genes have an increase in overall survival of around 16 months compared with those with IDH-WT tumours (30). IDH enzymes play vital roles in the metabolic processes such as the Krebs cycle and homeostasis. In lower grade gliomas, mutations in IDH are considered to be driving tumorigenesis, which is in contrast to in GBM where IDH mutations are favourable (30, 31). IDH mutation in GBM leads to cells to growing slower which is thought to be due to changes in metabolic events and reduction in ATP synthesis (32).

1.2.1.2 EGFR

Mutations in the epidermal growth factor receptor (*EGFR*) are another common molecular aberration in GBM. *EGFR* is a receptor tyrosine kinase (RTK) that acts as a receptor for epidermal growth factor (EGF) members (33). Amplification of *EGFR* is associated with an aggressive phenotype, with amplification in 50% of primary GBM and recognition as a molecular marker of GBM by the WHO (2, 34, 35). Furthermore, *EGFR* is typically stable over the course of the disease as around 80% of GBM patients still have amplification on recurrence (36). In contrast, only 8% of secondary GBMs have *EGFR* amplification (37). In around 50% of these cases, there is a specific *EGFR* mutation observed that is caused by the deletion of exons 2 and 7 from the *EGFR* gene resulting in a 267 amino acids loss from the EGFR protein. This specific mutation is known as EGFRvIII and prevents *EGFR* from binding its associated ligands, inducing constitutive signalling (38). EGFRvIII has been shown to be tumorigenic in GBM and is linked to increasing tumour survival through increased proliferation and invasion that contributes to GBM progression (38).

EGFR amplification is also recognised as tumorigenic in multiple cancers such as lung and breast cancer, and EGFR inhibitors have had therapeutic success in these tumour types (39, 40). In contrast, in GBM, despite having promising effects in preclinical research, EGFR inhibitors have failed to have a clinical impact to patients (41-43). There are many reasons thought to contribute to this including heterogeneity in *EGFR* mutations and compensatory signalling pathways, so a better understanding of its pathways and signalling network is essential to be able to target *EGFR* successfully in GBM (44).

1.2.1.3 TERT promoter

Mutations in the promoter region of the telomerase reverse transcriptase (*TERT*) gene are seen in around 80% of GBM tumours and are recognised by the WHO as a molecular marker of GBM (2, 45). The *TERT* gene is one subunit of telomerase and is involved in the maintenance of telomeres protecting chromosome ends from degradation by filling the gaps left at the end of the chromosome following DNA replication (46-48). Telomerase is not active in differentiated cells, and therefore the telomeres of these cells will gradually shorten over time, leading to cell death (49). In GBM, mutations in the promoter region of the *TERT* gene have been shown to result in an upregulation of *TERT*

expression that leads to a significant increase in telomerase activity (50). This gives cancerous cells the ability to extend and stabilise their telomere length allowing them to continually divide and survive (51).

The debate on whether the presence of *TERT* promoter mutations in glioblastoma can independently predict a better or worse prognosis has been debated over the years. Many studies claim that *TERT* promoter mutations can predict a worse survival for patients (52-54). In contrast, numerous studies have claimed that *TERT* promoter mutations is not an independent prognostic factor and instead is correlated to other factors such as IDH mutation and age at diagnosis (55, 56). Regardless, it is clear that its dysregulation is implicated in GBM. Therefore, numerous studies have attempted to target telomerase with inhibitors as a therapeutic strategy. However, to date there has only been one telomerase inhibitor that has entered clinical trials, and this was shown to cause toxicity to solid tumours (57, 58).

1.2.1.4 Chromosome 7/10 translocation

The final WHO defined molecular characteristic used to determine a GBM tumour, in combination with the other markers, is chromosome 7 gain and chromosome 10 loss (7+/10-) (2). This is commonly seen in GBM and loss of chromosome 10q has been linked to a worse prognosis in high grade gliomas (59). The role of gain of chromosome 7 on survival in GBM patients is unclear but patients do exhibit shorter survival (60). One reason for this is thought to be that the *EGFR* gene is located on chromosome 7, and *EGFR* increase is related to worse prognosis in GBM (61). Due to the nature of this characteristic, it is used solely as a diagnostic marker and not for therapeutic targeting.

EGFR amplification, IDH-WT status, *TERT* promoter mutation and 7+/10- signature are commonly associated with GBM. However, having one of these molecular characteristics alone does not automatically indicate GBM as some of these characteristics are seen in other gliomas; for example *EGFR* amplifications in diffuse midline glioma and *TERT* promoter mutations in oligodendroglioma (2). However, a combination of two of *EGFR* amplification, *TERT* promoter mutation and 7+/10- signature is highly indicative of IDH-WT GBM and having all three of these characterises is exclusively seen in GBM (62). However, mutation profiles are not the only way to subclassify GBM. Work has been done to show that tumours can also be grouped based on their transcriptional profile.

1.2.2 GBM transcriptional subtypes

The Cancer Genome Atlas (TCGA) has been used to define three unique GBM subtypes based upon gene expression. These are termed proneural, classical and mesenchymal based on the expression of signature genes. These subtypes were identified using bulk sequencing of GBM tumours. Analysing the patterns of DNA copy number changes and somatic mutations revealed that genetic aberrations were more commonly associated with some transcriptional subtypes than others. The key mutations for each subtype as determined by Verhaak *et al.*, are described below (63-65). Originally a fourth subtype was identified, neural, but this was deemed to be non-tumour specific upon further analysis (66, 67).

1.2.2.1 Classical

In 100% of classical tumours, the chromosome 7 gain and chromosome 10 loss is seen. Subsequently, in almost all classical tumours *EGFR* was significantly amplified in comparison to the other subtypes (4-fold higher in classical tumours). There are low levels of mutation of *TP53* gene even though it is the most highly mutated gene in GBM. Furthermore, deletion *CDKN2*, a gene that is responsible for encoding several tumour suppressor genes was also seen in 94% of classical tumours. Finally, there are high expression levels of Nestin a neural precursor and stem cell marker as well as genes that are part of the Notch and Sonic hedgehog signalling pathways.

1.2.2.2 Mesenchymal

Deletion of the gene *NF1* occurred most often in the mesenchymal subtype and 53% of the samples containing *NF1* abnormalities fell into the mesenchymal subtype. Markers previously associated with mesenchymal phenotype for example *MET*, and *CHI3L1* were also expressed. Other genes that are highly expressed are those in the in the NF- κ B pathway and tumour necrosis factor super family pathway including *RELB* and *TRADD*.

1.2.2.3 Proneural

The proneural subtype was associated with IDH1 point mutations and amplification of the *PDGFRA* gene. Both mutations in *TP53* and LOH were also seen frequently in this subtype. Chromosome 7 loss and chromosome 10 gain was seen in the proneural subtype but a lot less frequently than in the classical subtype (54%). High levels of oligodendrocytic developmental genes including

OLIG2 and *NKX-2* were seen as well as several proneural development genes including *SOX* and *ASCL1*.

1.2.2.4 Intratumoral heterogeneity of subtypes

Although a GBM tumour can be assigned a subtype based on the above, single cell RNA sequencing (scRNAseq) showed that individual cells within a GBM tumour variably express the tumour subtype signatures, and that patients with tumours that showed a higher level of heterogeneity had decreased survival (68). Furthermore, the sequencing of multiple areas of a tumour showed evidence that each tumour harboured a mix of different subtypes (67, 69). In addition, the GBM subtype frequently changes going from primary to recurrent tumour (70).

1.2.3 Cellular states heterogeneity

As well as being caused by genetic mutations, ITH in GBM is also thought to result from variation in epigenetic and transcriptional profiles independent of genomic subclone. A study by Neftel *et al.*, determined that each GBM cell in IDH-WT tumours exists in one of four main cellular states and these reflect unique brain cell types, show plasticity and can interconvert (71). These states are based on expression signatures of around 39-50 key genes discovered from scRNAseq of GBM cells from IDH-WT tumours. This study found that there were high levels of ITH across the samples tested but despite this, the gene signature patterns pulled out often share fundamental biological process signatures. The four neoplastic cell states are termed Neural-progenitor-like (NPC-like), Oligodendrocyte-progenitor-like (OPC-like), Astrocyte-like (AC-like) and Mesenchymal-like (MES-like). As the names suggest, each gene signature is related to a brain cell type and the signatures were most highly expressed in each of these corresponding cell types. For example, astrocytes-like cancer cells most highly expressed genes associated with normal astrocytes.

NPC-like is associated with stem and progenitor markers such as *SOX11* and *SOX4*. It is subdivided into two further categories termed NPC1 which included genes related to oligodendrocyte progenitor cells and NPC2 which included genes related to neuronal lineage genes. OPC-like is correlated with oligodendroglia lineage markers for example *OLIGO1*, *OMG* and *TNR*. AC-like is correlated with astrocyte markers such as *GLAST*, *GFAP* and *SLC1A3*. MES-like is further subdivided into two categories. Those signatures that are strongly

associated with hypoxia response genes (for example *HILPDA* and *DDIT3*) and those that are not associated with hypoxia.

Each of the states contained proliferating cells however these were higher in NPC and OPC-like states. The majority of the cells tested correlated to one of these four main cell states however there was around 15% of cells that were correlated to more than one cell state and were considered as 'hybrid'. Each tumour tested was seen to have cells in at least two but typically all four of the cellular states, further demonstrating the levels of heterogeneity within a tumour. The cellular states seen within a tumour are reflective of their bulk tumour subgroup assignment; classical subtype had a higher abundance of AC-like cell state, mesenchymal subtype had a higher abundance of MES-like cell type and proneural subtype had a higher amount of both NPC and OPC-like states.

There are genetic drivers that predispose the cell states. For example, point mutations in the *NF1* gene were more associated with the MES-like state, and tumours with a higher proportion of cells in the AC-like state are also seen to have high-levels of genetic amplifications of the *EGFR* gene.

The plasticity of the cell states was also assessed in this study. Populations of cells from different cell states were isolated and implanted *in vivo* orthotopic patient derived xenograft models and all were seen to have tumour initiating properties. The tumours were analysed and found to contain equal distribution of cells belonging to all the cell types, suggesting that they have the potential to switch cell type. How the implication of these findings will reflect upon GBM patient treatment is yet to be discovered but it is clear that one standard treatment will not provide effective therapy for all GBM patients given the high level of heterogeneity at a genetic subtype and cellular state level.

1.3 Cancer stem cells

Cancer stem cells (CSCs) are so called because they possess the intrinsic properties of stem cells i.e. they are able to differentiate or self-renew, giving them the capability to drive tumour formation (72, 73). CSCs have been identified in multiple cancer types including breast, leukaemia, colorectal and brain cancer (74-77). Like stem cells, CSCs have the ability to remain dormant for prolonged periods of time or begin rapidly dividing to populate areas of the body. For CSCs, these features mean they can resist cytotoxic chemotherapies by remaining

quiescent, but many studies have also found that many CSCs have the ability to proliferate rapidly to dominate tumour formation when circumstances allow (78). CSCs have been linked to the recurrence of many cancers long after apparently successful treatment (79). Therefore, many studies aimed to target CSCs specifically to prevent tumour recurrence (80).

1.3.1 Glioma stem cells

Glioma stem cells (GSCs) is the term given to CSCs found in glioma. GSCs have been shown to drive tumour growth and recurrence, in part through their ability to resist chemoradiotherapy (72). GSCs exhibit a high level of invasiveness, and therefore are able to persist after debulking surgery to seed tumour recurrence (81). GSCs were first identified in GBM by Singh *et al.*, who discovered a population of cells that had the ability to initiate tumour growth *in vivo* (76). Furthermore, these GSCs were shown to express the marker CD133+, and were able to differentiate in culture into tumour cells. GSCs can be further identified by the expression of *CD15*, *SOX2* and *Nanog*; markers of normal neural stem cells (82-84). GSCs have been shown to initiate formation of recurrent tumour as well as recapitulating tumour heterogeneity *in vivo* after injection into mice (85). Due to their contribution to disease progression and treatment resistance in gliomas, GSCs have been deemed as a promising therapeutic target but, to date, targeting them has not been completed successfully (86).

1.4 Current treatment for GBM

To effectively treat GBM, mechanisms that confer resistance to standard treatment must be identified and therapies targeted to these. Despite GBM biology being increasingly understood, there has been no advancement of treatments in recent years. Multiple clinical trials look at the effects of new treatment of GBM each year, but these typically show no significant findings at phase III (87). This can be attributed to, but not limited to, a lack of translation from current *in vitro* and *in vivo* models into the clinic, the heterogeneity of GBM and the design of the clinical trials (88). Therefore, the same standard of care treatment protocol developed in 2005 is still used today as described below.

Following diagnosis, standard treatment for GBM includes a harsh treatment regimen of debulking surgery followed by combination treatments of chemotherapy with temozolomide (TMZ) and radiation (89). Debulking surgery is

performed on average around 13 days post diagnosis (90). The aim is to remove as much of the tumour as feasibly possible without damaging normal neuronal functions as preventing further neurological damage is prioritised over extending the resection margin (1). Methods to enable a higher extent of surgical resection include performing awake craniotomy, or performing fluorescence guided surgery using 5-aminolvalulinic acid (5-ALA) (91, 92). 5-ALA is an orally consumed substance that results in accumulation of fluorescent porphyrins in GBM tissue, allowing for more of the tumour to be identified and removed during surgery (93). Following this, patients receive radio and chemotherapy. Radiation is used to target the tumour in 2Gy fractions per day, for 5 days a week up to a total of 60Gy. Alongside this, patients receive daily TMZ until the last day of radiation (75mg/m²). Patients then receive a four week break before continuing with TMZ treatment for five days, repeating every 4 weeks for up to six cycles (17).

Inevitably due to the highly infiltrative nature of GBM, there will be cells left behind from surgery and some of these cells are able to evade the chemo and radiotherapy and form a recurrent tumour (94). There have been no major advances in GBM treatment since the development of TMZ and all targeted drugs have failed to give a clinical impact (95). However, other chemotherapeutic agents including etoposide and procarbazine are sometimes used for patients with recurrent GBM despite no data suggesting they are beneficial (1).

1.4.1 Temozolomide

TMZ is an alkylating agent that was first discovered to have anti-tumour properties in 1987 and was routinely used in clinics to treat GBM in 2005 after the establishment of the Stupp protocol. Stupp *et al.*, discovered that the combination of TMZ and irradiation significantly increased overall survival in GBM patients to 14.6 months, an increase of 2.4 months compared to radiotherapy alone (17). Since then, TMZ has been given to patients alongside radiation therapy as part of the standard treatment for GBM. TMZ metabolism is dependent on pH. At a neutral or alkaline pH, TMZ is broken down non-enzymatically to 5-(3-methyltriazene-1-yl)imidazole-4-carboxamide (MTIC) and MTIC is broken down to 5-aminoimidazole-4-carboxamide (AIC) and a methyl-diazonium cation (96). The methyl-diazonium cation alkylates the DNA. This is a rapid process and the half-life of TMZ is only 1.9 hours (97).

TMZ induces a number of harmful DNA damaging lesions and of these is the cytotoxic O⁶-methylguanine (O⁶-MeG) that is created by the addition of a methyl group to the O⁶ position of guanine (98). During DNA replication, O⁶-MeG pairs with thymine instead of cytosine. The mismatch repair (MMR) machinery within the cell then recognises the mis-paired O⁶-MeG and thymine pair and excises the incorrect base from the strand that was just synthesised. Thymine is therefore excised and the O⁶-MeG in the original strand remains present. This process repeats with another thymine being added and the ongoing excision and incision of thymine ultimately stalls DNA replication and leads to cell arrest and apoptosis (99, 100) (Figure 1.1).

O⁶-methylguanine-DNA-methyltransferase (MGMT) is an enzyme that acts to remove alkyl groups from O⁶-MeG. In cells expressing *MGMT* the alkyl group is removed from guanine and transferred to an internal cysteine in MGMT allowing the cell to replicate its DNA as usual and no longer be forced into apoptosis. This enables a cell to survive the effects of TMZ. MGMT is degraded in this process (101, 102). Promoter methylation of *MGMT* silences its expression, inducing susceptibility to TMZ, as alkyl groups remain on DNA and disrupt DNA replication (103). Therefore, GBM patients expressing *MGMT* respond less well to TMZ chemotherapy and have a shorter overall survival post-diagnosis (104). *MGMT* promoter methylation is therefore one of the main predictors of response to TMZ and is correlated with an increase in overall survival in GBM patients (102, 105). Currently GBM patients receive TMZ regardless of their *MGMT* status as in some cases patients with unmethylated *MGMT* see a benefit to TMZ, and some with a methylated *MGMT* have no benefit. This is likely due to the fact that some patients who are tested for *MGMT* status fall into a category where *MGMT* status cannot be fully determined (106).

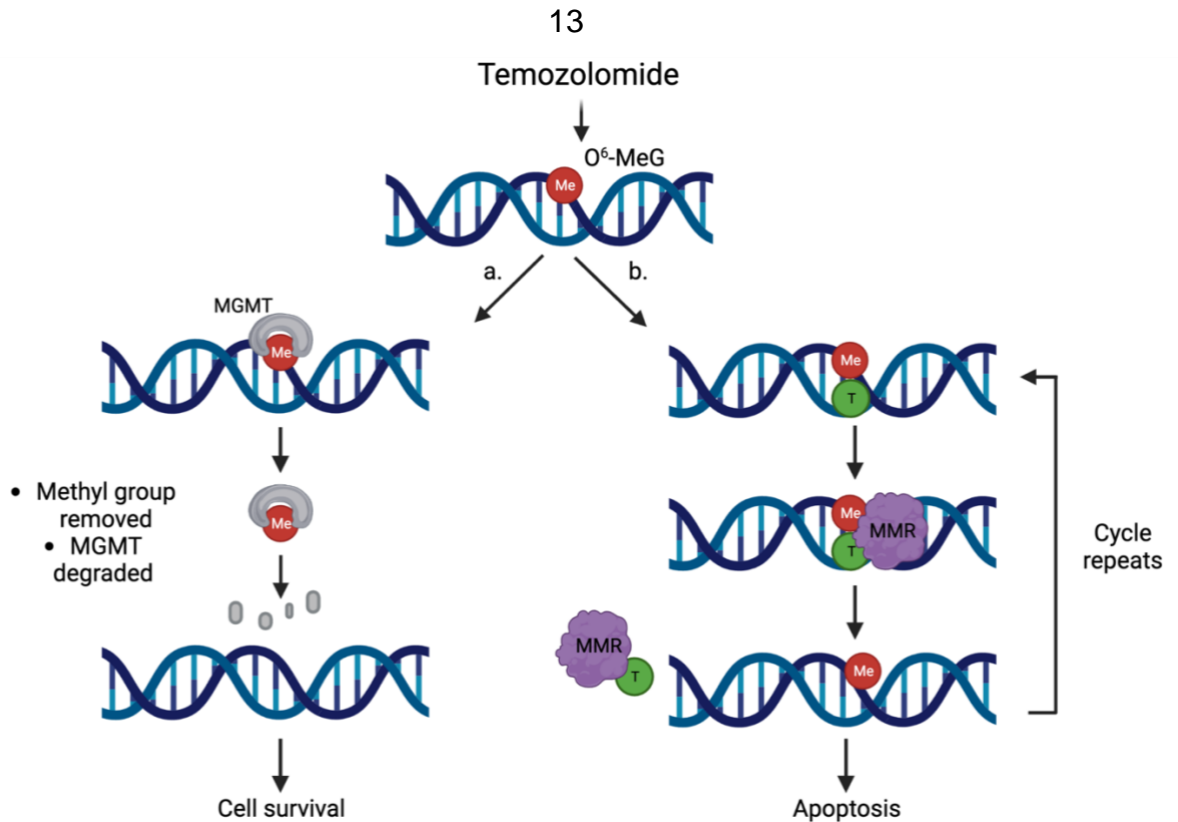


Figure 1.1. TMZ induces the harmful lesion O⁶-methylguanine (O⁶-MeG) to DNA. a) MGMT (O⁶-methylguanine-DNA-methyltransferase) removes the alkyl group from the DNA meaning the cell survives DNA replication. MGMT is lost in this process b) Thymine (T) pairs with O⁶-MeG. Mismatch repair (MMR) machinery recognises and attempts to repair the O⁶-MeG lesion. It continually excises the thymine leaving the O⁶-MeG present and the repair process is repeated. This eventually leads to DNA strand breaks and apoptosis.

1.5 RNA sequencing

Since its development, RNA-sequencing (RNA-seq) has become a powerful tool in molecular biology, in helping to shape the understanding of the transcriptome in a wide range of systems from examining microbial communities to understanding cancer genomics. RNA-seq has enabled insights into many aspects of biology, for example demonstrating the regulation of gene expression via non-coding RNAs and revealing the vast amount of mRNA splicing (107, 108). RNA is often highly dysregulated in human cancers, which can enable initiation and progression of the disease (109). RNA-seq provides biological information on ITH and helps to establish the molecular basis of formation of many cancers (110). Furthermore, it has been used in many aspects of cancer research

including biomarker discovery and identification of drug resistance mechanisms (110).

To date, there are over 100 unique methodologies stemming from the standard RNA-seq protocol (111). Many of these are based on short-read sequencing from the Illumina SBS (“sequencing-by-synthesis”) methodology. However, the more recent developments in long-read sequencing have enabled further advances in the field (111). Two well established categories of RNA-seq are bulk RNA-seq and single cell RNA-seq. Bulk RNA-seq refers to sequencing approaches that take the average gene expression from a cell population and therefore are used to identify differences between different conditions and allows insights into the representation of highly regulated pathways (112). There are two main categories of bulk RNA-seq: creating mRNA only libraries; and creating whole transcriptome libraries to look at all RNA species excluding ribosomal RNA (109). The most commonly used method of bulk RNA-seq is the use of short read sequencing. This enables the user to understand the molecular mechanisms involved at different stages of tumour progression by looking at differentially expressed genes. Long read sequencing is less commonly used but can provide insights into alternative splicing, point mutations and long non-coding RNAs (109). scRNA-seq allows an insight into the transcriptome at a single cell resolution and was first published in 2009 (113). scRNA-seq allows for a more comprehensive understanding into the changes inside a cell. However, the data from scRNA-seq is often noisier both in a technical sense from RNA capture efficiency and in a biological sense from cell cycle states and stochastic gene expression (113). One of the most common analysis methods following RNA sequencing is to perform differential gene expression analysis (114).

1.5.1 Differential gene expression analysis

Analysis of paired primary and recurrent GBM samples aims to allow the identification of features, present in primary tumours, that have become more dominant in recurrent samples and are, therefore, potentially involved in mechanisms of treatment resistance (115). Differential gene expression (DGE) analysis is a way of looking at this. DGE analysis is a method of analysing RNA-seq data that allows the discovery of the most differentially expressed (DE) genes across two or more conditions (114). Tools allow DGE to be performed based on count data i.e. the number of raw RNA-seq reads that aligned to a gene per

experimental condition. DGE analysis determines what genes have their expression changed, e.g. through treatment, and the extent of this change (114). There are multiple tools and packages available to perform DGE analysis and there is no consensus of the correct way in which this analysis should be performed (116). Broadly speaking, the steps involved in DGE analysis are quality control, alignment, gene expression quantification, and finally the differential gene expression analysis itself (117). DE can enable genes that are dysregulated following treatment to be identified which can help identify candidates for conferring resistance to therapy.

1.6 *SLC6A6* as a gene of interest in GBM

Work in the Glioma Genomics group at Leeds included RNA expression analysis on 17 pairs of IDH-WT primary and matched recurrent GBM samples. This showed that *SLC6A6* expression is significantly upregulated in recurrent versus matched primary GBMs (Figure 1.2a) In addition, single-cell GBM experiments were performed. This involved isolating cancer cells from a newly resected GBM, which were then cultured as spheroids. Half of the spheroids were treated with TMZ and irradiation and seven days later, RNA was sequenced from single cells from untreated and treated groups. This showed that *SLC6A6* was significantly upregulated post-treatment (Figure 1.2b). Previous associations with *SLC6A6* and treatment response in other cancers (118, 119) and the fact that high *SLC6A6* expression associates with poor prognosis in GBMs according to data from The Cancer Genome Atlas (plotted using GlioVis (120) (Figure 1.2c), have led us to investigate its potential role in treatment resistance in GBM.

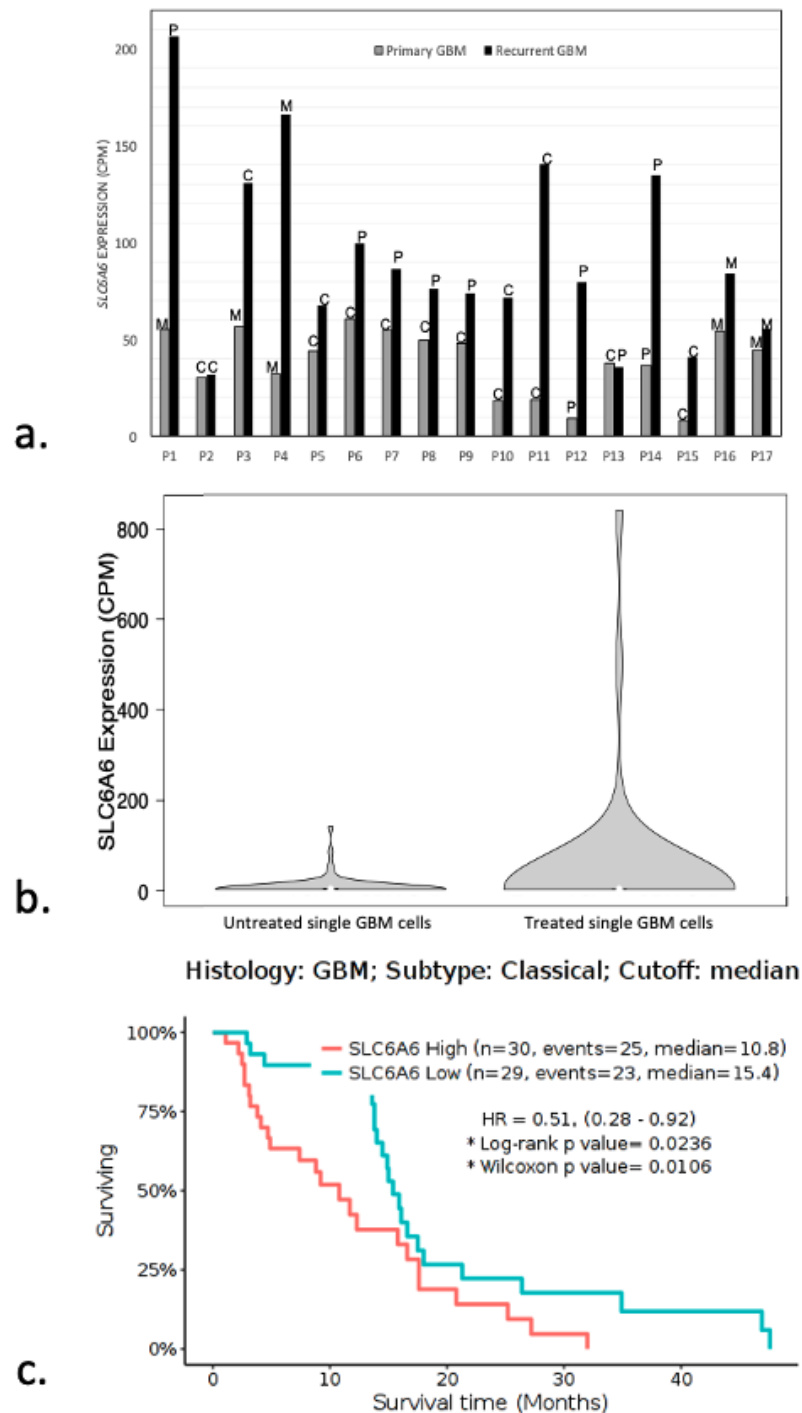


Figure 1.2. *SLC6A6* expression. a) Expression level from RNA-sequencing in counts per million (CPM) of *SLC6A6* in seventeen pairs of primary and recurrent GBM tumours. Letters indicate the subtype of the tumour. C = classical, M = mesenchymal, P = proneural. b) *SLC6A6* expression level (CPM) in single cells from spheroids derived from a primary patient GBM. *SLC6A6* is upregulated in spheroids treated with TMZ and irradiation. c) GBM patients with increased *SLC6A6* expression have a significantly worse overall survival. Data from The Cancer Genome Atlas and plotted using GlioVis (120).

1.6.1 Solute Carrier Family 6 Member 6 (*SLC6A6*)

Solute Carrier Family 6 Member 6 (*SLC6A6*) is a gene located on Chromosome 3p25.1 and contains 19 exons. The main isoform encodes 620 amino acids but alternative splicing results in multiple transcript variants including coding transcripts and those subjected to nonsense mediated decay. Expression of *SLC6A6* is seen in many areas of the body including the heart, kidney, stomach, ovary and brain (121, 122). *SLC6A6* encodes an intracellular taurine transporter, TauT, expressed in embryonic and adult neural progenitor cells (NPCs) (123).

TauT is a solute carrier transporter which belongs to a superfamily of around 400 membrane bound proteins that aid in transporting substrates across membranes (124). Membrane transporters from the SLC superfamily typically have a role in transporting small, hydrophilic molecules into cells and are required as these molecules cannot easily diffuse across membranes and must be transported via channels for cellular or organelle entry or exit (124, 125). Many transporters in the SLC group can transport a broad range of molecules, however some have only a narrow range such as the SLC6 group that are neurotransmitter transporters (124). SLC transporters are often drug targets as targeting them can block transport of endogenous substrates (126).

The SLC6 family are a group of sodium and chloride dependant transporters and have been deemed responsible for fundamental roles, including in the central nervous system where they provide crucial nutrients and osmolytes to glial cells and neurons (127). They can be further divided into four groups based on sequence similarity and substrate specificity. These are the monoamine transporters, the γ -aminobutyric acid (GABA) transporters, the amino acid transporters group I and the amino acid transporters group II. The GABA transporter group also comprises the transporters of the osmolyte taurine, known as *SLC6A6* (128).

SLC6A6 has been found to play a role in promoting the survival of colorectal cancer cells (129). This study found that *SLC6A6* was highly expressed in colorectal cancer cells, and that knockdown reduced the cell numbers in the cancer stem cell population. *In vivo* experiments with *SLC6A6* knockdown cells conferred significantly smaller tumours than wildtype cells. Furthermore, they found that *SLC6A6* correlated to multi-drug resistance in colorectal cancer

demonstrated by the enhanced number of multi-drug resistance cells following *SLC6A6* over expression.

SLC6A6 has been linked to various other disease phenotypes, briefly summarised here. High levels of *SLC6A6* have been correlated with gastric cancer and associated with a worse prognosis (130). *SLC6A6* has additionally been identified as a potential biomarker in the early stages of colorectal adenocarcinoma (131). Mutations in *SLC6A6* have been linked to retinal degeneration and *SLC6A6* expression has been linked to cardiomyopathy (132). Long term taurine supplementation in patients with both retinal degeneration and cardiomyopathy because of a homozygous mutation in *SLC6A6* have had their disease phenotypes halted (retinal degeneration) or reversed (cardiomyopathy) (133).

1.6.2 Taurine transporter (TauT)

In humans, TauT is a 70 kDa protein (134). Like most members of the SLC6 family, TauT is comprised of 12 hydrophobic membrane spanning domains with intracellular N and C termini. TauT is an osmolyte transporter which is part of the GABA transporter family. Its main function is to regulate taurine transport based on factors such as temperature, pH and ionic environment (135). In hypertonic and isotonic conditions TauT utilises a Na⁺ gradient to couple passive transport of Na⁺ with active transport of taurine across the membrane (136). Taurine is the primary molecule TauT transports. However, TauT also transports GABA, beta-alanine and hypotaurine which is an intermediate molecule in taurine biosynthesis (137-139). TauT is regulated post-translationally by phosphorylation of serine 322 by Protein Kinase C (PKC) that results in a reduction of taurine transport via TauT. PKC is activated by processes such as oxidative stress and increased calcium levels, and upon its activation it phosphorylates serine 322 which subsequently decreases taurine transport (140).

1.6.3 Taurine

Taurine is an amino sulfonic acid, sometimes termed as a non-essential amino acid as it is one of the few amino acids that is not involved in protein synthesis. However, this name is contradictory due to the essential roles that taurine has in the human body that includes neuroprotective functions (141). The chemical formula of taurine is C₂H₇NO₃S with a molecular weight of 123.15, and its

chemical name is 2-aminoethanesulfonic as it is the 2-amino derivative to ethanesulfonic acid (142). Taurine is found throughout the body, but levels are highest in the heart, brain, retina and muscles (143). A normal part of a human diet, taurine is found in many common foods such as chicken, turkey, white fish and shellfish. Upon entering the body, taurine is absorbed by the small intestine before being transported to the liver via the portal vein. Here it is released into circulation and can be transported into cells via TauT (144). Taurine cannot be transported via any other transporter (145). As well as entering the body via food, taurine can also be biosynthesised within the cytoplasm in a process using cysteine. In this reaction, which takes place in the liver, the sequential action of two enzymes named cysteine dioxygenase (CDO) and cysteine sulfonic acid decarboxylase (CSAD) catalyses cysteine to taurine. During this process CDO catalyses the oxidation of cysteine to cysteinesulfonate which then undergoes decarboxylation to hypotaurine catalysed by CSAD. Hypotaurine is the precursor for taurine and is oxidised to taurine in a step thought to be independent of enzymatic activity (146). As well as being synthesised in the liver, taurine has also been reported to be synthesised in the brain, lungs and mammary glands (147). However, only low amounts of taurine are synthesised this way due to the low amounts of CSAD in the body, therefore the primary method of getting taurine into a cell is through the diet (144).

The importance of taurine was first observed in 1975 when it was discovered that taurine deficiency led to retinal degeneration in cats (148). Since then, many beneficial and protective effects of taurine have been investigated such as regulating calcium levels to prevent the progression of arteriosclerosis, reduction in heart failure, providing protection to cells from neurotoxicity in mice and reducing oxidative stress (149-151). Taurine is important in brain development and has numerous fundamental roles in human brains, for example regulating osmotic pressure with cytoprotective effects in various cell types (152). This comes from the ability of taurine to increase membrane stability, eliminate inflammation, and prevent calcium accumulation (153). Taurine has also been shown to promote neural development in the embryonic brain, and regions of the adult brain; glycine, GABA or alanine are not able to mimic this affect. This was evidenced in mice brains, where it was shown that the olfactory bulb contains the highest taurine. Furthermore, levels therein do not decline over brain maturation unlike in other regions, suggesting a highly important role. Neural progenitor cells

(NPCs) migrate from the subventricular zone to the olfactory bulb during adulthood, wherein they differentiate into neurons. The unusually high levels of taurine here is thought to play a role in this process (123). Due to its important role in brain development, taurine deficiency can have serious consequences and has been linked to a delay in cell differentiation and migration in multiple cell types in cats and monkeys including in the cerebellum, pyramidal cells and visual cortex (154-157).

Taurine association with glioma is understudied. One study found that taurine levels have been linked to increased malignancy in glioma, and a higher concentration of taurine is found within the tumour than the surrounding brain (158). A recent study in 2021 investigated the effects of taurine and TMZ combination on the survival of U251 cells. They demonstrated that taurine results in a reduction in cell proliferation resulting in a decrease in viable cells after treatment. Furthermore, they showed that the combined effect of taurine and TMZ exhibited synergistic effects on glioblastoma cell lines and resulted in a reduction in proliferation and an increase in apoptosis (159).

1.7 Current models in GBM research

1.7.1 Patient derived cell lines and established cell lines

Established cell lines have been extensively used in GBM research, thus they are well characterised. However preference is now shifting towards the use of patient derived cell lines cultured in serum-free media (160). Serum causes GBM cells to differentiate, thereby reducing cells stem-like properties and diverting away from the phenotype of patient tumours (161, 162). Patient derived lines cultured in serum-free media are enriched for stem cells and are referred to as GSC lines. These recapitulate the heterogeneity of patient samples and retain important features such as the ability to self-renew, and undergo multi-lineage differentiation, which established cell lines lack (163). Furthermore, both histopathological and molecular differences are observed between established and patient-derived cell lines (163). Included in this is differing gene expression profiles seen between established and patient derived cell lines, with the patient derived cell lines at lower passage number resembling that seen in patient tumours. Furthermore GSCs are thought to contribute heavily to disease pathology as described in section 1.3.1 (164).

Despite the mounting evidence that patient derived GBM cell lines better represent the biology of patient tumours, it is important to use both established and patient-derived serum-free cell lines to inform on the different types of GBM biology when investigating treatment resistance. This is because established cell lines represent the differentiated population of cells in GBM therefore should not be discounted (160).

1.7.2 3D cell culture

Over the years, 2D cell culture has been used as a major part of scientific research. While 2D cell culture offers many advantages, there are issues with the reproducibility upon progression to *in vivo* work, perhaps due to their oversimplified nature (160). Despite not being a full representation of the tumour microenvironment, 3D spheroid cultures contain many features that make them more closely mimic *in vivo* than 2D models (165). For example, spheroids have natural gradients for oxygen, metabolite, pH and drug penetration. Cell-to-cell interactions with neighbouring cells affect gene expression and can only be modelled in 3D culture (166). Furthermore, spheroids above around 400 μm in diameter begin to develop a hypoxic core. Hypoxia has been associated with chemotherapy and radiotherapy resistance resulting in a worse patient prognosis and this feature of spheroids is difficult to replicate in 2D models (167). Spheroid models are therefore more physiologically relevant and allow a better platform for the testing of drug delivery thus lead to more reproducible findings *in vivo* (168).

Organoids are another 3D culture method where miniature versions of organs are grown from either pluripotent embryonic stem cells/induced pluripotent stem cells, or organoid restricted adult stem cells (169). When these stem cells are allowed to replicate in culture under the influence of certain growth factors, they self-organise into structures that resemble that of organs (170). Organoids possess all the main advantages that spheroid culture provides in terms of physiologically relevant features such as oxygen and nutrient gradient, however their differentiation allows them to be made of multiple different cell types which differs from spheroids that are typically only made up of one cell type. Organoids have been successfully created to model a range of organ types including liver, kidney, lung and brain and organoids can be derived from both normal tissue and malignant tissue (171-174).

The drawback of organoid use is that maturation of organoids to a state that most closely resemble the complexity of organs require a prolonged period of time in culture, often around 2-3 months (175). Therefore, it is hard to perform high-throughput assays using organoids.

1.7.3 Mouse models

In vivo models are valuable resources for studying human disease and over 95% of *in vivo* work is performed in mice (176). There are two main categories of mouse models, genetically modified mice and xenograft models.

Xenograft mouse models implant tumour cells from a human cancer into a mouse. The mouse must be immunocompromised to avoid the mouse immune system recognising and killing the implanted human tissue. There are two main types of xenografts, cell-line based xenografts and the more biologically relevant patient-derived xenografts (PDX). PDX are grown from primary tumour tissue and when implanted are believed to recapitulate the features of the original tumour, such as the cellular heterogeneity and gene expression profiles (176). Xenograft models are often used to assess how a tumour will respond to a certain drug or treatment regime (177). However, the absence of the immune system from the mice is a disadvantage as they cannot be used to study any treatment involving immunotherapies. Additionally, the importance of the immune system in GBM biology is becoming increasingly studied, and therefore the PDX may not represent the whole picture in terms of response to a drug and immune response, as well as in tumour recurrence.

Genetically engineered mouse models (GEMMs) have been used in GBM to alter the genetic of mice to mimic disease phenotypes and observe role of genetic mutations in GBM tumorigenesis. GEMMs can model disease phenotypes in a mouse model with a functioning immune system, a major advantage compared to PDXs as they can be used to model the interactions between tumour cells and the tumour microenvironment (178). Furthermore, they capture tumour formation more accurately and the blood brain barrier is not disturbed as it is in PDX. The disadvantages of GEMMs for use in GBM research include the tumour formation in any region of the brain, which contrasts with a PDX where tumours typically form near the standardised injection site. Furthermore, GEMMs often lack ITH (179). Different levels of genetic manipulation exist and are summarised in Figure 1.3. These include the manipulation of a small number of cells for example using

viruses for delivery, targeting a group of tissue cells, for examples using conditional and inducible promoters, and targeting the whole tissue for example using knockout mice (180).

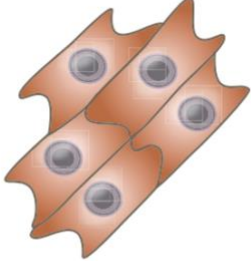
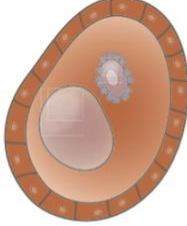
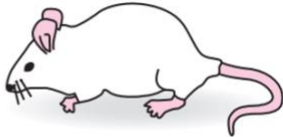
Tissue scale	A small number of cells	A specific group of tissue cells	Whole tissues and germ line
			
Methodology	Hit and run Head-to-head loxP Virus-mediated delivery	Conditional and inducible knockout Transgenic with a tissue-specific promoter	Knockout Transgenic with a ubiquitous promoter

Figure 1.3. Genetic manipulations in mice. Summary of the different genetic manipulations, and the scale of these manipulations to create genetically engineered mice. Taken from (180).

1.8 Aims and Objectives

Through its significant upregulation following treatment of GBM, it is clear that *SLC6A6* is of interest however it is unclear what role *SLC6A6* is playing in treatment resistance in GBM.

My hypothesis is that *SLC6A6* is impacting treatment resistance in glioblastoma.

To investigate my hypothesis, I have three aims:

1. Optimise the experimental set up and parameters for the experiments to be used in this study. This would ensure that all experiments could be run in a consistent and standardised way. To achieve this, the following objectives were set:

- Objective 1 - Determine suitable cell lines for use in the project.
 - Objective 2 - Develop an automated imaging and analysis platform for spheroid measurements.
 - Objective 3 - Select an appropriate taurine concentration for use in experiments.
 - Objective 4 - Optimise treatment doses and timings of temozolomide and irradiation in 2D culture.
 - Objective 5 - Optimise treatment doses and timings of temozolomide and irradiation in 3D culture (spheroids).
 - Objective 6 - Determine appropriate end point assays to be used
2. Investigate the association between *SLC6A6* expression and sensitivity to standard treatment in GBM *in vitro*.
 - Objective 1 – Knockdown the expression of *SLC6A6* in three chosen cell lines.
 - Objective 2 – Assess differential treatment sensitivity in the chosen 3D model using spheroid size measurements and CellTiter-Glo 3D assay.
 - Objective 3 – Investigate the effect of TauT antagonists and GABA_A receptor agonists on response to standard treatment.
 3. To define the effect of *SLC6A6* inhibition on GBM cell transcriptomes in response to standard treatment.
 - Objective 1 - Analyse RNA-sequencing data from experiments looking at the effect of TauT antagonists and GABA_A receptor agonists on response to standard treatment.

Chapter 2

Materials and Methods

2.1 Preparation of stock solutions

Temozolomide (TMZ) was resuspended to 50 mM in dimethyl sulfoxide (DMSO) and stored at -20°C. Gaboxadol hydrochloride (GAB) and Guanidinoethyl sulfonate (GES) were both resuspended in high purity water to 100 mM and stored at -20°C. New stocks of GAB and GES were made every 6 months. epidermal growth factor (EGF) and fibroblast growth factor (FGF) were suspended in Dulbecco's phosphate buffered saline (PBS) to a final concentration of 2000 ng/mL and stored at -20°C. Poly-L-ornithine was diluted to 10 mg/mL in tissue culture (TC) grade water and stored at -20°C. Laminin was stored in aliquots of 1 mg/mL in TC at -20°C. Catalogue number of the reagents are listed in Table 2.1.

Table 2.1. Reagents prepared for stock solutions. The reagents used, supplier information, and catalogue of commonly used stock solutions.

Reagent	Supplier	Catalogue number
Temozolomide	Merck	T577-100MG
THIP Hydrochloride (Gaboxadol)	Merck	T101-500MG
Guanidinoethyl sulfonate	Cayman Chemical	17572-500mg-CAY
Human FGF-basic	R&D systems	100-18B-100
Recombinant Human EGF, CF	Peptotech Inc. USA	236-EG-200
Poly-L-ornithine	Sigma	P3655-50MG
Laminin	Sigma	L2020-1MG

2.2 Cell culture

2.2.1 Cell passage

Reagents used for cell culture are listed in Table 2.2. The A172 established GBM cell line was acquired from American Type Culture Collection (ATCC, Manassas) and authenticated using STR profiling (December 2018). A172 cells were maintained in A172 medium (Table 2.3), maintained at 5% CO₂ at 37°C and passaged 1:5 twice a week. Two primary patient-derived cell lines (GBM58 and GBM63), cultured in Leeds, were maintained in Neurobasal (NB) media (Table 2.3), maintained at 5% CO₂ at 37°C and passaged when at 80% confluency at a 1:3 dilution. Primary patient derived cell lines were cultured in flasks coated with 10 µg/mL ornithine and 2 µg/mL laminin. On passage of the cells, they were washed with 5mL PBS before addition of Trypsin-EDTA solution at 1 mL/75cm² flask. Cells were placed in the incubator until detached before being collected in the appropriate medium and centrifuged for 5 minutes at 300g before media being removed. Cells were resuspended in medium and split at appropriate confluency.

Table 2.2. Reagents used in cell culture procedures. The catalogue number and suppliers of all reagents used in cell culture protocols.

Reagent	Supplier	Catalogue No.
Foetal Calf Serum (FCS)	ThermoFisher Scientific (Life Technologies)	10270106
Dulbecco's modified eagle medium (DMEM), high glucose	Merck	D6429
Neurobasal (NB) medium	ThermoFisher Scientific (Life Technologies)	10888022
Human FGF-basic	R&D systems	100-18B-100
Recombinant Human EGF, CF	Peprotech Inc. USA	236-EG-200
N-2 supplement	ThermoFisher Scientific (Life Technologies)	17502048
B27 serum free supplement	ThermoFisher Scientific (Life Technologies)	17504044

Poly-L-ornithine	Sigma	P3655-50MG
Laminin	Sigma	L2020-1MG
Trypan Blue	SLS	T8154-20mL
10 x Trypsin-EDTA solution	Sigma	59418C-100ML
DMSO	Sigma	D2650-100ML
Dulbecco's Phosphate Buffered Saline	ThermoFisher Scientific (Life Technologies)	D8537-500ML
Sterile double process cell culture water	Merck	W3500

Table 2.3. Cell lines used and their required growth medium. Suppliers and catalogue number (where appropriate) for cell lines are shown and the and the basal media and required supplements for culturing.

Cell line	Supplier and catalogue No.	Basal Media	Supplements
A172	ATCC. Cat. No. CRL-1620	DMEM high glucose	<ul style="list-style-type: none"> • 10% FCS
GBM58	LIMR	Neurobasal	<ul style="list-style-type: none"> • 40 ng/mL recombinant human EGF • 40 ng/mL recombinant human FGF • 0.5 x B27 serum free supplement • 0.5 x N2 supplement
GBM63	LIMR	Neurobasal	<ul style="list-style-type: none"> • 40 ng/mL recombinant human EGF • 40 ng/mL recombinant human FGF • 1:200 dilution of B27 serum free supplement • 1:200 dilution x N2 supplement

2.2.2 Cell freezing and thawing

Cells were frozen in their growth media (Table 2.3), supplemented with 10% DMSO. 1 mL of cells were frozen per cryovial at a density of 1×10^6 cells/mL. Cells were frozen at -80°C initially in a Mr Frosty then transferred to liquid nitrogen. On thawing cells, cryovials were placed in a water bath at 37°C until defrosted and added to 10 mL prewarmed media before being centrifuged at 300g for 5 minutes. Media was removed and replaced with 5 mL of fresh media and then placed in a T25. Media was replaced after 24 hours. Once confluent, cells were split into a T75 as described above.

2.2.3 Cell counting

To determine the number of cells in solution, 20 μL of cell suspension was diluted with 20 μL of Trypan blue solution. 10 μL of this mixture was transferred to a haemocytometer and the cells in each four quadrants counted to calculate and the concentration calculated as below:

$$\text{Concentration} = \left(\frac{\text{Cell count}}{2} \right) \times 10^4 \text{ cells/mL}$$

The dilution factor was then calculated to determine the dilution needed for experiments using:

$$\text{Dilution factor} = \frac{\text{Current concentration}}{\text{Desired concentration}}$$

The dilution factor was used to calculate the volume of cell suspension required which was then made up to the total volume required using fresh media.

$$\text{Volume of cell suspension} = \frac{\text{Required volume}}{\text{Dilution factor}}$$

2.2.4 Coating plates

Poly-L-ornithine stocks were diluted to 10 $\mu\text{g}/\text{mL}$ in TC grade water. 10 mL working solution was added to each T75 flask, 5 mL to each T25 flask, 1.5 mL per well of a 6-well plate, and 100 μL per well in a 96-well plate. After one hour at room temperature, the solution was removed and flasks rinsed with TC grade water. Laminin stocks were diluted to 2 $\mu\text{g}/\text{mL}$ in PBS (cat. no. D8537, ThermoFisher Scientific). 10 mL working solution was added to each T75 flask, 5 mL to each T25 flask, 1.5 mL per well of a 6-well plate, and 100 μL per well in a 96-well plate. Flasks and plates were wrapped in parafilm and left at room temperature overnight before storing at -20°C .

2.3 MTT assay

MTT assays were used to determine the number of viable cells present in 2D cultures. Cells were trypsinised and resuspended at 1.5×10^4 cells per mL in normal culture medium and 200 μL plated into each well of a 96-Well Clear Flat Bottom Microplate. Cells were left overnight before any treatment added (described below). For each time point, cells were pre-incubated with 3-(4,5-dimethylthiazol-2-yl)-2,5-diphenyltetrazolium bromide (MTT) (cat. no. 6494, ThermoFisher) at a final concentration of 0.5 mg/mL for three hours before all media and MTT was replaced with 100 μL DMSO. Viability was measured by absorbance of MTT/100 μL DMSO at 540 nm (Thermo Scientific Multiskan EX).

2.4 Spheroid culture

For 3D culture, cells were trypsinised and resuspended at 1.5×10^4 cells per mL in normal culture medium and 200 μL plated into each well of a 96-Well Clear Round Bottom Ultra-Low-Attachment Microplate (Scientific Laboratories Supplies, 7007). Any empty wells were filled with 200 μL PBS to avoid evaporation. Spheroids were imaged every two to three days using the Confocal Nikon AR1 and medium changed every three days by removing 100 μL of medium and replacing this with 100 μL fresh medium. On most experimental set ups 60 spheroids per condition were originally seeded.

2.5 Spheroid imaging and growth curves

To measure spheroid growth, a bespoke automated plate-imaging and analysis programme was developed using the Confocal Laser Scanning Microscope-Nikon A1R as described in section 3.3.2.1. Using the confocal microscope and the software currently available, it is not yet possible to obtain Z-stacks of an entire spheroid in order to determine the volume. Therefore, it was decided that area (μm^2) would be the measurement used to represent spheroid size. Data was analysed using SpheroidAnalyseR described in section 3.3.3 (<http://spheroidanalyser.leeds.ac.uk/>) which uses a pre-set threshold to remove obvious outliers for example empty wells, and then removes further statistical outliers using a robust z-score of +/- 1.96 (181).

2.5.1 CellTiter-Glo 3D cell viability assay

Spheroids to be analysed via CellTiter-Glo 3D cell viability assay were removed from the spheroid plate in a total volume of 100 μL and transferred to 96-well white opaque edged plates (Cat. No. 655098 – Grenier Bio-one Ltd) and left at room temperature for 30 minutes. CellTiter-Glo reagent was left to come to room temperature before 20 μL was added to each well. Plates were placed on a plate shaker for 30 minutes at room temperature before the luminescence read on a Cytation 5 Imaging Plate Reader (BioTek).

2.6 Treating with temozolomide and irradiation

2.6.1 In 2D cultures

GBM cells were seeded in 96-well plates at 3000 cells per well in 100 μL media for 24-, 48- and 72-hour treatment time points and 1500 cells per well for 144-hours post-treatment. Cells were left to attach for 24 hours before adding TMZ in 100 μL of media to reach concentrations of 0.1 μM , 0.3 μM , 1 μM , 3 μM , 10 μM , 30 μM , 100 μM , and 300 μM . Cells were irradiated using a RadSource RS-2000 irradiator with either 1Gy, 2Gy, 5Gy or 10Gy one-hour after treatment with TMZ. MTT assays were performed at time points of 24, 48, 72 and 96 hours post treatment.

2.6.2 In 3D cultures

Spheroids were seeded at 3000 cells per spheroid as described above and were treated at 5 days post-seeding. 100 μL of medium was removed from a total of

200 μL and replaced with medium containing TMZ diluted from the 50 mM stock solutions to concentrations of 6 μM , 20 μM , 60 μM , 200 μM and 600 μM giving final concentrations when added to spheroids of 3 μM , 10 μM , 30 μM , 100 μM and 300 μM . For irradiation treatments, cells were irradiated using a RadSource RS-2000 X-ray irradiator with either 2Gy, 4Gy or 6Gy one hour after TMZ treatment and imaged every two to three days thereafter.

2.7 Taurine supplementation

2.7.1 2D cultures

Cells were seeded in 96-well plates at 3000 cells per well in 100 μL media for 24, 48, 72 and 96-hour time points post-seeding. 100 μL of standard cell culture media containing taurine at concentrations 10 mM, 20 mM and 40 mM was added to the cells to give a final concentration of 5 mM, 10 mM and 20 mM respectively.

2.7.2 3D cultures

Cells were seeded at 3000 cells per well in 100 μL media. Immediately after, 100 μL of normal cell culture media containing taurine at concentrations 10 mM, 20 mM and 40 mM was added to the cells to a final concentration of 5 mM, 10 mM and 20 mM respectively. Spheroids were imaged every two to three days and media was changed every two to three days by removing 100 μL media and replacing with 100 μL of 10 mM taurine media.

2.8 Combined treatment and taurine supplementation

Cells were seeded at 3000 cells per well and cultured as spheroids in media containing 10 mM taurine. On day five post seeding, treated plates were treated with 30 μM TMZ and 2Gy irradiation. Spheroids were imaged every two to three days and media was changed every two to three days by removing 100 μL media and replacing with 100 μL of 10 mM taurine media.

2.9 Inhibitor treatment on spheroids

2.9.1 Inhibitor dose response

Cells were seeded at 3000 cells per well and cultured as spheroids in media containing 10 mM taurine. On day five post seeding, a 1:10 serial dilution was

made of both GES and GAB from 100 mM stock solutions diluted into normal culture medium ranging from 100 mM to 0.0001 mM. Following this, 120 μ L of media was removed from each spheroid and replaced with 100 μ L fresh media containing 10 mM taurine, and 20 μ L of inhibitor so that spheroids were treated with between 10 mM and 0.001 mM of GES or GAB. 20 μ L dH₂O was added to vehicle control spheroids. Spheroids were imaged every two to three days. CellTiter-Glo 3D assay was performed 7 days post treatment.

2.9.2 Inhibitor and standard treatment

Cells were seeded at 3000 cells per well and cultured as spheroids in media containing 10 mM taurine. On day five post seeding, 120 μ L of media was removed from each spheroid. For vehicle control spheroids 20 μ L dH₂O and 100 μ L fresh media containing 10 mM taurine was added. 20 μ L of 100 mM GES or GAB was added to remaining spheroids. Untreated spheroids received 100 μ L of media containing 10 mM taurine, and the spheroids to be treated with standard treatment received 100 μ L media containing 10 mM taurine and 60 μ M TMZ to give a final concentration of 30 μ M TMZ. Treated plates were subjected to irradiation treatment using a RadSource RS-2000 X-ray irradiator with 2Gy one hour after TMZ treatment. Spheroids were imaged and media replaced every two to three days thereafter. CellTiter-Glo 3D assay was performed 7 days post treatment on 10 spheroids per condition, and the remaining 50 spheroids used to extract RNA from section 2.10.1.2.

2.10 qPCR

2.10.1 RNA extraction

2.10.1.1 RNA from cells in 2D

Cells were cultured in T75cm³ flasks until confluent. Cells were trypsinised, collected, and spun at 300g for 5 minutes before being lysed in 600 μ L of buffer RLT. RNeasy mini kits (Cat. No. 74134 Qiagen) were used to extract RNA as per the manufacturer's instructions. RNA was quantified using Nanodrop spectrophotometer (ThermoFisher) assessment before being stored at -80°C.

2.10.1.2 RNA from spheroids for sequencing

Around 50 spheroids per condition were collected in a 15 mL centrifuge tube and centrifuged at 800 rpm for 5 minutes. Media was aspirated and spheroids washed in PBS and centrifuged at 800 rpm for 5 minutes. PBS was removed and spheroids washed in PBS and centrifuged at 800 rpm for 5 minutes. PBS was removed and 600 μ L of Qiazol added from Qiagen Lipid Tissue Mini Kit. Spheroids in Qiazol were frozen at -80°C for 24 hours before being defrosted. Once defrosted, Qiagen Lipid Tissue Mini Kit was used to extract RNA as per the manufacturer's instructions. RNA was quantified using Nanodrop spectrophotometer (ThermoFisher) assessment before being stored at -80°C .

2.10.2 cDNA synthesis

500 ng of total RNA was reverse transcribed to cDNA using High-Capacity RNA-to-cDNA Kit (Cat. No. 4387406, Applied Biosystems) following the manufactures instructions. Samples were placed in a thermal cycler and incubated at 37°C for one hour, heated to 95°C for 5 minutes, held at 4°C . 55 μ L of RNase free water was added to each sample before being stored at -20°C .

2.10.3 qPCR

TaqMan qPCR (ThermoFisher) was performed using TaqMan Gene Expression Master Mix (Cat. No. 4369016, ThermoFisher) in triplicate for each sample. 7.5 μ L Master Mix, 0.75 μ L Taqman gene expression assay consisting of a pair of primers and a TaqMan probe (Table 3.4), 3.75 μ L of RNase free water and 3 μ L of cDNA was used per sample. Plates were run on the QuantStudio 5 System (Applied Biosystems) with a two-minute incubation at 50°C then 95°C for 20 seconds. Following this, 40 cycles at 95°C for 1 second then 60°C for 20 seconds were performed. Relative gene expression was quantified using the ddCt method using Beta Actin as the internal housekeeping gene.

Table 2.4. TaqMan probes. TaqMan human gene expression assays used in qPCR. All probes were specific to the human gene of interest.

Gene	TaqMan genbe expression assay reference
<i>ACTB</i>	Hs01060665_g1
<i>SLC6A6</i>	Hs00161778_m1

2.11 Western blotting

2.11.1 Protein extraction

Cells for western blotting were lysed using Radioimmunoprecipitation (RIPA) buffer (50 mM Tris-HCl pH 7.4, 1% NP40 (Igepal), 0.25% Na-deoxycholate 150 mM NaCl, 1 mM EDTA), supplemented with protease inhibitor cocktail (cat. no. 539134, Merck) and centrifuged for 20 minutes at 4°C. The supernatant was collected and quantified in triplicate using the Pierce BCA assay (ThermoFisher Scientific), as per the manufacturer's instructions.

2.11.2 Western blotting

Equal amounts of protein (minimum of 5 µg) were combined with 7.5 µL of 4x Laemmli buffer (Bio-Rad), made up to a final volume of 30 µL with Tris/Glycine/SDS running buffer (Bio-Rad), then heated at 100°C for 5 minutes before being placed on ice. Samples were run on 4–15% Mini-PROTEAN® TGX™ Precast Protein Gels (Bio-Rad) and transferred using NuPage transfer buffer onto Polyvinylidene Fluoride (PVDF) membranes (both ThermoFisher Scientific). Membranes were blocked in TBST (TBS with 0.1% Tween-20) with 5% added milk powder (Oxoid) for an hour at room temperature. Membranes were incubated overnight at 4°C with primary *SLC6A6* antibody (Abcam, ab196821 or 26898) at a dilution of 1:1000 in blocking solution or GAPDH (Cell Signalling Technology, 2118S) for one hour at a dilution of 1:10000 in blocking solution. Membranes were washed three times in TBST before incubation with secondary antibody at a dilution of 1:2000 in blocking solution (Cell Signalling Technology, Anti-Rabbit IgG, HRP-linked Antibody, 7074S) for an hour at room temperature. Membranes were washed four times in TBST and developed using SuperSignal™ West Femto Maximum Sensitivity Substrate (ThermoFisher Scientific) and imaged using the ChemiDoc MP Imaging System. Bands were analysed in ImageJ, signals were normalised to GAPDH.

2.12 *SLC6A6* knockdown using siRNA

A172, GBM63 and GBM58 cells were plated at a density of 25 x 10⁴ cells per well in a total of 2 mL per well, in a 6-well plate. Cells were plated in normal media supplemented with 10 mM taurine. Cells were left to attach for 5 hours in an incubator before transfection with *SLC6A6* siRNA (cat. no. 4392420,

ThermoFisher Scientific) or a negative control (cat. no. 4390846, ThermoFisher Scientific). For each well to be transfected, a transfection solution containing 1.2 mL of opti-MEM (cat. no. 51985026, Gibco), 7 μ L of Lipofectamine RNAiMAX transfection Reagent (cat. no. 13778030, ThermoFisher Scientific) and siRNA to a final concentration of 50 nM) was combined and incubated for 20 minutes at room temperature. Following this, media was removed from the cells and replaced with the incubated transfection solution. 24 hours later, cells were trypsinised and resuspended at 9000 cells per 100 μ L in their normal cell culture medium, supplemented with 10 mM taurine and plated into 6 wells of a 96-well plate per condition. The remaining cells were collected, and spun at 300g for 5 minutes before being lysed in 600 μ L of buffer RLT. RNeasy mini kits (Cat. No. 74134 Qiagen) were used to extract RNA as per the manufacturer's instructions. Cells in 96-well plates were left for two hours to attach. Following this, cells were treated with 30 μ M of TMZ and irradiated with 2Gy radiation one hour later. 48 hours later, cells were subjected to MTT assay as described above (2.3).

2.13 SLC6A6 knockdown using GIPZ Lentiviral shRNA

Glycerol stocks of 4 GIPZ lentiviral Human *SLC6A6* shRNA constructs were used (V2LHS_153000, V3LHS_348816, V2LHS_121007, V3LHS_406826, all Horizon Discovery). Agar plates were made using 12 grams of agar dissolved in distilled water and autoclaved at 121°C (cat. no. 22700025). Glycerol stocks of shRNA constructs and lentiviral components (psPAX2 vector pMD2.G vector) and were streaked onto the agar and placed in an incubator at 37°C overnight. A single colony was picked from the agar using an inoculation loop and placed into 6 mL LB broth (cat. no. 12780052). this was placed in a shaking incubator at 37°C overnight. Plasmid DNA was harvested using a Qiagen Plasmid Mini Kit (cat. no. 12323) (as per the Manufacturers' instructions).

HEK293 cells were cultured in DMEM high glucose with 10% FCS, and maintained at 37°C at 5% CO₂. One day before transfection, 10 cm dishes were coated with 10 μ g/mL fibronectin (cat. no. 33016015, ThermoFisher Scientific) and 4x10⁶ HEK293 cells seeded into each. A transfection mixture consisting of 10 μ g of one of four construct plasmids, 7 μ g of psPAX2 vector, 3 μ g pMD2.G vector, 500 μ L of Opti-MEM and 40 μ L of Lipofectamine 2000 (cat. no. 11668030, ThermoFisher Scientific) was added dropwise to the HEK293 cells. After 24

hours, the media was completely removed and replaced with fresh medium. After 24 hours, media from each well was collected and filtered through a 0.45 μM Millex HV filter and the media replaced with fresh media, which was collected 24 hours later. 2 mL of lentivirus was added to 1×10^5 of A172, GBM58 or GBM63 cells seeded in 6-well plates. Once confluent, cells were transferred to a T25 and then a T75 flask in normal culture medium supplemented with 2.5 $\mu\text{g}/\mu\text{L}$ puromycin. Cells were then lysed using RIPA buffer to extract protein or with RLT buffer to extract RNA for subsequent western blot and qPCR analysis.

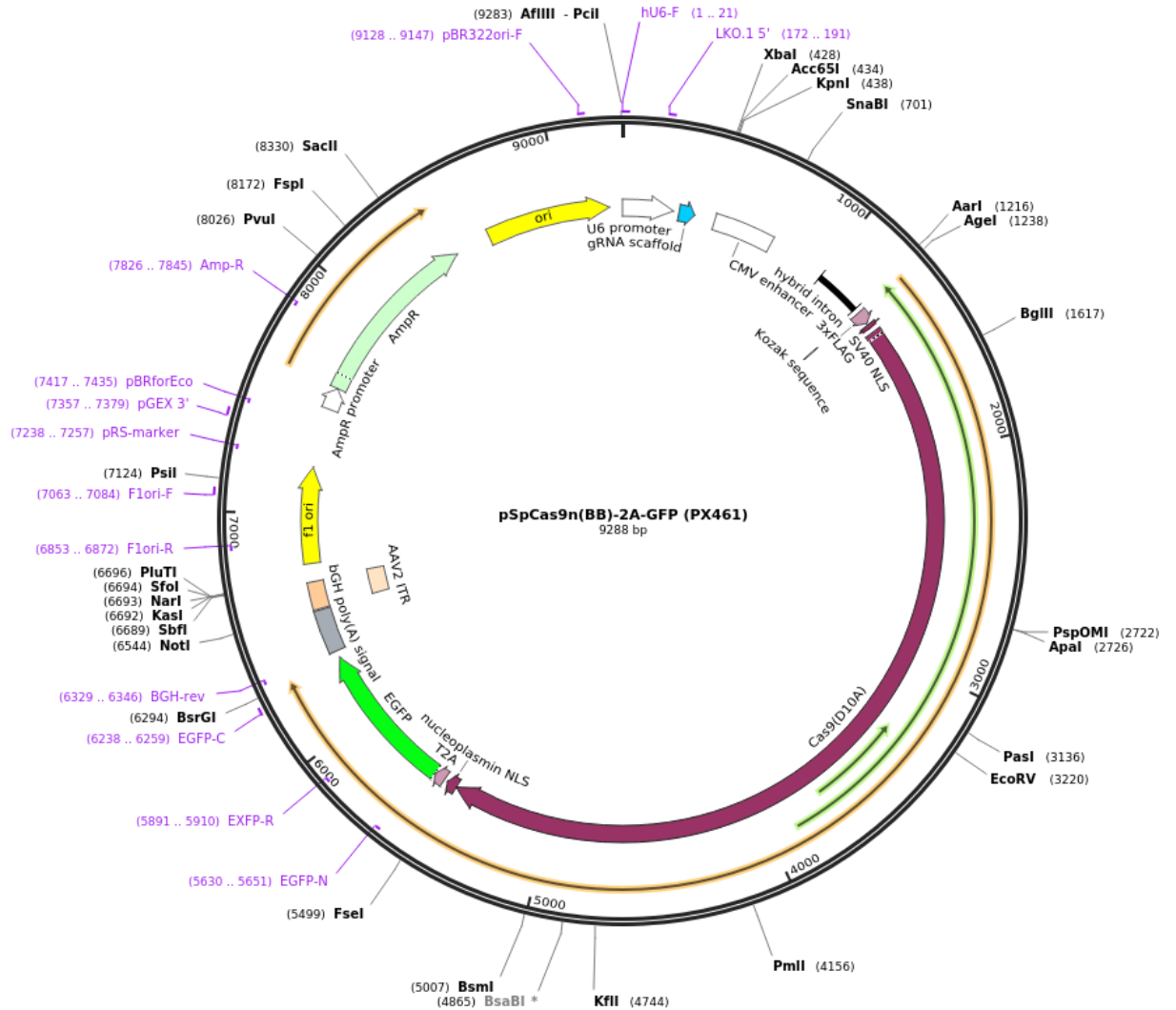
2.14 *SLC6A6* knockout using CRISPR

2.14.1 Cloning

Oligos to generate single guide RNAs (sgRNAs) were designed using Benchling (<https://www.benchling.com>) based on the exon 5 sequence, shared between all known splice variants of *SLC6A6* (NCBI). Oligos were resuspended to 100 μM in dH_2O and 1 μL of each oligo added to 8 μL dH_2O . To anneal, oligos were heated to 95°C for 5 minutes, and then cooled at a rate of 0.1°C/sec to 50°C, held for 10 minutes, then further reduced to 4°C at a rate of 1°C/sec. In parallel, Crispr/Cas9 vectors (px461 (Green Fluorescent Protein - GFP) or px462 (Puro) (Figure 2.1) were digested at 37°C in a mastermix consisting of 2 μL of 10x CutSmart buffer (cat. no. B7204, New England BioLabs), 16 μL of dH_2O , 250 ng plasmid and 1 μL of BbsI enzyme (cat. no. R0539S, New England BioLabs). After 1 hour, 1 μL of annealed oligos, 1.5 μL of T4 DNA ligase (cat. no. EL0014, ThermoFisher Scientific) and 2.5 μL of T4 ligation buffer (cat. no. B69, ThermoFisher Scientific) was added to the digested vectors and incubated for an hour at room temperature.

For transformation, 2 μL of ligation product was added to 25 μL of competent DH5 α cells (cat. no. 12297016, ThermoFisher Scientific) and placed on ice for 20 minutes, heat shocked at 42°C for 30 seconds, and incubated on ice for 2 minutes. 475 μL SOC medium (cat. no. S1797, Sigma) was added and cells placed in a shaking incubator at 37°C for one hour. Cells were spread onto prewarmed agar plates containing LB and ampicillin and grown overnight at 37°C. The following day, individual colonies were isolated and grown overnight in a shaking incubator at 37°C in 5 mL of LB and ampicillin. Plasmid DNA was

extracted and purified using a QIAprep Spin Miniprep kit (cat. no. 27104, Qiagen) following the manufacturer's instructions and quantified using Nanodrop spectrophotometer (ThermoFisher).



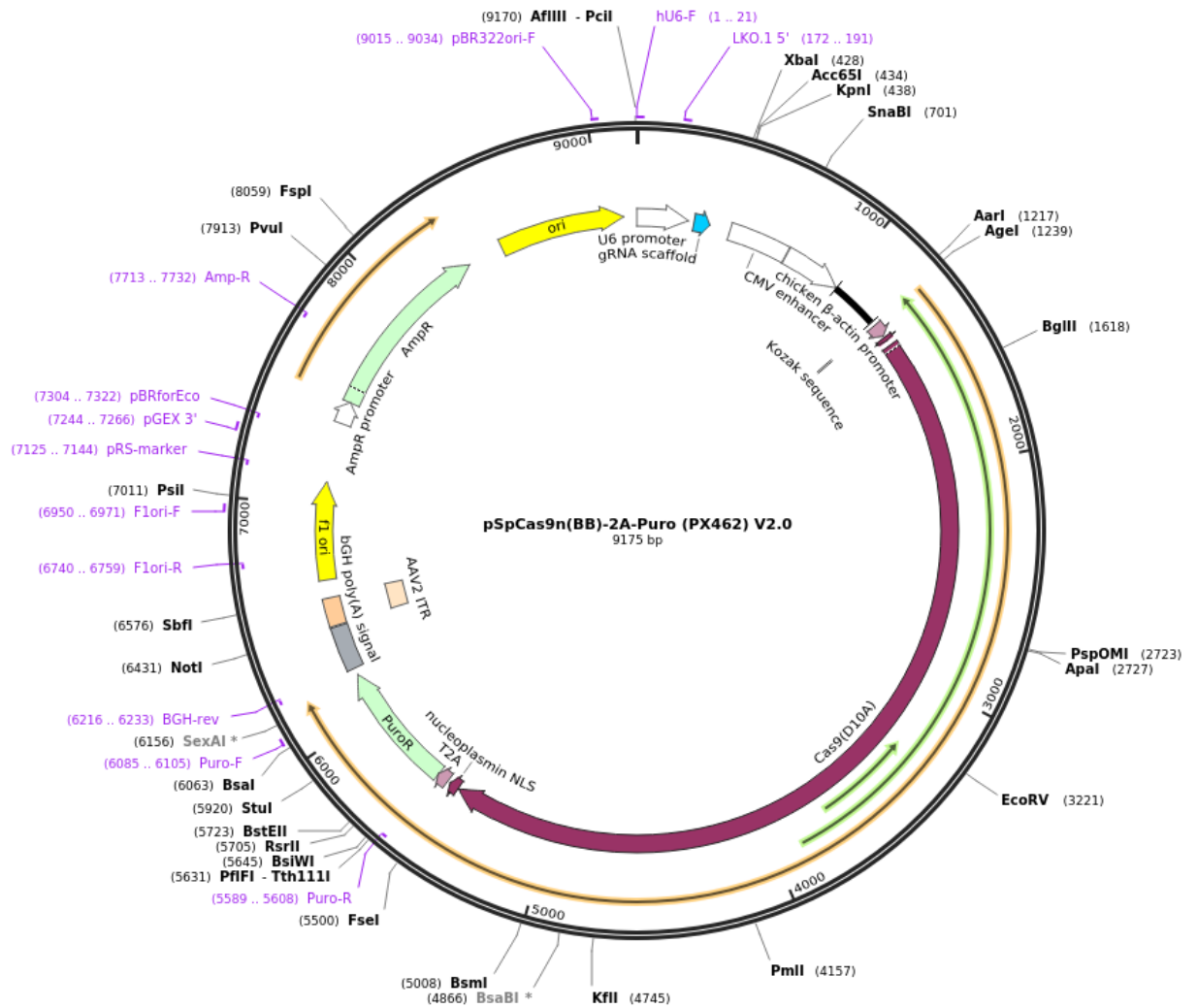


Figure 2.1 Plasmid maps. Plasmid maps for both plasmid vectors used in CRISPR/Cas9 knockout of *SLC6A6*. Maps for plasmid PX461 and PX462 are shown.

2.14.2 Sanger Sequencing to confirm insertion of oligo into plasmid

A sequencing mastermix was made up of 14 μ L of BigDye v3.1 (cat. no. 4337454, ThermoFisher), 22 μ L BigDye sequencing buffer (cat. no. 4336701, ThermoFisher), 14 μ L of 1.6 μ M U6-F primer (sequence - ATAATTTCTTGGGTAGTTTGCAG) and 77 μ L nuclease free H₂O. 9 μ L of mastermix and 1 μ L DNA was added per well and run on a thermocycler (Biorad) using the conditions in Table 2. DNA was subsequently precipitated using 60 μ L of 100% ethanol and 5 μ L 125 mM EDTA and centrifuged for 30 minutes at 22°C and 4000 rpm. Excess liquid was removed and allowed to dry before pellets were

resuspended in 10 μ L of HiDi formamide (cat. no. 17899, ThermoFisher). Sequencing was performed on a Genetic Analyzer 3130xl (Applied Biosystems).

Table 2.5. Sequencing reaction thermocycler conditions.

Temperature ($^{\circ}$ C)	Ramp	Time	
96	1 $^{\circ}$ C/sec	1 minute	x25
96	1 $^{\circ}$ C/sec	10 seconds	
50	1 $^{\circ}$ C/sec	5 seconds	
60	1 $^{\circ}$ C/sec	4 minutes	
4	1 $^{\circ}$ C/sec	∞	

2.14.3 Transfection of CRISPR plasmids

Each cell line was seeded at 70% confluency into 2 wells of a 6-well plate and one well per cell line was transfected with 1 μ g of each plasmid and 6 μ L Lipofectamine 2000 (cat. no. 11668030, ThermoFisher Scientific) or Lipofectamine Stem (cat. no. 15783605, ThermoFisher Scientific). After 24 hours, the media was supplemented with puromycin, to a final concentration of 2.5 μ g/ μ L, and cells incubated overnight. Media was replaced (without puromycin) and one GFP-positive cell was sorted per well into 96-well plates, and incubated for 2-3 weeks. Any propagating colonies were grown to confluency and transferred into 6-well plates. Genomic DNA was extracted from positive colonies using a DNeasy Blood and Tissue Kit (cat. no. 69504, Qiagen) as per the manufacturer's instructions before Sanger sequencing described as above.

2.15 Immunofluorescence

2.15.1 Sample preparation – OCT embedded spheroids

10 spheroids per condition were collected in falcon tube and centrifuged at 800 rpm for 5 minutes. The pellet was reconstituted with 1 mL PBS and centrifuged for 30 minutes at 4 $^{\circ}$ C. PBS was removed and spheroids fixed with Paraformaldehyde (PFA) (4% (w/v)) for 30 minutes at 4 $^{\circ}$ C. Spheroids were washed three times with PBS before being resuspended in sucrose solution (30%

(w/v)) and left at 4 °C overnight. Spheroids were removed from the falcon with a 1000 µL pipette tip and placed into cryo-moulds containing Optimum Cutting Temperature (OCT) solution (cat. no. 36160E, VWR). Spheroids were sectioned on a cryostat at 20 µm thickness. Slides containing spheroids sections were placed at -20°C until staining.

2.15.2 Immunofluorescent Staining

Before staining, slides were left at room temperature for 20 minutes then washed in PBS twice. Each individual spheroid was drawn around using an ImmEdge hydrophobic pen (cat. no. H-4000, 2B Scientific) before a single drop of Bloxall (cat. no. SP-6000, 2B Scientific) was added using a 200 µL pipette and left for 20 minutes. Slides were placed in TBST for 5 minutes before casein (cat. no. SP-5020, 2B Scientific) was diluted 1:20 in antibody dilutant (cat. no. 003218, ThermoFisher Scientific) and placed on the slides for 20 minutes. Ki-67 primary antibody (cat. no. 151210, Biolegend) was diluted 1:150 and left at 4°C overnight. Slides were washed in TBST, three times before secondary antibody added for two hours at room temperature in the dark. Slides were washed in TBST three times then incubated with Hoescht (diluted 1:10,000 in PBS) for 10 minutes. Slides were washed once in TBST before a drop of Prolong Gold Antifade (P36930) added and coverslips mounted. Fluorescence signal was detected using an EVOS digital inverted fluorescence microscope (Life Technologies) and quantified using ImageJ.

2.16 RNA sequencing

RNA for sequencing was extracted using the method in section 1.10.1.2. Strand directional whole transcriptome paired end RNA-sequencing libraries were created and sequenced by Novogene. FASTQ data were trimmed of low-quality bases, phred threshold=20, and adapters via Trim Galore v0.4.3, wrapping Cutadapt v1.8.3 (182). Trimmed reads were quality checked using FASTQC and then aligned to human reference genome GRCh38.13 using STAR v020201. Gene and transcript count and gene expression was quantified via CuffQuantv2.2.1 taking directional specifics of the library as input, using probabilistic weighting of multireads and quantifying against the GENCODEv27 human genome annotation with haplotypes and scaffolds included. Differential gene expression analysis was performed using Deseq2 using a paired design

(183). An adjusted p-value of < 0.05 was used as the significance threshold. Gene Ontology analysis was performed using ShinyGo v0.75 (184). Over-representation analysis (ORA) using WebGestalt (WEB-based Gene Set AnaLysis Toolkit) using the molecular signature database gene set named “the hallmark of cancer” (185, 186).

2.17 Statistical analysis

Shapiro-Wilk and Kolmogorov-Smirnov tests were used to check for normal distribution using Prism version 8.0.2. Unpaired Student t-tests were used to analyse significance levels with a confidence limit of 95% on a minimum of three biological replicates for each experimental assay unless stated otherwise. On figures, * means p-value < 0.05 , ** <0.005 , *** <0.0005 , and **** <0.0001 . Error bars denote the standard error of the mean (SEM) or standard deviation (SD) as stated.

Chapter 3

Optimisation of models

3.1 Introduction

The first requirement for my PhD research project was to establish the details of the preclinical models I would use and determine the appropriate treatment regime and other relevant experimental parameters. This chapter describes the work completed to determine the experimental setup that would be used routinely throughout in order to provide consistency between results, including selection of cell lines most suited to the project, treatment schedules, treatment doses, taurine supplementation and end point assays.

3.1.1 Use of cell line models in GBM

It is important that different aspects of GBM biology are accounted for when choosing appropriate models for use in this project. Different types of cell lines are available for use which include commonly used established cell lines and less commonly used patient-derived cell lines, the differences of which are described in more detail in section 1.7.1. Established cell lines typically come from a clonal origin meaning they are homogeneous in nature and have phenotypically similar cells (187). This means they undergo similar cell cycle durations so have distinct doubling times when cultured in 2D (188). They also require standard cell culture plastics and are usually grown in media supplemented with foetal calf serum (FCS). Due to their ease of use and commercial availability, they are used commonly throughout cancer research. There are a multitude of established GBM cell lines that can be bought commercially with several commonly used models, including A172, M059K and U87. U87 have however been shown to be insufficient for use in GBM research due to the lack of similarity to human GBM (189).

Similar to a GBM tumour, patient-derived cell lines are heterogeneous in nature and contain many glioma stem cells (GSCs) that are often regarded as the cells responsible for disease recurrence (190). They commonly have spontaneous and unpredictable growth patterns in culture and are grown without FCS. The lack of FCS maintains the stem-like properties of the cells which often need special growth requirements including flasks coated in ornithine and laminin to allow their attachment and growth in 2D. The expression profiles of patient derived cell lines

are more similar to that of patient tumours than established cell lines so they are arguably a more relevant model to study GBM (190). Leeds Institute of Medical Research has molecularly characterised 13 GBM cell lines derived from patient materials using serum-free media for experimental analysis. These were available for use in this project.

There are fundamental differences in established and patient-derived cell lines and each are thought to represent a different part of tumour biology. GBM cells cultured in serum are thought to be enriched for the differentiated components of the tumour. By contrast, patient-derived cell lines, typically cultured with no serum, are enriched for the stem cell component of GBM biology (162, 191). It was therefore important that I used both types of GBM cell lines to represent important but unique parts of GBM biology.

3.1.2 3D cell culture and assays

As referenced in section 1.7.2, the use of three-dimensional (3D) models such as spheroids has become an intermediate step between two-dimensional (2D) cell culture and *in vivo* models. This is especially true in cancer research, with 3D models providing a more physiologically relevant environment for cancer cells in comparison to being grown as 2D monolayers. This results in a more clinically relevant recapitulation of the biology or therapeutic response observed *in vivo* (168). The genomic profile of glioblastoma is more highly preserved in spheroids in comparison to cells grown in 2D (192). One important aspect of 3D cellular interactions that is relevant to this project is the expression of the membrane protein TauT, encoded by the *SLC6A6* gene. Simulations performed by Xie *et al.*, showed that the membrane proteins CD2 and CD58 had 100-fold lower protein dissociation in 2D than when in 3D (193). However there are no records of experiments looking at taurine transport via TauT in 2D vs 3D.

Additionally, cells in 3D are exposed to different levels of nutrients from the culture medium than cells in 2D (194). TauT transports the amino acid taurine from the extracellular environment so we might expect that this will differ between cells in 2D and those grown as a spheroid. Furthermore, GBM spheroids often have a hypoxic core when they reach 300 μm and have an outer layer of proliferating cells (168). Hypoxia is a common and important feature of GBM, especially in relation to *SLC6A6* as variants in this gene has been associated with a GBM hypoxia-dependent subtype (71). Thus, it is important that the spheroids

used in this project reach this diameter so that they possess this physiologically-relevant feature.

3.1.2.1 Methods of spheroids culture

There are multiple methods available for growing spheroids. U-bottomed-low-adherence plates provide an easy way of culturing spheroids. Cells resuspended in media are aliquoted into each well and the low adherence properties of the plate allow cells to aggregate together to form spheroids with typically just one spheroid forming per well. With this method it is easy to adjust spheroid size as cell numbers can be adjusted to create smaller or larger spheroids. Additionally, media can be easily replaced every few days with minimal disturbance to the spheroid (195). The hanging drop method allows cells to form spheroids by aggregating together in droplets that can be controlled via the amount of cell suspension and which in turn controls spheroid size. The cell suspension is pipetted into wells of a plate which are then turned upside down after the lid is put on (196). The advantages of hanging drop methods are that they are inexpensive and it is easy to make a lot of spheroids in a single experiment. It is also easy to change the size of the spheroid depending on the number of cells in the starting cell suspension. Despite this, however, spheroids in one set up often vary in size from one another and this technique is technically challenging (197). Using spinner flasks is another commonly used method of generating spheroids. In this methodology, a cell suspension is placed into a spinner flask which continually stirs the cells to aggregate them together to form spheroids. The rate of spinning is key and can result in spheroids that are either damaged (if spun too fast) or that sink to the bottom (if spun too slow). Spheroids generated in the same spinner flask can also vary dramatically in size that can serve as both an advantage and disadvantage depending on the experiment (196). However, once purchased, spinner flasks are cheap to run and require minimal maintenance.

Despite the numerous advantages and many ways to culture spheroids, they are not widely used in biomedical research because they are unsuitable for high-throughput assays and the lack of reliable analysis methods (198). Many spheroid assays are endpoint only, meaning that changes occurring between initial set up and the assay end point are not recorded. Evaluation of spheroid measurement changes over time, including parameters such as area, diameter, and circularity, could be a valuable tool for many biological studies. In many cases, obtaining

these results involves manual imaging of each spheroid with subsequent manual application of imaging tools to obtain quantification metrics that are individually collated and then laboriously analysed. This is time-intensive, resulting in fewer technical repeats per condition being studied, and introduces subjectivity and, thus, human error.

At the start of this PhD, the method routinely used to quantify spheroid size was via manual imaging of each well of a 96-well plate using the EVOS Cell Imaging System; a fluorescent and transmitted light microscope capable of producing high resolution images. ImageJ software, a Java-based image processing programme, was then used to manually draw around each spheroid and automatically quantify perimeter, diameter and area (199). To image and analyse a full 96-well plate using this method took approximately two hours.

With all the methods to consider, it was important to determine and adapt the approach used for generating 3D models to find a way that could be adapted to for high throughput methods both in terms of culturing and subsequently imaging the spheroids.

3.1.3 Taurine, temozolomide and irradiation doses to be used

Using physiologically relevant model parameters is important for this project to study the conditions in which *SLC6A6* is upregulated in recurrent tumours. This will allow me to investigate its importance in treatment resistance observed in patient samples.

In my experimental setup it was important that I mimicked physiological taurine levels found within the normal brain. Although taurine can be biosynthesised within a cell from cysteine, the main source of taurine is through transport via TauT. This is particularly important for glioma cells that rely heavily on taurine transport into the cell due to biosynthesis defects and demand for cysteine in other cellular processes. Therefore it is important that any cell media is supplemented with taurine so that cells can transport this into the cell. Numerous previous studies looking at various brain cell types used 10 mM taurine, based on the levels of taurine found within the brain, which provided a starting point for taurine supplementation experiments (123, 200-202).

Using a physiological treatment regime to treat the cells is also an important consideration. Primary GBM patients are treated with temozolomide (TMZ) and

irradiation. Irradiation is given in 2 Gy fractions to a total of 60 Gy and studies have shown that the level of TMZ that reaches GBM tumour cells is around 30 μM (17). When deciding upon doses of radiation and TMZ to use, it is important to consider that the aim is not to eradicate all GBM cells, as it would be when treating a patient. Instead I needed to find a dose which causes a significant cytotoxic effect, but with which we can still observe any changes in treatment response following modification of cells, for example with a gene knockdown.

3.1.4 Dose response curves

Dose response curves are a way in which the response of an organism, in this case cells, to a compound, can be measured after a certain amount of time. It is important that dose responses are determined and optimised to work out the most appropriate concentration a compound should be used at to answer the research question. For this project, it was important that a response to a treatment is observed, but not to a level where any further changes would cause no further response. For example, I wanted to observe a significant reduction in survival or spheroid size without killing every cell in the spheroid, so that further manipulations of the cell can be performed and changes still observed.

For a GBM patient, the size of the tumour is a very important factor. GBM patients with smaller tumours have significantly longer survival times than patients with larger tumours (203). If the size of the tumour could be reduced, this would impact both the quality of life of the patient as well as their life expectancy. Therefore one method to measure the response of spheroid models to treatment is to measure the size of the spheroids. This is not a direct measure of cell survival as other things could be causing the spheroid to be smaller other than cell death, for example cell shrinkage or a change in the density. However, this metric would directly affect a patient's survival, so I used spheroid size as a valid representation when optimising experimental conditions to be used in subsequent experiments.

3.2 Aim and Objectives

The aim of the work described in this chapter was to optimise the experimental set up and parameters for the experiments to be used in this study. This would ensure that all experiments could be run in a consistent and standardised way. To achieve this, the following objectives were set:

Objective 1 - Determine suitable cell lines for use in the project.

Objective 2 - Develop an automated imaging and analysis platform for spheroid measurements.

Objective 3 - Select an appropriate taurine concentration for use in experiments.

Objective 4 - Optimise treatment doses and timings of temozolomide and irradiation in 2D culture.

Objective 5 - Optimise treatment doses and timings of temozolomide and irradiation in 3D culture (spheroids).

Objective 6 - Determine appropriate end point assays to be used

3.3 Results

3.3.1 Determining suitable cell lines for use

It was important to include both established and patient-derived cell lines in this project, with all suitable cell lines having promoter methylation, and therefore consistent responses to TMZ (see section 1.4.1). TMZ is part of the standard treatment for GBM patients, regardless of *MGMT* promoter methylation status, and therefore I wanted to mimic this as closely as possible in my assays. *MGMT* promoter methylation data for all available GBM patient derived cell lines was determined by DNA extraction (by Ruth Morton) and DNA methylation profiling using the Illumina Human Methylation EPIC array (DFKZ, Heidleberg, Germany). This enabled GBM63 and GBM58 to be identified as both *MGMT* promoter methylated. *SLC6A6* RNA expression was confirmed in both these cell lines by qPCR (Figure 3.1) making them suitable for use in this project. For established GBM cell lines, M059K has an unmethylated *MGMT* promoter sequence deeming it unsuitable for use in this project, whereas A172 was confirmed to have a methylated promoter sequence for *MGMT* and expressed *SLC6A6* RNA (Figure 3.1) (204) (205).

A172 is a fast growing cell line, making it an ideal candidate for developing the automated imaging and analysis system and for treatment optimisation of TMZ and irradiation. All optimised variables were subsequently verified for applicability in the patient derived cell lines (GBM58 and GBM63).

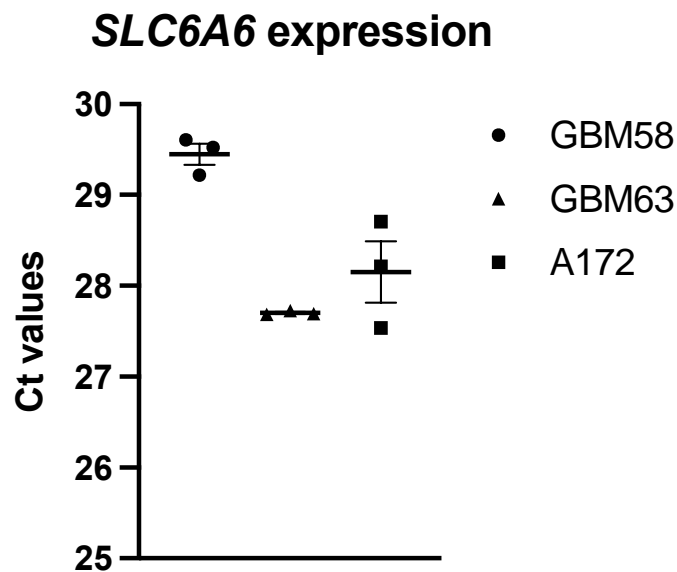


Figure 3.1. Expression levels of *SLC6A6*. Expression levels represented by Ct Values determined by qPCR of *SLC6A6* in GBM58, GBM63 and A172. Ct values are used as the measurement as the aim was to simply show if *SLC6A6* was expressed in the cell line or not, and not to show the relative changes in gene expression. Individual values from each biological repeat plotted along with the mean \pm SEM, n=3.

3.3.2 Developing an automated imaging and analysis platform for spheroid measurements.

I chose low-adherence 96-well plates to culture GBM spheroids as they allowed multiple plates to be cultured simultaneously. Additionally, a single spheroid can be grown per well, meaning that spheroids are all a consistent size after seeding with the same cell number and therefore each individual spheroid can be tracked and monitored over time using imaging techniques. Historically, the drawback to culture and analysis of spheroids using this method is the time taken to image the spheroids. Traditionally, this was done manually which was time inefficient. Therefore, I developed a more efficient method of imaging and analysis. In collaboration with specialists from Nikon, we developed an automated plate-imaging and analysis programme using the Confocal Laser Scanning Microscope-Nikon A1R. This involved the creation of a bespoke JOB (computationally scripted series of commands) that uses a threshold-based method to automate the imaging and analysis of spheroids. This was a significant

breakthrough in spheroid assay analysis for use in this project. The method is described in more detail below (3.3.2.1).

The automated JOB reduced imaging and analysis to under two minutes per plate, making measuring spheroid growth every two to three days over a period of weeks achievable. This automated approach was used to measure spheroid diameter, area, perimeter and circularity based on a 2D image of each spheroid taken from above the spheroid at its widest point. Using the confocal microscope and the software currently available, it is not yet possible to obtain Z-stacks of an entire spheroid in order to determine the volume. Therefore, it was decided that maximal cross-sectional area (μm^2) would be the measurement used to represent spheroid size in the majority of experiments.

3.3.2.1 Bespoke method developed for using the confocal imaging technique

Import the JOB file (Spheroid_Imaging_Single_Plane_with_Area.bin) into the software by clicking import and then open the JOB by going to file, JOBS and double clicking. The confocal should be set up as standard using the 10x lens and focusing on a spheroid within a well. The fluorescence bulb does not need to be switched on as the programme uses brightfield light only. In the tab 'Use plate with 96 wells', select the plate type used. The 'Align plate.wellplate' tab is used to align the plate in relation to where the spheroids sit within a well. If the spheroids are in relatively the same place in each well, only one well will need to be aligned. Focus on a spheroid in a well, use the align plate tab to click on the well in focus, and move the yellow grid to show the position of the spheroid in the well as seen in Figure 3.2. If necessary, multiple wells can be aligned per plate. This will need to be redone for each plate imaged. On the 'WellSelection' tab, select the wells containing spheroids that are to be imaged. If necessary, the wells can be labelled in the 'WellLabelling' tab. The JOB works more effectively if the confocal Perfect Focus is available to use. This is specified to turn on and be in use on the 'PFSON' tab – this tab should not need to be altered. In order to set the threshold for determining a spheroid, a still image of a spheroid in a well needs to be taken. Following this, double click on the 'Spheroid_Area on Capture_Image' tab to open a box, and adjust the arrows in the threshold, size and circularity tabs as required as seen in Figure 3.3. Click OK when complete. The play button at the bottom right-hand side of the JOB can now be pressed.

This will open a dialogue box in which every tab will have to be viewed order to press the next play button and continue on to the next step. Press play. A further dialogue box will open to act as a reminder to set the focus on a spheroid. Once complete press 'OK' and the imaging will begin.

Upon completion of imaging, a plate map showing an image of each spheroid in the well will appear. Using this view it is easy to compare spheroids to look for anything that will cause obvious outliers (e.g. empty wells as the result of losing spheroids when media changing). In Figure 3.4, the outer wells of the plate contain no spheroids.

Figure 3.5 shows an example of a heat map produced based on area (μm^2) from imaging a plate of spheroids. These are also produced for other measurements including perimeter, diameter, circularity. The highlighted square appears to have a spheroid bigger than the rest – a quick click in this shows the corresponding spheroid with a black line coming from it which has skewed the area of this spheroid and can be removed from the analysis. The buttons circled show how to view the plate as a heat map showing the area of each spheroid. These can be copied to be pasted into another document using the copy button. The Grid button shows all the data from the imaging in a grid format which can be exported to an excel document to be used in the SpheroidAnalyseR pipeline (Section 3.3.3).

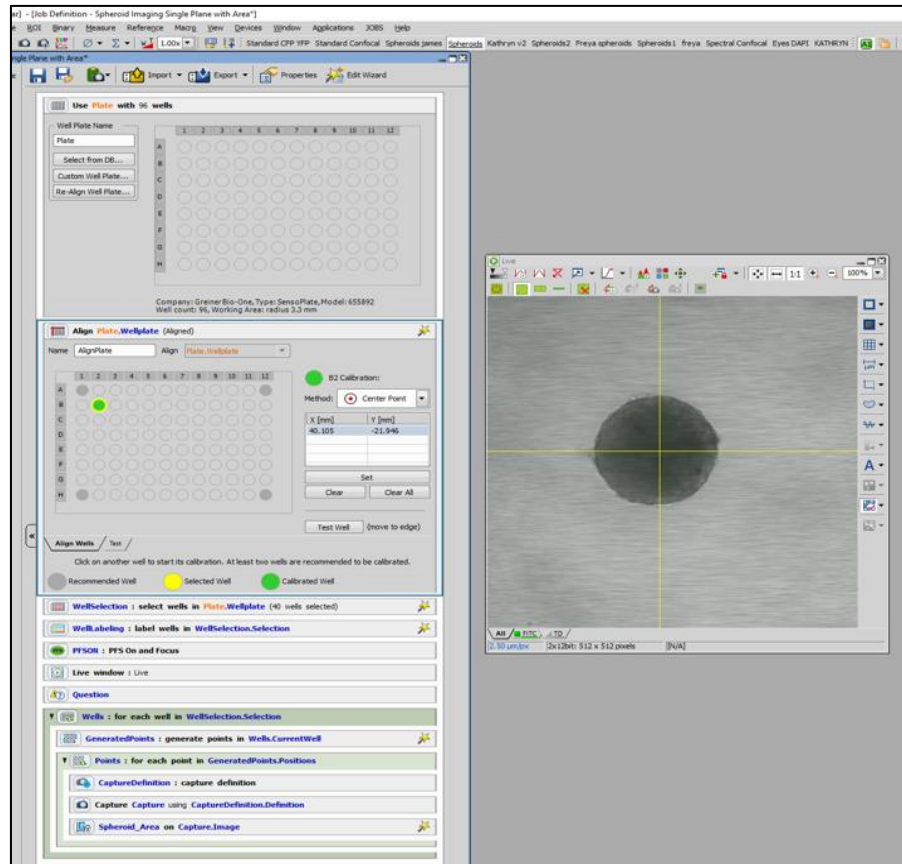


Figure 3.2. The confocal JOB stages and plate spheroid alignment in a well. The multiple stages of the JOB are shown on the left hand side. On the right hand side, a spheroid is being aligned in a well. A spheroid should be located and the corresponding well selected. The yellow grid should be aligned to the centre of the spheroids and the 'set' button on the left hand side pressed to align the spheroid to this well.

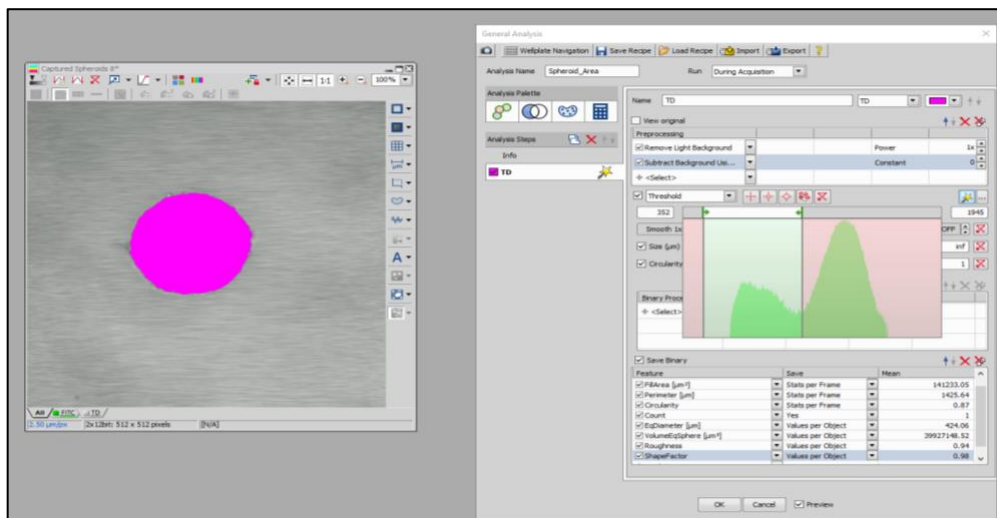


Figure 3.5. Heat map of spheroid measurements. A heat map showing the area of each spheroid imaged in the location for the well it corresponds to. In the blue oval are the buttons to click between this view and the view in figure 3.4. Circled in red is the option to export the data to an excel spreadsheet. The colours represent the size of the spheroid in a heat map method with red being the largest area and purple being no measurement recorded.

3.3.3 Creation of SpheroidAnalyseR

This high-throughput method using the confocal microscope generated a lot of data that was becoming increasingly harder to manually analyse. Therefore, in collaboration with a visiting computer science researcher (Joseph Wilkinson) and bioinformaticians from the University of Sheffield, I developed an R Shiny App named SpheroidAnalyseR to analyse the data. I was responsible for driving and directing the creation of the app; I led the project and directed the computational scientists with regards to what was needed for the app to be fit for purpose for use by a non-computational expert. I did the testing of the app to ensure it worked and helped with the design and format. I wrote this method as a paper which is available at (<https://www.biorxiv.org/content/10.1101/2022.02.18.481039v1>) to enable the app to be adopted by the wider research community (181).

The R programming language is a highly regarded open-source platform for data manipulation, visualisation and statistical analysis. Despite numerous training initiatives, there is still a steep learning curve for those without prior programming experience to adopt the language in their daily work. SpheroidAnalyseR takes advantage of the user-friendly 'Shiny' which allows R developers to make their code and analyses accessible to the wider community through a web interface.

SpheroidAnalyseR starting point is inputting size measurements from spheroids grown in 96-well plates. This data can be acquired in multiple ways including manual imaging and measuring for example using an EVOS fluorescent and transmitted light microscope capable of producing high resolution images. ImageJ, a Java-based image processing programme, can be used to manually draw around each spheroid (199). Next, data can then be uploaded into the template spreadsheet provided and analysed by SpheroidAnalyseR. Alternatively, published methods such as SpheroidSizer provide a way to calculate the area and other key spheroid measurements from images (206). In

addition, the Excel file output from the confocal job as seen above can be inputted straight into the app. Users can use SpheroidAnalyseR to preview the data, remove outliers, merge result files and plot graphs. SpheroidAnalyseR identifies and visualises outliers in spheroid data giving the user the option to remove some or all of them. It does this by converting user-defined technical replicate data into a statistical measure known as a robust z-score, which is a method of determining outliers based on how many standard deviations they are away from the median (207). The user can set a threshold score for the robust z-score, with the default set as ± 1.96 , which equates to a 95% confidence interval. The webpage, after data input, includes graphical visualisation of spheroid measurements across multiple predefined parameters i.e. time, cell-type and treatment(s). The workflow for analysing the data is in five main steps as follows:

3.3.3.1 Method developed for the bespoke Shiny App SpheroidAnalyseR

1. Data input

On the *Data Input* tab, three types of files are required to be uploaded to allow processing. These are:

Raw data file - Files can be uploaded either directly from the output file from the bespoke JOB on the confocal (raw data template 1) or, data can be manually inputted into the second template file (raw data template 2). Several parameters can be inputted including treatment date and time, cell line, passage number, drugs used and their concentrations, and irradiation dose. Any columns in which no data is present should have '0' for each row. If the user is analysing multiple plates of data with the same layout, then multiple raw data files can be uploaded simultaneously to allow for faster processing.

Plate layout file - This file defines the layout of treatments on the 96-well plate for each spheroid or organoid. Each plate can contain spheroids or organoids with multiple different treatments. 1-12 represents columns 1-12 of the 96-well plate and A-H represents rows A-H of a 96-well plate. A number corresponding to the treatment index assigned in the treatment file should be in each cell that a spheroid measurement was for. Only one plate layout can be uploaded at any one time. If a raw data file has a different plate layout to the last file analysed, then a new plate layout will need to be uploaded.

Treatment file - This file defines the treatment index numbers corresponding to the plate layout file. An index denotes a specific treatment, or combination thereof, and cell line as detailed in the corresponding row of the treatment template. If desired, users can input the time and date of treatment, the cell lines used, the passage number, the dose of radiation used and multiple drugs and subsequent concentrations. Multiple wells with the same index constitute technical replicates. Multiple different combinations of treatments can be defined as required.

Templates for these files are available to download on the *Data Input* tab of the SpheroidAnalyseR web page. The column names of any input files must match those given in the supplied templates, and the sheet name must match the template's sheet name. Four template sheets are provided:

1. Raw data template 1 - This is the file created after running the bespoke JOB on the Confocal Nikon AR1. It can be uploaded straight to SpheroidAnalyseR.
2. Raw data template 2 – This template allows users to input their own spheroid measurements obtained. Users must have the Well.Name column completed and at least one of measurements from the other columns which are: area, perimeter, circularity, count (number of spheroids per well), diameter and volume. If any measurements are not inputted, then a '0' should be inputted in each cell. Optional: – the user can input the time and date the spheroids were analysed, if not required then '0' should be inputted in each cell.
3. Plate layout template.
4. Treatment template.

2. Previewing files in the *Data Input* tab

Raw data files can be previewed on the *Data Input* tab. A drop-down list enables users to select each raw file if multiple files were uploaded simultaneously. Treatment and layout information based on the templates uploaded can also be reviewed here: the plate layout is shown, and a dropdown list allows the user to colour the plate according to each parameter in the treatment file (i.e. cell line, drug used, or time treated). An image of the plate layout along with its designated treatment index is shown. It is recommended to review your uploaded data to ensure that the plate layout and treatment index are correct before proceeding.

3. Outlier removal

Once data has been inputted and reviewed, the user can move to the *Outlier Removal* tab and determine if any of the data points are spurious and should be removed as an outlier. On the *Outlier Removal* tab, choose the raw file to be analysed from the 'Chose a raw file' drop-down list. A spheroid measurement value (e.g. diameter, area, etc.) for which the outliers should be determined for can be selected from the 'Choose a value to plot the outliers' drop-down list. In the shaded beige/yellow box (Figure 3.7) users can adjust the robust z-score (if required) and choose to apply pre-screen thresholds. These are automatically applied with default settings but can be adjusted if necessary. The pre-screen threshold removes spheroid measurements where the value falls outside the upper or lower limits set by the user. This ensures any wells in which there is an extreme outlier, for example due to an empty well, will be removed prior to outlier analysis. After clicking the 'Remove outliers' button, outliers will be removed and three images will be displayed. The top figure shows the plate layout after wells with spheroids that are determined to be outliers have been removed based on the pre-screen thresholds and robust z-score limits. Below that, Plot 1 and Plot 2 can be viewed with the selected measurement (e.g. diameter, area, etc.). These plots show the columns of the plate and the measurement each spheroid in these columns has (for example diameter). Plot 2 shows spheroids grouped by technical replicates, i.e., with the same treatment index as defined on the previously inputted treatment file. It is advised to apply pre-screen threshold to remove any values that are obvious outliers before running the robust z-score. This could include measurements that have been taken of empty wells or when the imaging technique failed to recognise and measure a spheroid. Using the 'Toggle Cell Status normal/outliers' drop-down list, users can manually override individual results of the outlier process. The user must select a cell or multiple cells and choose the 'apply manual adjustment' button. At this point, if the spheroid in that well was determined to be an outlier, it will now be classed as a normal result, and vice-versa. This is to give the user full control over the data and inclusion in subsequent analysis. The report of the selected file with outliers removed can be downloaded by clicking the Download button. This will automatically be downloaded and be titled <the file name of the raw file>. The file contains multiple tabs each showing a different measurement (area, diameter etc.) with two plots per tab showing the data for each treatment index with and

without outliers. The main dataset tab shows all the data uploaded with new columns added with the outliers removed (OR) (Area_OR etc). This data can be used by the user to create their own graphs and perform statistical analysis in their preferred method. The downloaded files can also be re-uploaded at a later date on the *Merging* tab by selecting 'Use previous reports' checkbox and using the file selection tool to upload the previously processed files.

4. Merging

The *Merging* tab allows multiple files to be merged into one master file to create plots in the *Plotting* tab. If the user is only analysing one file, then the 'Merge' button should be chosen and then progress straight to the next tab. On the main panel on the *Merging* tab, a table of raw files that have been uploaded on the *Data Input* tab will be shown. The third column (column name: Processed) shows whether the file has been processed through the outlier removal step on the *Outlier Removal* tab. The rest of the columns show the configuration (e.g. robust z-score value or Pre-screen thresholds) used in outlier removal so that the user has a record of the parameters should they need to re-analyse a file, or analyse future files in the same way at a later date. Files that have been previously analysed on the *Outlier Removal* tab can also be uploaded directly to the *Merging* tab. To do this, select the 'Use previous reports' checkbox and browse for the correct files. The merged file is only available when selected raw files have been processed. Once all the raw files have been processed on the *Outlier Removal* tab, press the Merge button. This will allow plots to be created using the data from multiple files on the *Plotting* tab. The user can rename (using the 'Merged file name' textbox) and download (using 'Download the merged file' button) the merged file if required.

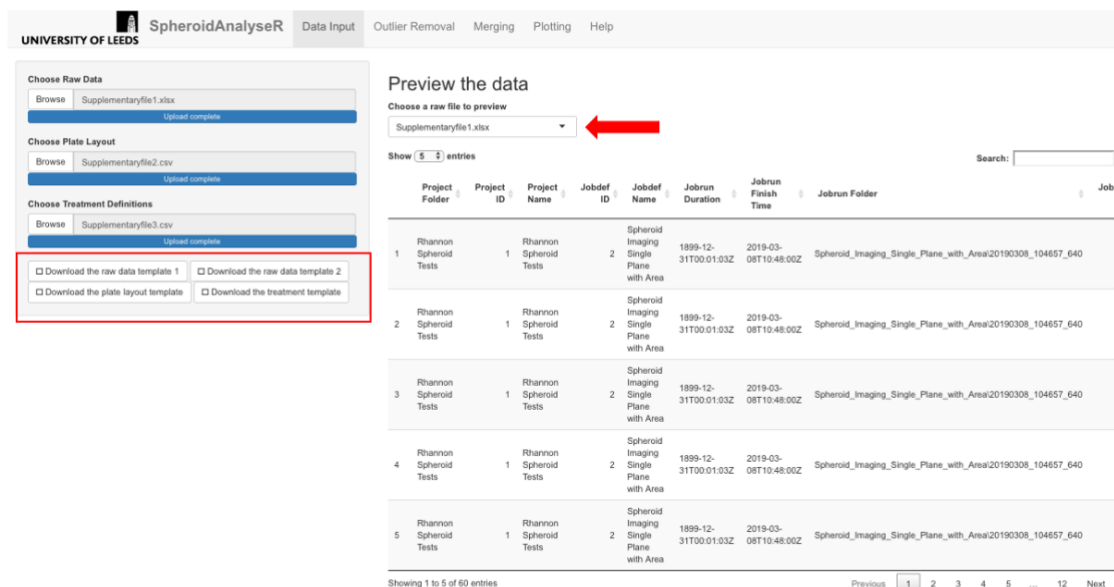
5. Plotting

Plots of the merged data can be created and viewed on the *Plotting* tab. SpheroidAnalyseR supports bar plots, point plots, dot plots and box plots. The user must select a plot type (bar plot by default) followed by a spheroid/organoid measurement type for the Y-axis (Area by default) and a grouping parameter for the X-axis (Treatment.Label by default) from the drop-down lists. If required, up to two grouping parameters can be specified to be distinguished by different colouring. The plot can be named and there is an option to colour the plot in black and white if desired. Press the 'Plot' button to view the plot on the tab, and the

'Add to the report' button to add it to the report which can be downloaded using the 'Download the report of plots' button. Multiple plots can be added to the report before downloading.

3.3.3.2 Example work through

A series of screenshots taken from SpheroidAnalyseR highlighting the process of uploading data, data analysis and data presentation is given in Figures 3.6 – 3.9. Key steps are described in the associated figure legends. The example data files are available at provided in the supplementary materials (raw data is in Supplementaryfile1, plate layout is supplied in Supplementaryfile2 and treatment definitions within Supplementaryfile3).



The screenshot shows the SpheroidAnalyseR web interface. On the left, there are three sections for data upload: 'Choose Raw Data', 'Choose Plate Layout', and 'Choose Treatment Definitions'. Each section has a 'Browse' button and an 'Upload complete' button. Below these sections, there are four checkboxes: 'Download the raw data template 1', 'Download the raw data template 2', 'Download the plate layout template', and 'Download the treatment template'. A red box highlights these checkboxes. On the right, the 'Preview the data' section shows a dropdown menu with 'Supplementaryfile1.xlsx' selected, indicated by a red arrow. Below this is a table with 5 entries, showing columns for Project Folder, Project ID, Project Name, Jobdef ID, Jobdef Name, Jobrun Duration, Jobrun Finish Time, and Jobrun Folder. The table contains 5 rows of data for 'Rhannon Spheroid Tests'.

Project Folder	Project ID	Project Name	Jobdef ID	Jobdef Name	Jobrun Duration	Jobrun Finish Time	Jobrun Folder
1	Rhannon Spheroid Tests	Rhannon Spheroid Tests	2	Spheroid Imaging Single Plane with Area	1899-12-31T00:01:03Z	2019-03-08T10:48:00Z	Spheroid_Imaging_Single_Plane_with_Area/20190308_104657_640
2	Rhannon Spheroid Tests	Rhannon Spheroid Tests	2	Spheroid Imaging Single Plane with Area	1899-12-31T00:01:03Z	2019-03-08T10:48:00Z	Spheroid_Imaging_Single_Plane_with_Area/20190308_104657_640
3	Rhannon Spheroid Tests	Rhannon Spheroid Tests	2	Spheroid Imaging Single Plane with Area	1899-12-31T00:01:03Z	2019-03-08T10:48:00Z	Spheroid_Imaging_Single_Plane_with_Area/20190308_104657_640
4	Rhannon Spheroid Tests	Rhannon Spheroid Tests	2	Spheroid Imaging Single Plane with Area	1899-12-31T00:01:03Z	2019-03-08T10:48:00Z	Spheroid_Imaging_Single_Plane_with_Area/20190308_104657_640
5	Rhannon Spheroid Tests	Rhannon Spheroid Tests	2	Spheroid Imaging Single Plane with Area	1899-12-31T00:01:03Z	2019-03-08T10:48:00Z	Spheroid_Imaging_Single_Plane_with_Area/20190308_104657_640

Showing 1 to 5 of 60 entries

Previous 1 2 3 4 5 ... 12 Next

Show the treatment groups on the plate

Choose the value to view the layout

Index

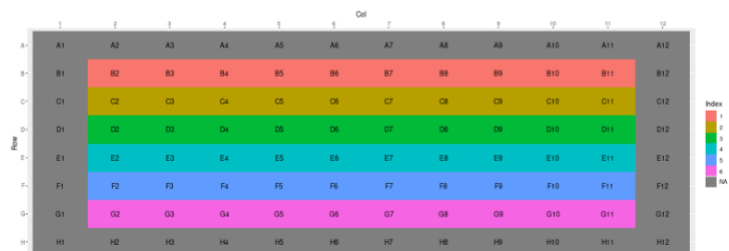


Figure 3.6. The *Data Input* tab. The view of the Data Input tab once raw data has been uploaded. Template files are available to download (see red rectangle). A raw file (Supplementaryfile1), plate layout (Supplementaryfile2) and treatment file (Supplementaryfile3) have been uploaded. A preview of the raw data is shown in the main panel, and a map of the plate coloured by treatment index is displayed underneath. Red arrows show the dropdown menus to select a different file to view, and to choose a value to view the layout for.

UNIVERSITY OF LEEDS SpheroidAnalyseR Data Input Outlier Removal Merging Plotting Help

Choose a raw file
Supplementaryfile1.xlsx

Choose a value to plot the outliers
Area

Download
Report generated, please download the report. These cells may have empty measurements: B04. Please Check the raw file. Please run the outlier removal before downloading the report.

Remove outliers
The remove outlier button will plot the data based on the metric selected above. If you are happy to proceed with default settings which will remove outliers based on the pre-set thresholds in the blue box then click remove outliers. Please use the blue box settings below if you would like to manually adjust settings prior to outlier removal (this can be done any number of times).

Toggle cells status normal/outliers

Once you have performed outlier removal, if you are unhappy with any of the automated choices you have an option here to manually change the status of any given well and then go to the top and press remove outliers again

Robust z-score
1.96
Robust Z-Score looks at the spread of the data and removes things that are classed as outliers by a Robust-Z-Score [1].

Apply Pre-screen thresholds?
Pre-screen thresholds are to allow you to say that you will only include spheroids that lie within a range. This is because there could be an empty well, or an error with imaging that has produced a value that you don't want to be included in any analysis.

Area lower limit
1

Area higher limit
1630000

Diameter lower limit
100

Diameter higher limit
1440

Volume lower limit
1000

Volume higher limit
1567543610

Perimeter lower limit
100

Perimeter higher limit
6276

Circularity lower limit
0.01

Circularity higher limit
1

Plate layout after robust Z-score outlier removal

Col	1	2	3	4	5	6	7	8	9	10	11	12
A1	A01	A02	A03	A04	A05	A06	A07	A08	A09	A10	A11	A12
B1	B01	B02	B03	B04	B05	B06	B07	B08	B09	B10	B11	B12
C1	C01	C02	C03	C04	C05	C06	C07	C08	C09	C10	C11	C12
D1	D01	D02	D03	D04	D05	D06	D07	D08	D09	D10	D11	D12
E1	E01	E02	E03	E04	E05	E06	E07	E08	E09	E10	E11	E12
F1	F01	F02	F03	F04	F05	F06	F07	F08	F09	F10	F11	F12
G1	G01	G02	G03	G04	G05	G06	G07	G08	G09	G10	G11	G12
H1	H01	H02	H03	H04	H05	H06	H07	H08	H09	H10	H11	H12

Plot 1
Area data by treatment index with outliers in red

Plot 2
Area - Mean +/- SE (outliers removed)

Area status
 Not an outlier
 Outlier determined by robust Z score
 Outlier determined from pre-set thresholds
 Invalid cells

Figure 3.7. The *Outlier Removal* tab. Inside the beige box are the adjustable outlier settings of Pre-screen-thresholds and robust z-score. After pressing the 'Remove outliers' button, the outliers have been identified on the plate layout seen at the top of the panel. Orange shows outliers removed via pre-screen thresholds and red shows outliers removed after robust z-score. The results of either of these can be modified using the 'Toggle cell status, normal/outlier' drop down menu. The user should select the wells to adjust and press 'Apply manual adjustment'. The data can be downloaded as an excel spreadsheet via the Download button.

Figure 3.8. The *Merging* tab. The status of the file processing is shown 'true' or 'false' in the Processed column. The Merge button must be pressed before moving to the next stage even if there is only one file to be analysed. Files that have been downloaded from the 'Outlier Removal' tab can be uploaded here if required.

Figure 3.9. The *Plotting* tab. The default plot type is a bar plot, but different plot types can be selected in the 'Choose plot type' drop-down list. Values to plot on the Y-axis and X-axis can be selected from the drop-down lists. The plot can be displayed in black and white if desired. Plots can be added to the report via the 'Add to report' button and then a file of the plots can be downloaded.

The combined result of the confocal imaging and SpheroidAnalyseR allowed imaging and subsequent analysis to be reduced from hours per plate to minutes. This was then used in any spheroid experiments going forward.

3.3.4 Determining seeding densities for spheroid models

In order to determine the number of cells per spheroid to seed for future experiments, the size of A172 spheroids seeded with different starting numbers was recorded at days 2 and 5 post seeding. Studies show that 400 μm diameter spheroids are known to develop a hypoxic core which is a common feature of GBM tumours (168). In a hypoxic environment, cells can undergo certain adaptations that enable them to have a more aggressive tumour phenotype, including a decrease in proliferation and a reduction in pro-apoptotic signalling, due to activation of DNA damage repair signalling pathways (167). Chemotherapy and irradiation are often less effective on tumours containing a hypoxic core (208). It was important that we seek ways in which our model could more physiologically represent a GBM tumour, therefore, a diameter of at least 400 μm must be observed at the start point of the experiment. On day 2, spheroids were not yet compact or circular. By day 5, spheroids were compact and spherical and their diameter appeared to be reduced from that measured at day 2 (Figure 3.10). Therefore, day 5 was chosen as an appropriate experimental time point following seeding in subsequent experiments. The diameter of spheroids at day 5 was around 360 μm for 2000 cells and around 420 μm for 4000 cells. Therefore a mid-point of 3000 cells was chosen to be the start point for experiments. This was consistent with previous spheroid work done in the lab using different cell lines that meant these results could be comparable to previous data collected if required. GBM63 and GBM58 both reached at least 400 μm in diameter at day 5. Therefore, this cell number and start time of any treatments following seeding was also appropriate for these cell lines.

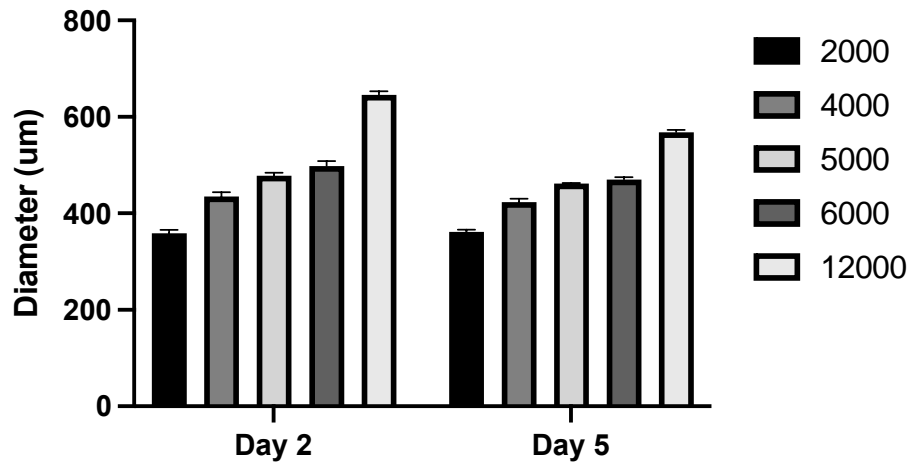


Figure 3.10. Diameter of A172 spheroids. Diameter measured in μm of A172 spheroids with different starting numbers of cells on day 2 and days 5 post-seeding. The mean spheroid diameter (μm) \pm SEM is plotted, $n \geq 6$ for each data point.

3.3.5 Optimising treatment doses and timings of TMZ and irradiation

To determine whether inhibiting *SLC6A6* alters the response of GBM cells to standard TMZ and irradiation treatment administered following surgery, doses and timepoints had to be identified whereby cell death was observed but not so much that no cells were available for analysis following treatment. Furthermore, to make these studies clinically relevant, treatment combinations needed to be comparable to those administered to patients: around 3-30 μM TMZ and fractionated irradiation of 2Gy doses to a total of 60Gy (17). Initially, treatments were optimised in 2D culture in case future work would benefit from assays only available in this format (Figure 3.11).

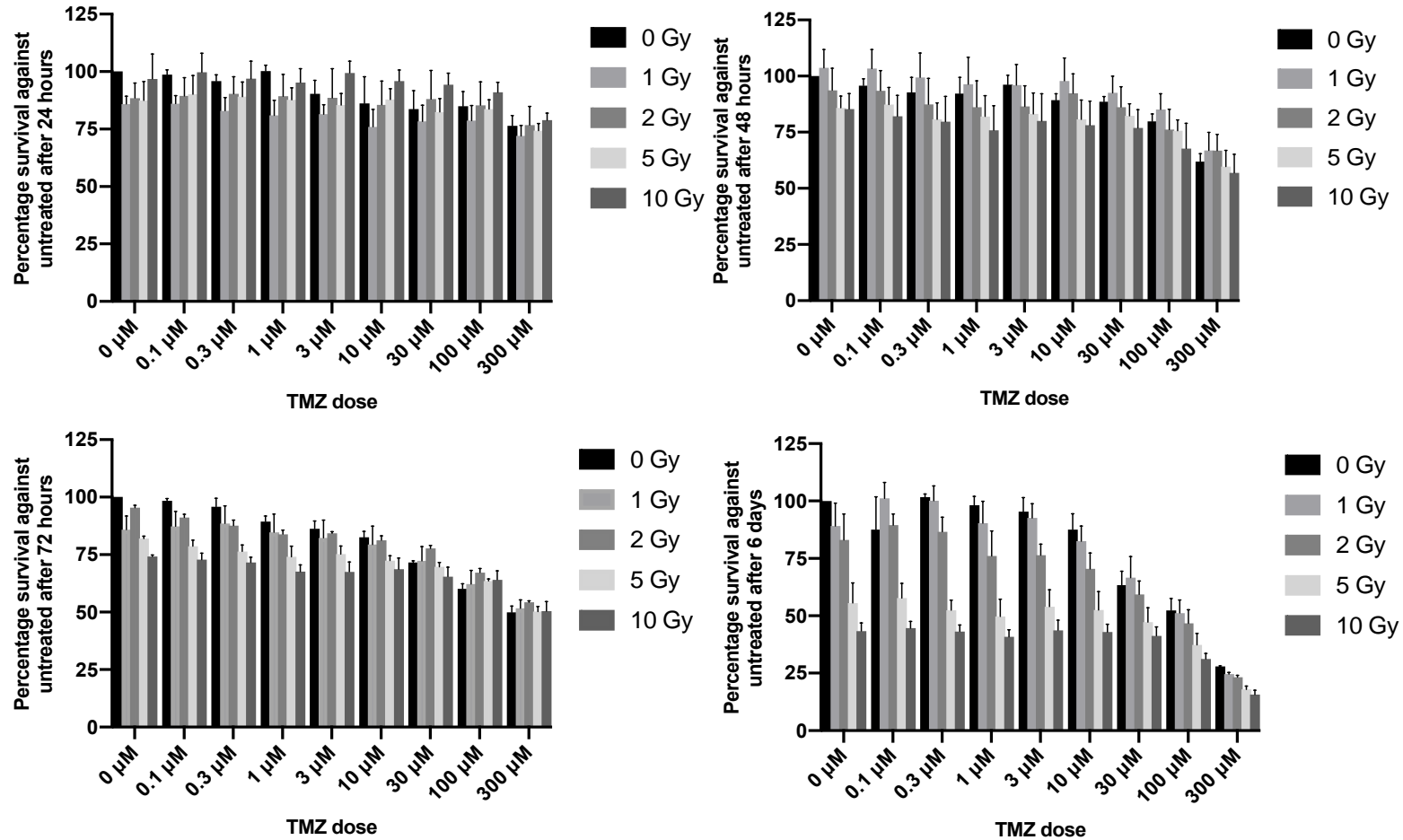


Figure 3.11. 2D dose response to TMZ and irradiation in A172. Dose response in 2D determined by MTT assay on A172 cell line at 24-, 48-, 72-, 96- hours after treatment. Mean \pm SEM is plotted, n=3.

Treatment of A172 cell spheroids with irradiation or TMZ alone shows a clear separation in growth curves at 30 μM TMZ (Figure 3.12a) and at 4Gy radiation (Figure 3.12b). In combination, there is no significant difference in treatment response between 2Gy + 30 μM TMZ and 4Gy + 30 μM TMZ (unpaired t-test, $p=0.322$)(Figure 3.13). Therefore, 30 μM TMZ and 2Gy irradiation were chosen as this most closely aligns with the treatment doses given to patients (17, 209). Spheroid area was measured up to day 37. However, from day 22 the variability in spheroid growth in both untreated and treated spheroids increased significantly and confounded results (Figure 3.14), and therefore an end point of 22 days was used.

A combination treatment of 30 μM TMZ and 2Gy irradiation elicits a significant response compared to untreated spheroids from day 14 ($p<0.05$)(Figure 3.12) so this timepoint was selected as the experiment endpoint for future work. Further testing showed a significant effect in GBM58 and GBM63 also resulted from treatment with 30 μM TMZ and 2Gy irradiation at day 14 ($p<0.05$) meaning that this treatment combination was sufficient for use in all three chosen cell lines (Figure 3.15).

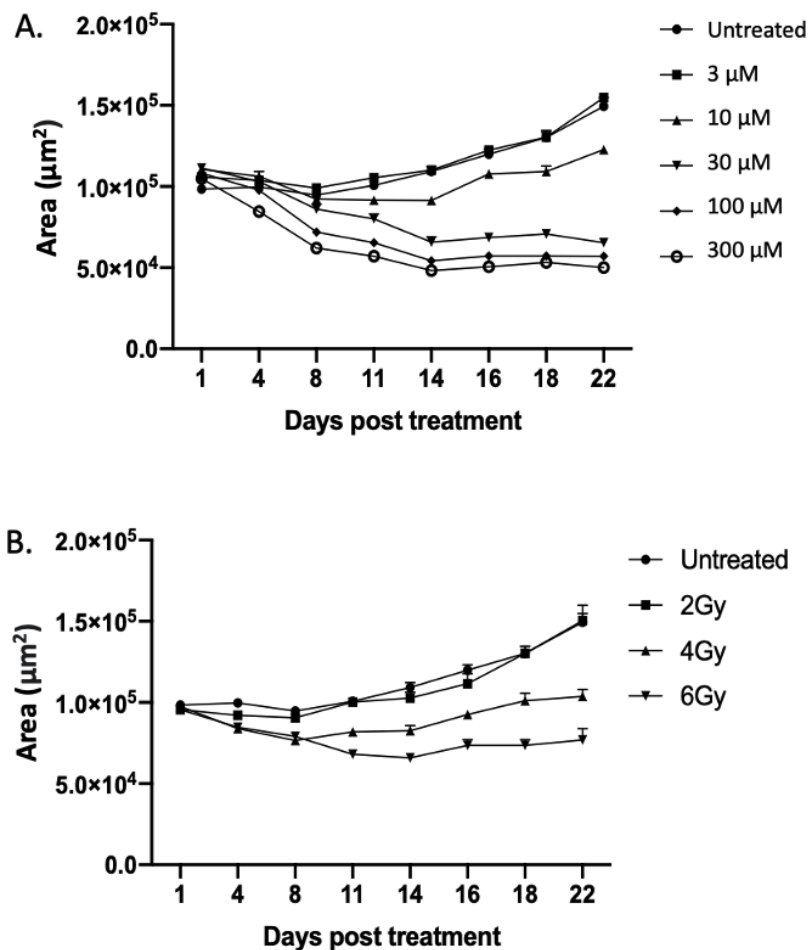


Figure 3.12. Area of A172 spheroids with TMZ or irradiation. Area measured in μm^2 of A172 spheroids treated over a period of 22 days with a) TMZ alone (from 0 μm to 300 μm) and b) irradiation alone (from 0Gy to 6Gy). The mean spheroid area (μm^2) \pm SEM is plotted, $n \geq 6$ for each data point.

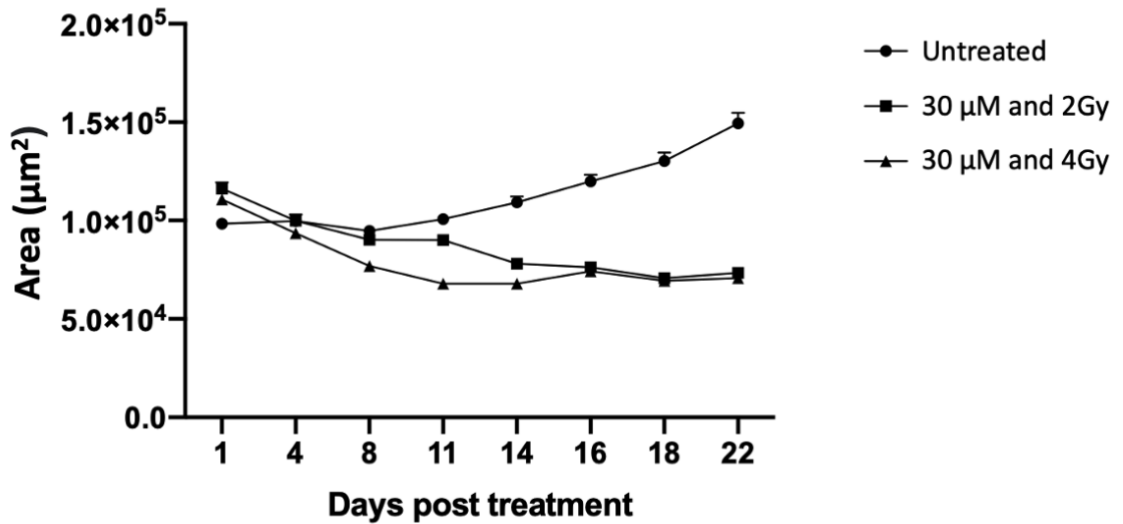


Figure 3.13. Area of A172 spheroids with TMZ and irradiation combined. Area measured in μm^2 of A172 spheroids for untreated or treated with 30 μM TMZ and 2Gy irradiation and 30 μM TMZ and 4Gy irradiation. The mean spheroid area (μm^2) \pm SEM is plotted, $n \geq 6$ for each data point.

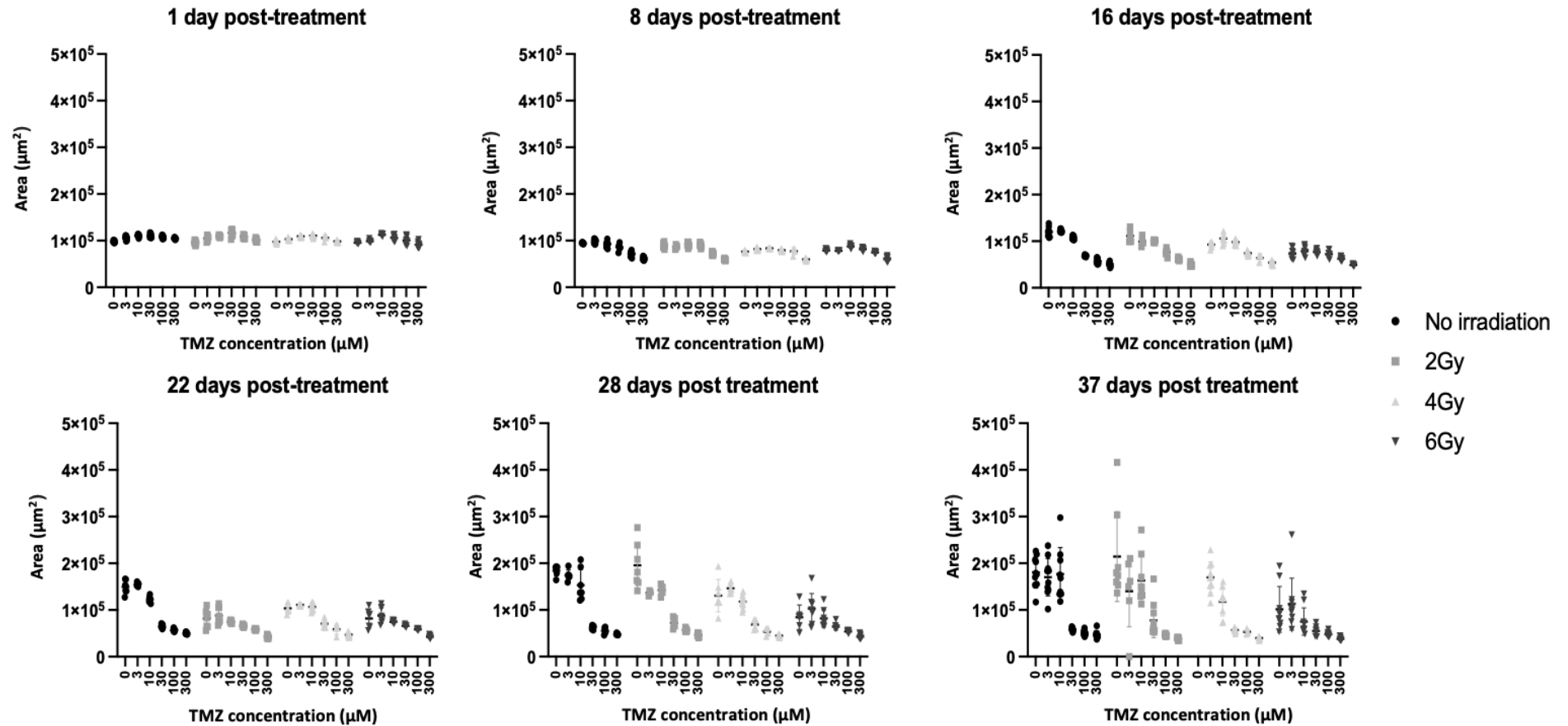


Figure 3.14. Area of A172 spheroids treated with TMZ and irradiation over a period of 37 days. Area measured in μm^2 of treated spheroids using treatment combinations of TMZ (30 μM to 300 μM) and irradiation (2Gy to 6Gy) measured on the Nikon confocal A1R. Six time points post-treatment are shown. In each treatment for each time point, $n \geq 6$.

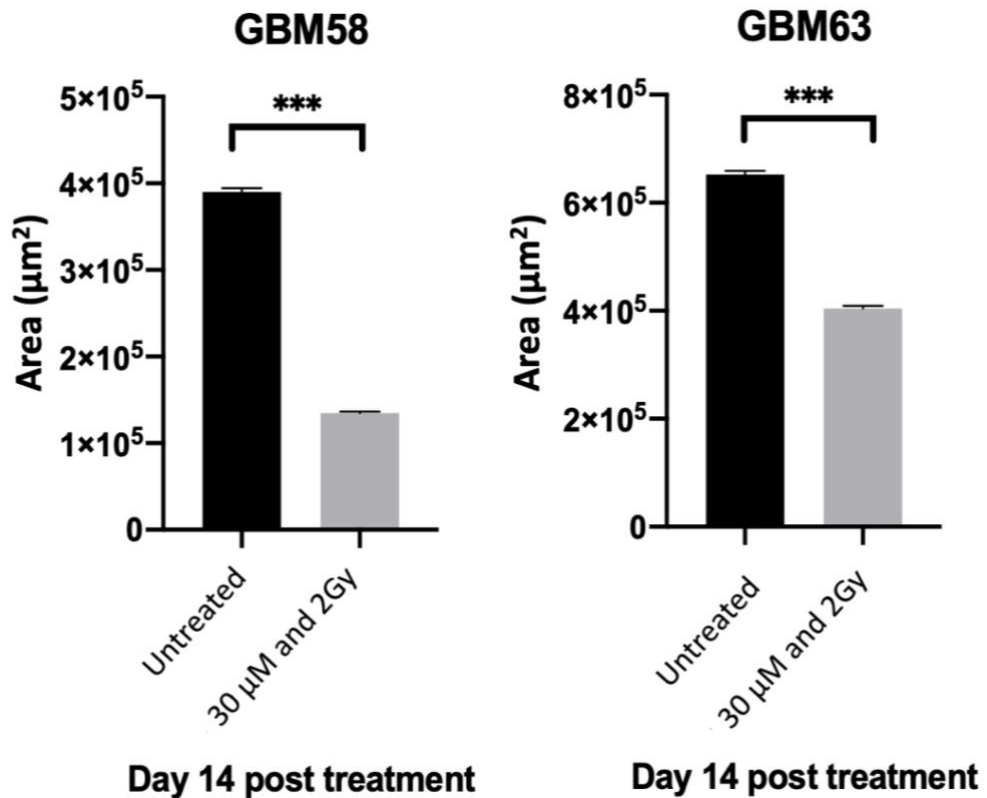


Figure 3.15. Area of GBM58 and GBM63 spheroids treated with the chosen treatment. Area measured in μm^2 of spheroids for untreated, or treated with 30 μM TMZ and 2Gy irradiation in both GBM58 and GBM63. The mean spheroid area (μm^2) \pm SEM is plotted, $n \geq 6$. Statistical significance of pair-wise comparisons are based on an unpaired Student's t-test and shown as *($p < 0.05$), **($p < 0.005$), and ***($p < 0.0005$).

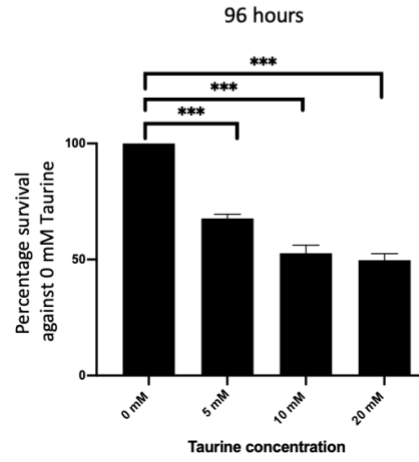
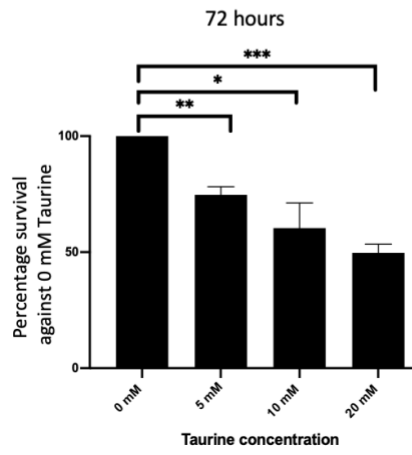
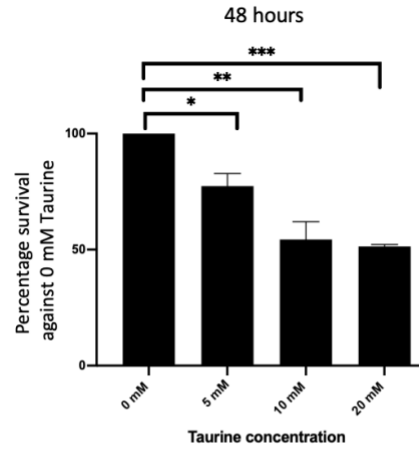
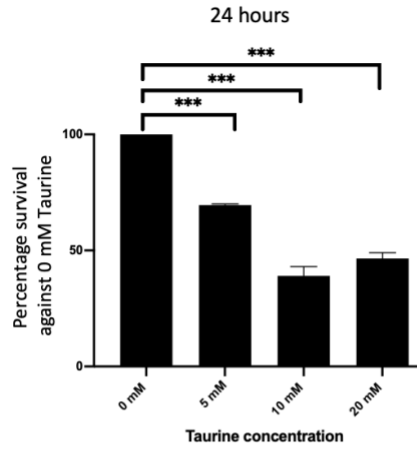
3.3.6 The effect of taurine on spheroid growth

SLC6A6 encodes a protein called TauT for which the primary function is to transport taurine into the cell. It was therefore important to observe any effect that taurine has on spheroid growth. To assess the effect of taurine on cell growth, viability and determine optimal taurine concentrations for further work, cell culture media was supplemented with increasing concentrations of taurine. The number of viable cells present following addition of taurine was measured in 2D by MTT assay at 24, 48, 72 and 96hrs after addition of taurine (Figure 3.16). Unpaired Student's t-tests were performed comparing no taurine control to each concentration of taurine for each cell line. This is because the only information

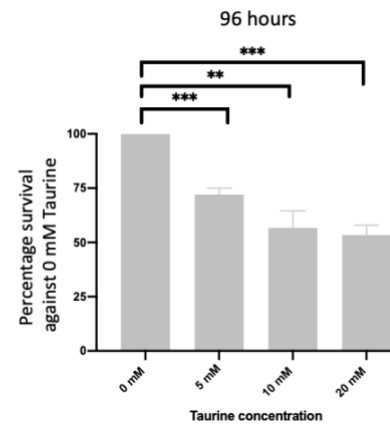
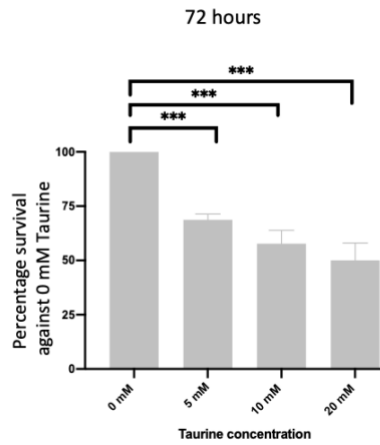
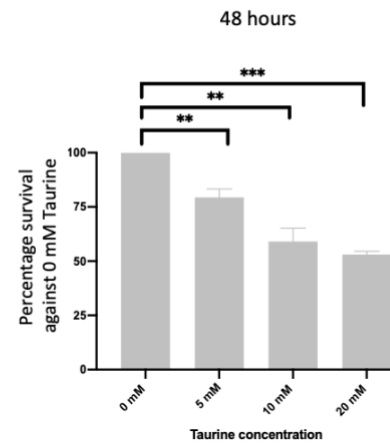
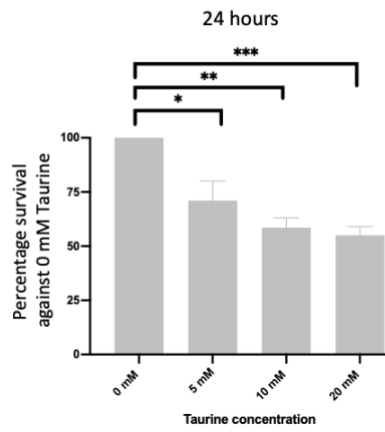
needed from this experiment was to observe the difference adding taurine has compared to the no taurine control therefore comparing only two groups. Pair-wise comparisons on the effect of each different concentration of taurine to one another was not necessary. Increasing the level of taurine in culture media resulted in significantly fewer viable cells, compared to 0 mM taurine, present in all three cells lines at all time points, with the exception of A172 supplemented with 5 mM taurine for 24 hours where there was a non-significant reduction. The effect of taurine is more apparent in the primary patient derived cell lines (GBM58 and GBM63).

The effect of taurine on 3D spheroids was assessed by supplementing the media with 0, 5, 10 or 20 mM taurine and measuring spheroid size over 21 days (Figure 3.17). Significant differences in growth were observed upon taurine supplementation but these were not extreme enough to indicate that the treatment doses, or determined end point of 14 days, required re-optimising. Interestingly, with 10 mM taurine, A172 spheroids show a trend toward increased growth compared to no treatment controls whereas a significant reduction in growth in GBM58 and GBM63 was observed (unpaired Student's t-test, $p < 0.05$) (Figure 3.17). 10 mM taurine supplementation was chosen for subsequent assays as this is a physiologically relevant concentration for brain tissue. However, the differences in the effect of this concentration of taurine on the established and (more differentiated) cell line and the patient-derived (more stem-like) cell lines could be due to fundamental biological differences which also become apparent in subsequent results chapters.

GBM58



GBM63



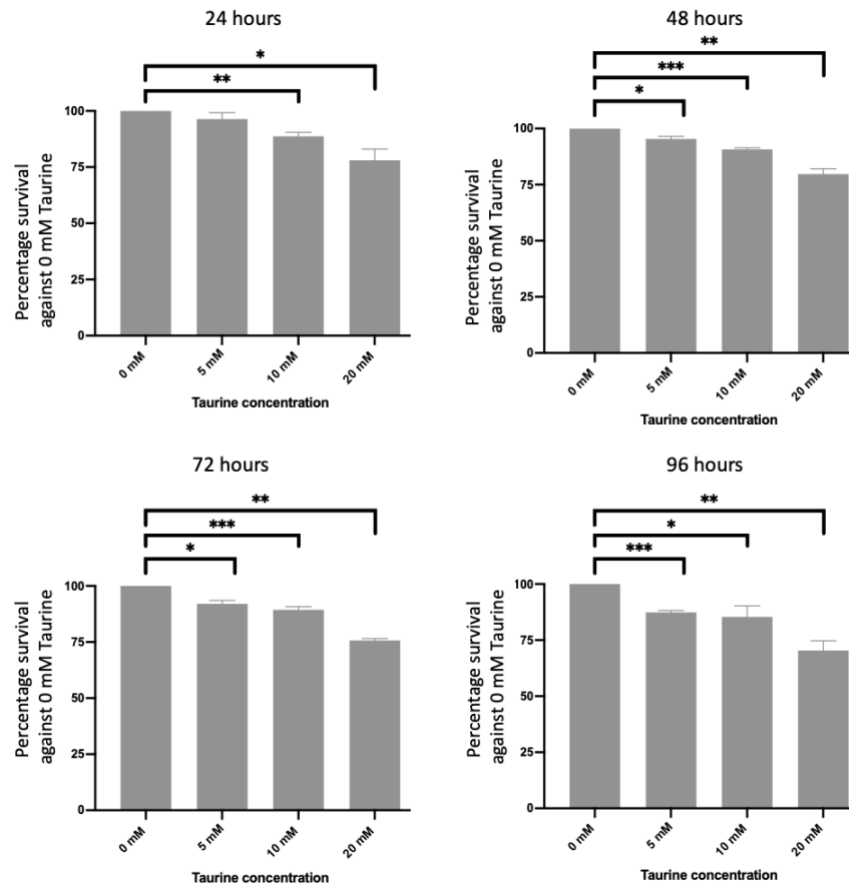


Figure 3.16. MTT assay in 2D looking at response to taurine. MTT assay results in 2D: mean percentage survival compared to 0 mM taurine \pm SEM (n=3) showing the effect of 5 mM, 10 mM and 20 mM taurine on GBM58 and GBM63 and A172 at 24, 48, 72, and 96 hours. The information sought from this assay was to determine the effect of each concentration of taurine compared to no taurine control only. The difference between each concentration of taurine to another was not required. Therefore, statistical significance of pair-wise comparisons are based on an unpaired Student's t-test and shown as *($p < 0.05$), **($p < 0.005$) and ***($p < 0.0005$).

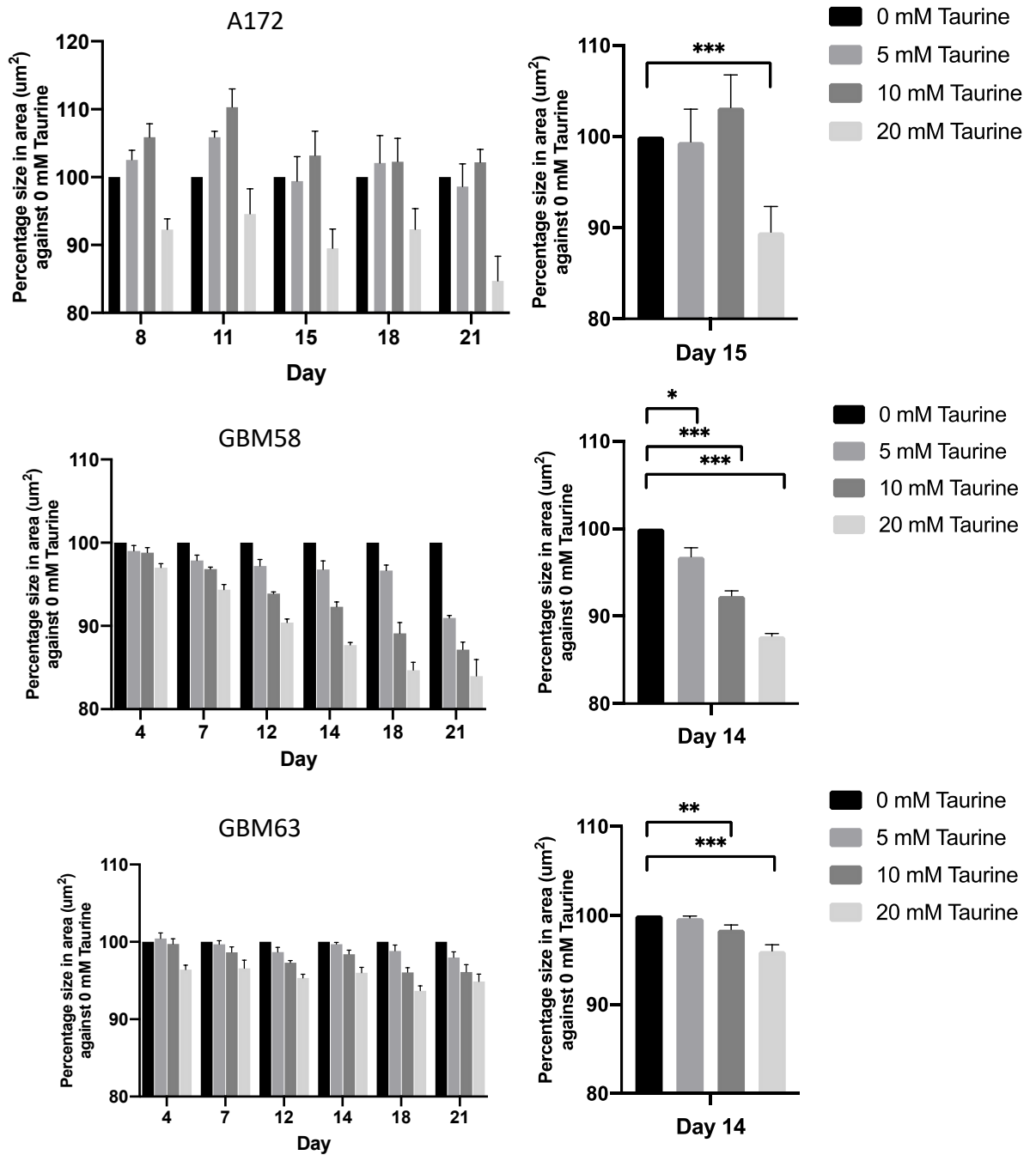


Figure 3.17. Spheroid size when supplemented with taurine. Percentage size of spheroid area (μm^2) against 0 mM taurine in three GBM cell lines – A172, GBM58 and GBM63. $n \geq 6$ for each data point, mean percentage size of spheroid area \pm SEM in every case. The information sought from this assay was to determine the effect of each concentration of taurine compared to no taurine control only. The difference between each concentration of taurine to another was not required. Therefore, Statistical significance of pairwise comparisons are shown in right hand bar graphs and based on an unpaired Student's t-test and shown as *($p < 0.05$), **($p < 0.005$) and ***($p < 0.0005$).

3.3.7 Assaying growth effects

To confirm that the combination of optimised treatments and taurine supplementation were suitable, taurine-supplemented spheroids were treated with irradiation and TMZ for all three cell lines to determine the combined effect on spheroid growth. This is to ensure sufficient cell death is seen whilst allowing alterations in treatment response to be observable (e.g. from *SLC6A6* knockout vs wildtype spheroids). Treated spheroids supplemented with taurine are significantly smaller ($p < 0.05$) (Figure 3.18) than those that were treated and had no taurine supplementation. However, the spheroid sizes are not reduced enough to indicate that the optimised treatments and taurine concentrations are not suitable for downstream work.

This experiment additionally offers the chance to investigate the differential treatment response, indicated by the difference in size of treated versus untreated spheroids, of each GBM cell line when cultured with and without taurine. To assess this, each treatment group (+/- taurine) was normalised to its untreated control. Figure 3.19 shows that there is no significant difference in treatment response in GBM58 and GBM63 but that in A172, adding taurine to the media reduced their response to treatment.

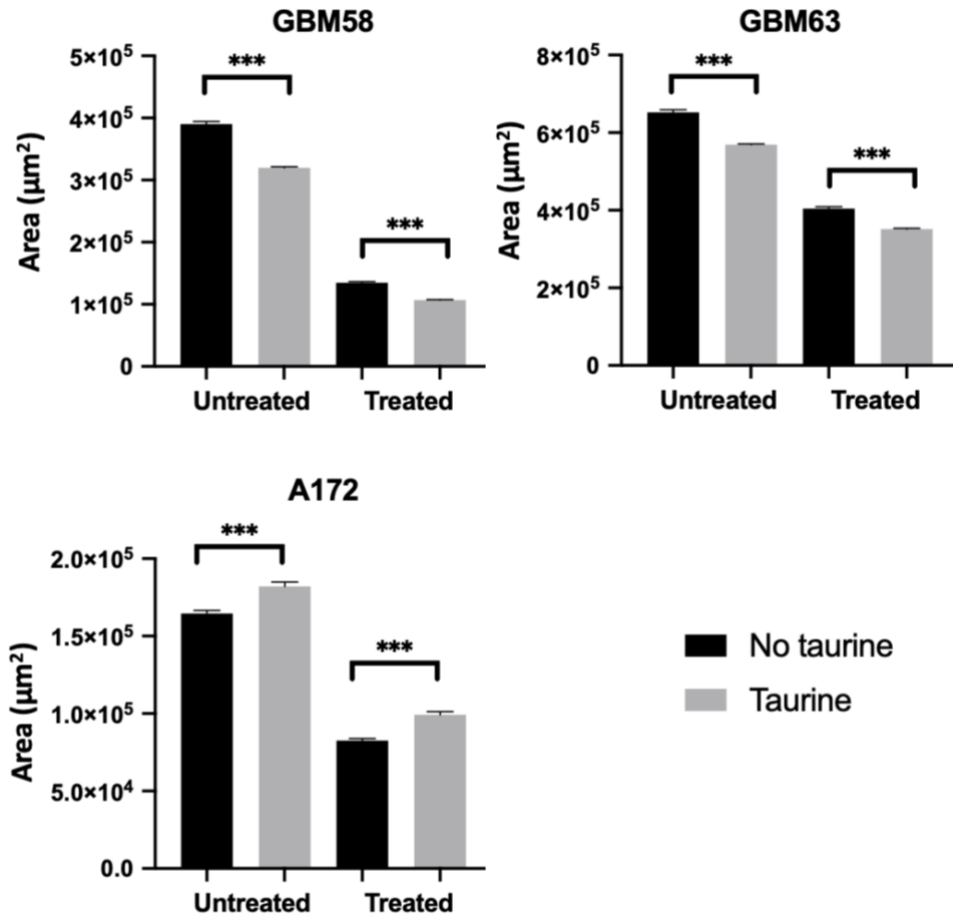


Figure 3.18. The effect of taurine and treatment combined on spheroids. Area measured in μm^2 of spheroids for untreated, 10 mM taurine supplementation, treated with 30 μM TMZ and 2Gy irradiation or treated with 30 μM TMZ and 2Gy irradiation with 10 mM taurine supplementation. The mean spheroid area (μm^2) \pm SEM is plotted, $n \geq 6$. Statistical significance of pair-wise comparisons are based on an unpaired Student's t-test and shown as *($p < 0.05$), **($p < 0.005$) and ***($p < 0.0005$).

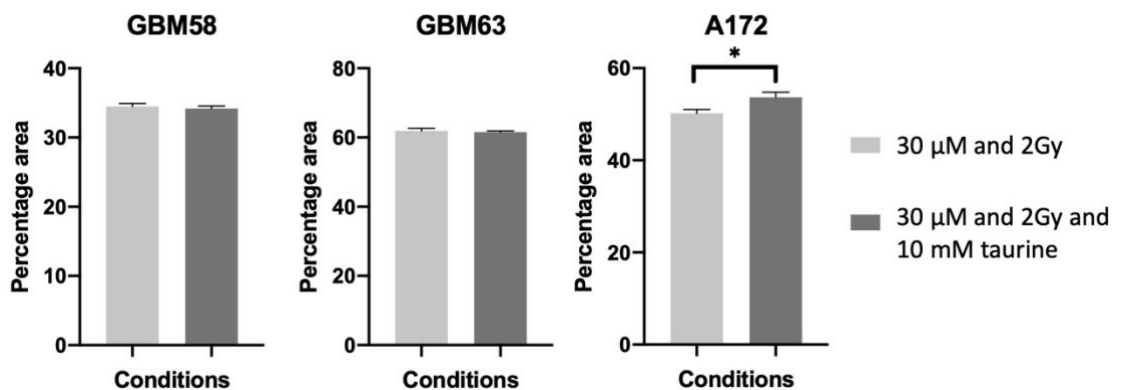


Figure 3.19. The effect of taurine on treated spheroids. Spheroid size at day 14 post treatment. 30 μm TMZ and 2Gy irradiation spheroid area expressed as a percentage of untreated spheroid area (\pm SEM is plotted, $n \geq 6$). 30 μm TMZ and 2Gy irradiation with 10 mM taurine spheroid area expressed as a percentage of 10 mM taurine spheroid area. Statistical significance of pair-wise comparisons are based on an unpaired Student's t-test and shown as $^*(p < 0.05)$.

3.3.8 Assessing proliferation

The addition of taurine to the media resulted in smaller spheroid sizes for GBM58 and GBM63 spheroids and larger spheroid sizes for A172 spheroids which was an unexpected finding. To try and understand the mechanisms underlying these differences, Ki67 immunofluorescence staining was performed as a marker of cell proliferation to determine if this was different between the cell lines. Spheroids grown in 0 mM and 10 mM taurine were embedded in OCT and 10 μm sections cut on a cryostat. Sections were stained with a Ki67 antibody (section 2.15) as a marker of proliferation. No significant difference in Ki67 staining was observed between 0 mM and 10 mM taurine in any of the cell lines (Figure 3.20) suggesting that changes in proliferation were not causing the differences in spheroid size upon taurine supplementation.

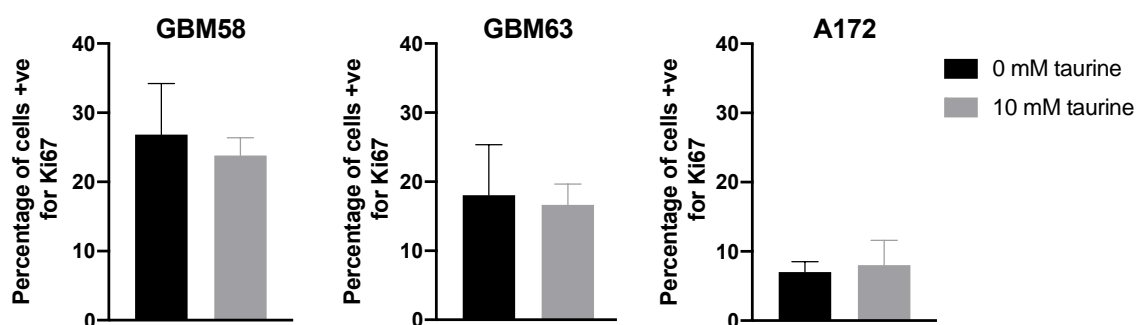


Figure 3.20. Ki67 staining in spheroids supplemented with taurine. The percentage of cells positive for Ki67 staining with no taurine or 10 mM taurine in GBM58, GBM63 and A172. No significant differences were observed from a Student's t-test. The mean percentage of +ve cells \pm SEM is plotted, $n \geq 6$.

3.4 Discussion

The aim of this chapter was to lay the foundations for future experiments by ensuring the right experimental set up and parameters were established to allow experiments to be run in a consistent and standardised way. To do this, several decisions had to be made starting with the choice of cell lines to be used for the duration of the project.

3.4.1 The use of cell lines in glioblastoma research

Established and patient-derived cell lines cover important but distinct parts of GBM tumour biology, so it was important to include both when deciding on cell lines of choice. Numerous studies have shown that established GBM cell lines have often been shown to be very dissimilar to the original tumour in terms of both gene expression and phenotype whereas patient-derived cell lines capture a lot more of the biology of glioblastoma primary tumours (163). This poses the question of “should we moving away from using established cell lines in GBM research and focusing solely on patient derived cell lines?”. Despite their differences from GBM tumours, established cell lines are still a valuable tool in GBM research due to their ease of use in terms of cell culture and availability for high-throughput assays. Therefore, they make an invaluable tool for optimisation purposes. Additionally, they represent the differentiated components of the tumour (162). Although this is not considered to be the most relevant aspect in GBM biology, as it is not regarded as the cell type causing the tumour to recur, it is nonetheless an important aspect that cannot be overlooked.

The decision to use both established and patient-derived cell lines allowed the fundamental biological differences between the two to be observed when they responded differently in experiments as discussed below.

3.4.2 Taurine effects on cells in 2D and 3D

There are two ways in which a cell gets taurine: through transport via TauT and from biosynthesis from cysteine inside the cell. Glioma cells often have biosynthesis defects which means they are more dependent on transport via taurine. For this reason, it is important that when we are setting up experiments looking at the effect of taurine in GBM cell lines we supplement the media with taurine to allow cell transport. The concentration to which the media should be supplemented had to be determined. Many previous studies looking at the effect

if taurine used concentrations around 10 mM, therefore this was the starting point used (123, 200-202). In addition, 5 mM and 20 mM were also investigated. Taurine supplementation had interesting and rather unexpected effects. The patient-derived cell lines GBM58 and GBM63 were both consistently and significantly smaller when supplemented with taurine in 2D from 48 hours post-taurine treatment onwards. The same findings were also observed for A172 cells which is in accordance with other studies in the literature that have found that taurine addition reduces the number of viable cells in GBM cell lines (159). However, when assayed in 3D spheroids, a greater variability was observed between cell lines. GBM58 was significantly smaller at all concentrations two weeks after taurine supplementation in spheroids, but GBM63 was only significantly smaller at 10 mM and 20 mM taurine. In contrast, for A172 there were no significant changes two weeks after taurine supplementation at 5 mM and 10 mM taurine but spheroids were significantly smaller when supplemented with 20 mM taurine. In interpreting these results, there are a number of issues to consider. Firstly, what is causing the general difference in size between patient derived and established cell lines? Secondly, what is causing the A172 spheroids to be larger when supplemented with 5 and 10 mM taurine and smaller with 20mM taurine? Thirdly, why is there variability between the results in 2D and 3D?

To determine what may be causing differences in cell size, Ki67 was used as a marker of proliferation to determine if addition of taurine affected cellular proliferation. However no significant differences were observed between the levels of Ki67 when taurine was added, suggesting that taurine was having no effect on cell proliferation. This contrasts with other studies in the literature that determined taurine resulted in a reduction of proliferation of cells in lung cancer cells, colon cancer cells and GBM cells (159, 210, 211). It may be that taurine was affecting the rate of cell death, cell density, or it was simply a change in the pH of the media that was causing the cells to divide slower. While the differential effect of taurine on cell growth was unexpected, it was not the main focus of this project. Therefore, it was decided that no more time would be spent on investigating exactly why taurine is causing a difference in spheroid size and, instead, the study would focus on the effect of treatment on spheroids. 10 mM taurine was decided to be the concentration of choice in subsequent experiments. Treatment experiments using standard treatment of 30 μ m TMZ and 2Gy irradiation were performed in the presence of 10 mM taurine. The difference

between treated and untreated was still observable which means we could continue adding 10 mM taurine for future experiments. In A172, spheroids supplemented with 20 mM taurine were smaller than those supplemented with 10 mM taurine. This was an unexpected finding but was not an outcome that was key to the investigation because 20 mM taurine would not be used in further experiments.

The variability between results in 2D and 3D is the other main observable difference. This difference could be due to the exposure to taurine, as cells cultured in 2D are subject to equal exposure to growth media and supplements. In 3D cell models, cells towards the centre of a spheroid will not be exposed to the growth media to the same degree as cells on the surface of the spheroid (196). This means that in 3D, not all cells may have been exposed to taurine which may be the reason behind the higher variability. Furthermore, the variability could be due to the cell-to-cell interaction differences in 2D and 3D and how cells are responding differently when exposed to taurine but in communication with other cells (194). Ultimately, the results are not as clear in 3D, but since 3D is more physiologically- relevant to tumours as previously discussed, it was decided I would use spheroids in subsequent experiments.

The effect of taurine and treatment combined was also investigated. Spheroids supplemented with taurine were generally smaller than those without taurine. When comparing spheroids treated with standard treatment vs untreated, to spheroids treated with standard treatment vs untreated in the presence of taurine, there was only one cell line (A172) with a small but significant difference between the two groups. To account for the changes taurine alone seems to be having on spheroid size, it was decided that taurine would be added to all spheroid assays going forward.

3.4.3 Alternatives to spheroid models

Spheroid models are becoming an increasingly popular experimental method especially in cancer research. Despite the numerous advantages previously discussed about spheroids, they lack elements that make them completely biologically relevant. For example, spheroids contain no tumour microenvironment. Recent studies are continually pointing to the tumour microenvironment in becoming an ever important aspect of GBM biology that is able to increase the heterogeneity of a GBM tumour (212). The tumour

microenvironment consists of many different cell types including fibroblasts, glial cells, endothelial cells, blood cells and immune cells such as tumour associated macrophages (213). The exact role that the tumour microenvironment has in GBM is unknown, but it is known that it can contribute to the evasion of GBM cells from the immune system (214). Therefore it is possible that drugs appearing to be successful in spheroids would not actually be successful in a model where more aspects of tumour microenvironment were present; for example *in vivo*. Obviously, we cannot recreate the tumour microenvironment perfectly outside of the human brain but there are other models that can help us with understanding the tumour microenvironment.

Organoids are small organ-like tissues that are most commonly derived from pluripotent stem cells and are therefore mimicking the process of organ formation *in vitro* (215). These model systems can be used to recreate the components of a human brain and therefore can be a more advanced model for studying GBM. Although these could be a more appropriate model for GBM treatment experiments, organoids are not without their own issues. They are grown from stem cells which is limited by access to patient tissue and there are ethical implications to consider. In addition, they are notoriously difficult to culture and need feeding daily. Furthermore, one major disadvantage is the absence of inter-organ communication meaning that they do not fully reiterate the tumour microenvironment (215).

In vivo Patient-Derived Tumour Xenograft (PDTX) models are another way in which GBM biology can be studied and overcomes the issue of interorgan communication. Commonly, immunocompromised mice are used so that tumours are more likely to form after the injection of tumour cells. However the lack of immune system is a drawback because the immune system itself is thought to play an important role in immune evasion in GBM (216). PDTX mouse models have been shown to represent many features of the original tumour including increased angiogenesis, necrosis and an increased level of invasiveness (217). However there are many ethical issues surrounding the use of mice and experiments, meaning they are not always accessible. Additionally, experiments using animals are technically challenging, very expensive and require extensive maintenance once set up making them inaccessible for many researchers (215). Ultimately, there is no perfect method of studying GMB

biology. However, due to their ease of use, cost-effectiveness and availability for high throughput assays, spheroids were deemed an appropriate model for these experiments and starting point into investigations into *SLC6A6*. The disadvantages of 2D cell culture, spheroids, organoids and PDTX are summarised in Table 3.1.

Table 3.1. Comparison of cell culture methods. The advantages and disadvantages of 2D cell culture, spheroids, organoids and Patient Derived Tumour Xenografts (PDTX). Table information adapted from (194, 218).

	Advantages	Disadvantages
2D cell culture	<ul style="list-style-type: none"> • Cultures are formed in a matter of hours after seeding • High reproducibility between experimental repeats • High throughput can be easily achieved • Easy to maintain cultures long-term • Commercially and readily available 	<ul style="list-style-type: none"> • Structure is not representative of the tumour • Cell-to-cell interactions are limited • No tumour microenvironment • Lack of tumour heterogeneity
Spheroids	<ul style="list-style-type: none"> • Cell-to-cell interactions present • Oxygen and nutrient gradients similar to that of a tumour • Often develop a hypoxic core over 400 μM in diameter which is also seen in GBM tumours • Easy to set up and maintain 	<ul style="list-style-type: none"> • Can take a few days for spheroids to form • Costly in comparison to 2D cell culture but cheaper than PDTX • No tumour microenvironment • Analysis tools are limited with common assays being end point only. • Difficult to do high throughput screens
Organoids	<ul style="list-style-type: none"> • Same advantages as seen in spheroids • Resemble an organ and therefore begins to 	<ul style="list-style-type: none"> • Can take a few days for organoids to form • Expensive media required for maintenance • No interorgan communication

	encapsulate some of the tumour microenvironment	<ul style="list-style-type: none"> • Require access to tissue • High maintenance
Patient Derived Tumour Xenografts (PDTX)	<ul style="list-style-type: none"> • Encapsulates a more of the tumour microenvironment • Interorgan communication • Tumour heterogeneity is maintained • Cells are interacting and communicating in the natural way 	<ul style="list-style-type: none"> • Require an immune deficient host so not representative of the true tumour microenvironment • Expensive to set up and run • Extensive maintenance required • Ethical approval required

In recent years, tissue-on-a-chip technologies have been developed that use microfluidic chips to hold a small section of tumour and culture it for up to 8 days by keeping it at a constant temperature and feeding with a constant supply of media whilst removing the effluent (219). In one study, the levels of lactate dehydrogenase (LDH) excreted into cell culture supernatant were determined. LDH is a cytosolic enzyme that is released into the media after plasma membrane damage to a cell. The amounts of LDH in the media can then be quantified and act as a reliable indicator of cellular toxicity (220). In addition, the tumour sample can be examined itself, for example by RNA-sequencing. These chips can be used in a similar way in which we perform treatment experiments with cell lines, by adding drugs in the media to monitor the treatment response of the tumour (219). The advantage of this is it uses real tumour tissue allowing observations into how the patient's tumour responds to a given treatment. The disadvantage is that access to frequent tissue samples is required and therefore high-throughput assays are not achievable. Despite being a more relevant model to GBM tumours, the Tumour-on-a-Chip method is still in its infancy so not a viable option for use in this project that requires a high-throughput method.

3.4.4 End point assays

In order to decide on the way in which treatment response will be measured, we have to determine what would generally be considered a success for a patient. While complete loss of all tumour cells would be the ideal scenario for any cancer patient, with GBM this is an impossible task. GBM tumours are in the brain which cannot be removed unlike a lung or kidney, so the best hope is resection of the

tumour. Unfortunately, GBM is a highly infiltrative tumour so it is inevitable some tumour cells are left behind (16). Making the margin of resection larger would inevitably jeopardise brain function, so the remaining tumour cells left behind are able, over time, to form a recurrent tumour. As GBM is so aggressive, resection of a small tumour causes significantly less damage to the brain. For a GBM patient, a smaller tumour generally equates to a better quality of life and a better prognosis (203). During optimisation of assays in this chapter, spheroid size was therefore used as a measure of response to treatment. A smaller spheroid upon treatment does not necessarily equate to increased cell death; other reasons for a reduction in size include cells becoming more tightly packed together or simply a reduction in cell division resulting in fewer cells compared to the control. Regardless of the underlying mechanism, the outcome of a smaller tumour, or in this case a smaller spheroid, is still desirable.

With the development of the spheroid imaging and analysis software, imaging of spheroids has been reduced from hours per plate to minutes, allowing an opportunity for high throughput analysis that previously was not viable. In addition, the development of SpheroidAnalyseR has allowed data to be analysed quickly and in an automated way, leading to reduced bias and human error. Altogether, this allowed multiple plates per experimental repeats to be setup and imaged. As well as allowing more spheroids to be assayed, additional downstream benefits were also identified. For example, to extract RNA from patient-derived spheroids is a challenge, and frequently numerous spheroids are required to obtain the required amounts of RNA. Previously, spheroids collected for RNA would not be imaged due to the length of time required for visualisation and analysis. Using the new method, spheroids can be assessed for any obvious outliers before being grouped together to harvest for RNA.

The R programming language is a highly regarded platform for data manipulation and statistical analysis but is often out of reach for those without previous programming skills. The Shiny platform used in developing SpheroidAnalyseR is a way of allowing users who are not knowledgeable about the R programming language to use the benefits of R through the use of a web interphase. Consequently, SpheroidAnalyseR can now be used by researchers from all backgrounds.

Although measuring the size of the spheroid helps to assess the effect of treatment, without further analysis it is hard to understand why the spheroid size is decreasing. For example, is this due to cell death or are there other mechanisms causing this reduction. To further explore the effects of treatment on spheroid size, cell viability assays can also be performed. Cell viability is commonly described as the number of healthy cells in a sample, common methods of measurements include Trypan Blue, MTT (3-(4,5-dimethylthiazol-2-yl)-2,5-diphenyltetrazolium bromide) and MTS (3-(4,5-dimethylthiazol-2-yl)-5-(3-carboxymethoxyphenyl)-2-(4-sulphophenyl)-2H-tetrazolium) (221). However these are not suitable for use in 3D as they cannot penetrate through the dense layers of cells. In order for a cell viability assay to work in 3D, there must have a strong lytic capability for the reagent (222). CellTiter-Glo 3D cell viability assay is one such assay what measures the amount of ATP present as a measure of viable cells. In this assay, ATP is used as a marker for the presence of metabolically active cells. The reagent can be added straight to cells and the luminescence signal read after 30 minutes though remains stable for around three hours. In addition, it is suitable for use in 96-well plates making it the perfect candidate for high throughput assays (223).

Cell viability assays such as CellTiter-Glo 3D use ATP as a measure of cell viability. However, it could be argued that this is not an accurate measure as cells may stop dividing and therefore produce less ATP but are nonetheless viable. An alternative measure of viability would be to dissociate the spheroids and count the ratio of alive: dead cells using Trypan Blue to stain the dead cells. However, the process of dissociating spheroids back to a single cell suspension can in itself kill the cell and therefore give a biased representation of cell viability. With this in mind, it was decided for this project that the CellTiter-Glo 3D cell viability assay would be used in parallel with the primary method of measuring the size of the spheroid. This methodology would allow the assessment of responses to treatment and whether these were due to cell death. In combination, these two methods of treatment response should give a clearer picture of the role of *SLC6A6* in treatment resistance in GBM.

With the models, timings and doses and end point assays decided upon, investigations into the role of *SLC6A6* in treatment response are described in the subsequent results chapter.

Chapter 4

SLC6A6 knockdowns and TauT inhibitors

4.1 Introduction

Once the models had been established, (Chapter 3), the role of *SLC6A6* in treatment response could be investigated. To do this, I planned to knockdown expression of *SLC6A6* and monitor response to treatment in the presence of taurine. There are multiple ways in which this could be achieved; siRNA, shRNA and CRISPR were chosen to knockdown or knockout the expression of *SLC6A6* and monitor its effect.

4.1.1 Gene knockdowns and knockouts

Gene knockdown involves reducing expression of a target gene either in a transient or permanent way. The gene will still be expressed but at a significantly lower level than the usual expression. Similar to this, gene knockouts aim to completely stop expression of the target gene. Knockdowns often target the RNA molecules produced by cells and do not affect the DNA. Knockout techniques such as CRISPR-Cas9 gene editing alter the DNA to negate the transcription of a functional RNA molecule or prevent translation of the protein, thereby creating a null allele (224, 225). Both shRNA and CRISPR-Cas9 can be inducible to allow for specific gene knockdown or knockout respectively both *in vivo* and *in vitro* (226, 227).

Knockdowns and knockouts are used extensively in molecular biology to determine the function of a given gene. Different methods are available, depending on the experimental need. CRISPR-Cas9 gene-editing targets the genomic DNA and therefore creates a stable, constitutive knockout of the gene. Knockdowns can be stable or transient depending on the method used: stable transduction or integration of shRNA constructs can create stable gene knockdown whereas siRNAs are usually transient over a matter of days (228, 229).

4.1.2 Small interfering RNA (siRNA)

Gene knockdown by small interfering RNA (siRNA) uses a technique called RNA interference (RNAi) to selectively induce a short-term reduction in translation of a target gene. siRNA are made up of sense and antisense strands that are around

21-25 nucleotides in length and are used for gene silencing in mammalian cells (230). First discovered in plants in 1999 by Baulcombe *et al.*, siRNA has been used widely in research since Elbashir *et al.*, first successfully used it for gene silencing in 2001 (231, 232). It has the ability to silence almost any gene through complementary binding to the RNA sequence selected for silencing. siRNA is used *in vitro* and *in vivo*, and the ability of siRNA to bind to and transiently silence any mammalian gene including those that have been deemed as 'undruggable' makes it a promising therapeutic approach. However, for this to be successful, an efficient method of delivering siRNA into the cells must be achieved (233). Achieving the desired amounts of siRNA in the correct tissue has presented many barriers including nuclease degradation of the siRNA reagents and immune response (233, 234). Despite these challenges, two siRNA therapeutics are now approved for clinical use: ONPATRO® (patisiran) used to treat hereditary amyloidogenic transthyretin amyloidosis with polyneuropathy in adults since 2018, and GIVLAARI™ (givosiran) used to treat adults with acute hepatic porphyria (235, 236).

The process of siRNA-based gene knockdown is depicted in Figure 4.1. It involves long double strand RNA (dsRNA) entering the cell cytoplasm where Dicer, an RNase III-related endonuclease processes these dsRNAs into siRNA molecules. Dicer binds to the 5' phosphate of two nucleotide 3' overhang before cleaving the dsRNA. The siRNA associates with the RNA-Induced Silencing Complex (RISC) that contains the protein Argonaute-2 (Argo-2). Argo-2 cleaves the sense strand which leaves the antisense strand free to bind to mRNA complementary to its sequence. Once the siRNA is bound to the complementary mRNA, the mRNA is degraded by Argo-2, which silences expression. This is achieved through endonucleolytic cleavage at a specific point towards the 5' end of the antisense siRNA strand (233, 237, 238). This process is repeated multiple times. As siRNA nucleic acids are not integrated into the genome of the host, they become degraded by the cell and therefore only result in transient gene silencing (239).

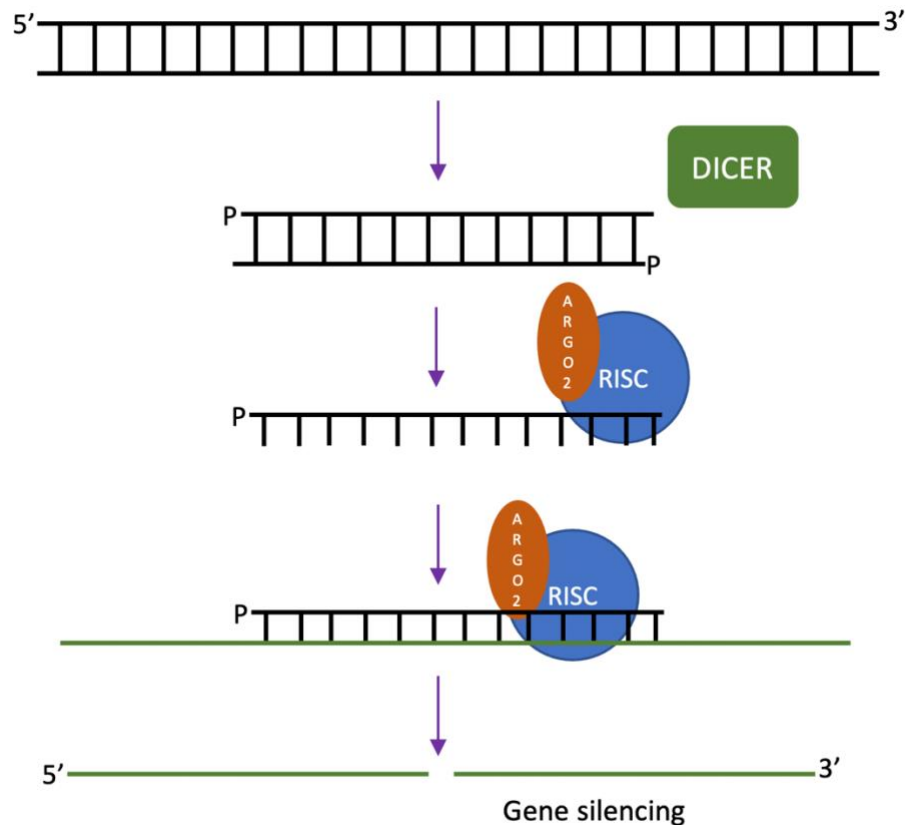


Figure 4.1 siRNA process. Long dsRNA enters the cell cytoplasm where Dicer processes these dsRNAs into siRNA molecules. The siRNA associates with the RNA-Induced Silencing Complex (RISC) which contains the protein Argonaute-2 (Argo-2). Argo-2 cleaves the sense strand which leaves the antisense strand free to bind to mRNA complementary to its sequence. Once the siRNA is bound to the complementary mRNA, the mRNA is degraded by Argo-2 which silences expression. This is achieved through endonucleolytic cleavage at a specific point towards the 5' end of the antisense siRNA strand.

4.1.3 Short hairpin RNA (shRNA)

Short hairpin RNA (shRNA) is used for stable gene knockdown. This uses an RNA interference pathway similar to that for siRNAs. The structure of shRNA is as a hairpin loop, hence its name. It has a stem region consisting of the sense and antisense strands with a loop in between consisting of unpaired nucleotides (240) (Figure 4.2). shRNA expression vectors are stably integrated into the genome allowing long term knockdown of the target gene to be achieved. Other advantages of shRNA are that they are thought to have fewer off-target effects compared to siRNA and they can silence gene expression more effectively than siRNA (241, 242). shRNA are synthesised and processed inside the cell nucleus

before being transported via Exportin-5 to the cytoplasm. Once in the cytoplasm, shRNA molecules are processed by Dicer into 20-15 nucleotide siRNA molecules before being loaded onto the RISC complex (228). This process activates the RISC complex and facilitates binding to the complementary mRNA sequence, followed by cleavage of this sequence as seen in siRNA processing.

shRNA transcription can be controlled using inducible promoter systems, the most common of which is the tetracycline-inducible system. This allows transcription to be turned on when tetracycline is not present, or off when the antibiotic tetracycline is added, due to the interaction between tetracycline and the tetracycline-controlled transactivator protein. This technique can be used *in vivo* to provide higher control over the target gene (240).

Viral vectors are a common and effective method expressing shRNA constructs in a cell. There are many different viral vectors available including the RNA viruses, lentivirus and retrovirus that are capable of integrating into the chromosomes using a reverse transcriptase and allowing continual expression of the shRNA inside the cell (243). Non-replicating viruses are commonly used for this method, introduced as *GAG*, *POL* and *ENV* genes in different plasmid vectors so that following one round of viral infection, the shRNA is stably integrated into the host genome and no infectious virus produced. Vectors using RNA viruses can also include selection markers to maintain selection pressure on the cell to maintain the shRNA. These are usually antibiotic resistance genes, but fluorescent protein markers are also commonly used for visualisation purposes (229).

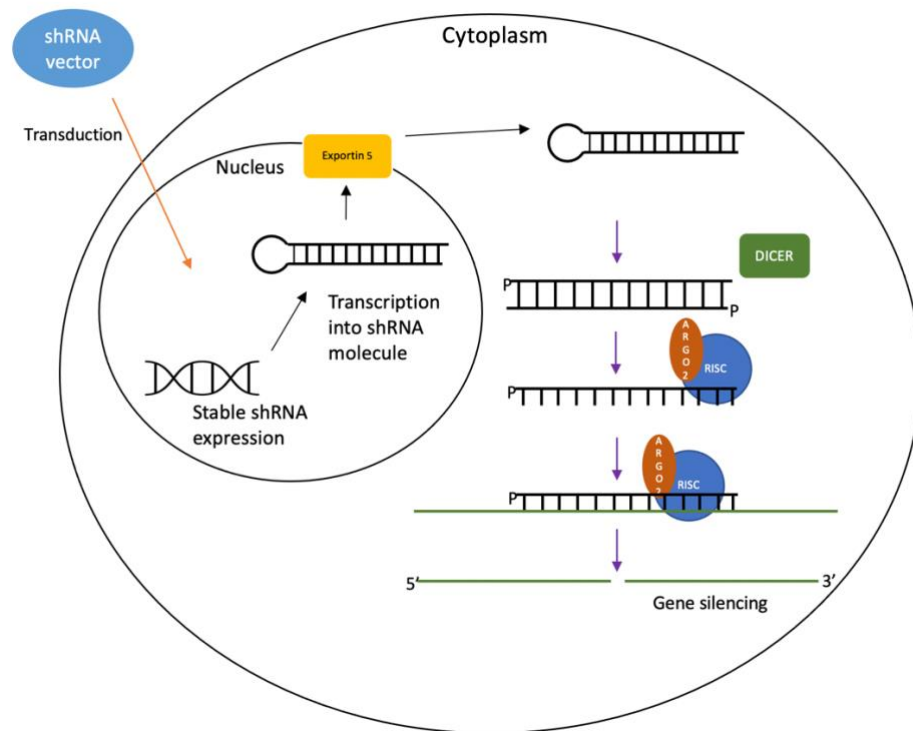


Figure 4.2. shRNA process. shRNA expression vectors transduced into the cell and stably integrate into the genome. shRNA are synthesised and processed inside the cell nucleus before being transported via Exportin-5 to the cytoplasm. Once in the cytoplasm, shRNA molecules are processed by Dicer into 20-15 nucleotide siRNA molecules before being loaded onto the RISC complex. This process activates the RISC complex and facilitates binding to the complementary mRNA sequence, followed by cleavage at this sequence.

4.1.4 Delivery of siRNA and shRNA into a cell

There are numerous ways in which siRNA or shRNA can be delivered into a cell. These include transfection, electroporation, and viral-based delivery. The advantages and disadvantages of each method are summarised in Table 4.1. Physical methods of delivery include electroporation that uses a high voltage electrical pulse to open pores in the cell membrane and allow siRNAs or shRNAs to diffuse into the cell (244). The most common method of nucleic acid delivery is via transfection using lipofection or lipid transfection using liposome particles. The liposome encapsulates the nucleic acid, which are then endocytosed by the cell or fuse directly with the cell membrane to release the nucleic acid into the cell (245). This method of transfection is easier to use than viral vectors but tends to have a lower transfection efficiency (246). Cationic polymers are also used for

nucleic acid delivery. These bind to the nucleic acid molecule and create an overall positive charge under the correct conditions allowing attachment and internalization via endocytosis or fusion with the cell membrane (246). Viral-mediated delivery is commonly used to transfer shRNA molecules into the cell and integrated into the genome as described in section 4.1.3. siRNA is usually easier to transfect into a cell than shRNA due to shRNA acting in the nucleus whereas siRNA acts in the cytosol and does not require transport to the nucleus. Additionally siRNAs are significantly shorter making it easier for delivery into the cell (247).

Table 4.1 Nucleic acid delivery into a cell. The advantages and disadvantages of each method of nucleic acid delivery into a cell

	Delivery mode	Advantages	Disadvantages
Transfection	<ul style="list-style-type: none"> • Cationic polymers • Liposomes (248) 	<ul style="list-style-type: none"> • Can be used on the majority of cell types (248) 	<ul style="list-style-type: none"> • Transfection reagents can be toxic to some cell types • Low efficiency (249)
Physical methods	<ul style="list-style-type: none"> • Electroporation – uses electrical pulse (250) 	<ul style="list-style-type: none"> • A higher frequency of cells gain the molecule • Effective on cells that are notoriously hard to transfect (251) 	<ul style="list-style-type: none"> • Decreases cell viability by around 60% (230) • Requires expensive equipment
Viral mediated Delivery	<ul style="list-style-type: none"> • Lentivirus • Retrovirus 	<ul style="list-style-type: none"> • Can be used in vivo • Can be used for stable knockdowns (250) 	<ul style="list-style-type: none"> • Requires BSL2 facilities (252)

4.1.5 CRISPR-Cas9

CRISPR (clustered regularly interspaced short term repeats)-Cas9 (CRISPR associated protein 9) is a genome editing tool that utilises the Cas9 nuclease to cleave genomic DNA via small RNAs that target cleavage through complementary base pairing (253). CRISPR sequences are short palindromic repeats that were first identified in bacteria where they are an important immune system component to prevent viral infection (254). Cas9 is an endonuclease that cleaves DNA creating double strand breaks (DSB) after being guided to it by guide sequences inside the CRISPR complex (255). Following the double strand breaks, the cell attempts to mend the break by non-homologous end joining (NHEJ). This type of repair often results in insertions, deletions, and frame shift mutations that can result in nonsense mediated decay of the transcript, leading to a null allele and therefore gene knockout (256) (Figure 4.3). So far, three CRISPR-Cas systems have been identified, each of which comprises a set of CRISPR-associated Cas genes, an array of unique repetitive elements and non-coding RNAs (257). The unique repetitive repeats are interspaced by protospacers that are short variable sequences derived when invading viral DNA is cleaved into small fragments by the Cas nuclease and inserted into the CRISPR locus. In combination, this is known as CRISPR RNA (crRNA). crRNAs are always associated with protospacer adjacent motifs (PAMs) (258). Cas9 from different bacterial species have different PAM requirements, which means that the site to be targeted must contain a specific sequence and precede a PAM site. For example, in the system derived from *Streptococcus pyogenes*, the DNA target must come directly before a 5'-NGG PAM where N represents either A, C, G or T (259).

CRISPR-Cas9 (type II) is the simplest and best-characterised CRISPR system to date (260). This system only requires one Cas gene (Cas9) and in total three components which are the Cas9 protein, the crRNA and transactivating crRNA (tracrRNA). Each unit of crRNA contains a guide sequence of approximately 20 nucleotides which enables the binding to the correct complementary sequence (254). The function of the CRISPR-Cas9 system can be recreated in mammalian cells where the crRNA and the tracrRNA can be joined together to create one single guide RNA (sgRNA). The 20 nucleotide sequence within this guide RNA can be specified so that the Cas9 nuclease can be directed towards any gene of

interest if it is adjacent to a PAM sequence. This base pairing makes it a highly efficient method of gene editing (254, 261).

The dual nickase CRISPR-Cas9 approach uses two mutant nickase versions of Cas9 (Cas9n) in combination with two sgRNAs. The guide sgRNAs are complementary to opposite strands of the target sequence. The Cas9n only nicks one strand of the DNA. When two nicks occur together the repair is usually carried out by NHEJ which results in gene knockout as described above. However, when just one nick is made the type of repair is usually a less error prone method such as base excision repair (262). Both nicks are required to result in NHEJ and subsequent gene knockout, which only happens when both nicks are made at their target sites. Therefore, the dual nickase approach reduces the chances of off-target effects (263).

CRISPR is used widely in molecular biology as a tool for gene knockout and genetic manipulation to study gene function, in a similar way to siRNA and shRNA. The advantages of CRISPR compared to siRNA and shRNA is that a complete gene knockout can be achieved. This is important as in some cases, even the low amount of RNA remaining after gene knockdown can result in the retention of protein function even at low levels of expression. It is hoped that gene editing may one day be used as a therapeutic intervention to treat genetic conditions such as Huntington disease and cystic fibrosis (264). Currently, CRISPR-Cas9 technology is being tested in *in vivo* mouse models. Non-Small Cell Lung Cancer (NSCLC) cells were modified using CRISPR to lose resistance to a drug called Osimertinib, a growth factor receptor tyrosine kinase inhibitor, and injected into nude mice. These cells formed tumours *in vivo* and Osimertinib inhibited the growth at the same rate as the control, showing that the CRISPR modification had reduced the cells' resistance to Osimertinib (265). So far, no tests have been successfully completed that have modified cells in an *in vivo* setting; this is due to the problem of delivering the CRISPR construct to the target cells.

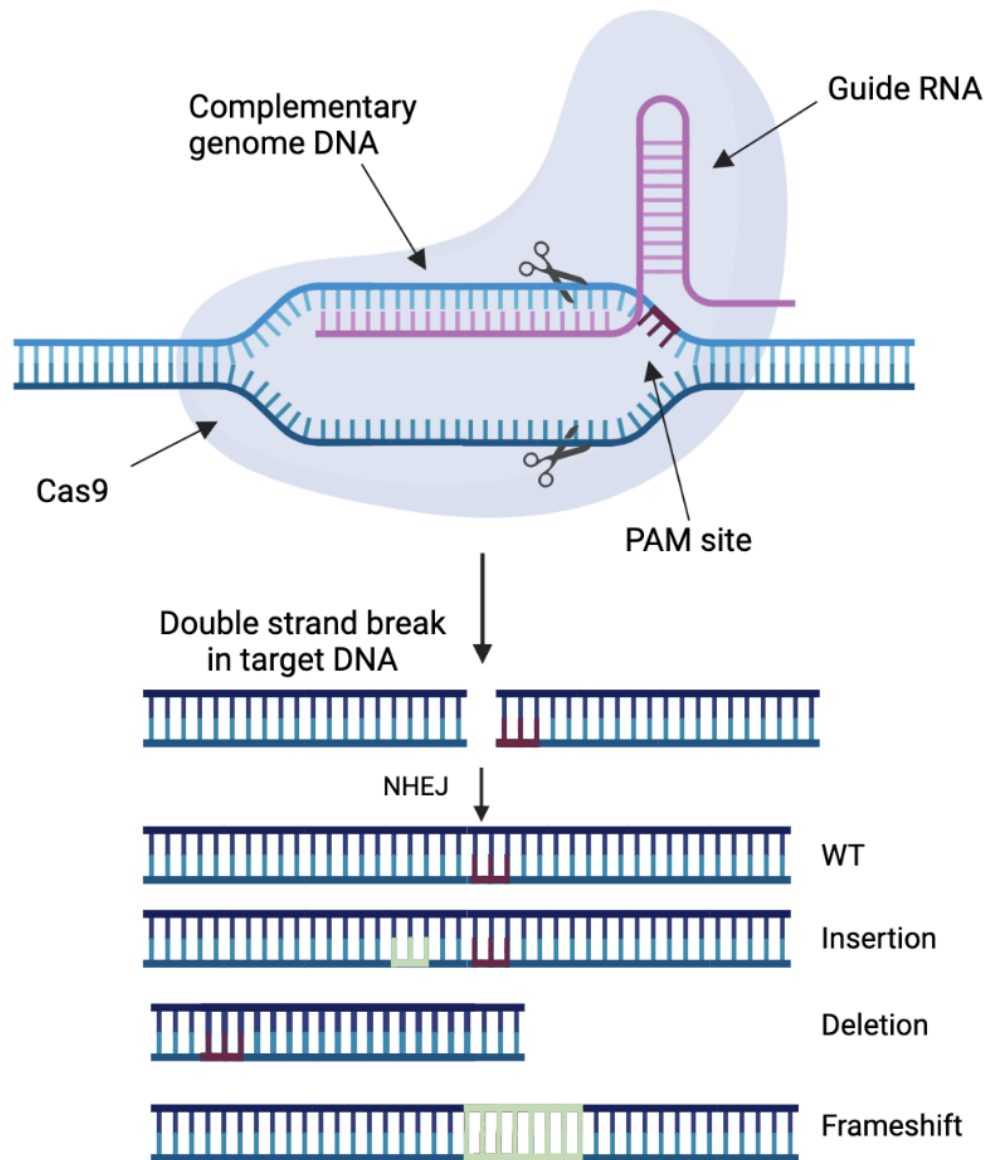


Figure 4.3. CRISPR-Cas9 genome editing. Cas9 binds to the guide RNA and is guided to the complementary DNA sequence immediately before a PAM sequence. A double strand break is created by the Cas9 that results in Non-Homologous End Joining (NHEJ) causing insertions, deletions or frameshift mutations.

4.1.6 Validation of knockdowns

4.1.6.1 Quantitative Polymerase Chain Reaction (qPCR)

Upon gene knockdown or knockout, expression of the gene and often the associated protein must be validated. One of the most common methods of gene expression validation is via quantitative Polymerase Chain Reaction, more

commonly referred to as qPCR (266). qPCR is a nucleic acid quantification method used extensively in molecular biology. RNA can also be quantified via qPCR but must first be transcribed to complementary DNA (cDNA) before amplification (267). The term 'quantitative' is used because the amplification of the DNA is monitored in real-time and allows the user to determine the exact starting amounts of DNA present in the sample.

qPCR uses a thermostable DNA polymerase originally identified in the bacterium *Thermus aquaticus* (268). At each cycle, the cDNA is denatured allowing the primers to bind, and the polymerase to amplify a short part of the cDNA. After each cycle the amount of DNA present is doubled so that total DNA is increased exponentially over a number of cycles. In order to quantify the DNA, fluorescent dyes that intercalate with any double stranded DNA present, or fluorescently labelled sequence specific probes are also added to the reaction. The amount of DNA present can therefore be monitored using the fluorescent signal seen when the DNA is doubled. The qPCR process lasts around 35-40 cycles, and a threshold for the fluorescence is set. The number of quantitation cycles (C_q) it takes for the threshold fluorescent signal to be reached is proportionate to the starting amount of DNA present. Therefore, a lower C_q value means there was more DNA present to start with. By determining at the C_q value of a given gene in a sample, and standardising this to a house-keeping gene across all samples, the user can determine the relative starting amount of DNA present in each sample (269). Therefore, qPCR can be used to determine if a sample has reduced expression of a target of interest following knocked down.

One major advantage of qPCR is the ability to analyse data easily and without the need for the user to develop complex bioinformatic scripts. A disadvantage is only a limited number of target molecules can be assessed at one time. Other more complex techniques might be favoured to look at multiple targets, such as next generation sequencing (NGS) of cDNA. However, NGS and qPCR are orthogonal methodologies that meaning that qPCR can be used to further validate NGS findings (270).

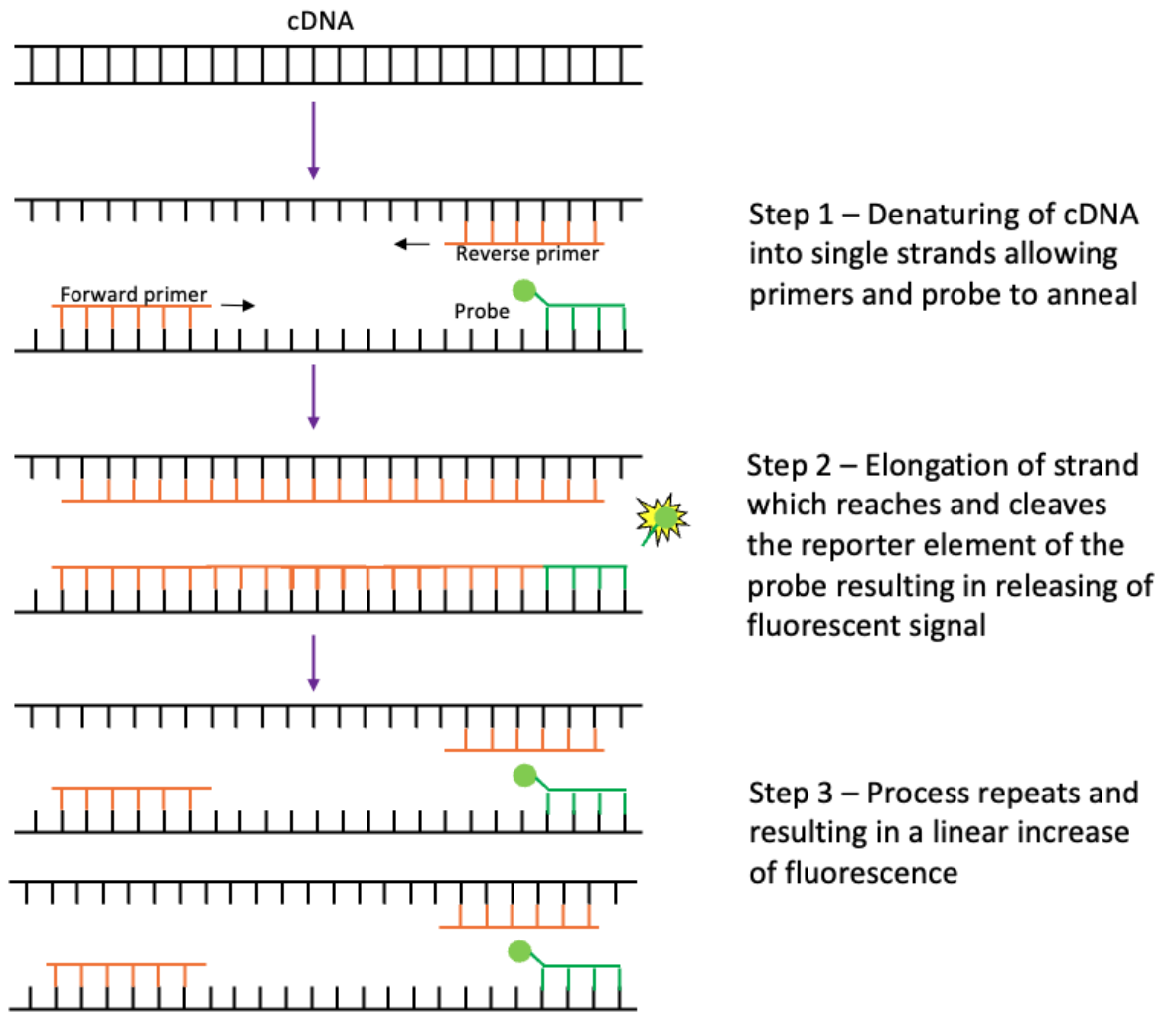


Figure 4.4 qPCR process. Double stranded cDNA is denatured allowing the probe and primers to bind. Elongation of cDNA strand begins, and this reaches and cleaves the reporter element of the probe which results in the release of a fluorescent signal. The process repeats resulting in a linear increase in fluorescence.

4.1.6.2 Western blotting

Western blotting is a method that can be used to validate the reduction in protein expression levels following gene knockdown or knockout or to validate the size of a given protein within a mixture of all the proteins that have come from a certain cell type (271). The western blotting technique involves three main steps. The first is to separate the proteins by size which is followed by transferring these proteins to a membrane and finally the visualisation of the desired proteins using

primary and secondary antibodies and detection. The main steps of the process are summarised in Figure 4.5.

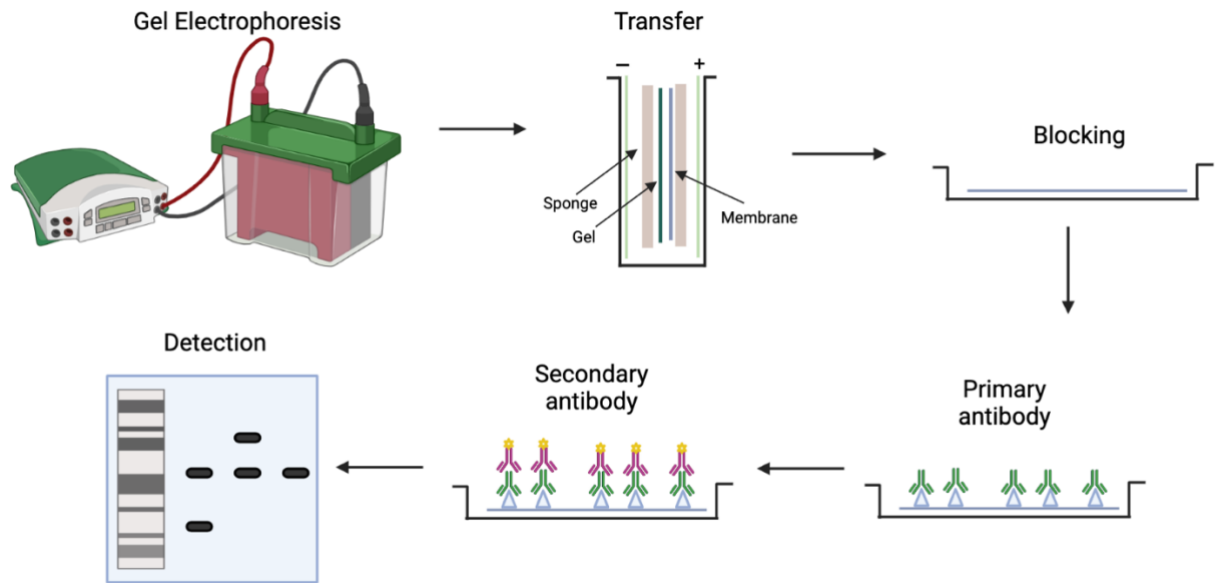


Figure 4.5. Western blot overview. Gel electrophoresis separates the proteins by size. Following this, transfer allows the separated proteins to be transferred from the gel to a membrane. Following transfer, blocking of the membrane is performed to ensure no non-specific binding of the primary and secondary antibodies to the membrane where there is no protein attached. Detection must occur to be able to visualise where the bands are for the desired protein.

4.1.7 Inhibitors

Inhibitors are widely used to investigate the role of proteins within a cell. By reducing the function of a protein, the effect on molecular processes or phenotypes, such as the ability to evade treatment, can be observed. Inhibitors often have very potent effects across cells grown as a monolayer meaning so that high scale experiments can be easily established, particularly those that vary inhibitor concentrations resulting in inhibition of the protein at varying levels (272, 273). Furthermore, some inhibitors are reversible meaning subsequent re-activation of the protein can be achieved (273).

However compared to direct gene-targeting methods, their use can be problematic. For example, because inhibitors target the protein product of the gene and not the gene directly, there may be non-canonical functions of the gene that contribute to treatment resistance, which inhibition of the protein will not

model. Therefore, if there is no difference seen upon inhibition of a protein, that does not rule out that the gene of interest is important and could be acting in a different unknown way. Furthermore, inhibitors are often not specific to one protein and instead target a number of proteins with varying levels of potency leading to either off-target or even pleiotropic effects (274).

4.1.7.1 TauT Inhibitors

There are many TauT inhibitors available and often these have effects on both TauT and the γ -aminobutyric acid type A (GABA_A) receptor. Guanidinoethyl sulfonate (GES) and imidazole-4-acetic acid (IAA) and gaboxadol (GAB) (275-278) are three examples of compounds that have been shown to interact with both TauT and GABA_A receptor. Each of these known TauT antagonists has an inhibitory effect on both TauT and GABA_A receptor, but to differing extents (Table 2). GES is a strong antagonist for TauT resulting in inhibition of taurine transport via TauT but is also a weak GABA_A receptor inhibitor (279). In experiments by Suarez *et al.*, the level of γ -aminobutyric acid (GABA) in the brains of rats did not decrease following treatment with of GES (275, 280). In addition, GES inhibits both PAT1 and GAT1, both of which transport taurine and GABA into the cell. Furthermore, GES is a competitive inhibitor of the glycine-receptor mediated taurine response in mice but is not able to decrease the level of glycine or GABA in the brains of rats or mice (275, 280). IAA is also a strong TauT antagonist and was identified by Valembois *et al.*, as a lead structure for interaction with the taurine transporter TauT (275). In addition, IAA inhibits the GABA_A receptor at a medium to low level but there are no other known targets of this compound. In contrast, GAB is a weak TauT antagonist with no significant difference on taurine influx seen on the addition of 2 mM GAB in the ARPE-19 retinal pigment epithelium cell line (275). Furthermore, GAB is a strong GABA_A receptor agonist that resulted in 78% agonist-induced response in a human embryonic kidney (HEK293) cell line (276). So overall GAB is a GABA_A agonist, and a weak TauT antagonist.

There are no recorded studies on the effect of pentylentetrazol (PTZ) on TauT, however PTZ is an antagonist of the GABA_A receptor in a concentration-dependent manner, making it a useful tool for investigating the effect of GABA transport independent of TauT (281). Using combinations of agonists and

antagonists can help dissect the mechanism of TauT that transports both taurine and GABA into a cell.

Table 4.2. The inhibitory effect on TauT and GABA_A receptor. The inhibitory effect of four compounds on TauT and GABA_A receptor.

Compound	Effect on TauT	Effect on GABA _A Receptor
Guanidinoethyl sulfonate (GES)	Strong antagonist (276)	Weak antagonist (280)
Imidazole-4-acetic acid (IAA)	Strong antagonist (275)	Medium to low inhibition (276)
Gaboxadol (GAB)	Weak antagonist (275)	Strong agonist (276)
Pentylentetrazol (PTZ)	Unknown	Strong antagonist (281)

4.2 Aims and objectives

The aim of this chapter was to investigate the association between *SLC6A6* expression and sensitivity to standard treatment in GBM *in vitro*.

Objective 1 – knockdown the expression of *SLC6A6* in the three chosen cell lines; A172, GBM58 and GBM63.

Objective 2 – Assess differential treatment sensitivity in the chosen 3D model using spheroid size measurements and CellTiter-Glo 3D assay.

4.3 Results

4.3.1 *SLC6A6* siRNA knockdown does not result in differential treatment response

To assess whether *SLC6A6* contributes to treatment resistance in GBM cell lines, siRNA knockdowns were performed, followed by treatment with temozolomide (TMZ) and irradiation. This was to investigate two main points: the first was to see the effect of knocking down *SLC6A6* and the second was to assess the impact of TauT on treatment response in *in vitro* experiments.

siRNA knockdown was performed successfully in all three cell lines with over 90% knockdown of *SLC6A6* achieved at the RNA level at 24 hours post-transfection validated via qPCR (Figure 4.6). 24 hours after transfection, cells were treated with 30 μ m TMZ and 2Gy irradiation. MTT assays were performed 48 hours after treatment to assess the effect of standard treatment on cell viability following *SLC6A6* knockdown. No significant differences in treatment response were seen between the non-targeting (NT) control and the *SLC6A6* knockdowns in GBM58, GBM63 and A172 cell lines (Figure 4.7). For the GBM58 cell line only one biological experiment was performed, and no differences were observed. To investigate the effect of treatment resistance in a more stable spheroid model, shRNA knockdown was used.

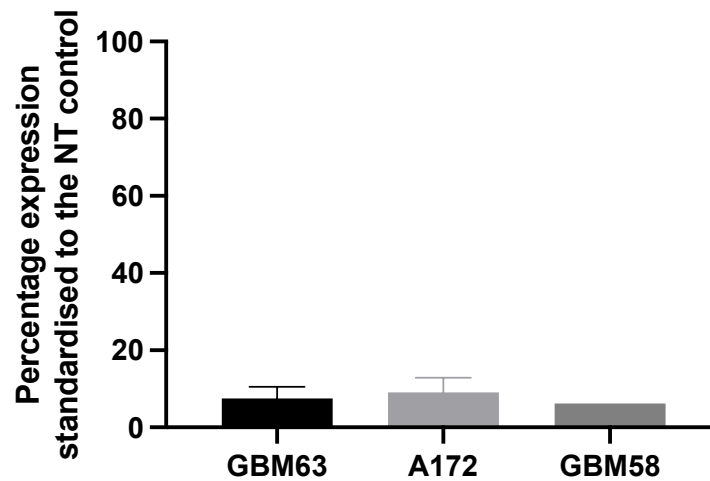


Figure 4.6 siRNA knockdown of *SLC6A6*. qPCR validation of expression of *SLC6A6* compared to the NT control 24 hours post-transfection with siRNA. A172 = 9.1% (n=2), GBM63 = 7.5% (n=3) and GBM58 6.2% (n=1). Percentage expression \pm SEM is plotted.

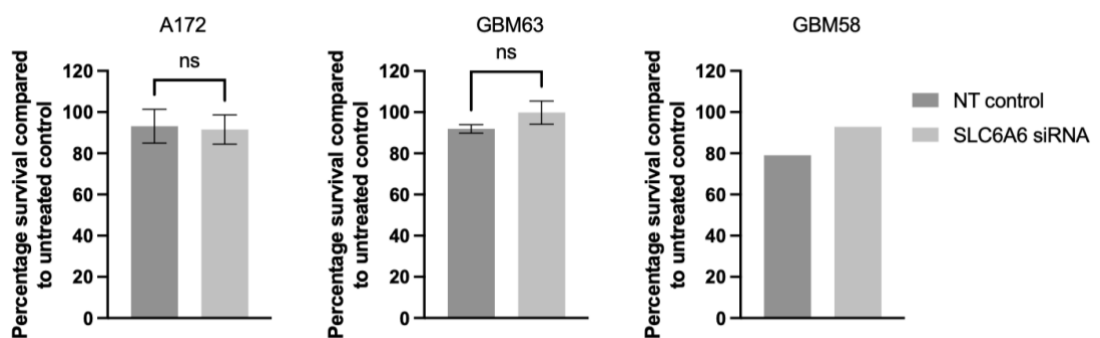


Figure 4.7 Treatment response following siRNA knockdown. The treatment response to 30 μ M TMZ and 2 Gy irradiation in A172 (n=2), GBM63 (n=3) and GBM58 (n=1) following siRNA knockdown. Percentage survival of treated versus untreated cells \pm SD is plotted. Statistical significance of pair-wise comparisons based on an unpaired Student's t-test showed no significant differences between the NT control cells and matched *SLC6A6* knockdown cells in any of the cell lines. ns = non-significant.

4.3.2 shRNA knockdown of *SLC6A6* in A172 and GBM63

4.3.2.1 Knockdown and validation

As *SLC6A6* siRNA appeared to have no effect on treatment resistance in 2D cultures I decided to use shRNA to permanently *SLC6A6* knockdown allowing longer term experiments in spheroids. The aim was to determine if TauT expression can affect treatment resistance in GBM cell lines using a more physiologically relevant model. Initially, I used four different shRNA constructs co-expressing GFP and a puromycin resistance gene in the A172 cell line.

A puromycin response assay was performed to determine the optimal puromycin concentration for selection of A172, GBM58 and GBM63 post transfection (Figure 4.8) and indicated an optimal dose of 2.5 μ g/mL.

48 hours after transfection, cells expressed GFP indicating successful transfection. Puromycin selected cells were subsequently analysed via qPCR which revealed successful knockdown of *SLC6A6* mRNA in the A172 cell-line for all four constructs (Figure 4.9). Construct 153000 had the most significant reduction in *SLC6A6* expression (65 \pm 5% reduction, p=0.0002). To determine protein expression of TauT, western blotting was performed on each of three biological repeats created for each of the four constructs and the NT control. Protein knockdown could not be validated, with no band of the expected 70 kDa size for *SLC6A6*, and furthermore of the protein bands that were visualised, none decreased in the knockdown samples (Figure 4.10). It is important to note that none of these antibodies had been previously validated for TauT expression.

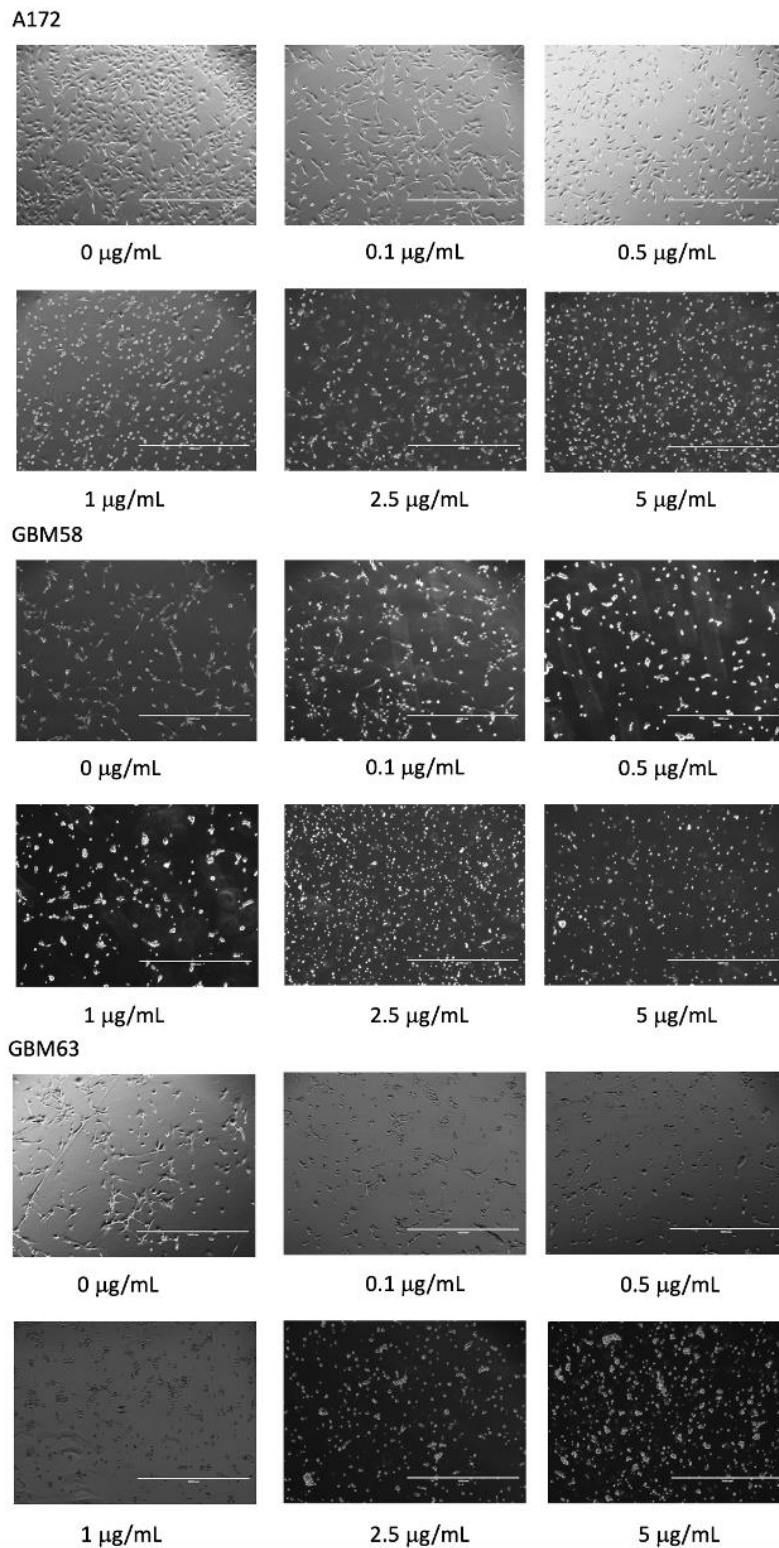


Figure 4.8. EVOS images of puromycin response. EVOS images of puromycin response at different concentrations of puromycin ranging from 0 $\mu\text{g/mL}$ to 5 $\mu\text{g/mL}$ for untransfected A172, GBM58 and GBM63 cell lines after 24 hours treatment. For all three cell lines, 2.5 $\mu\text{g/mL}$ resulted in complete cell death and was chosen as the optimal dose for selection.

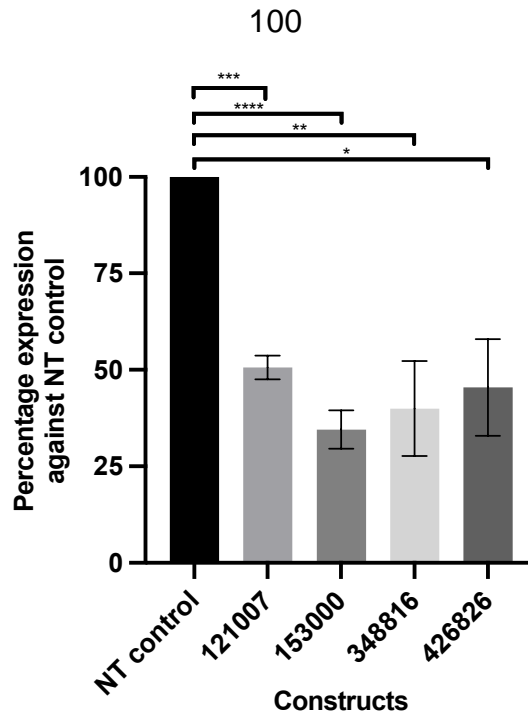


Figure 4.9. qPCR validation of four shRNA constructs each used to knockdown the expression of SLC6A6 in A172. The mean percentage expression compared to the NT control \pm SEM is plotted, $n=3$. Construct 153000 has the most significant reduction in SLC6A6 expression ($65\pm 3\%$ reduction). The information sought from this assay was to determine level of knockdown compared to the NT control. The difference between the levels of knockdown for each construct compared to another was not required. Therefore, Statistical significance of pair-wise comparisons are based on an unpaired Student's t-test and shown as *($p < 0.05$), **($p < 0.005$), ***($p < 0.0005$), and ****($p < 0.0001$).

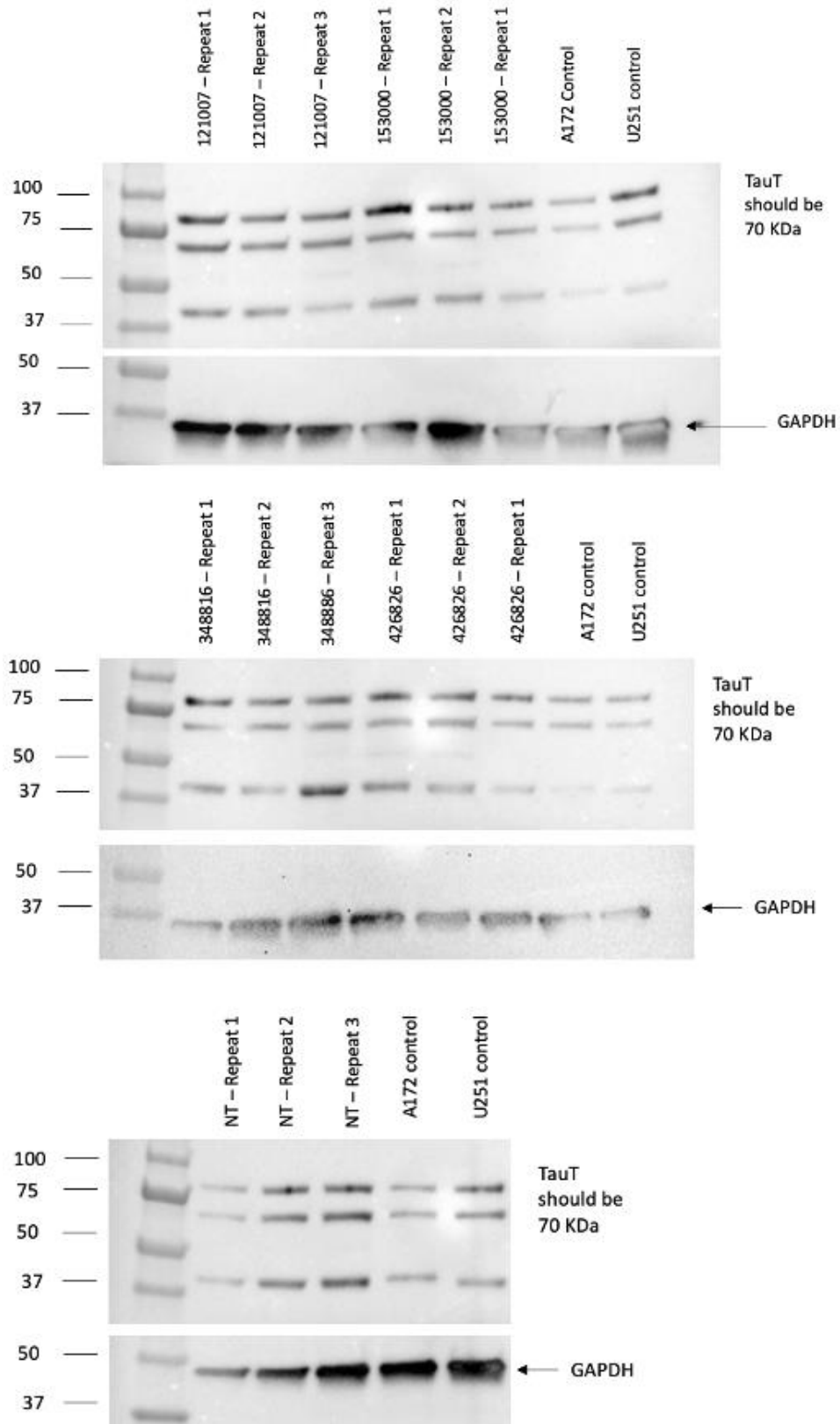


Figure 4.10 Decreased TauT protein levels were not observed by western blot following shRNA transfection. An example of a Western blot analysis using abcam antibody ab196821. A band a bit bigger than the 70 kDa expected for TauT was seen. Smaller bands are also seen, assumed to be smaller protein isoforms or non-specific bands are also observed.

To investigate if there was an experimental error in the shRNA knockdowns, qPCR probes were mapped onto the different *SLC6A6* isoforms along with the location of the shRNA targets and the location that the antibodies bind (Figure 4.11). From this analysis, the isoform detected by the antibody should be the isoform determined by qPCR. The lack of evidence for protein loss may be because the anti-TauT antibodies do not have validated specificity, or mRNA knockdown was insufficient to give rise to a detectable decrease in protein levels. Nonetheless, without creating a complete knockout, it cannot be determined if cells stably expressing the shRNA constructs result in knockdown of TauT. However, *SLC6A6* knockdown is still of interest as it could be involved in treatment resistance independently of the expression levels of TauT.

With this in mind, shRNA construct 153000 was used to create an *SLC6A6* knockdown in GBM63 and GBM58. GBM58 shRNA was unsuccessful with multiple attempts at knockdown each resulting in loss of GBM58 cells following transfection. shRNA in GBM63 appeared successful with cells expressing GFP and puromycin resistant. However, qPCR analysis showed that *SLC6A6* expression was not knocked down (Figure 4.12). Therefore, survival analysis if shRNA cell lines culture as spheroids was only performed in A172.

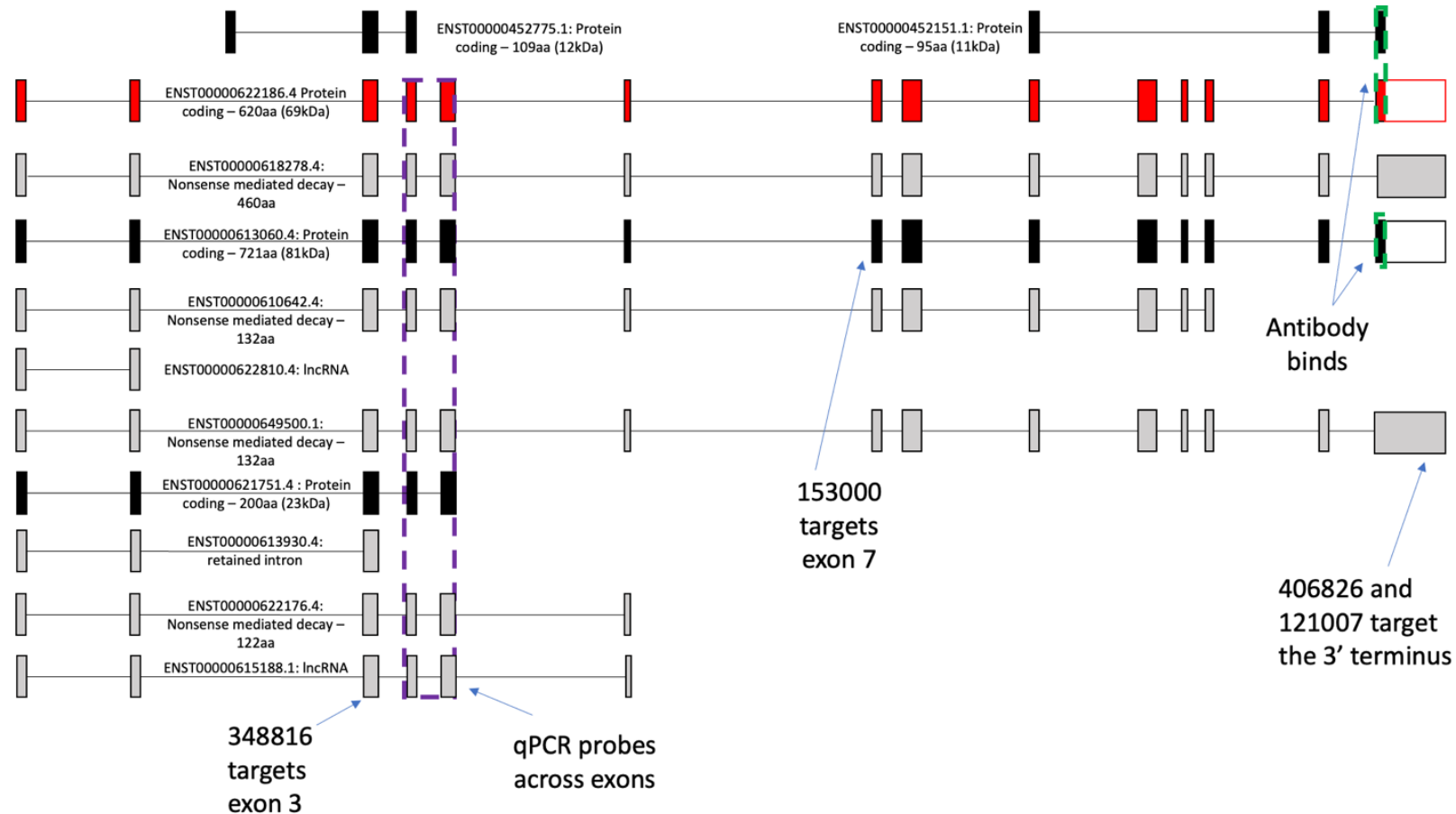


Figure 4.11. Map of *SLC6A6* isoforms. *SLC6A6* isoforms with the locations of the antibody, qPCR probes and shRNA constructs (153000, 406826, 121007, 348816) shown. shRNA constructs bind to the exons shown. Canonical Ensembl transcript is shown in red, all other protein coding *SLC6A6* isoforms are shown in black.

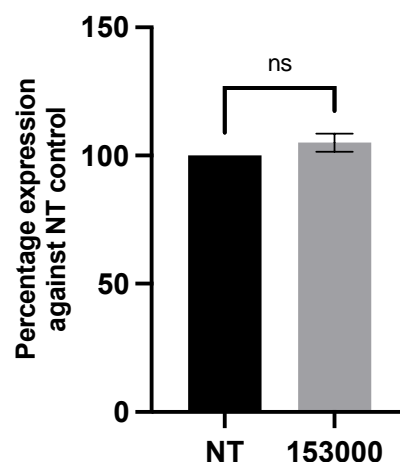


Figure 4.12. qPCR validation of *SLC6A6* shRNA knockdown in GBM63. qPCR validation of shRNA construct 153000 used to knockdown the expression of *SLC6A6* in GBM63. The mean percentage expression compared to the NT control \pm SEM is plotted, $n=3$. P-values are based on an unpaired t-test and shown as ns = non-significant, *(< 0.05), **(<0.005), ***(<0.0005), and ****(<0.0001).

4.3.2.2 Treatment experiments on shRNA spheroids show differential treatment response

Experiments using spheroids and the chosen treatment were setup using A172 and GBM63 shRNA cell lines. The shRNA construct used for these experiments was 153000 as this proved to mediate the most successful knockdown in A172 cells. As optimised in section 2.4 spheroids were set up for 5 days following seeding, before being treated with 30 μ M TMZ and 2Gy irradiation. 14-days post-treatment, spheroid area (μm^2) was assessed using the bespoke confocal imaging and analysis platform described in section 3.3.2.1 and 20 spheroids were subject to the CellTiter-Glo 3D cell viability assay to measure ATP levels. For A172, a significant difference in treatment response (assessed as the change in size of treated versus untreated spheroids) was observed in the *SLC6A6* knockdown spheroids compared to the non-targeting ($p<0.05$) with knocked down spheroids being more affected by treatment than the control (Figure 4.13). CellTiter-Glo 3D cell viability assays showed that in *SLC6A6* knockdown A172 cells there was a non-significant trend towards less metabolically active cells (as denoted by the amount of ATP present) compared to their NT control (Figure 4.14). This result indicates that knocking down *SLC6A6* causes A172 cells to be more sensitive to standard treatment.

The protein levels for TauT could not be validated due to the lack of antibodies. In addition, GBM58 and GBM63 *SLC6A6* shRNA was never achieved as the cells repeatedly died upon transfection or did not show reduced *SLC6A6* levels after transfection. Therefore, I attempted to use CRISPR-Cas9 gene editing as an alternative knockdown method to validate the A172 results.

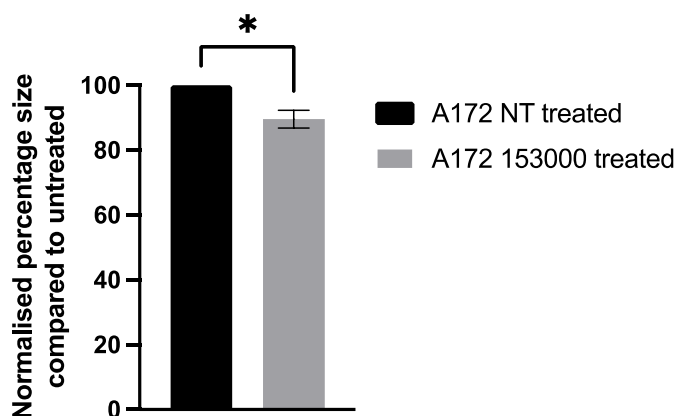


Figure 4.13. Percentage area of spheroids compared to untreated. The percentage size (mean area, μm^2) difference \pm SD between treated and untreated spheroids is plotted, comparing A172 NT control and *SLC6A6* knockdown (153000) spheroids. $n=3$, $p<0.05$ based on an unpaired t-test.

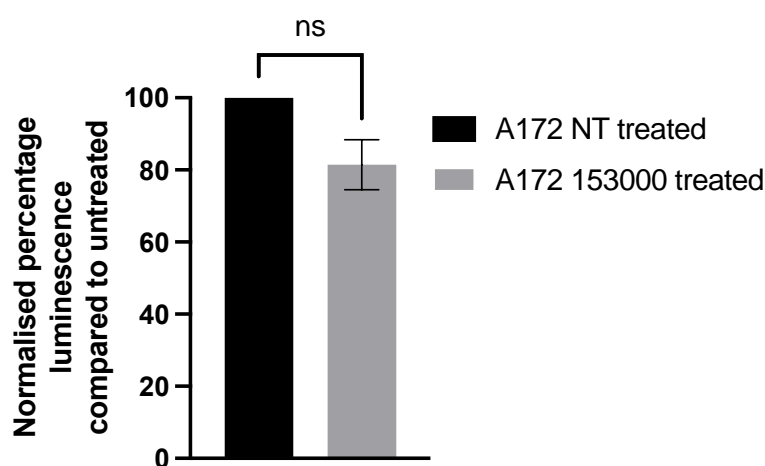


Figure 4.14. Percentage luminescence of spheroids compared to untreated. The mean luminescence of A172 NT control and 153000 spheroids shown as a percentage \pm SD in comparison to their untreated counterparts. $n=3$, ns = non-significant determined by an unpaired t-test.

4.3.3 Knockout of *SLC6A6* using CRISPR-Cas9 gene editing

CRISPR-Cas9 gene editing was attempted to knockout the expression of *SLC6A6* in all three cell lines. The dual nickase approach was chosen due to its lower off target effects. I designed two pairs of sgRNA that would target *SLC6A6* exon 5 of the canonical transcript. The guides were cloned into the px461(GFP) or px462 (puromycin resistance) plasmid vectors (Figure 4.15) and their insertion verified by Sanger sequencing (not shown). Transfection of the plasmids into the cells has been attempted multiple times with varying ratios of lipofectamine to DNA and a range of lipofectamine reagents. This included Lipofectamine 2000, Lipofectamine 3000, and Lipofectamine Stem, but unfortunately each attempt proved unsuccessful with complete loss of cells following transfection. To determine if these cells were not transfectable with plasmids or if these constructs were cytotoxic, each cell line was transfected with an empty px461 construct containing no guide RNA. Cells were successfully transfected and showed GFP expression (Figure 4.16) showing that these cell lines were capable of being transfected.

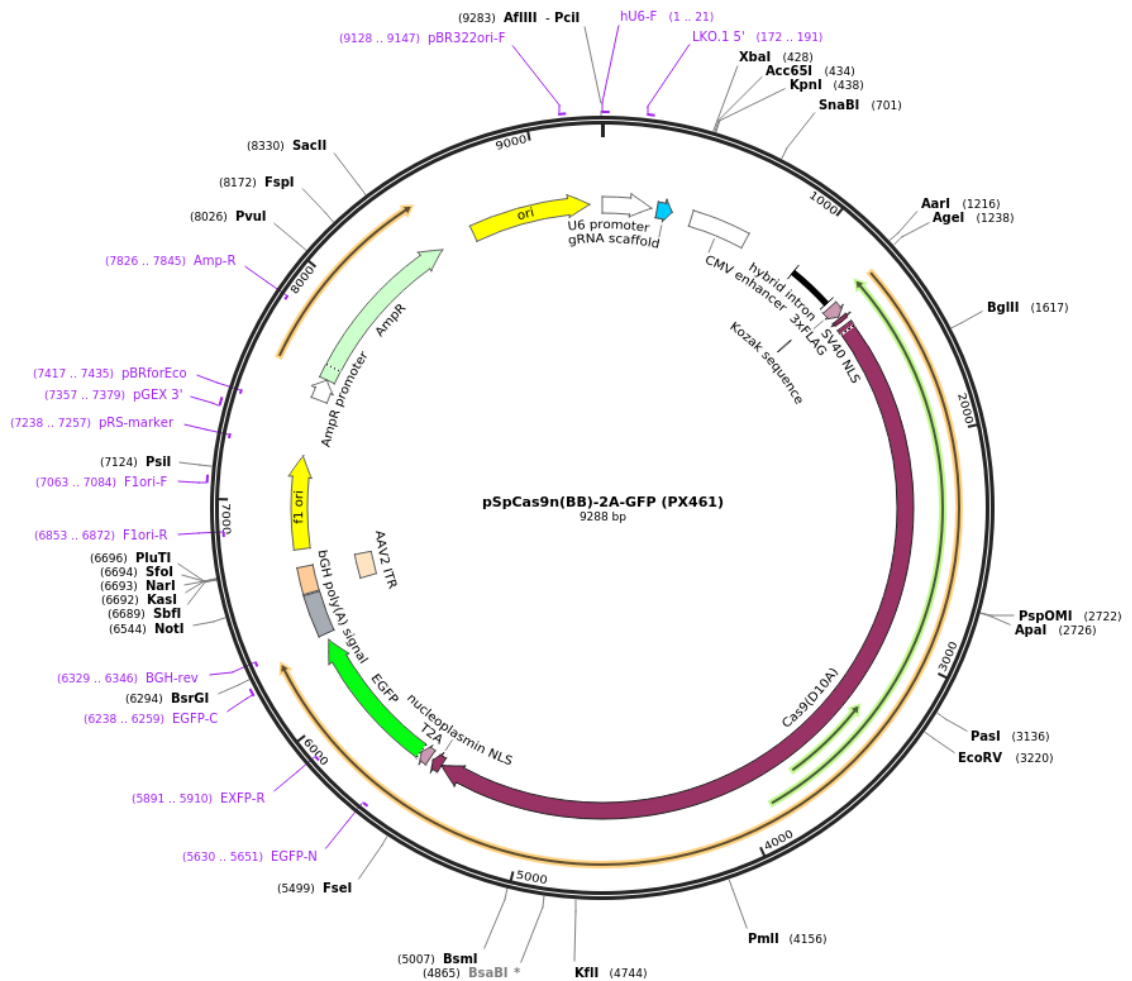


Figure 4.16. Cells expressing GFP. A172, GBM63 and GBM58 cells expressing GFP after transfection with an empty px461 construct containing no guide RNA using Lipofectamine 2000 demonstrating that these cells have the capability to be transfected. |Scale bar is 400 μm .

To test the efficiency of the CRISPR guides, *SLC6A6* knockout was attempted in HEK293T cells which are easier to transfect. Following transfection, cells were cultured in puromycin to confirm the uptake of plasmid PX462, and it was confirmed by EVOS microscopy that surviving cells were also positive for GFP. Individual GFP positive cells were FACs sorted into wells in 96-well plates and left to form clones. All clones that formed were cultured further and cells were pelleted prior to extraction of protein and RNA harvesting. Sanger sequencing was used to confirm the presence of a DNA mutation in the 6 clones that formed. Sanger sequencing showed that the targeted region was still present, meaning *SLC6A6* was not knocked down.

The results so far showed that CRISPR was unsuccessful. This in combination with the impact of the COVID-19 pandemic and the potential short term closing of the lab meant the decision was made to move onto experiments that could be performed on a shorter time scale. This meant that work to optimise CRISPR was halted and instead experiments focusing on antagonists and agonists used instead.

4.3.4 The use of inhibitor to target TauT

4.3.4.1 The effect of TauT inhibitors on cell lines

Previously, efforts have focused on knocking down or knocking out *SLC6A6* and assessing the response to treatment. As the protein levels following knockdown could not be validated, it was not possible to determine if treatment effects are due to the decrease in levels of *SLC6A6* protein, an unknown non-coding function of the *SLC6A6* transcript or an off-target effect. Using inhibitors that directly target TauT will provide key insight into its role in treatment response. Two inhibitors, guanidinoethyl sulfonate (GES) and gaboxadol (GAB), were chosen for use.

A range of concentrations of GES and GAB were used and added onto day 5 A172 spheroids and incubated for 7 days. I aimed to identify a concentration for both inhibitors that resulted in a large difference in spheroid size compared to the control, providing a high enough dose to have an effect and allow any differences

in treatment response to be seen in later experiments. The information sought from these assays was to determine the effect each concentration of drug compared to the solvent. The effect of each concentration of drug compared to another was not important. Therefore to compare the two groups, unpaired Student's T-tests were used (unless stated otherwise) between solvent controls and each dose of the inhibitor.

For A172, concentrations of 1 and 10 mM of both GAB and GES significantly increased the size of spheroids, compared to vehicle control ($p < 0.005$ and 1 mM and $p < 0.0005$ for 10 mM). For GBM58, only 10mM GES or GAB showed any significant differences ($p < 0.05$ and $p < 0.0001$ respectively), however these changes were in the opposite direction to those observed in the A172 cell-line resulting in a reduction in spheroid size compared to the control. No significant differences were seen in GBM63 at any concentration of GES. Similarly to GBM58, the addition of 10 mM of GAB resulted in significantly smaller spheroids in GBM63 ($p < 0.0001$) (Figure 4.17). To ensure consistency between treatment experiments with the inhibitor, 10 mM concentration of each inhibitor was used for all three cell lines.

The effect of GES and GAB and the vehicle control on spheroid size was performed with a higher number of technical repeats (Figure A.1). When observing the effect of GES alone on spheroid size, in all three replicates the addition of GES resulted in significantly larger spheroids derived from the A172 cell-line ($p < 0.0001$). In GBM58, GES resulted in significantly smaller spheroids in two of the repeats ($p < 0.0001$) with no significant differences seen in the third repeat. This is also the case in GBM63. When observing the effect of GAB alone on spheroid size, in A172 GAB results in an increase in spheroid size in two out of three repeats ($p < 0.0001$) and no significant differences in the third repeat. For GBM58, GAB results in significantly smaller spheroids in two of the repeats ($p < 0.0001$) with no significant changes seen in the third repeat whereas GAB results in significantly smaller spheroids across all three repeats in GBM63 ($p < 0.0001$).

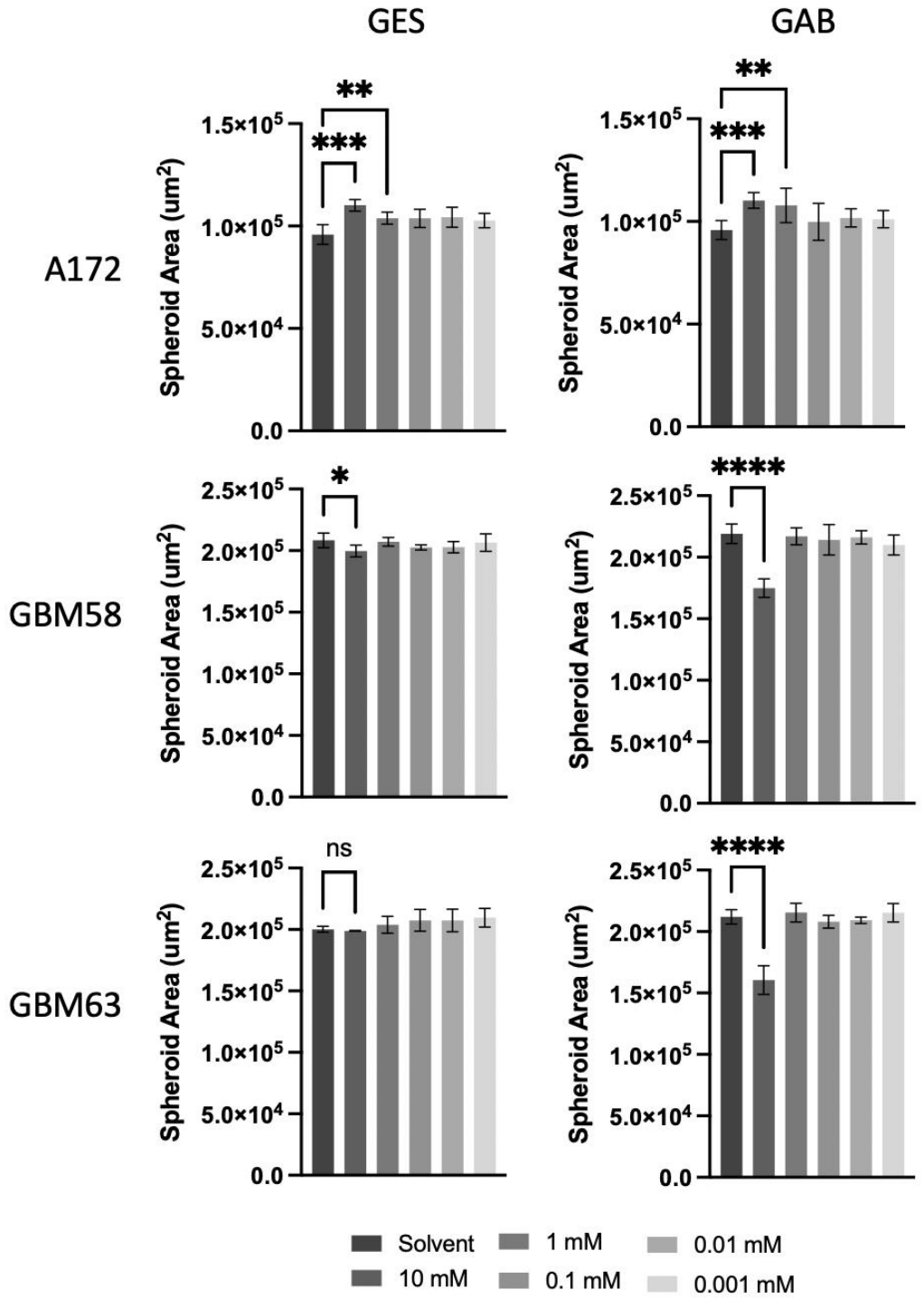


Figure 4.17. Effect of guanidinoethyl sulfonate and gaboxadol on cell lines.

The mean spheroid area (μm^2) \pm SD of A172, GBM58 and GBM63 one week post treatment with 10 mM, 1 mM, 0.1 mM, 0.01 mM, 0.001 mM of guanidinoethyl sulfonate (GES) and gaboxadol (GAB) and a vehicle control of water. One biological repeat performed with n=4 technical repeats (one experimental repeat with 4 spheroids treated per dose). The information sought from this assay was to determine the effect each concentration of drug compared to the solvent control to determine a single suitable dose for future assays. The effect of each concentration of drug compared to another was not important. P-values are based on an unpaired t-test and shown as *(<0.05), **(<0.005), ***(<0.0005), and ****(<0.0001).

4.3.4.2 Effect of guanidinoethyl sulfonate (GES) and of gaboxadol (GAB) on standard treatment

The effect of GES, GAB or vehicle control on response to standard treatment of 30 μM TMZ and 2 Gy irradiation was measured. The main aim of these experiments is to observe the effect of standard treatment on spheroid size in the presence of GES or GAB, and to determine if this was significantly different to the effect of vehicle control. This is to see what effect, if any, GES and GAB have on standard treatment.

In order to determine the effect that GES or GAB had on the treatment (30 μM TMZ and 2 Gy irradiation), the size of treated spheroids were each expressed as a percentage size against untreated controls, resulting in a value referred to as normalised percentage spheroid size.

For A172, normalised percentage spheroid size was significantly reduced in the presence of GES or GAB compared to the vehicle control. This shows there is a significant difference in treatment response in the presence of either GES or GAB in A172 ($p < 0.05$) (Figure 4.18). These results are confirmed by the CellTiter-Glo 3D cell viability assay for GAB but were non-significant for GES (Figure 4.19).

For both GBM58 and GBM63, the normalised percentage size significantly increased in the presence GAB, compared to vehicle control ($p < 0.005$) (Figure 4.18). These results are also confirmed by the CellTiter-Glo 3D assay ($p < 0.05$) (Figure 4.19). For GBM63 spheroids, the normalised percentage size significantly increased in the presence GES compared to vehicle control ($p < 0.05$) but this

increase was not significant in the CellTiter-Glo 3D assay (Figure 4.19). For GBM58 there was no significant difference on spheroid size in the presence of GES. These results are mirrored in the CellTiter-Glo 3D assay (Figure 4.19).

There are two main findings from these results. The first is that the effect that GES and GAB have on treatment response is different in the established cell-line A172 compared to the patient-derived cell lines. Secondly, the magnitude of this effect is usually larger in the presence of GAB than GES. This is unexpected because, if TauT was conferring an effect, then there should be a larger magnitude of change in the presence of GES since this is a strong TauT antagonist. However, the inhibitors have an opposite effect on the GABA_A receptor. As well as transporting taurine, TauT also transports GABA but at a lower affinity, and inhibitory effects on GABA signalling may therefore contribute to the treatment response phenotypes.

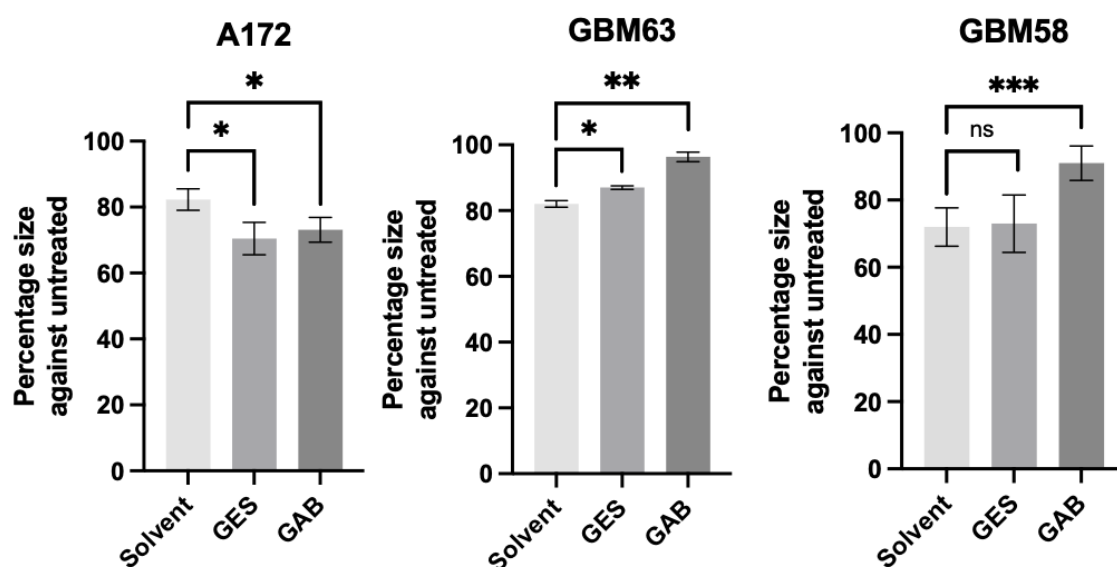


Figure 4.18. Standardised effect of Guanidinoethyl sulfonate and Gaboxadol and standard treatment on cell lines. The mean spheroid area (μm^2) \pm SEM of A172, GBM58 and GBM63 spheroid lines one week post treatment with 10 mM of guanidinoethyl sulfonate (GES) or gaboxadol (GAB) in addition to standard treatment of 30 μM TMZ and 2Gy irradiation. Results are expressed as a percentage of the size untreated spheroid with the same inhibitor. $n=3$. P-values are based on a paired t-test and shown as *(< 0.05), **(<0.005), ***(<0.0005). The direct comparison between GES and GAB was not necessary.

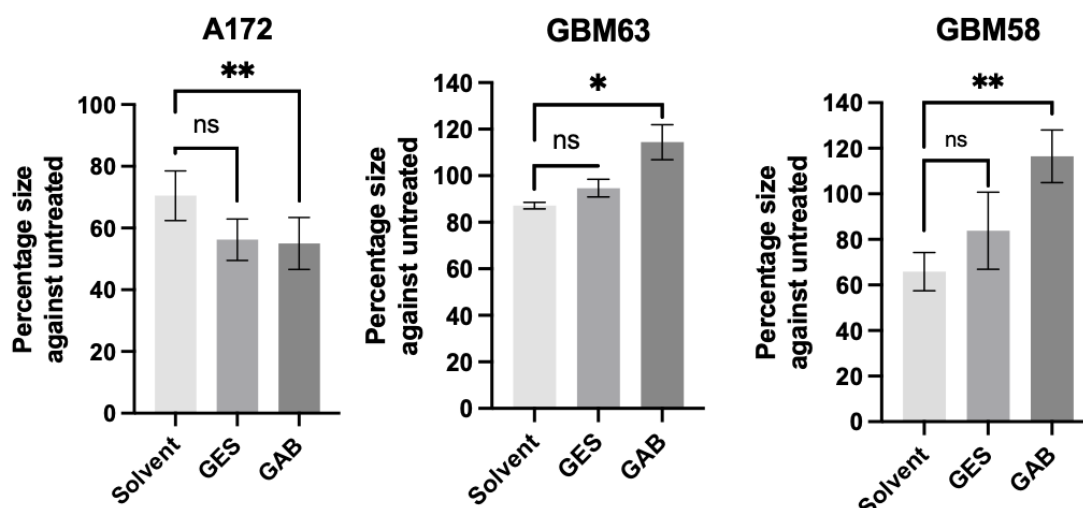


Figure 4.19. Standardised effect of Guanidinoethyl sulfonate and Gaboxadol and standard treatment on cell lines. The mean luminescence from CellTiter-Glo 3D assay \pm SEM of A172, GBM58 and GBM63 spheroid lines one week post treatment with 10mM of guanidinoethyl sulfonate (GES) or gaboxadol (GAB) in addition to standard treatment of 30 μ M TMZ and 2 Gy irradiation. Results are expressed as a percentage of the size untreated spheroid with the same inhibitor, and standardised as a percentage of the solvent control. $n=3$. P-values are based on a paired t-test and shown as ns = non-significant, *(< 0.05), **(<0.005), ***(<0.0005), ****(<0.0001). The direct comparison between GES and GAB was not necessary.

4.4 Discussion

In order to fulfil the aim of investigating the association between *SLC6A6* expression and sensitivity to standard treatment in vitro, I attempted to knock down *SLC6A6* in GBM cell lines and used these as cellular models to assess treatment response to TMZ and irradiation in relation to *SLC6A6* levels.

4.4.1 siRNA showed no difference in treatment response

The logical first step in looking at the effect of *SLC6A6* was to perform an siRNA knockdown to demonstrate if *SLC6A6* was a gene that could successfully be knocked down. siRNA transfections were therefore performed, and the knockdowns validated via qPCR proving that *SLC6A6* mRNA levels could be significantly reduced in all three cell lines.

Treatment response experiments performed after knocking down *SLC6A6* using siRNA showed no difference when compared to the control. This is contrary to what would be expected if *SLC6A6* was contributing to treatment resistance. Recently, *SLC6A6* has been associated with a hypoxic phenotype in multiple types of cancer including GBM. Neftel *et al.*, observed gene signatures associated with single cells in GBM tumours and was able to assign these to one of six main cellular states (71). Each GBM tumour will be made up of a combination of the different cellular states, but one cell type is usually more dominant than the others. Neftel *et al.*, characterised malignant cells within GBM tumours and used this to identify expression signatures of individual cells referred to as 'meta-modules' that varied across different tumours. These expression signatures were highly consistent over cells from different tumours and overlapped the signatures of multiple other tumours. This indicates that although there are these distinct signatures, there is a lot of intra-tumour heterogeneity which suggests that many biological processes in GBM biology are shared across tumours. Their analysis identified six meta-modules, two of which showed high expression of mesenchymal-associated genes. Out of these, one was associated with hypoxia response genes, and one was not, which led these to be named hypoxia-dependant and hypoxia-independent signatures. *SLC6A6* was a key gene in the hypoxia-dependant signature. The hypoxia-dependant subtype harboured high expression of multiple genes associated with hypoxia, indicating that *SLC6A6* could be closely related or even involved in the hypoxia response within GBM.

Another study looking at hypoxia-related differentially expressed genes in hepatocellular carcinoma identified *SLC6A6* as one of 12 key hypoxia-related genes that could be used a prognostic predictor for hepatocellular carcinoma (282). This could therefore be a reason why *SLC6A6* knockdown in 2D siRNA experiments is showing no effect on treatment resistance as perhaps its role in treatment resistance can only be observed or become relevant in a hypoxic environment.

There are other ways in which hypoxia could be mimicked in cell monolayers, for example with the use of a hypoxia chamber which is a sealed air-tight chamber that provides a hypoxic environment. However, hypoxia chambers can be expensive and mean that access to cells cannot be possible during the time

course of the experiment without exposing them to oxygen (283, 284). Given that spheroids often contain a hypoxic core which is one of the ways making them more physiologically relevant to GBM, and that a long-term knockdown of TauT levels is preferable, it was decided that shRNA should be used to achieve stable *SLC6A6* knockdown to enable treatment experiments in spheroids.

4.4.2 shRNA showed a difference in treatment response

shRNAs are a reagent that can be used in stable knockdown experiments. This is preferable to siRNA because it enables longer-term knockdown in a 3D model such as spheroids, whereas siRNAs typically only last around 3 days, so will be ineffective by the time the spheroids have formed. *SLC6A6* shRNA was attempted on GBM58, GBM63 and A172 cell-lines. This was successful in GBM63 and A172 but could not be achieved in GBM58 because of cytotoxicity following transfection. Due to the stem like nature of patient-derived cell lines described in section 1.7.1 they are extremely heterogeneous in nature and each cell line is entirely unpredictable, so it is common that they can act very differently to one another.

Validation of the *SLC6A6* mRNA levels following shRNA knockdown showed that *SLC6A6* transcript levels had been significantly reduced. A Western blot was performed to show the knockdown at the protein level, however the results from blotting with the *SLC6A6* antibody were inconclusive due to the inability to determine what the antibody was actually detecting.

Creating a *SLC6A6* knockout using CRISPR-Cas9 would produce a null allele and would rule out the possibility that any protein would be translated and be detected on a western blot. Without being able to validate protein levels of TauT, it is uncertain if siRNA or shRNA knockdown has been successful at the protein level. However, *SLC6A6* gene expression is the main focus of the research project, regardless of whether this is as a result of TauT, as the original observation was of elevated *SLC6A6* levels determined by RNA-seq. Therefore, any effect in my experiments can be measured at the RNA level rather than the protein level to support the original findings. With this in mind, it was still crucial that investigation into the effect of standard treatment on the knocked down *SLC6A6* cell lines was performed.

In A172 spheroids, knockdown of *SLC6A6* had a significant effect on treatment response with the size of treated *SLC6A6* knocked-down spheroids be significantly smaller than the NT control in all three repeats. This trend is also seen using CellTiter-Glo 3D assay as a measure of cell viability however is not significant. This result is expected if *SLC6A6* is contributing to treatment resistance in GBM because, without expression of this gene, cells are less viable than when subjected to standard treatment.

SLC6A6 appears to be correlated to treatment resistance in A172. Without further investigations into the levels of TauT, it is impossible to say if *SLC6A6* is acting via increased TauT expression, or if *SLC6A6* has a non-canonical function that we are unaware of which does not involve TauT.

A172 and GBM63 show differences in their response to treatment when *SLC6A6* is knocked down. This is expected because in previous experiments, such as the investigation of taurine both in monolayers and 3D (Figure 3.16 and Figure 3.17), these cell lines have different responses. This is likely due to the fundamental biological differences between A172 and GBM63 and the differences in the cellular makeup. A172 being an established cell line is highly homogeneous whereas GBM63 is highly heterogenous being a patient derived cell line.

4.4.3 Exploring CRISPR-cas9 attempt

Attempts to knockout the expression of *SLC6A6* in the cell lines was unsuccessful because no viable cells remained following transfection with plasmids. Patient-derived cell lines are often very sensitive to transfection, as seen with inability to successfully transfect GBM58 cells with the shRNA construct. However, transfection of A172, the established cell line, with shRNA constructs was successful on the first attempt so this should be able to be transfected with the CRISPR-Cas9 plasmid construct. One possibility was that plasmid preparations were cytotoxic because they contained bacterial endotoxin (285). Transfections with an empty GFP plasmid were successful in the lines, indicating that they could be transfected and therefore the cell death observed is likely due to the presence of the Cas9/gRNA or something related to the plasmid preparation. Transfection of the plasmids into a HEK293 cell-line however was successful, with transfected cells conferring both resistance to puromycin and GFP expression. Therefore, we can assume that the plasmids were not in themselves causing cell death. Despite

taking up the plasmids, sanger sequencing confirmed that there was no *SLC6A6* knockout present.

This still does not explain the cell death in the GBM cell lines upon transfection with the plasmids. One possibility is that the cells, being more sensitive and less amenable to transfection than HEK293T cells, were not cable of handling both plasmids needed for a dual nickase CRISPR approach. Each plasmid was going to be transfected into the cell without the other one to test this hypothesis, however due to the pandemic lockdown this had to be abandoned. Following the lockdown, the decision was made to move away from CRISPR due to time constraints.

4.4.4 Inhibitors of TauT and GABA_A Receptor showed differences in response to standard treatment

Agonists and antagonists are important tools for investigating protein function in molecular biology. However, one disadvantage of using these is that often they are not specific to one protein and can therefore have off-target or pleiotropic effects on other protein targets. Although the use of agonists and antagonists, can begin to dissect the differences in treatment responses, the molecular mechanisms that cause these effects remain unclear.

The inhibitors initially chosen for the investigation of TauT were guanidinoethyl sulfonate (GES) and gaboxadol (GAB). GES is a strong TauT antagonist, therefore if TauT is contributing to treatment resistance then in the presence of GES, smaller spheroids would result after standard treatment of 30 μ M TMZ and 2Gy irradiation, compared to controls. This was the case for A172, however the opposite was seen in the patient-derived cell lines, resulting in spheroids that were larger than the spheroids without GES.

As stated previously in chapter 1.7.1 the cellular homogeneity of the A172 line is an obvious biological difference with the other more heterogenous lines, a difference supported by gene expression profiles (163). Despite the heterogeneity of the GBM58 and GBM63 lines, the inhibitor results are consistent which suggests that this is due to treatment response. GBM58 and GBM63 are grown in media without FCS, which encourages the stem-like population to be maintained whereas A172 is grown in media containing FCS which enriches for the differentiated components of GBM (286). This enrichment of either stem cell

or differentiated cells could be driving the differences in treatment response. Adding FCS to the media of GBM58 and GBM63 would cause the cells to differentiate (286). It would be interesting to do this and observe the response to the inhibitors, with and without standard treatment, to see if the response changes. A previous study found that the cell culture media is critical to the treatment response of a cell line, and that culturing in different media can promote different populations of cells growing which results in a differential treatment response (286, 287).

Furthermore, the results from the inhibitor experiments reiterate those seen in treatment experiments with *SLC6A6* shRNA cell lines. Therefore, this would indicate that the change in treatment result is due to the changes in TauT levels or activity due to shRNA or inhibitors respectively, and not due to a non-canonical function of *SLC6A6*.

In general, the effect of GAB is greater than GES in comparison to normalized controls. GES is a strong TauT antagonist and a weak GABA_A receptor antagonist but has found to not affect the levels of GABA rats brains (275). GAB is weak TauT antagonists and a strong GABA_A receptor agonist. As well as transporting taurine, TauT also transports GABA but at a lower affinity (138). If TauT was conferring the effect on treatment, then we would expect a larger magnitude of change in the presence of GES as this is a strong TauT antagonist. However, the opposite of this is true with respect to what effect these inhibitors have on the GABA_A receptor. Therefore, as the inhibitors GAB results in a higher magnitude of change than GES, could this mean that the GABA signalling is being affected and causing this change in phenotype? The direction of treatment response is still different between A172 and the patient derived cell lines. GABA is transported via TauT and via the GABA_A receptor so this could still explain why *SLC6A6* expression is increased. Perhaps in GBM the focus of TauT shifts to GABA instead of taurine transport resulting in increased GABA levels. A study looking at the associations of different types of cancer including colon adenocarcinoma and NSCLC showed that increased GABA levels are seen in the higher stages of the cancer demonstrating that increase in GABA levels is linked to higher morbidity levels (288). The association of GABA and cancer progression has also been shown in pancreatic cancer and prostate cancer (289, 290).

Determining the gene expression differences after RNA-sequencing might allow us to see gene expression changes are linked to genes associated with GABA or taurine. Would this help indicate which, if any, is predominantly contributing to treatment resistance and if not then what treatment resistance mechanisms are actually in play.

Chapter 5

RNA-sequencing analysis

5.1 Introduction

In the previous chapter I found that functional modification of TauT, by genomic or pharmaceutical means, does significantly alter the response of glioblastoma (GBM) cells to chemoradiation. However, the direction of this altered response i.e. whether it increases or decreases the efficacy of the treatment, was cell line dependent. Furthermore, by using drugs with different strength of inhibition of TauT, but that also act as agonists of γ -aminobutyric acid type A (GABA_A) receptors, I determined that it may be GABA signalling through TauT that impacted treatment response, rather than taurine transport. These are confounding results. However, work performed in parallel in the Stead Group raised a possible explanation based on the need to stratify patients into two subclasses based on how they respond to standard of care treatment, and the role of γ -aminobutyric acid type A (GABA) signalling in the differential biology of the two so-called 'responder subtypes'. In this chapter I used RNA sequencing to delve further into this hypothesis in the context of my own research findings.

5.1.1 GABA and GABA_A receptor

Neurotransmitters are molecules secreted by nerves that have inhibitory or excitatory neuronal functions upon binding to their receptors. Their chemical structures allow them to be classed into one of three categories; these are amino acids, biogenic amines and peptidergic neurotransmitters often termed neuropeptides. GABA is primarily an inhibitory neurotransmitter that falls into the first class of amino acids (291). Many neurotransmitters have medicinal properties and are used to treat a variety of human diseases. This applies to GABA, which is commonly used to treat anxiety and sleep deprivation related disorders as well as being used to treat Attention Deficit Hyperactivity Disorder (ADHD) (292). However, over the years, neurotransmitters have been increasingly implicated in human cancers and can be produced by cancer cells directly (291). Neurotransmitters are primarily synthesised inside neurons that have a sophisticated ability to regulate production, release and degradation of neurotransmitters (293). Furthermore, many neurotransmitters occur naturally in

human food and GABA is no exception to this, naturally occurring in many foods such as broccoli, sweet potato, and soya bean (294).

GABA was discovered in plants and bacteria long before the discovery in 1950 of high amounts of GABA in the mammalian CNS despite being almost undetectable in other tissues (295). GABA is one of the earliest neurotransmitters present in the developing nervous system where it acts by depolarizing radial glial cells and immature neurons. In the developing brain, GABA is the main excitatory drive and is involved in the modulation of progenitor proliferation and neuronal migration (296). In contrast, GABA adopts a different role and acts as the primary inhibitory neurotransmitter in the adult central nervous system (CNS) (296, 297). Here, GABA's physiological roles involve promoting neuronal development and the modulation of synaptic transmission. GABA enters the cell either via transporters such as those in the solute carrier 6 (SLC6) family for example GAT1 and TauT. GAT1, encoded by *SLC6A1* and GAT2, encoded by *SLC6A13* are the most well characterised GABA transporters (145). Alternatively, it is synthesised inside neuroblasts and mature GABAergic neurons from the excitatory neurotransmitter glutamate in the brain, by the action of the glutamate decarboxylase (145, 295).

GABA acts primarily by binding GABA_A or GABA_B receptors (296). GABA_A or GABA_B have distinct biochemical and pharmacological properties as GABA_A is a GABA-gated chloride channel located on the post-synaptic membrane and GABA_B is located on both pre and post synaptic membranes and is a G protein coupled receptor (292). The GABA_A receptor is a Cl⁻ channel, and GABA activation causes Cl⁻ influx and membrane hyperpolarization in the mature brain due to low intracellular Cl⁻ concentrations at resting potential (296). This then reduces the excitability of the cell, inhibiting the cell activity. In neural precursors, GABA_A receptor activation depolarises instead of hyperpolarises. This depolarisation still works to cause an inhibitory effect by blocking excitatory currents (295). The distinction between hyperpolarisation and depolarisation partly depends on expression of Na-K-Cl transporter NKCC and the accumulation of intracellular chloride ions. The activation of GABA_A receptors by GABA in neural precursors leads to efflux of chloride ions and an influx of calcium ions which acts to reduce the proliferation of neural stem cells (298). However, cancer

cells have often been shown to use neurotransmitters to their advantage by activating signalling pathways that lead to uncontrolled proliferation (291).

5.1.2 Up and Down responder subtypes in glioblastoma

RNA sequencing was performed on 168 longitudinally paired de novo IDH-WT GBM tumours from patients who received standard treatment of temozolomide (TMZ) and irradiation and had locally recurrent tumours. These data were analysed within the Stead group. A validation cohort consisting of 23 further pairs from samples matching the same criteria were collected and analysed via a pipeline developed in the Glioma Longitudinal Analysis Consortium (GLASS) (299). Analyses of these data led to the identification of two responder subtypes in GBM based on the changes in gene expression of a subset of genes following treatment. In two thirds of patients, gene expression of a subset of genes is upregulated in recurrent tumours and, in one third, expression of this same subset of genes is downregulated in recurrent tumours. These have been termed the Up and the Down responders respectively. Different biological characteristics are seen in Up or Down responders, which may give insight into the specific mechanisms of treatment resistance occurring in these patients.

Up and Down responders were discovered via a bespoke analysis applied to all primary and recurrent pairs. The genes differentially expressed between primary and recurrent samples were first inspected and found to be enriched for normal neurodevelopmental processes, which are regulated by transcription factors that work together with chromatin remodelling complexes to open up DNA to allow expression or inhibition of certain genes. Gene sets for DNA-binding factors were created to determine whether certain regulators were involved in the gene dysregulation seen between primary and recurrent tumours. This showed that genes containing a JARID2 (Jumonji and AT-Rich Interacting domain) binding site in the promoter were consistently altered across the patient tumour pairs. There was a total of 5234 genes containing a JARID2 binding site (“JBSgenes”). The leading edge (LE) 70 genes are those that consistently (in >70% of the patients) have the highest \log_2 fold-change (\log_2FC) in expression between paired samples from the “JBSgenes” data-set. There are around 80 LE70 genes and these are dysregulated in a consistent direction within a patient, but this direction changes between patients, through treatment.

The difference between the responder subtypes were further investigated. GBM tumours are often characterised into different molecular subtypes known as classical, mesenchymal and proneural as described in section 1.2.2. In Up and Down responders, no differences were seen between the prevalence of these molecular subtypes in the primary tumours. Furthermore, there were no differences between the probability of subtype switching from primary to recurrent between Up and Down responders. However, a significant difference was seen in the molecular subtypes seen at recurrence between the Up and Down responders. Up responders most commonly switched to be proneural however Down responders display a therapy-driven switch to the mesenchymal subtype.

Furthermore, GBM biology specific gene sets were collated within the Stead group, and joined with those from the molecular signature database, so that gene set enrichment analysis could be investigated separately in Up and Down responders. In Up responders there was an upregulation of developmental glioma stem cell (GSC) states. Single cell transcriptional analysis of GBM tissues performed by Wang *et al.* showed that there is a single axis of transcriptional variation for neoplastic cells in GBM. Proneural GSCs reside at one end of this axis, and mesenchymal GSCs at the other; differentiated malignant cells appear more centrally. Through treatment, Up responders become enriched for proneural GSCs signatures and Down responders become enriched for mesenchymal GSC cell signatures. Genes associated with epithelial to mesenchymal transition are also enriched in the Down responders which is more accurately termed the proneural to mesenchymal transition in GBM, as GBM is a non-epithelial cancer.

Down responders have an upregulation in cell cycle genes and of marker genes associated with proliferation. On the other hand, Up responders have an upregulation of stem cell quiescence markers along with differentiated neuroblasts and oligo cell types.

In survival analysis, considering known prognostic markers such as *MGMT* promoter methylation, there was no significant differences in the overall survival between Up and Down responders. This evidence of Up and Down responders summarised in Table 5.1 suggests differential mechanisms of treatment response which may mean that Up and Down responders should be stratified and given responder subtype specific treatments. To assess this, subtype-specific drug

targets need to be identified. Up responder samples show an upregulation in GABA neurotransmitter signalling components as well as an increase in gene signatures for neurons and oligodendrocytes. The opposite is seen for Down responders. This suggests an increase in interactions between cancerous cells and normal brain cells in the Up responders and the opposite for Down responders. Therefore, potentially GABA signalling pathways components could be drug targets. This includes GABA_A receptor which might need targeting by antagonists or agonists depending on the responder subtype. In GBM63 and GBM58 a differential treatment response is seen to A172 when treated with the GABA_A receptor agonists GES and GAB. This suggests that GBM63 and GBM58 might be different responder subtypes to A172. To investigate this, RNA sequencing was performed to determine if A172 and GBM63 recapitulate Up and Down responder subtypes by looking at changes in expression of key genes and pathways in response to standard treatment.

Table 5.1. Biological characteristics of Up and Down Responders. Summary of the Biological characteristics of the Up and Down responder subtypes.

Biological characteristic	Up responder subtype	Down responder subtype
Prevalence of subtype in primary tumours	No difference in prevalence	
Prevalence of subtype in recurrent tumours	Most commonly switched to proneural subtype	Most commonly switched to mesenchymal subtype
Glioma Stem Cell (GSC) signature type	Enriched for proneural GSC signatures	Enriched for mesenchymal GSC signatures
Key marker gene expression	Upregulation of stem cell quiescence, differentiated neuroblasts and oligo cell type markers	Upregulation in cell cycle and proliferation markers
Survival	No difference in survival	

5.1.2.1 Deciding on inhibitor experiments to be sequenced

I used RNA-sequencing (RNA-seq) to develop a better understanding of the changes seen upon treatment, and upon treatment in combination with the TauT antagonists Guanidinoethyl sulfonate (GES) and Gaboxadol (GAB). The RNA from experiments on A172, GBM58 and GBM63 with 10 mM of GAB or GES or solvent control, and with and without standard treatment was harvested at the end point of each experiment. This meant it was available for RNA-seq if required, as below.

I chose two cell lines for sequencing. As there were two apparent response phenotypes to GES and GAB across the cell lines, one cell line from each of these response phenotypes was chosen: A172 and GBM63. GBM63 was chosen instead of GBM58 because it is more widely used within the group so further characterisation could be beneficial to other projects. The inhibitor that had the greatest effect on standard treatment across the cell lines was GAB and therefore this was chosen to be sequenced along with the solvent control. 10 mM GES and GAB, and the same end points as used in section 4.3.4.2. were used.

5.1.3 Differential gene expression

Following RNA-seq, I performed differential gene expression (DGE) on my samples to understand the changes through treatment in each of the cell lines and to see if these treatment specific gene expression effects in A172 and GBM63 reflected those seen in Up and Down responders.

5.2 Aims and Objectives

The aim of this chapter was to define the effect of *SLC6A6* inhibition on GBM cell transcriptomes in response to standard treatment.

Objective 1 - Analyse RNA-sequencing data from experiments looking at the effect of TauT inhibitors on response to standard treatment

5.3 Results

5.3.1 Establishing a differential gene expression analysis pipeline

To perform DGE analysis, a pipeline must be set up in order to process and quantify the gene expression data. I designed a pipeline to achieve this, starting with literature searching to find the best tools for each step of the analysis before

integrating these tools into the pipeline. The main steps and tools used are shown in Figure 5.1. The first step is performing quality control of the data and is typically performed by the JAVA tool FastQC. FastQC performs quality control checks on raw sequence data and gives outputs that help the user determine if their data is satisfactory and without problems that may need to be factored into the further analysis (300). The output is easy to interpret, with multiple graphs and figures each with a green tick to indicate the test was passed and data looks as expected, a yellow “!” if the test result shows slight abnormalities that need to be further investigated, or a red cross if there is a significant issue. From performing FastQC analysis I saw my data was without issues.

The next step is Trimming of reads to ensure that adaptor sequences and low-quality bases are removed before downstream analysis. Each base is assigned a Q-value which is a probability score that the base was scored incorrectly. The Q-value tends to decrease towards the 3' end of the sequence, meaning more chance a base is scored incorrectly. It is important that lower quality regions typically with a Q-value of below around 30, are removed to improve downstream alignment to the genome. Cutadapt was developed to perform this role and was chosen for use. Cutadapt uses the first 13bp of illumina standard adapters which are suitable for both ends of a paired end fragment (301). I decided to use a wrapper script called Trim Galore, which incorporates FastQC and Cudadapt together in order to make this process more efficient (302).

The next step is alignment of the sequencing reads to a reference genome or transcriptome. The choice between aligning to a genome or transcriptome depends on the purpose of the analysis. For those wishing to identify new transcripts then alignment to the genome would be preferred. However, for simpler gene quantification purposes then aligning to the transcriptome is generally used (303). Aligning to the genome is complicated in eukaryotes due to the alignment being affected by splicing and poly-adenylation. Additionally, aligning to the genome takes a lot longer as the total length of the genome far exceeds the total length of all the transcripts (303). Bowtie2 is alignment tool for aligning reads to the reference transcriptome. I decided this would be suitable for my analysis as Bowtie2 is capable of aligning reads that vary in length from 50 base pairs (bp) to 1000s of bp and is ultrafast, and has a very low number of false positives (304). RSEM (RNA-Seq by Expectation Maximization) is a transcript

quantification tool that works without the use of a reference genome and is used in conjunction with Bowtie2 (117). RSEM maps both isoform and gene level abundance and is effective when aligning to the reference transcriptome (303). The output of RSEM can be Transcript per million (TPM) or fragments per kilobase of transcript per million mapped fragments (FPKM) and FPKM was chosen (305). I decided to use RSEM alongside Bowtie2.

Once reads have been aligned to the genome and quantification performed, the process of differential expression analysis can be carried out. DESeq2 was chosen for this step due to its higher precision, sensitivity, and few false positive than other commonly used differential expression platforms such as DESeq, EBSeq and EdgeR (183). The output of interest for DESeq2 was the adjusted p-value (adj.p). The adj.p is a stringent filtering method that assumes 5% of all the significant tests will result in false positives, in contrast to a p-value which assumes that 5% of the total tests will result in false positives. Where needed, ggplot2 was used as a visualisation tool for the DGE results (306).



Figure 5.1. RNA-sequencing and Differential gene expression steps. The main steps involved in RNA-sequencing and differential gene expression analysis and the tools chosen for which step of the process.

5.3.2 Number of genes differentially expressed

The number of genes differentially expressed (DE) for each comparison was calculated using DESeq2 and presented in Table 5.2. Upon running differential gene expression analysis in DESeq2, I found that there were very few DE genes in some of the comparisons (Table 5.2). To check these results were correct, I decided to use a second tool for DGE comparisons that enabled paired analysis. EdgeR was chosen for this. The results from this independent analysis method (Table 5.2) correlated with DESeq2. Furthermore, using EdgeR I was able to identify the Biological Coefficient of Variation (BCV) value (Table 5.2). The BCV is the relative variability of expression between biological replicates so is a

measure of how much biological variance there is within a condition (307). The lower the BCV, the lower the variation and therefore the greater number of differentially expressed genes can be detected. The BCV value shows that there is a more noise in the GBM63 samples, which indicates that it is harder for genes to be defined as being differentially expressed. Therefore, I decided to proceed with my original DGE analysis using DESeq2, but for the comparisons with fewer DE genes I reduced the stringency to identify the most significantly DE genes even if they did not meet the original cut-off of $\text{adj.}p < 0.05$. This would enable me to search for pathways that are DE between one sample or another, even when the BCV is high. This would result in more genes reported as DE being false positives which would make pathway enrichment more difficult to detect. Therefore, if a pathway is still seen to be enriched, I can be certain that it is not due to false positives.

Table 5.2. Differentially expressed gene numbers. The number of genes differentially expressed at an adjusted p -value ($\text{adj.}p$) of 0.01 or 0.05 using either DESeq2 or EdgeR. The Biological coefficient of variation is displayed for each comparison.

Comparison	Number of genes DE in DESeq2. Adjusted p -value		Number of genes DE in EdgeR. Adjusted p -value		Biological coefficient of variation
	0.05	0.01	0.05	0.01	
A172 Solvent untreated vs treated	2978	2038	4249	2912	0.082
A172 Gaboxadol untreated vs treated	3577	2472	4289	2954	0.106
A172 untreated Solvent vs Gaboxadol	547	320	864	482	0.133
GBM63 Solvent untreated vs treated	511	307	485	255	0.193
GBM63 Gaboxadol untreated vs treated	1	0	0	0	0.226

GBM63 untreated	1046	465	1371	504	0.144
Solvent vs Gaboxadol					

5.3.3 Gene expression direction change between A172 and GBM63 upon standard treatment

Differential gene expression analysis tells us which genes are DE, but it is also important to look at the direction of this expression change. A172 and GBM63 were both affected by standard treatment with spheroids becoming smaller when treated (Figure 3.13 and Figure 3.15). To observe if the effect of standard treatment is the result of the activation of the same mechanisms, the DE genes between these two groups were compared. Figure 5.2 shows the direction of gene expression changes between A172 treated and untreated and GBM63 treated and untreated. Genes in red are those significantly differentially expressed with an adjusted p-value of less than 0.05. The genes in the green boxes are differentially expressed in opposite directions between the two cell lines, and the ones in orange boxes are differentially expressed in the same direction. There are 151 genes in the green boxes and only 38 genes in the oranges boxes which means significantly more genes are differentially expressed in opposite directions between A172 and GBM63 even though the same cytotoxic effect was seen after both were subjected to the same standard treatment of 30 μM TMZ and 2Gy irradiation ($P < 0.0001$, chi-squared).

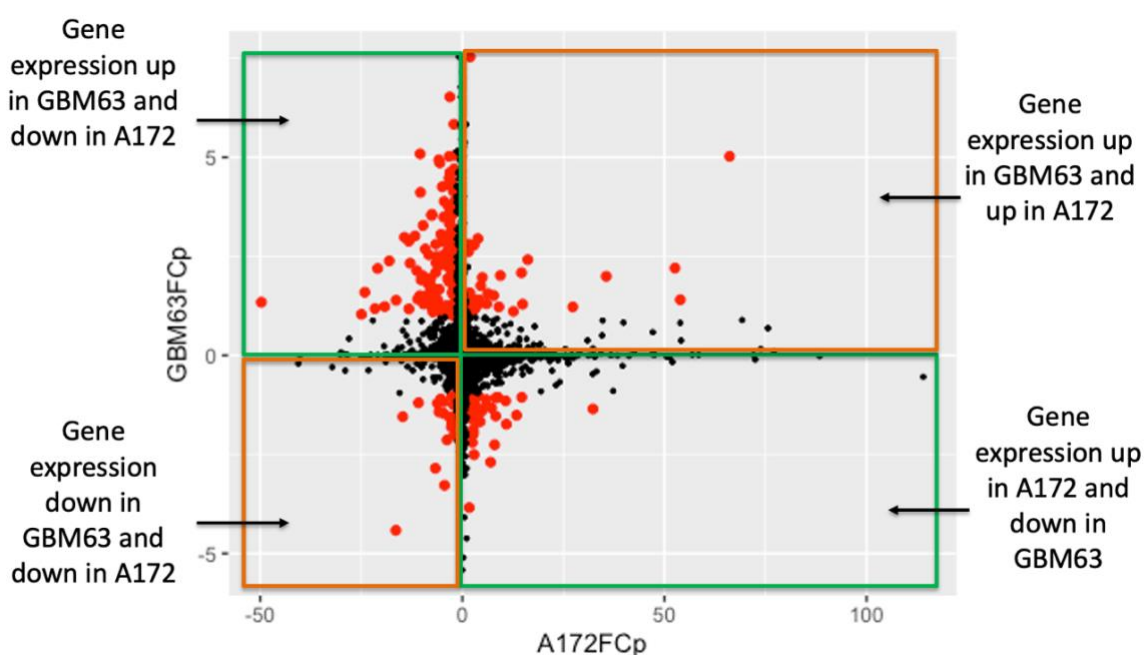


Figure 5.2. Gene expression direction of genes in A172 and GBM63 with standard treatment. Direction of fold change multiplied by $-\log_{10}\text{adj.p}$ for A172 (x) and GBM63 (y) results from DEseq2 for three biological replicates and looking at genes DE between treated and untreated. Black = gene expression for a particular gene. Red = genes with $p\text{-value} < 0.05$ on both experiments. Green boxes indicate genes expressed in opposite directions between A172 and GBM63 and genes in the orange boxes represent those expressed in the same direction between A172 and GBM63.

5.3.4 The effect of standard treatment on A172 and GBM63

To further investigate the reason for the phenotypic effect of spheroids becoming smaller when subjected to standard treatment in both the cell lines, Gene Ontology (GO) enrichment analysis was performed using ShinyGO v0.75 to look for pathways that could explain the change in spheroid size. In A172, cell population proliferation and programmed cell death were of particular interest as both are mechanisms that could result in smaller spheroids (Figure 5.3). The GO terms means that a significant number of genes relating to this category are DE between treated and untreated, but this did not provide me with an indication into if these genes were upregulated or downregulated through treatment. The expression of some key genes commonly relating to proliferation decreased in A172 following treatment i.e. causes treated spheroids to be smaller than the untreated spheroids (Figure 5.4).

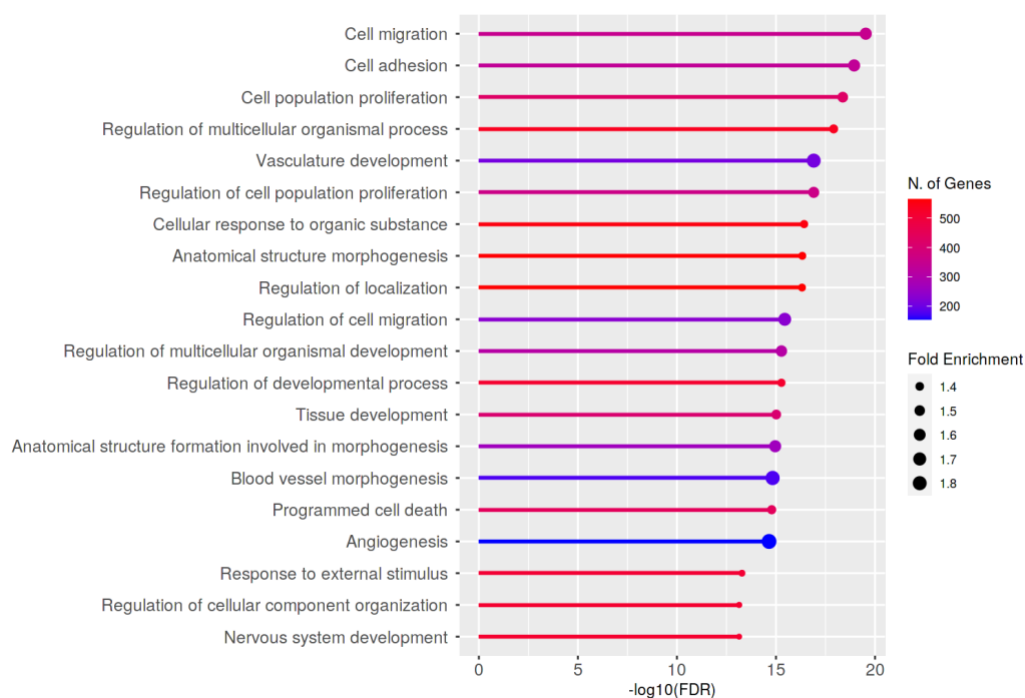


Figure 5.3. Gene Ontology in A172. ShinyGO v0.75 gene ontology enrichment analysis was performed for genes DE in A172 upon standard treatment.

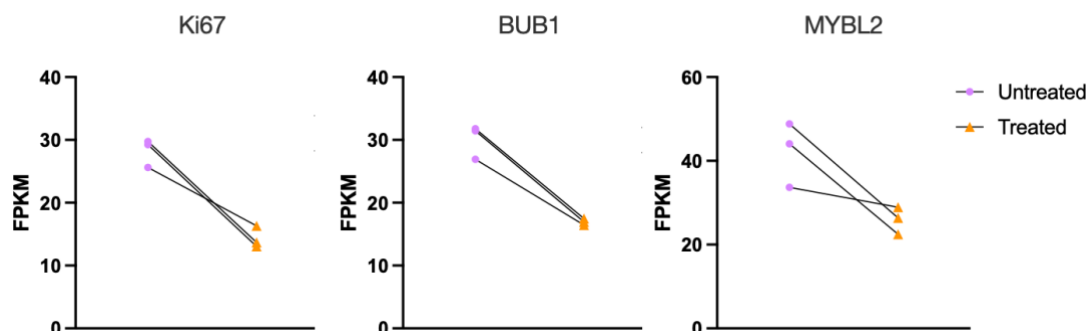


Figure 5.4. Normalised expression of genes related to proliferation in A172. The normalised expression (FPKM) of three genes commonly associated with proliferation, in three paired replicates of treated and untreated A172 spheroids.

The same ShinyGo GO analysis was performed for the genes differentially expressed in GBM63 treated vs untreated. Interestingly, none of the exact same GO terms were identified meaning that the same standard treatment of 30 μ M TMZ and 2Gy irradiation has a different transcriptional effect in both the cell lines despite having the same phenotypic effect. However, in GBM63, several GO terms did still relate to cell cycle, cell division and cell cycle process (

Figure 5.5). Inspecting the expression of key genes associated with the cell cycle show these are upregulated in treated versus untreated (Figure 5.6), the reverse of what we see in A172. As rapidly dividing cells are targeted by irradiation and alkylating chemotherapy agents, such as TMZ, increased cytotoxicity could explain the decrease in spheroid size despite the increase in dividing cells. The results from A172 and GBM63 show that standard treatment causes different distinctive effects on the transcriptome.

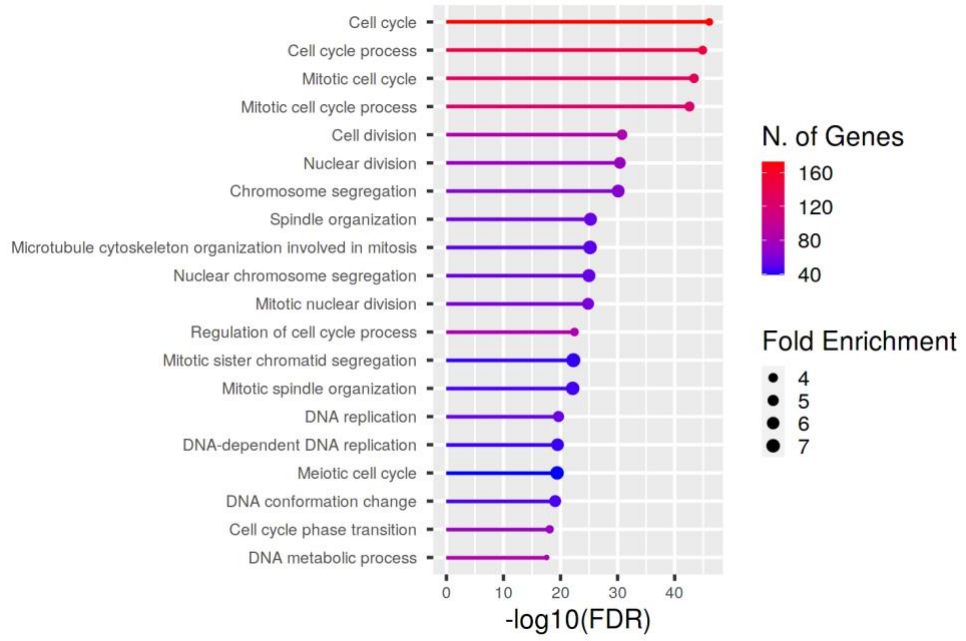


Figure 5.5 Gene Ontology in GBM63. ShinyGO v0.75 gene ontology enrichment analysis was performed for genes DE in GBM63 upon standard treatment.

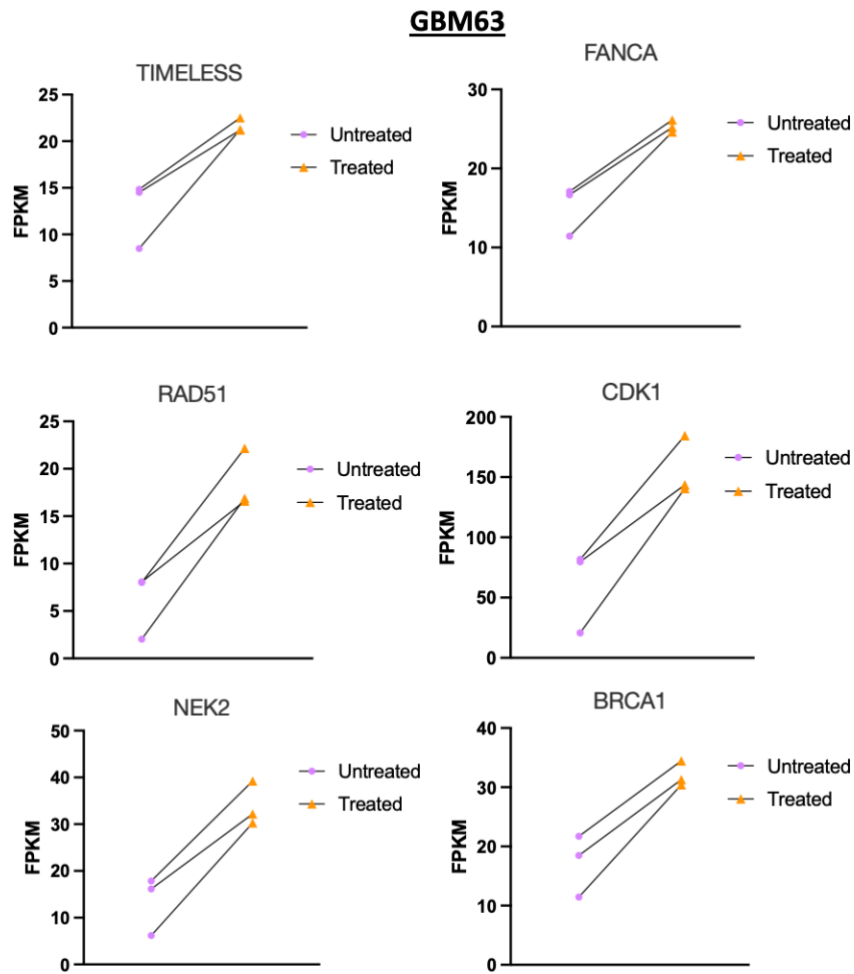


Figure 5.6. Normalised expression of genes related to the cell cycle. The normalised expression (FPKM) in treated vs untreated GBM63 spheroids of six genes associated commonly associated with the with cell cycle.

5.3.5 A172 and GBM63 are Up and Down responder cell lines respectively

The opposite direction of gene expression changes between A172 and GBM63 in response to standard treatment suggest that these may be different responder subtypes. Dr Georgette Tanner, a post-doc within the group has developed a pipeline to determine whether a patient is an Up or Down responder based on the direction of genes expression change in a subset of key genes over the course of treatment. We used this to determine if A172 and GBM63 recapitulate the therapy-driven transcriptional reprogramming that delineates Up and Down responders. Figure 5.7 shows that A172 is an Up responder and GBM63 is a Down responder.

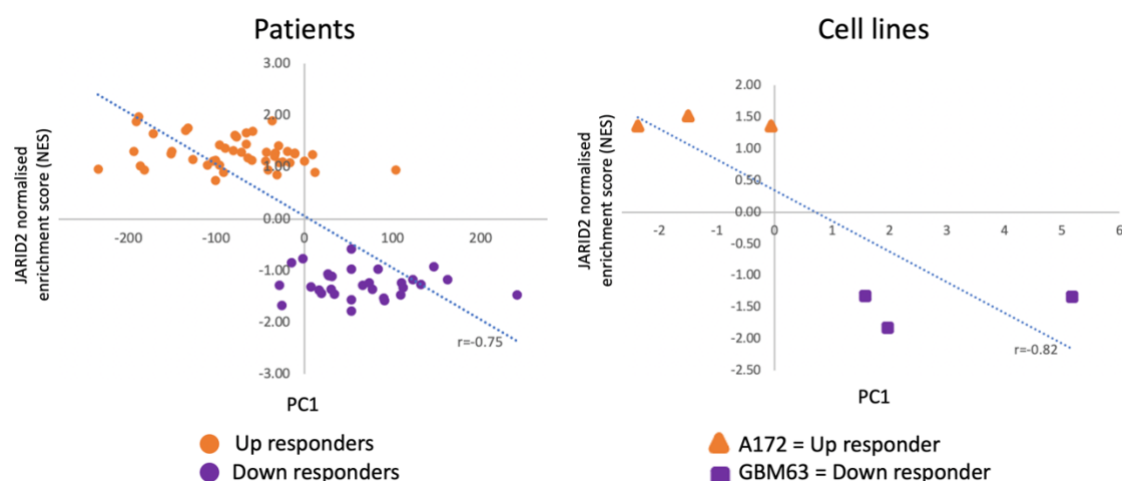


Figure 5.7. Responder subtype scatter plot. Left: Scatter plot showing the separation in Up and Down responders when plotted according to Principal Component 1 (PC1) of PC analyses of samples based on the \log_2 fold-change of all genes through treatment against the JARID2 normalised enrichment score (NES). Right: The same metrics plotted for A172 and GBM63 replicates indicating that they are Up and Down responders, respectively.

5.3.6 Biological similarities in the DEGs and enriched functions through treatment with regards: A172 and U responder patients; GBM63 and D responder patients

If A172 and GBM63 are different responder subtypes, I would expect them to have different gene expression features unique to their responder subtype. Gene lists of genes DE for A172 or GBM63 with and without standard treatment are referred to as “A172_UnVsT” and “GBM63_UnVsT” from now on.

Down responders have been shown to upregulate cell cycle genes going from primary to recurrent.

Figure 5.5 shows that in GBM63_UnVsT, the GO term with the greatest number of genes is “cell cycle”. FPKM plots from some key genes associated with the cell cycle are plotted in Figure 5.8. This shows that their expression is upregulated through treatment, as seen in the Down responders. These genes are downregulated in A172_UnVsT responders (Figure 5.8), as seen in the Up responder subtype. Furthermore, Down responders have an upregulation of marker genes of proliferation/progenitor (PPR) neoplastic GBM cells identified by Garofano *et al.*, who performed single cell sequencing on GBM cells to identify marker genes of PPR neoplastic GBM cells (308). These PPR genes included those associated with cell cycle progression, mitosis, DNA replication and DNA damage repair (308). These are downregulated in the Up responders. Over-representation analysis (ORA) using WebGestalt (WEB-based Gene SeT Analysis Toolkit) was performed. ORA is a statistical method that determines if genes from a pre-defined set of genes appear more than what would be expected in the data. In GBM63_UnVsT, ORA showed that the Garofano PPR signature had an enrichment ratio of 9.6366 and in A172_UnVsT there was an enrichment ratio of 2.2751 for the same signature. The direction of gene expression change for some of the genes in this signature was examined for both A172 and GBM63 (Figure 5.9). This showed that in A172 these genes were typically downregulated after treatment, as observed in patient Up responders, and in GBM63 these genes were typically upregulated after treatment, as for patient Down responders.

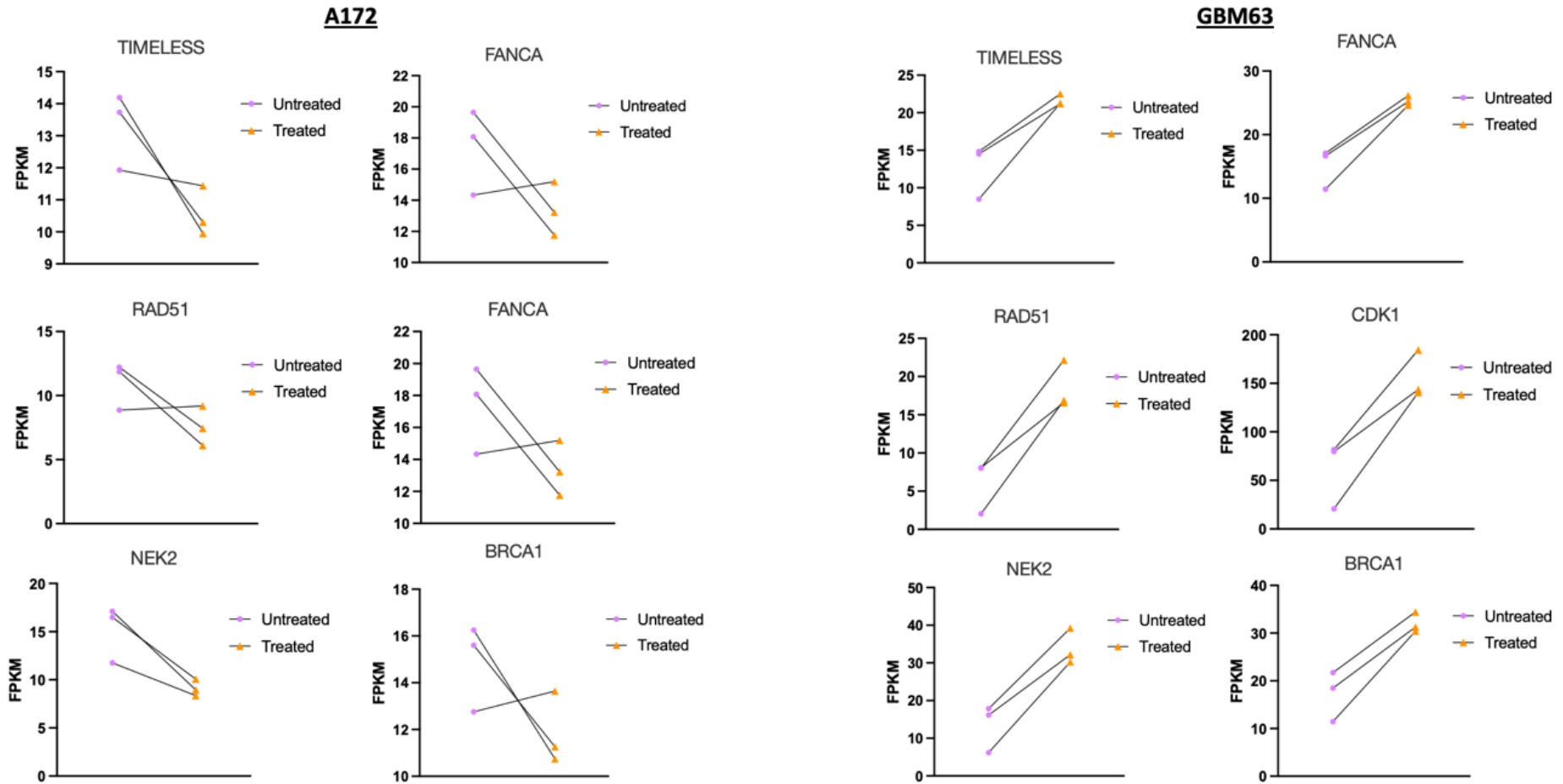


Figure 5.8. Normalised expression of genes related to the cell cycle. The normalised expression (FPKM) of six cell cycle genes in paired triplicates of treated and untreated A172 (left) and GBM63 (right) spheroids.

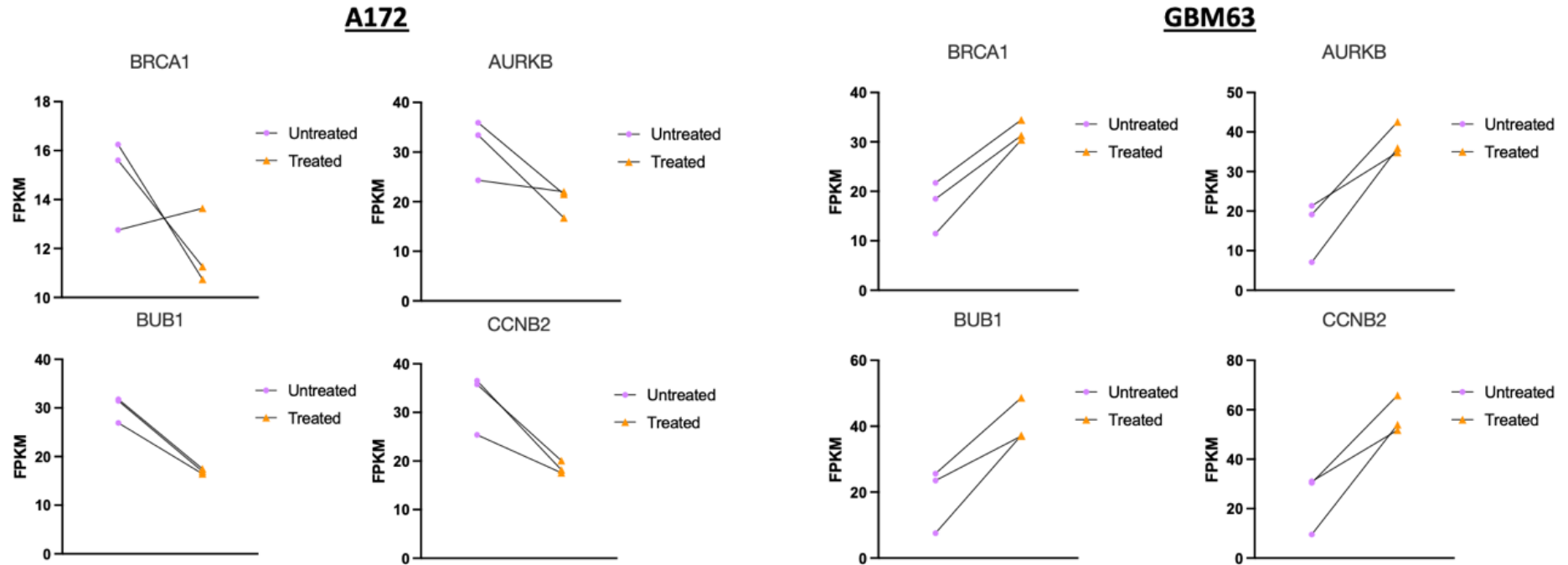


Figure 5.9. Normalised expression of genes related to the proliferation/progenitor (PPR) neoplastic GBM cells signature. The normalised expression (FPKM) of four genes associated with the PPR signature in A172 and GBM63 paired triplicates.

Figure 5.3 shows that cell population proliferation is an identified GO term in A172_UnVsT. To look at the direction of dysregulation in A172_UnVsT, expression of three genes commonly associated with proliferation were inspected (Figure 5.10). This showed a downregulation of these genes through treatment as seen in up responders. On the other hand, these same genes increased in expression following treatment in GBM63_UnVsT as seen in down responders. In A172_UnVsT, the gene that is the most highly DE is *BTG2*. *BTG2* is known as both B-cell Translocation Factor 2 and BTG Anti-Proliferation Factor 2, and is a protein-coding gene that has an anti-proliferation effect. *BTG2* has been previously linked to Diffuse Large B-cell Lymphoma Activated B-Cell Type but is often seen downregulated in many human cancers and acts as a tumour suppressor gene (309). The expression of *BTG2* significantly increases after treatment in A172 (adj.p<0.0001) (Figure 5.11). In GBM63, there is a non-significant trend in a reduction of *BTG2* after treatment (adj.p=0.286).

Codega *et al.* extracted Neural Stem Cells (NSCs) from adult mouse brains, used label retention approaches to separate those which were quiescent (qNSCs) from those which were activated (aNSCs), and identified differentially expressed genes which could then be used to identify GO terms of importance. Up responders have a significant number of qNSC markers upregulated, with the same genes downregulated in Down responders. The qNSCs were enriched for GO terms such as cell adhesion and response to stimulus, which are both identified in A172_UnVsT (Figure 5.3). The aNSCs were enriched for GO terms relating to the cell cycle and DNA replication which are also seen in GBM63_UnVsT (

Figure 5.5). Additionally, aNSCs were enriched for DNA repair genes. ORA for the molecular signature database gene set named “the hallmark of cancer”, on differentially expressed genes in GBM63 has an enrichment pathway for DNA repair genes (1.6119 enrichment ratio from WebGestalt) (185). Additionally, in GBM63_UnVsT, four out of the top five most DE genes in response to standard treatment are involved in DNA damage repair pathways and in each one of these is upregulated after treatment. These genes are *FANCD2*, *XRCC2*, *POLQ* and *MASTL* suggesting that GBM63_UnVsT has a higher ability to repair its DNA after treatment, correlating with the increase in the PPR signature as seen above. In

A172, these four genes are downregulated after treatment, though not significantly.

These results show significant similarities of GBM63_UnVsT with Down responder subtype and A172_UnVsT with an Up responder subtype, which may provide a reason for the difference in response to GES and GAB seen in chapter 2. Cumulatively, these results suggest two distinct mechanisms of treatment evasions for A172 and GBM63. As seen for Up responders, A172 evade treatment by slowing their proliferation and moving towards a more quiescent phenotype. This may enable them to evade chemotherapy treatment which targets proliferating cells. Conversely, GBM63 responds similarly to Down responders by moving towards a more aggressive mesenchymal phenotype and increasing proliferation following treatment, relying on DNA damage repair pathways to survive the cytotoxic effect of irradiation and TMZ, both of which rely on DNA damage to kill the cell.

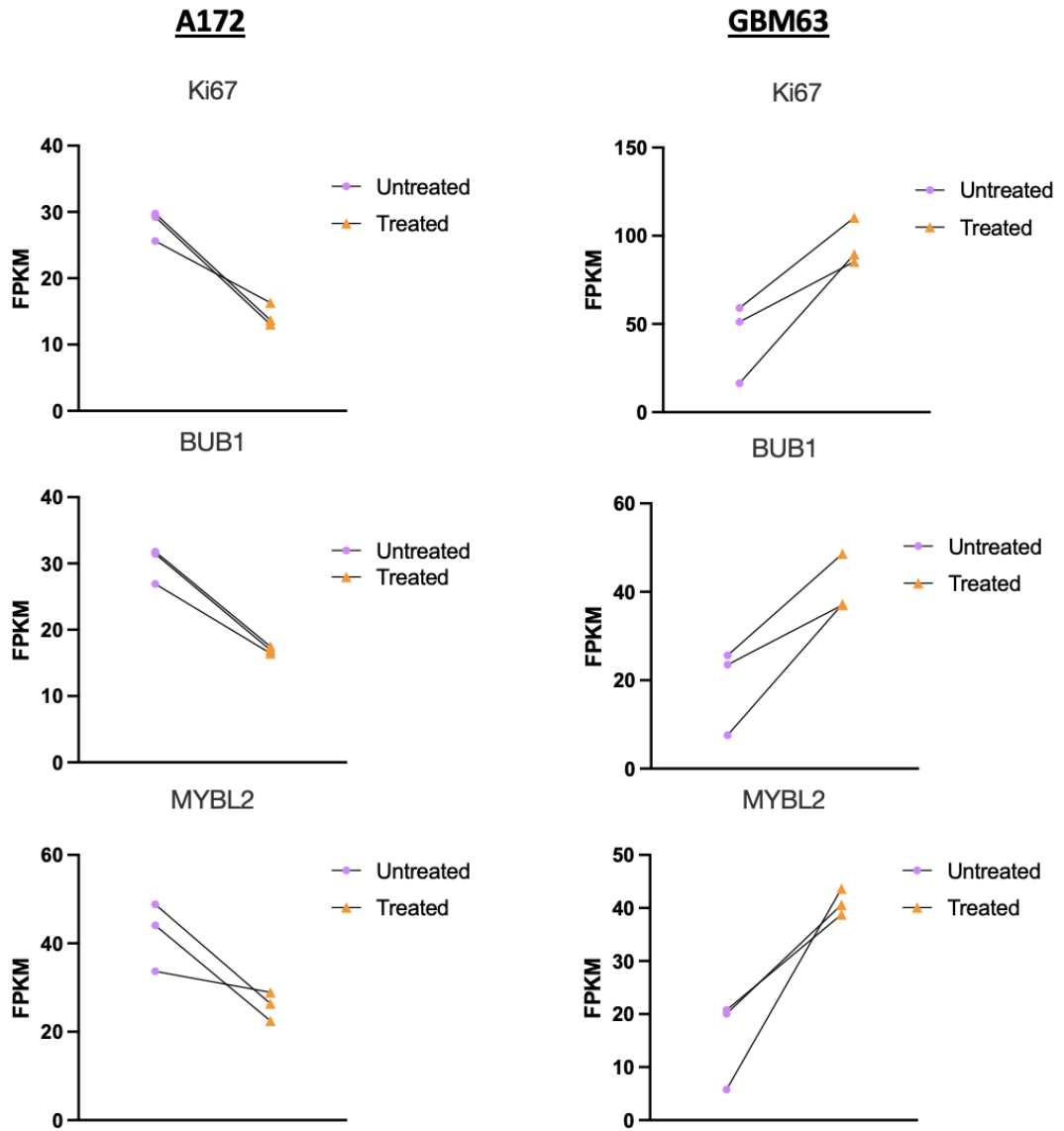


Figure 5.10. Normalised expression of genes related to proliferation. The normalised expression (FPKM) in treated and untreated samples of A172 and GBM63 of three key genes associated with cell proliferation.

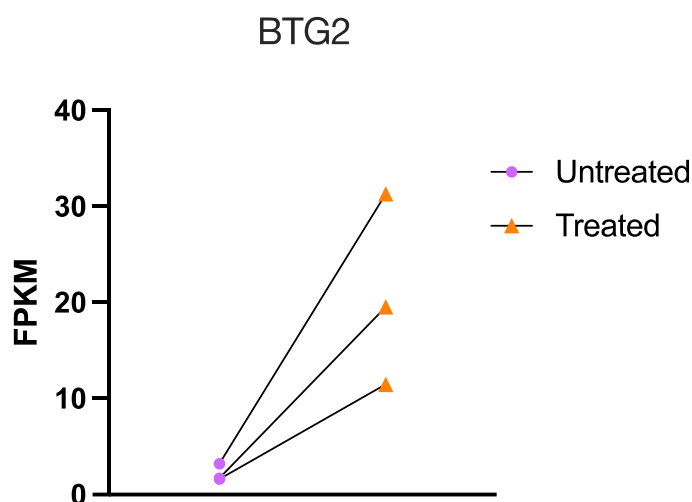


Figure 5.11. The normalised expression of BTG2 in A172. The normalised expression (FPKM) of *BTG2* in treated and untreated samples of A172. *BTG2* is the most differentially expressed gene between untreated and treated samples in A172.

5.3.7 Different responder subtypes for GBM63 and A172 suggest stratified treatments are needed.

Differences in biological response to standard treatment might mean that stratified treatment approaches are needed for different drug targets depending on the responder subtype. GABA neurotransmitter signalling is one druggable pathway that differs between Up and Down responders. Up responders are those that significantly upregulate GABA neurotransmitter signalling components and Down responders significantly downregulate these. In A172_UnVsT, GABA type A receptor associated protein like 1 and 2 (*GABARAPL2* and *GABARAPL1*) are significantly upregulated in treated vs untreated samples (Figure 5.12a.) reflecting the Up responders. These are not significantly DE in GBM63_UnVsT (Figure 5.12b.). However, treatment experiments in Chapter 4 show that the addition of GAB, a GABA_A Receptor agonist that has an effect on GABA signalling, has a differential effect in GBM63 to A172. This causes A172 to be more affected by standard treatment when present, although GBM63 is less affected by standard treatment. To get a better insight into the reasons for the difference, the impact of GAB with and without standard treatment on the transcriptome of A172 and GBM63 was investigated in section 5.4.

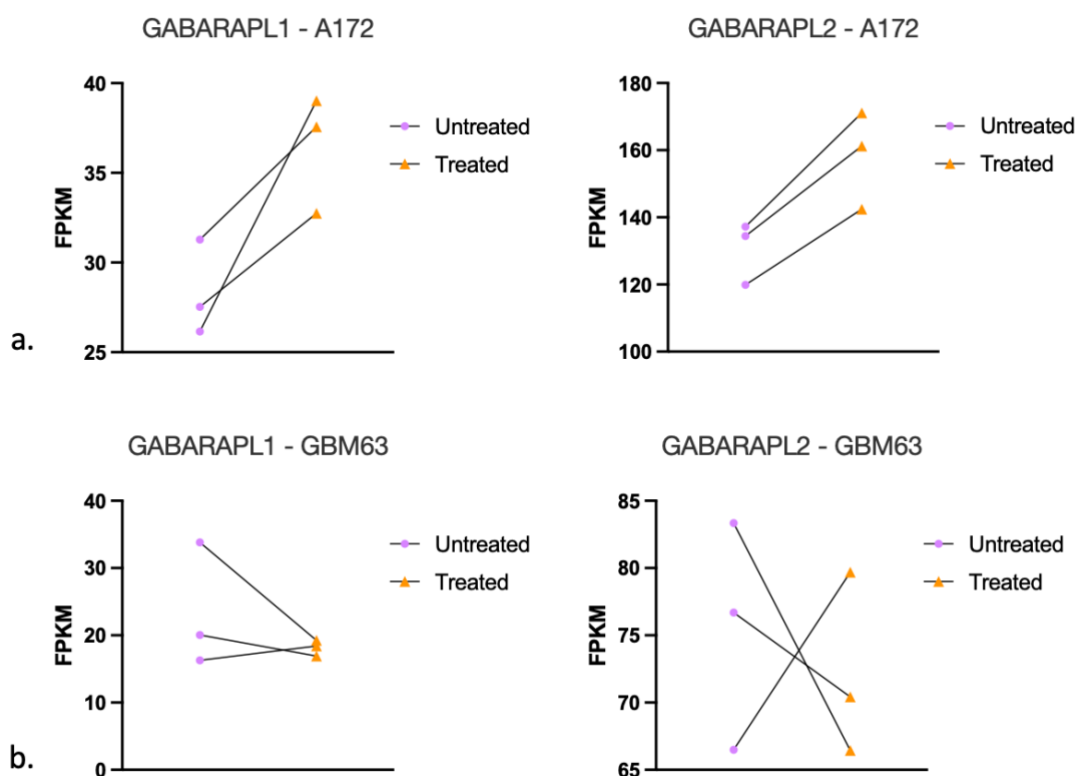


Figure 5.12. GABA type A receptor associated protein like 1 and 2 (*GABARAPL2* and *GABARAPL1*) normalised expression. a. *GABARAPL2* and *GABARAPL1* normalised expression (FPKM) in A172 untreated and treated. b. *GABARAPL2* and *GABARAPL1* normalised counts in GBM63 untreated and treated.

5.3.8 Differences between the DEGs/enriched functions through treatment with regards: A172 and Up in patient; GBM63 and Down in patients

Despite the many similarities A172 and GBM63 have with Up and Down responders, respectively, these are cell lines rather than patient samples so, undoubtedly, there are important biological differences. One key difference between GBM63 and Down responders is that GBM63 does not significantly downregulate GABA_A receptor components in response to treatment. There is a trend that GABA signalling components are downregulated post-treatment but this is not significant (Figure 5.12).

In addition, upon analysis performed on WebGestalt looking at the genes associated the molecular signature database gene set named “the hallmark of

cancer” there is an enrichment for genes associated with an epithelial-to-mesenchymal transition in A172 (enrichment ratio of 1.9929) (185). This is something that is usually observed in Down, and not Up, responders.

5.4 GAB affects the transcriptional changes observed following treatment

To determine if GAB is having an effect on GABA signalling components at the transcriptome level, expression of genes involved in GABA signalling were examined in comparison to the vehicle control. There was no differential expression observed for genes associated with the GABA receptor upon the addition of GAB in A172 or GBM63 in either treated or untreated samples. GAB is a small molecule inhibitor, that exerts its action by binding to protein complexes (TauT and GABA_A receptor). My results indicate that its effect on associated downstream pathways is not at the transcriptome level, so more likely affects the protein level.

To determine the effect on the transcriptome of treatment in the presence of GAB, differential expression analysis on the genes found to be significantly DE between treated and untreated in the presence of GAB was performed. This was followed by Gene ontology analysis using ShinyGo or ORA using WebGestalt with custom gene sets. These comparisons are termed “A172_UnVsT_GAB” or “GBM63_UnVsT_GAB”. In A172, many of the same GO terms identified as dysregulated through standard treatment alone are also dysregulated upon standard treatment in the presence of GAB. These include cell migration, cell adhesion, angiogenesis and cell population proliferation (Figure 5.13) suggesting the same mechanisms of action are responsible for spheroid size change. In addition, three of the top five DE genes in A172_UnVsT are also in the top five DE genes in A172_UnVsT_GAB. These are *FAS*, *FDXR* and *BGT2*. The direction of gene expression change between untreated and treated remains the same for these three genes in the presence of GAB and vehicle control (Figure 5.14). However, for each of these genes the counts are higher in treated samples in the presence of GAB. My interpretation of this data collectively suggests that for A172, GAB dysregulated the same genes that are already DE through treatment but at higher fold changes, exacerbating the therapy-driven transcriptional reprogramming. This aligns with the larger phenotypic response to the standard

treatment in the presence of GAB. The number of DE genes, identified by DESeq2 analysis and shown in

Table 5.2, further support this interpretation. In A172_UnVsT_GAB, the number of DE genes is increased suggesting that the effects on the transcriptome have been amplified in the presence of GAB.

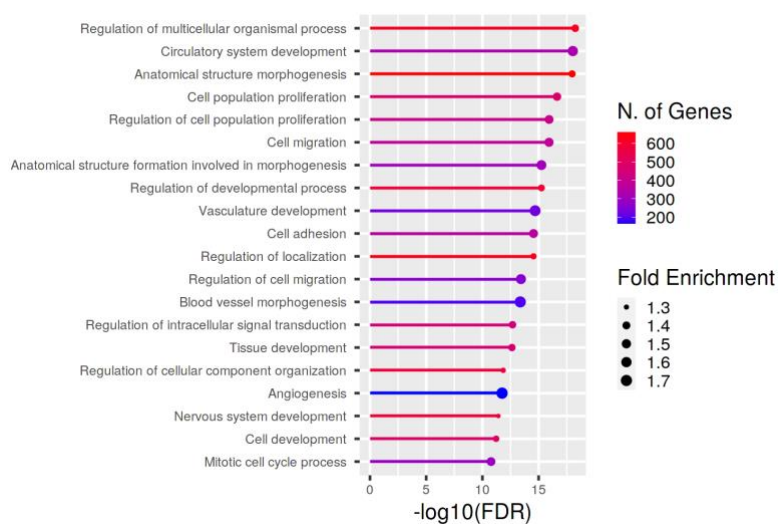


Figure 5.13. Gene ontology enrichment analysis in A172_UnVsT_GAB.

ShinyGO v0.75 gene ontology enrichment analysis was performed for genes DE in A172 upon standard treatment in the presence of Gaboxadol.

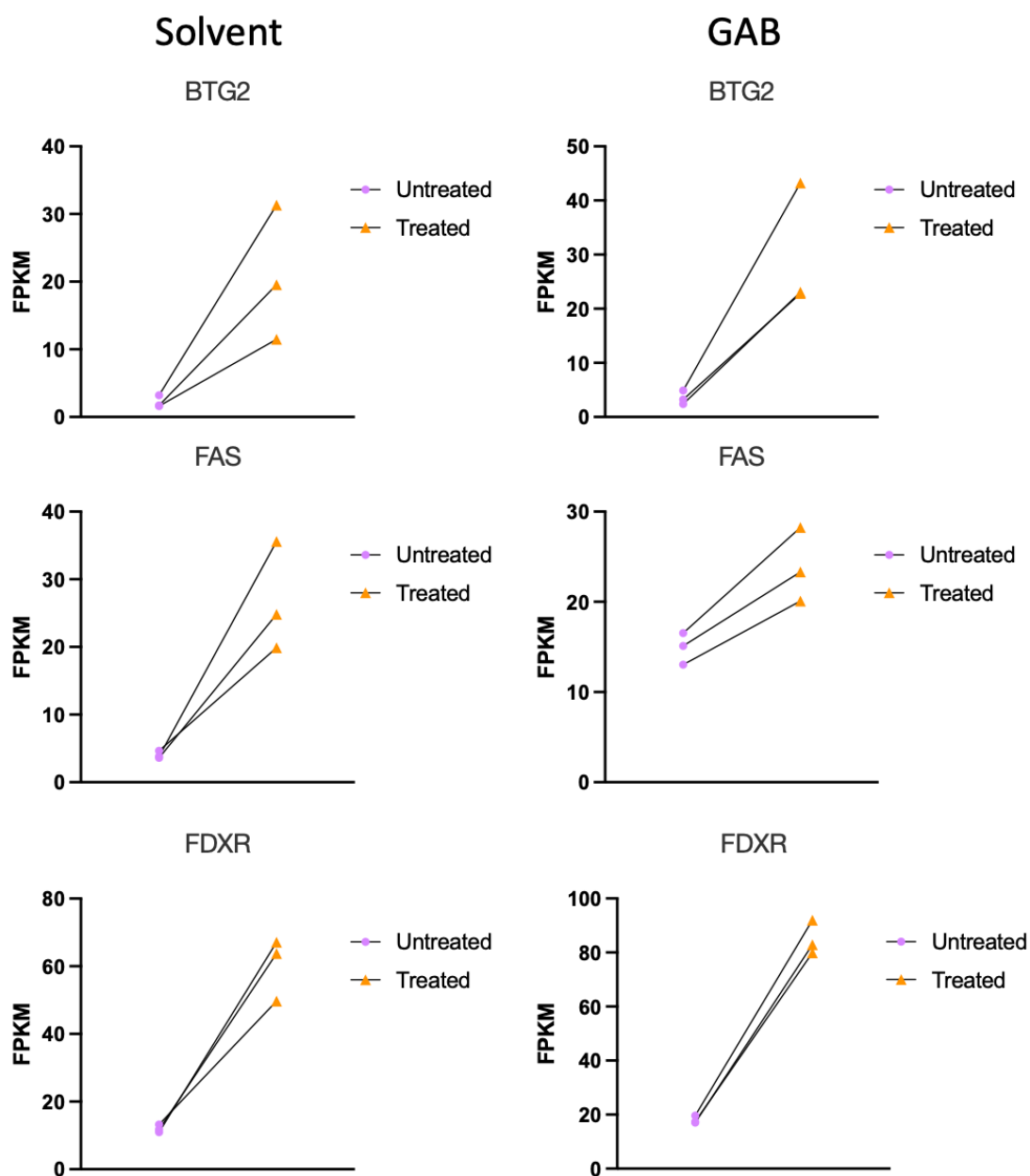


Figure 5.14. Normalised expression data for A172 genes. The normalised expression (FPKM) data for 3 out of 5 of the top DE genes in both A172 untreated vs treated in the presence of the solvent and A172 untreated vs treated in the presence of GAB.

For GBM63_UnVsT_GAB there was only one gene that was differentially expressed with an adjusted p-value of less than 0.05. The BCV is greater for GBM63 than in A172, with the BCV being the second highest for GBM63 untreated vs treated in the presence of GAB. Therefore, I lowered the significance threshold to 0.5. Using this threshold, there were still only 51 genes DE. The gene pathways that were identified, despite the limited number of genes, are similar to

those expressed in GBM63_UnVsT with many of the same GO terms such as “cell division”. WebGestalt analysis identified that enriched gene-sets were associated with cell cycle terms such as G2M checkpoint (enrichment ratio of 13.307 and mitotic spindle (enrichment ratio of 10.977). These results are similar to those observed for GBM63_UnVsT and suggest that the opposite effect on the transcriptome is occurring compared to A172. In GBM63, the treatment is causing genes to be DE, but GAB appears to be blocking these gene expression changes which results in far fewer genes DE. Therefore, GAB appears to be blocking the transcriptional reprogramming of genes that usually would happen through treatment. This correlates with what I observe for spheroid size because GAB causes standard treatment to be less effective. This appears to be because the pathways that normally are responsible for smaller spheroids after treatment are being suppressed.

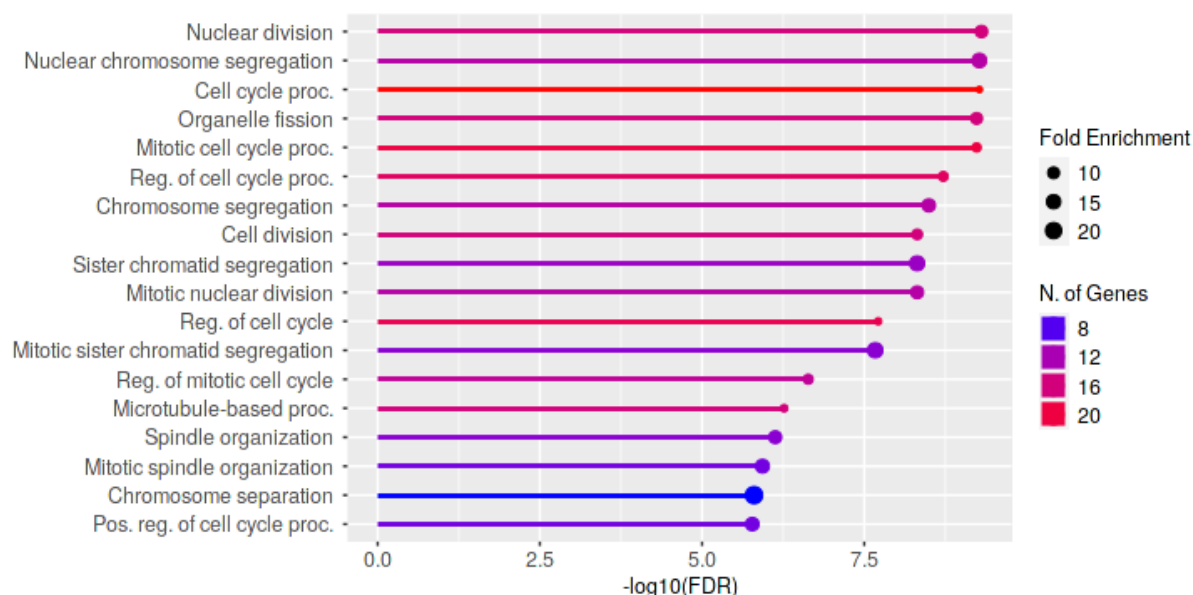


Figure 5.15. Gene ontology enrichment analysis in GBM63_UnVsT_GAB. ShinyGO v0.75 gene ontology enrichment analysis was performed for genes DE in GBM63 upon standard treatment in the presence of Gaboxadol.

5.4.1 Transcriptional changes with GAB

5.4.1.1 A172

To further inspect the effect of GAB, the genes DE between GBM63_UnVsT and GBM63_UnVsT_GAB were inspected to see how many genes were shared between, or unique to either group. Between A172_UnVsT and A172_UnVsT_GAB there are 2195 genes that are shared, 702 that are unique to

A172_UnVsT and 1247 that are unique to A172_UnVsT_GAB (Figure 5.16). In those gene-sets shared between A172_UnVsT and A172_UnVsT_GAB, the GO terms of interest include cell population proliferation and regulation of cell proliferation, which are the same terms seen in Figure 5.3 when just looking at A172_UnVsT. As stated earlier, this is likely as the mechanisms resulting in a treatment response in A172 are amplified in the presence of GAB so is no surprise that these same pathways are identified in genes shared between the vehicle control and GAB treatments. Interestingly, in the genes unique to A172_UnVsT_GAB, there are no GO terms that are enriched. This is unusual because there are 1247 genes identified in this category, which implies that other than amplifying the genes already DE following standard treatment, GAB is having a random effect on the transcriptome in A172.

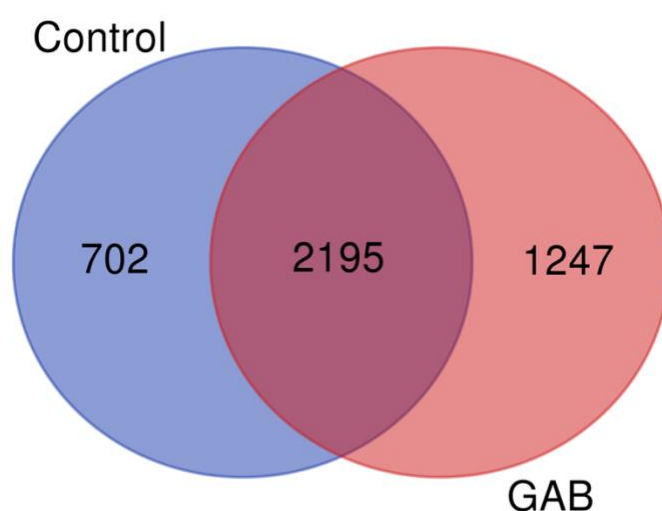


Figure 5.16. Venn diagram of genes DE in A172. Venn diagram of the number of genes shared between A172_UnVsT and A172_UnVsT_GAB. Made using <https://bioinformatics.psb.ugent.be/webtools/Venn/>.

5.4.1.2 GBM63

To further inspect the effect of GAB, the genes DE between GBM63_UnVsT and GBM63_UnVsT_GAB were analysed to identify the genes shared between, or unique to either group. There are 31 genes that are shared, leaving 21 to be unique to GAB and 462 to be unique to the solvent control (Figure 5.17). As expected, both the genes unique to GBM63_UnVsT and the shared genes have GO terms associated with cell division and the cell cycle, which is expected

because my earlier findings indicated that standard treatment affected both of these pathways. Despite only including 21 genes, those that are unique to GAB include shared terms such as “regulation of cell division”, but also unique terms such as “engulfment of apoptotic cells” (Figure 5.18). This suggests that gaboxadol has a novel mechanism in altering gene expression in spheroids which is not normally present during standard treatment alone (Figure 5.5). However, this has to be viewed with caution considering the 21 genes in this category were identified using a less stringent filtering cut-off value (adj.p <0.5 instead of 0.05) compared to other data-sets.

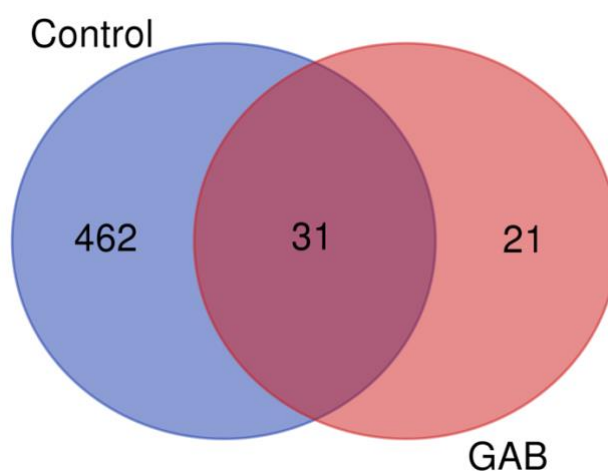


Figure 5.17. Venn diagram of genes DE in GBM63. Venn diagram of the number of genes shared between GBM63_UnVsT and GBM63_UnVsT_GAB. Made using <https://bioinformatics.psb.ugent.be/webtools/Venn/>.

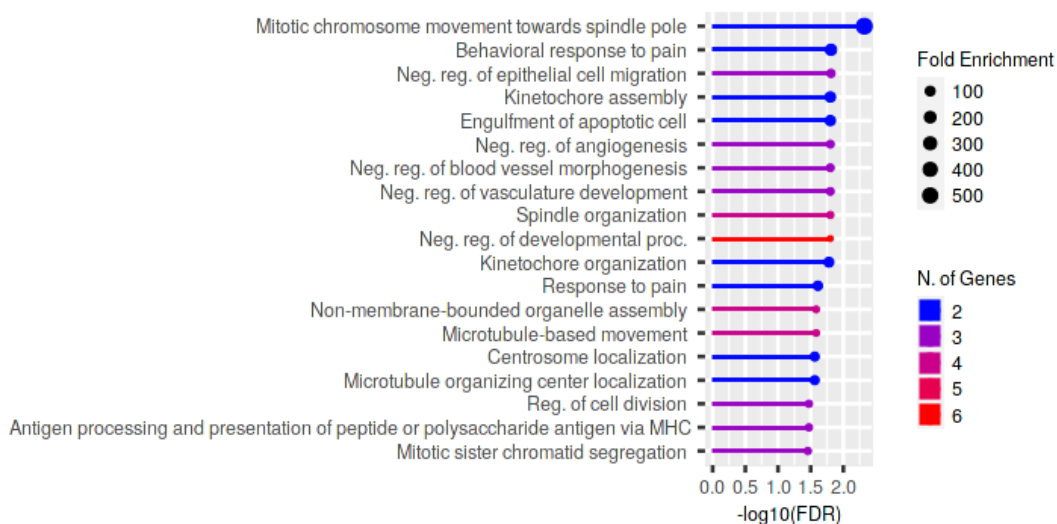


Figure 5.18. Gene ontology enrichment analysis in GBM63. ShinyGO v0.75 gene ontology enrichment analysis was performed for the DE genes shared between GBM63_UnVsT and GBM63_UnVsT_GAB.

5.5 Discussion

Through analysis of their transcriptomes, it is clear that A172 and GBM63 reflect the transcriptome of Up and Down responders subtypes, respectively. Therefore, these results show that, as observed for Up responders, A172 cells evade treatment by decreasing their proliferation. This move them towards a more quiescent phenotype which enables them to evade chemotherapy treatment that targets proliferating cells. On the other hand, GBM63 responds in a similar way to Down responders by increasing proliferation following treatment, and moving towards a more aggressive mesenchymal phenotype.

5.5.1 Treatment evasion of Up and Down responders

In GBM, the mesenchymal phenotype is associated with an aggressive phenotype and has the worst prognosis out of the GBM subtypes (310). One reason for this is that it expresses neural stem cell markers, and NSCs are associated with a high invasiveness and a resistance to chemoradiotherapy both in vitro and in a clinical environment (311, 312). This resistance comes from their ability to self-renew and proliferate extensively helping to form a heterogenous recurrent tumour, and for their ability to repair DNA damage allowing for continued division (86). Therefore, NSCs are often thought to be responsible for the tumour progression of glioblastoma following standard chemotherapy (313). A recent review by Tang *et al.*, summarised the therapies currently aimed at targeting NSCs in gliomas. This includes targeting signalling pathways commonly found in NSCs and over expressed in GSCs such as the Notch, Wnt and Sonic Hedgehog signalling pathways (86). The Notch pathway has been associated with stem cell fate, proliferation and metastasis, all common features of treatment resistance in GBM. It becomes highly activated in GSCs and maintains stem like properties which inevitably leads to increased tumorigenesis (314). Blocking the Notch signalling pathway would therefore contribute to a reduction in the tumorigenic properties of NCSs.

Up responders reduce proliferation and move to a quiescent phenotype in order to evade treatment. This is a common mechanism of treatment evasion in cancer

which works by allowing the cells to exit the cell cycle and sit in the G_0 phase indefinitely to evade chemotherapy treatment that targets rapidly dividing cells (315). Cells can remain in a quiescent state for longer periods of time before starting to divide again after treatment when conditions are favourable, leading to tumour recurrence. This makes them different to senescent cells which are unable to begin dividing again (316). These quiescent cancer cells (QCCs) express reduced amounts of Ki67, which are also observed in Up responders and in A172 (315). Approaches to specifically target QCCs have been trialled, including blocking of QCCs from re-entering the cell cycle through using CDK4/6 inhibitors to halt the transition into G_1 phase, or by therapeutically targeting cells which are in the G_0 phase specifically (317-319).

These distinct mechanisms of treatment resistance observed in GBM63 and A172 require differential target treatment approaches, alongside standard treatment in order to target the chemo-resistant populations unique to them. Targeting pathways that would result in a reduction of proliferation may therefore help Up responder tumours to further evade treatment. By contrast, targeting pathways that target cells in the G_0 phase would not provide any advantage to Down responders in a mesenchymal phenotype. Therefore, more specific treatments are needed to target characteristics unique to the responder subtype, that can be given alongside standard chemotherapy to enable this to be more effective.

However, Up and Down responders are currently identified based on the change in gene expression from primary to recurrent tumours and recurrent GBM tumours are resistant to standard treatment so targeting specific aspects of the tumour is still unlikely to have a profound effect. Ideally, a patient's responder subtype needs to be identified based solely on the expression of the primary tumours alone which would allow the primary tumours to be targeted more specifically with treatment in the hopes of preventing a recurrent tumour. Work within the group is aiming to look at this possibility and find ways of identifying Up and Down responders based on the primary tumour alone.

5.5.2 Gaboxadol effect on the transcriptome

I have been able to show that the phenotypic effect of GAB, which differs between the two cell lines, is likely because of transcriptional changes upon GAB addition. In A172, gene expression of the DE genes through treatment is amplified which

results in standard treatment being more effective. Many of the same GO analysis terms that were identified between treated and untreated are still present but with more significance and more genes in the categories showing the strengthening of these same mechanisms in the presence of GAB.

In contrast, in GBM63 the number of DE genes between treated and untreated under an $\text{adj.p} < 0.05$ threshold drops from 511 to 1 in the presence of GAB suggesting that gene expression changes are being halted by GAB and the standard treatment therefore becomes less effective. This is evidence that targeting Up and Down responders with the same treatment is not always the best option to ensure maximum treatment response. Furthermore, by lowering the significance threshold to 0.5, there is still only a total of 51 genes that are DE between treated and untreated in the presence of GAB. Despite this change in the threshold, meaning 50% of the genes identified could be false positives, the GO analysis showed the same terms as those expressed in GBM63_UnVsT to be identified such as terms related to cell division. This demonstrates the effects of GAB on halting gene expression changes as the most significantly DE genes are those DE in GBM63_UnVsT, even though their levels of DE in GBM63_UnVsT_GAB are very low. It is therefore no surprise that the phenotypic effect of this means that having GAB present alongside standard treatment results in spheroids increasing in size compared to the untreated counterparts than seen in the presence of standard treatment alone.

In A172, upon the addition of GAB, the expression of the genes are DE upon standard treatment are increased. This implies that GAB is working alongside standard treatment to increase the effect of treatment, meaning that the spheroids are smaller compared to the untreated than with standard treatment alone. The genes that are DE uniquely to GAB, and not those that are also DE upon standard treatment are not enriched for any GO terms. This implies that, other than amplifying the effect of standard treatment, in A172 GAB is having a completely random effect on the transcriptome. To date, there are no other studies that look at the effect of GAB on the transcriptome to compare and determine if GAB has a uniform or random effect on the transcriptome.

Again, as stated previously, it is important to remember that A172 and GBM63 are an established and a patient-derived cell line respectively, so maybe the mechanisms by which they respond to treatment with and without GAB could be

intrinsic differences in their biology. However, the data thus far does imply that A172 and GBM63 are Up and Down responders and therefore do require different treatments and different targets alongside standard treatment. As this study only used two cell lines, it would be beneficial to repeat these experiments in multiple cell lines, both established and patient-derived to determine if Up and Down responders can be identified, and if they respond in the same way as observed for GBM63 and A172.

5.5.3 GABA modulation

GABA modulation is evidently worth further inspection given the differences in phenotypic response to treatment in the presence of GAB between A172 and GBM63. There are many commercial GABA receptor agonists readily available, and often these have an ability to go through the blood brain barrier, such as GAB (320). This means that if GABA was of relevance then bespoke GABA targeting drugs would not need to be developed, and instead clinical trials involving already established drugs could begin.

Since GABA has been linked to multiple diseases in both a positive and negative way, it is plausible to think that GABA may be in part contributing to the treatment response seen in GBM. The impact of GABA in human disease has been widely investigated and evidence suggests that GABA seems to have both beneficial and disadvantageous impacts on varying diseases. GABA has been linked to many beneficial roles including in acting as a protective agent against toxin-induced damages in intestines, kidneys and livers, and having antioxidant, anti-microbial, and anti-inflammatory properties (292).

Furthermore, GABA has been associated with tumorigenesis in both a positive and negative outcome, although the mechanisms behind these associations are poorly understood. GABA is associated with the inhibition of tumour cell migration in colon carcinoma via the GABA_B receptor agonist baclofen (321). Cell migration is the starting point for metastasis and invasion in cancer, therefore inhibiting migration would have a positive outcome. In mouse models, GABA levels are seen to increase rapidly prior to tumour growth, allowing for a reduction in proliferation of glioma cells, particularly those expressing stem and progenitor markers. This is specifically a result of GABA_A receptor expression (322). In A172 there is a reduction in proliferation following treatment, so this might suggest why the addition of a GABA_A receptor agonist to A172 amplifies the DE genes involved

in these pathways. In addition, a study found that down regulation of GABA_A receptor results in the loss of GABA and this results in an increase in proliferation therefore promoting tumour growth in glioblastoma (323). This suggests that GABA has anti-proliferative effects in glioblastoma, which is consistent with a study by Labrakakis *et al.*, who noted that a loss of GABA in glioma cells resulted in uninhibited growth in malignant tumours, and for established glioblastoma cell lines (324).

On the contrary, GABA has also been associated with tumorigenesis in multiple tumour types including prostate cancer and gliomas and its inhibition has been suggested as a therapeutic target in cancers (325-327). Increased GABA levels have been linked to poor prognosis in a few types of solid tumours as breast, gastric and colon. Additionally, a study by Huang *et al.*, showed that increased GABA levels were seen in the higher-grade samples of individuals with colon adenocarcinoma (COAD), non-small cell lung cancer (NSCLC), and lung squamous cell carcinoma. Kaplan-Meier survival curves suggested that low GABA levels correlated with longer survival levels (288). Furthermore, Huang *et al.*, showed that GABA promoted proliferation in multiple NSCLC and COAD cell lines tested through activating β -catenin signalling, which is known to be oncogenic.

Although the mechanisms by which GABA and GABA_A receptors are involved in cancer in both a positive and negative way are often not clearly understood, it is clear GABA has the potential to be an interesting target and should be further explored. The experiments in this chapter only looked at the effect of GABA_A receptor agonists in combination with standard treatment, it would be interesting to observe the effect of a GABA_A receptor antagonist on response to standard treatment in A172 and GBM63 to determine if the opposite effect is observed in the presence of the agonists.

Chapter 6

Conclusion and future work

6.1 Summary of key findings

This study aimed to investigate the contribution of *SLC6A6* to treatment resistance in glioblastoma (GBM). To do this, models and treatment schedules were optimised, assays to determine treatment response chosen, gene knockdown performed, and protein targets inhibited.

In chapter 3, an automated spheroid imaging and quantification platform was developed in addition to a method of analysing this outputted imaging data via an R shiny app named SpheroidAnalyseR. This enabled the high throughput use of spheroids, which made it easier to set up experiments with multiple conditions such as different inhibitor and treatment combinations whilst setting up enough spheroids per experimental condition to be able to image spheroids, perform viability assays, and have enough spheroids remaining to be able to extract RNA from for sequencing.

In chapter 3 some experimental conditions that would be used in future experiments were optimised. One of which was looking at the effect of taurine on the chosen cell lines. MTT assays showed that taurine was found to decrease cell viability in 2D in all three cell lines. However, in 3D, taurine decreased spheroid size in GBM58 and GBM63 and increased it in A172. Ki67 staining in spheroids was assessed but no changes in Ki67 levels were seen, suggesting that changes in proliferation were not resulting in the change in spheroid sizes seen. At this point in the study, CellTiter-Glo 3D cell viability assay was not used therefore it is unknown if the changes in spheroid sizes on taurine addition were due to changes in cell viability. The matter appears more complicated in 3D with GBM58 and GBM63 showing a reduction in spheroid size as expected based on the 2D results, but A172 showing an increase in spheroid size. The difference seen in the effect of taurine on the cell lines is likely a result of the heterogeneity that exists within GBM and is replicated within GBM cell lines. Without further investigations to look at markers for biological process such as quiescence, apoptosis or senescence it is impossible to say how taurine is causing these differing effects.

Once models were established, *SLC6A6* targeting could be performed. This was described in chapter 4 where siRNA knockdown (KD) and 2D treatment assays were performed. In all three cell lines siRNA KD resulted in no significant difference in treatment response. Recent associations seen in the literature between *SLC6A6* and hypoxia in GBM suggest *SLC6A6* role in treatment response only causes an impact in hypoxic environments which was not reflected in these short term knockdown experiments. To further support this, shRNA KD of *SLC6A6* was successful in A172, and treatment assays in spheroids that more reflect the hypoxic environment of a GBM tumour showed that *SLC6A6* knockdown resulted in a significantly worse response to treatment, in fitting with the hypothesis that *SLC6A6* is contributing to treatment response. Unfortunately shRNA KD of *SLC6A6* was not successful in GBM58 and GBM63.

To try and understand if this difference in treatment response was because of taurine transport via TauT, TauT inhibitors were chosen for use in treatment response assays. Two inhibitors were used, one with a strong TauT inhibition and one with a weak TauT inhibition. The magnitude of change was larger when using the inhibitor that had a weak TauT inhibition. However, this TauT antagonist was also a strong GABA_A receptor agonist, which presented the possibility that changes in GABA signalling as a result of GABA_A receptor modulation were responsible for the treatment response phenotypes seen. Furthermore, the addition of these inhibitors had opposite effects on the impact of standard treatment in different cell lines. This could be as A172 is an established cell line, and GBM63 is a patient derived cell line. However, a parallel discovery in the group suggested there are two responder subtypes in GBM (the Up and Down responders) and RNA-sequencing of A172 and GBM63 show they fall into the Up and Down responder subtypes. This could help explain their differing responses to treatment, and the differences seen when treated in the presence of the inhibitors. These findings suggests that different adjuvant therapies alongside standard treatment might be needed to effectively target the different GBM responder subtypes. Targeting GABA alongside standard treatment appears to be a strong starting point for this, although the direction of GABA targeting (using agonists or antagonists) will need to be determined in a patient specific manner in association with up and down responder subtypes of GBM.

6.2 Discussion

6.2.1 Established vs patient derived cell lines

The difference between established and patient-derived cell lines has been an important subject throughout this project. Both are widely used in GBM research, and both have an important but distinct part to play. That being said, it is evident based on the literature looking at key similarities and differences between patient derived cell line, established cell lines, and GBM tumours, that patient derived cell lines far better represent the biology of GBM tumours (163).

The decision to use both established and patient-derived cell lines in this project allowed the fundamental biological differences between the two to be observed when they responded differently in experiments as discussed below. However as discussed previously, the glioma stem cells, represented by patient derived cell lines, are thought to contribute heavily to treatment resistance and drive recurrent tumour formation. Therefore, I believe they are a better model than established cell lines, and the results from these should be of higher value. In future, I think every effort should be made to use patient derived cell lines in GBM research.

There is debate as to whether cell lines themselves are good models for GBM research as the literature shows that the tumour immune environment plays a very important role in GBM biology (328-330). Additionally, recent findings have shown how GBM interacts with the surrounding normal brain tissue and uses these interactions as a way of migrating further into the normal brain, adding to the increased invasiveness of GBM (298). Using cell lines alone cannot recapitulate this immune environment or replicate the interactions between GBM and the surrounding brain. Recent advances in GBM models are helping to overcome these fallbacks. One way this is being looked at is using microfluidic devices, also known as tumour-on-chip devices (331-333). These are chambers that can hold a small piece of tissue or tumour. Upon surgery, small sections of brain tumour can be removed and inserted into the chip where it will be supplied with constant running media to keep the tissue viable. Inside this tissue piece there will be varying cell types found in a GBM tumour such as tumour cells, normal brain cells, immune cells, and blood cells meaning that treatments can be applied to these to see how actual brain tumour will respond when in a more relevant tumour microenvironment. This methodology would allow experimental

assays such inhibitor and treatment screening on the viability of the tumour to be performed.

6.2.2 Linking back to *SLC6A6* upregulation

SLC6A6 levels were found to be significantly increased in GBM tumours which is why it was of interest to us in the first place. As *SLC6A6* encodes a taurine transporter, it would be easy to assume that increased levels of *SLC6A6* result in an increase in taurine which could indicate taurine benefits tumour survival. However, when the cell lines were grown as spheroids and treated with standard treatment in combination with two TauT inhibitors, the inhibitor that resulted in the largest effect was actually only a weak TauT inhibitor. However, this was also a strong GABA_A receptor agonist. This led to my hypothesis that GABA modulation is contributing to treatment resistance in GBM. In gliomas, including GBM, GABA signalling and GABA_A receptor have been shown to be dysregulated (298). Perhaps this also occurs in GBM, and TauT is dysregulated resulting in increased levels of GABA, which would help to explain in part the results seen when inhibiting TauT but also explain the significant upregulation of *SLC6A6* in GBM tumours following treatment.

6.3 Future work

The experiments indicate that GABA_A receptor modulation by the TauT antagonists result in differential treatment responses between A172 and GBM58/GBM63. To get a better insight into the role of GABA_A receptor, treatment experiments should be repeated using a GABA_A receptor antagonist. If GABA_A receptor is contributing to the treatment response in the cell lines, then the opposite effect would be seen as when using GAB and GES. There are many readily available GABA_A receptor antagonists that could be used for this. An example is Pentylentetrazole which has no known effect on the levels of taurine in so would help to distinguish the role of taurine and GABA (334). RNA from these experiments should be sequenced and the pathways that are dysregulated compared to those seen to be affected by GAB.

More recent studies have optimised ways to successfully perform CRISPR-Cas9 in patient derived cell lines using methods that are more successful on harder to transfect cell lines such as electroporation. If CRISPR-Cas9 can be performed, then the differences between TauT knockout and GABA_A Receptor knockout can

be compared. This should help define the contributions each of these two transporters has on the treatment response in GBM.

Additionally, a mutant *SLC6A6* knockout method is available that allows either the inhibition of taurine transport via TauT or inhibits the transport of both taurine and GABA via TauT. This could help see the impact of TauT on treatment response and dissect if the impact is due to taurine or GABA transport. This would be a more precise mechanism of assessing different response to treatment in relation to GABA and Taurine transport than using inhibitors.

The response to TauT antagonists seems to be causing differential treatment response in the cell lines. This is thought to be due to the Up and Down responder subtypes. To validate this, more cell lines should be treated and their RNA sequenced to validate if they fall into the Up or Down responder subtypes and if their response to treatment mimics those seen in Up and Down responders. If this is the case, the experiments using inhibitors should be repeated on these cell lines to see if this reflects what was seen in A172 and GBM63. This would help get a better insight into these response subtypes, and whether TauT and/or GABA is implicated in this. This will hopefully pave the way towards a more stratified treatment regime in GBM whereby patients are treated based on their responder subtype. Of course, currently a responder subtype is assigned based on the gene expression changes after treatment. Therefore, to apply a stratified treatment response, the responder subtype needs to be identified at initial diagnosis. Work in the group is looking into if this is possible. Due to the complexity of GBM, it is unlikely that a treatment will be found that is applicable to all patients, however it is hoped that this work can be used towards improving therapeutic strategies by beginning to work towards a more personalised approach to GBM treatment based on each individual tumour profile.

Abbreviations

7+/10-	Chromosome 7 gain and chromosome 10 loss
AC-like	Astrocyte-like
ADHD	Attention deficit hyperactivity disorder
adj.p	Adjusted p-value
AIC	5-aminoimidazole-4-carboxamide
aNSCs	Activated neural stem cells
Argo-2	Argonaute-2
ATCC	American Type Culture Collection
BCV	Biological coefficient of variation
Bp	Base pairs
<i>BTG2</i>	BTG anti-proliferation factor 2
Cas9n	Mutant nickase versions of Cas9
cDNA	Complementary DNA
CNS	Central nervous system
COAD	Colon adenocarcinoma
CPM	Counts per million
CRISPR	Clustered regularly interspaced short term repeats-Cas9
crRNA	CRISPR RNA
CSCs	Cancer cells
CSDA	Cysteine sulfonic acid decarboxylase
DE	Differentially expressed
DE	Differentially expressed
DGE	Differential gene expression
DGE	Differential gene expression
DMEM	Dulbecco's modified eagle medium
DMSO	Dimethyl sulfoxide

dsRNA	Double strand RNA
EGF	Epidermal growth factor
EGF	Epidermal growth factor
EGFR	Epidermal growth factor receptor
FCS	Foetal calf serum
FGF	Fibroblast growth factor
FPKM	Fragments per kilobase of transcript per million mapped fragments
GAB	Gaboxadol hydrochloride
GAB	Gaboxadol
GABA	γ -aminobutyric acid
GABAa receptor	γ -aminobutyric acid type A receptor
GABARAPL1	GABA type A receptor associated protein like 1
GABARAPL2	GABA type A receptor associated protein like 2
GBM	Glioblastoma
GEMMs	Genetically engineered mouse models
GES	Guanidinoethyl sulfonate
GFP	Green fluorescent protein
GLASS	Glioma Longitudinal Analysis Consortium
GO	Gene ontology
GSC	Glioma stem cell
IAA	Imidazole-4-acetic acid
IDH	Isocitrate dehydrogenase
IRR	Irradiation
ITH	Intratumor heterogeneity
LDH	Lactate dehydrogenase
LE	Leading edge

LOH	Loss of heterozygosity
MES-like	Mesenchymal-like
<i>MGMT</i>	O ⁶ -methylguanine-DNA-methyltransferase
MTIC	5-(3-methyltriazen-1-yl)imidazole-4-carboxamide
MMR	Mismatch repair
MRI	Magnetic resource imaging
MTS	3-(4,5-dimethylthiazol-2-yl)-5-(3-carboxymethoxyphenyl)-2-(4-sulphophenyl)-2H-tetrazolium
MTT	3-(4,5-dimethylthiazol-2-yl)-2,5-diphenyltetrazolium bromide
NB	Neurobasal
NES	Normalised enrichment score
NGS	Next generation sequencing
NHEJ	Non-homologous end joining
NPC-like	Neural-progenitor-like
NPCs	Neural progenitor cells
NSCLC	Non-small cell lung cancer
NSCs	Neural stem cells
NT	Non-targeting
O ⁶ -MeG	O ⁶ -methylguanine
OPC-like	Oligodendrocyte-progenitor-like
ORA	Over-representation analysis
PAMs	Protospacer adjacent motifs
PBS	Phosphate buffered saline
PC	Principle Component
PDTX	Patient-derived tumour xenograft
PKC	Protein kinase C
PPR	Proliferation/progenitor

PTZ	Pentylenetetrazol
QCCs	Quiescent cancer cells
qNSCs	Quiescent neural stem cells
qPCR	Quantitative polymerase chain reaction
RISC	RNA-induced silencing complex
RNA-seq	RNA-sequencing
RNAi	RNA interference
RSEM	RNA-Seq by expectation maximization
RTK	Receptor tyrosine kinase
ScRNAseq	Single cell RNA sequencing
SD	Standard deviation
SEM	Standard error of the mean
sgRNA	Single guide RNA
shRNA	Short hairpin RNA
siRNA	Small interfering RNA
SLC6	Solute carrier 6
<i>SLC6A6</i>	Solute Carrier Family 6 Member 6
TauT	Taurine transporter
TC	Tissue culture
TCGA	The Cancer Genome Atlas
TERT	Telomerase reverse transcriptase
TMZ	Temozolomide
TP53	Tumour protein
TPM	Transcript per million
trancrRNA	Transactivating crRNA
WebGestalt	WEB-based Gene SeT AnaLysis Toolkit
WHO	World health organisation

References

1. Wen PY, Weller M, Lee EQ, Alexander BM, Barnholtz-Sloan JS, Barthel FP, et al. Glioblastoma in adults: a Society for Neuro-Oncology (SNO) and European Society of Neuro-Oncology (EANO) consensus review on current management and future directions. *Neuro Oncol.* 2020;22(8):1073-113.
2. Louis DN, Perry A, Wesseling P, Brat DJ, Cree IA, Figarella-Branger D, et al. The 2021 WHO Classification of Tumors of the Central Nervous System: a summary. *Neuro Oncol.* 2021;23(8):1231-51.
3. Perry A, Wesseling P. Histologic classification of gliomas. 2016. In: *Handbook of Clinical Neurology* [Internet]. 2016/03/08. [71-95]. Available from: <https://www.ncbi.nlm.nih.gov/pubmed/26948349>.
4. Ostrom QT, Bauchet L, Davis FG, Deltour I, Fisher JL, Langer CE, et al. The epidemiology of glioma in adults: a "state of the science" review. *Neuro Oncol.* 2014;16(7):896-913.
5. Lukas RV, Wainwright DA, Ladomersky E, Sachdev S, Sonabend AM, Stupp R. Newly Diagnosed Glioblastoma- A Review on Clinical Management. *Oncology.* 2019;33(3):91-100.
6. Philips A, Henshaw DL, Lamburn G, O'Carroll MJ. Brain Tumours: Rise in Glioblastoma Multiforme Incidence in England 1995-2015 Suggests an Adverse Environmental or Lifestyle Factor. *J Environ Public Health.* 2018;2018:7910754.
7. Tamimi AF, Juweid M. Epidemiology and Outcome of Glioblastoma. 2017. In: *Glioblastoma* [Internet]. Codon Publications; [143-55].
8. Brodbelt A, Greenberg D, Winters T, Williams M, Vernon S, Collins VP, et al. Glioblastoma in England: 2007-2011. *Eur J Cancer.* 2015;51(4):533-42.
9. Ostrom QT, Cioffi G, Gittleman H, Patil N, Waite K, Kruchko C, et al. CBTRUS Statistical Report: Primary Brain and Other Central Nervous System Tumors Diagnosed in the United States in 2012-2016. *Neuro Oncol.* 2019;21(Suppl 5):v1-v100.
10. Susan M. Chang, Ian F. Parney, Wei Huang, Frederick A. Anderson, Anthony L. Asher, Mark Bernstein, et al. Patterns of Care for Adults With Newly Diagnosed Malignant Glioma. *Journal of American Medical Association.* 2005;293:557-64.

11. Lyratzopoulos G, Abel GA, McPhail S, Neal RD, Rubin GP. Measures of promptness of cancer diagnosis in primary care: secondary analysis of national audit data on patients with 18 common and rarer cancers. *Br J Cancer*. 2013;108(3):686-90.
12. Gilard V, Tebani A, Dabaj I, Laquerriere A, Fontanilles M, Derrey S, et al. Diagnosis and Management of Glioblastoma: A Comprehensive Perspective. *J Pers Med*. 2021;11(4).
13. Alireza Mansouri, Jason Karamchandani, Das S. Molecular Genetics of Secondary Glioblastoma. 2017. In: Glioblastoma [Internet]. Codon Publications.
14. Ohgaki H, Kleihues P. The definition of primary and secondary glioblastoma. *Clin Cancer Res*. 2013;19(4):764-72.
15. Ohgaki H. Genetic pathways to glioblastomas. *Neuropathology*. 2005;25:1-7.
16. Glas M, Rath BH, Simon M, Reinartz R, Schramme A, Trageser D, et al. Residual tumor cells are unique cellular targets in glioblastoma. *Ann Neurol*. 2010;68(2):264-9.
17. Roger Stupp, Warren P. Mason, Martin J. van den Bent, Michael Weller, Barbara Fisher, Martin J.B. Taphoorn, et al. Radiotherapy plus Concomitant and Adjuvant Temozolomide for Glioblastoma. *The New England Journal of Medicine*. 2005;352(10):987-96.
18. Gilvert MR. Recurrent Glioblastoma: A Fresh Look at Current Therapies and Emerging Novel Approaches. *Seminars in Oncology*. 2011;38(4):21-33.
19. Birzu C, French P, Caccese M, Cerretti G, Idbaih A, Zagone V, et al. Recurrent Glioblastoma: From Molecular Landscape to New Treatment Perspectives. *Cancers (Basel)*. 2020;13(1).
20. Ringel F, Pape H, Sabel M, Krex D, Bock HC, Misch M, et al. Clinical benefit from resection of recurrent glioblastomas: results of a multicenter study including 503 patients with recurrent glioblastomas undergoing surgical resection. *Neuro Oncol*. 2016;18(1):96-104.
21. Suchorska B, Weller M, Tabatabai G, Senft C, Hau P, Sabel MC, et al. Complete resection of contrast-enhancing tumor volume is associated with improved survival in recurrent glioblastoma-results from the DIRECTOR trial. *Neuro Oncol*. 2016;18(4):549-56.
22. Helseth R, Helseth E, Johannesen TB, Langberg CW, Lote K, Ronning P, et al. Overall survival, prognostic factors, and repeated surgery in a

- consecutive series of 516 patients with glioblastoma multiforme. *Acta Neurol Scand.* 2010;122(3):159-67.
23. Barbagallo GM, Jenkinson MD, Brodbelt AR. 'Recurrent' glioblastoma multiforme, when should we reoperate? *Br J Neurosurg.* 2008;22(3):452-5.
 24. Woodroffe RW, Zanaty M, Soni N, Mott SL, Helland LC, Pasha A, et al. Survival after reoperation for recurrent glioblastoma. *J Clin Neurosci.* 2020;73:118-24.
 25. Becker AP, Sells BE, Haque SJ, Chakravarti A. Tumor Heterogeneity in Glioblastomas: From Light Microscopy to Molecular Pathology. *Cancers (Basel).* 2021;13(4).
 26. Eder K, Kalman B. Molecular heterogeneity of glioblastoma and its clinical relevance. *Pathol Oncol Res.* 2014;20(4):777-87.
 27. Friedmann-Morvinski D. Glioblastoma Heterogeneity and Cancer Cell Plasticity. *Critical Review in Oncogenesis.* 2014;19(5):327-36.
 28. Parker NR, Khong P, Parkinson JF, Howell VM, Wheeler HR. Molecular heterogeneity in glioblastoma: potential clinical implications. *Front Oncol.* 2015;5:55.
 29. Georgescu M-M. Multi-Platform Classification of IDH-Wild-Type Glioblastoma Based on ERK:MAPK Pathway- Diagnostic, Prognostic and Therapeutic Implications. *Cancers.* 2021;13.
 30. Han S, Liu Y, Cai SJ, Qian M, Ding J, Larion M, et al. IDH mutation in glioma: molecular mechanisms and potential therapeutic targets. *Br J Cancer.* 2020;122(11):1580-9.
 31. Choi BD, Curry WT. IDH mutational status and the immune system in gliomas: a tale of two tumors? *Transl Cancer Res.* 2017;6(Suppl 7):S1253-S6.
 32. Kayabolen A, Yilmaz E, Bagci-Onder T. IDH Mutations in Glioma: Double-Edged Sword in Clinical Applications? *Biomedicines.* 2021;9(7).
 33. Lemmon MA, Schlessinger J, Ferguson KM. The EGFR family: not so prototypical receptor tyrosine kinases. *Cold Spring Harb Perspect Biol.* 2014;6(4):a020768.
 34. Gan HK, Cvrljevic AN, Johns TG. The epidermal growth factor receptor variant III (EGFRvIII): where wild things are altered. *FEBS J.* 2013;280(21):5350-70.

35. Brennan CW, Verhaak RG, McKenna A, Campos B, Nounshmehr H, Salama SR, et al. The somatic genomic landscape of glioblastoma. *Cell*. 2013;155(2):462-77.
36. Lassman AB, Aldape KD, Ansell PJ, Bain E, Curran WJ, Eoli M, et al. Epidermal growth factor receptor (EGFR) amplification rates observed in screening patients for randomized trials in glioblastoma. *J Neurooncol*. 2019;144(1):205-10.
37. An Z, Aksoy O, Zheng T, Fan QW, Weiss WA. Epidermal growth factor receptor and EGFRvIII in glioblastoma: signaling pathways and targeted therapies. *Oncogene*. 2018;37(12):1561-75.
38. Hatanpaa KJ, Burma S, Zhao D, Habib AA. Epidermal growth factor receptor in glioma: signal transduction, neuropathology, imaging, and radioresistance. *Neoplasia*. 2010;12(9):675-84.
39. Mok TS. Personalized medicine in lung cancer: what we need to know. *Nat Rev Clin Oncol*. 2011;8(11):661-8.
40. Arteaga CL, Sliwkowski MX, Osborne CK, Perez EA, Puglisi F, Gianni L. Treatment of HER2-positive breast cancer: current status and future perspectives. *Nat Rev Clin Oncol*. 2011;9(1):16-32.
41. Wee P, Wang Z. Epidermal Growth Factor Receptor Cell Proliferation Signaling Pathways. *Cancers (Basel)*. 2017;9(5).
42. Raizer JJ. HER1/EGFR tyrosine kinase inhibitors for the treatment of glioblastoma multiforme. *J Neurooncol*. 2005;74(1):77-86.
43. Saleem H, Kulsoom Abdul U, Kucukosmanoglu A, Houweling M, Cornelissen FMG, Heiland DH, et al. The TICKing clock of EGFR therapy resistance in glioblastoma: Target Independence or target Compensation. *Drug Resist Updat*. 2019;43:29-37.
44. Westphal M, Maire CL, Lamszus K. EGFR as a Target for Glioblastoma Treatment: An Unfulfilled Promise. *CNS Drugs*. 2017;31(9):723-35.
45. Olympios N, Gilard V, Marguet F, Clatot F, Di Fiore F, Fontanilles M. TERT Promoter Alterations in Glioblastoma: A Systematic Review. *Cancers (Basel)*. 2021;13(5).
46. Smith EM, Pendlebury DF, Nandakumar J. Structural biology of telomeres and telomerase. *Cell Mol Life Sci*. 2020;77(1):61-79.
47. Heidenreich B, Kumar R. TERT promoter mutations in telomere biology. *Mutat Res Rev Mutat Res*. 2017;771:15-31.

48. Lu W, Zhang Y, Liu D, Songyang Z, Wan M. Telomeres-structure, function, and regulation. *Exp Cell Res*. 2013;319(2):133-41.
49. Yucheng Xu, Kaijie He, Goldkorn A. Telomerase Targeted Therapy in Cancer and Cancer Stem Cells. 2011;9(6):442-55.
50. Matthew Meyerson, Christopher M. Counter, Elinor Ng Eaton, Leif W. Ellisen, Philipp Steiner, Stephanie Dickinson Caddle, et al. hEST2, the Putative Human Telomerase Catalytic Subunit Gene, Is Up-Regulated in Tumor Cells and during Immortalization. *Cell*. 1997;90:785-95.
51. Colebatch AJ, Dobrovic A, Cooper WA. TERT gene: its function and dysregulation in cancer. *J Clin Pathol*. 2019;72(4):281-4.
52. Marianne Labussière, Blandine Boisselier, Karima Mokhtari, Anna-Luisa Di Stefano, Anais Rahimian, Marta Rossetto, et al. Combined analysis of TERT, EGFR, and IDH status defines distinct prognostic glioblastoma classes. *Neurology*. 2014;83(13):1200-6.
53. Spiegl-Kreinecker S, Lotsch D, Ghanim B, Pirker C, Mohr T, Laaber M, et al. Prognostic quality of activating TERT promoter mutations in glioblastoma: interaction with the rs2853669 polymorphism and patient age at diagnosis. *Neuro Oncol*. 2015;17(9):1231-40.
54. Mohamed Ali Mosrati, Annika Malmström, Malgorzata Lysiak, Adam Kryzstofiak, Martin Hallbeck, Peter Milos, et al. TERT promoter mutations and polymorphisms as prognostic factors in primary glioblastoma. *Oncotarget*. 2015;6(18):16663-73.
55. Arita H, Yamasaki K, Matsushita Y, Nakamura T, Shimokawa A, Takami H, et al. A combination of TERT promoter mutation and MGMT methylation status predicts clinically relevant subgroups of newly diagnosed glioblastomas. *Acta Neuropathol Commun*. 2016;4(1):79.
56. Arita H, Narita Y, Fukushima S, Tateishi K, Matsushita Y, Yoshida A, et al. Upregulating mutations in the TERT promoter commonly occur in adult malignant gliomas and are strongly associated with total 1p19q loss. *Acta Neuropathol*. 2013;126(2):267-76.
57. Salloum R, Hummel TR, Kumar SS, Dorris K, Li S, Lin T, et al. A molecular biology and phase II study of imetelstat (GRN163L) in children with recurrent or refractory central nervous system malignancies: a pediatric brain tumor consortium study. *J Neurooncol*. 2016;129(3):443-51.

58. Chiappori AA, Kolevska T, Spigel DR, Hager S, Rarick M, Gadgeel S, et al. A randomized phase II study of the telomerase inhibitor imetelstat as maintenance therapy for advanced non-small-cell lung cancer. *Ann Oncol.* 2015;26(2):354-62.
59. Wemmert S, Ketter R, Rahnenfuhrer J, Beerenwinkel N, Strowitzki M, Feiden W, et al. Patients with high-grade gliomas harboring deletions of chromosomes 9p and 10q benefit from temozolomide treatment. *Neoplasia.* 2005;7(10):883-93.
60. Korshunov A, Sycheva R, Golanov A. The prognostic relevance of molecular alterations in glioblastomas for patients age < 50 years. *Cancer.* 2005;104(4):825-32.
61. Munoz-Hidalgo L, San-Miguel T, Megias J, Monleon D, Navarro L, Roldan P, et al. Somatic copy number alterations are associated with EGFR amplification and shortened survival in patients with primary glioblastoma. *Neoplasia.* 2020;22(1):10-21.
62. Stichel D, Ebrahimi A, Reuss D, Schrimpf D, Ono T, Shirahata M, et al. Distribution of EGFR amplification, combined chromosome 7 gain and chromosome 10 loss, and TERT promoter mutation in brain tumors and their potential for the reclassification of IDHwt astrocytoma to glioblastoma. *Acta Neuropathol.* 2018;136(5):793-803.
63. Cancer Genome Atlas Research N. Comprehensive genomic characterization defines human glioblastoma genes and core pathways. *Nature.* 2008;455(7216):1061-8.
64. Verhaak RG, Hoadley KA, Purdom E, Wang V, Qi Y, Wilkerson MD, et al. Integrated genomic analysis identifies clinically relevant subtypes of glioblastoma characterized by abnormalities in PDGFRA, IDH1, EGFR, and NF1. *Cancer Cell.* 2010;17(1):98-110.
65. Teo WY, Sekar K, Seshachalam P, Shen J, Chow WY, Lau CC, et al. Relevance of a TCGA-derived Glioblastoma Subtype Gene-Classifer among Patient Populations. *Sci Rep.* 2019;9(1):7442.
66. Sturm D, Witt H, Hovestadt V, Khuong-Quang DA, Jones DT, Konermann C, et al. Hotspot mutations in H3F3A and IDH1 define distinct epigenetic and biological subgroups of glioblastoma. *Cancer Cell.* 2012;22(4):425-37.

67. Gill BJ, Pisapia DJ, Malone HR, Goldstein H, Lei L, Sonabend A, et al. MRI-localized biopsies reveal subtype-specific differences in molecular and cellular composition at the margins of glioblastoma. *Proc Natl Acad Sci U S A*. 2014;111(34):12550-5.
68. Patel AP, Tirosh I, Trombetta JJ, Shalek AK, Gillespie SM, Wakimoto H, et al. Single-cell RNA-seq highlights intratumoral heterogeneity in primary glioblastoma. *Science*. 2014;344(6190):1396-401.
69. Sottoriva A, Spiteri I, Piccirillo SG, Touloumis A, Collins VP, Marioni JC, et al. Intratumor heterogeneity in human glioblastoma reflects cancer evolutionary dynamics. *Proc Natl Acad Sci U S A*. 2013;110(10):4009-14.
70. Wang Q, Hu B, Hu X, Kim H, Squatrito M, Scarpace L, et al. Tumor Evolution of Glioma-Intrinsic Gene Expression Subtypes Associates with Immunological Changes in the Microenvironment. *Cancer Cell*. 2017;32(1):42-56 e6.
71. Neftel C, Laffy J, Filbin MG, Hara T, Shore ME, Rahme GJ, et al. An Integrative Model of Cellular States, Plasticity, and Genetics for Glioblastoma. *Cell*. 2019;178(4):835-49 e21.
72. Piper K, DePledge L, Karsy M, Cobbs C. Glioma Stem Cells as Immunotherapeutic Targets: Advancements and Challenges. *Front Oncol*. 2021;11:615704.
73. Battle E, Clevers H. Cancer stem cells revisited. *Nat Med*. 2017;23(10):1124-34.
74. Lapidot T, Sirard C, Vormoor J, Murdoch B, Hoang T, Caceres-Cortes J, et al. A cell initiating human acute myeloid leukaemia after transplantation into SCID mice. *Nature*. 1994;367(6464):645-8.
75. O'Brien CA, Pollett A, Gallinger S, Dick JE. A human colon cancer cell capable of initiating tumour growth in immunodeficient mice. *Nature*. 2007;445(7123):106-10.
76. Sheila K. Singh, Ian D. Clarke, Mizuhiko Terasaki, Victoria E. Bonn, Cynthia Hawkins, Jeremy Squire, et al. Identification of a Cancer Stem Cell in Human Brain Tumors. *Cancer Research*. 2003;63:5821-8.
77. Al-Hajj M, Wicha MS, Benito-Hernandez A, Morrison SJ, Clarke MF. Prospective identification of tumorigenic breast cancer cells. *Proceedings of the National Academy of Sciences*. 2003;100(7):3983-8.

78. Clevers H. The cancer stem cell: premises, promises and challenges. *Nat Med.* 2011;17(3):313-9.
79. Marzagalli M, Fontana F, Raimondi M, Limonta P. Cancer Stem Cells—Key Players in Tumor Relapse. *Cancers.* 2021;13(3):376.
80. Yang L, Shi P, Zhao G, Xu J, Peng W, Zhang J, et al. Targeting cancer stem cell pathways for cancer therapy. *Signal Transduct Target Ther.* 2020;5(1):8.
81. Cheng L, Wu Q, Guryanova OA, Huang Z, Huang Q, Rich JN, et al. Elevated invasive potential of glioblastoma stem cells. *Biochemical and Biophysical Research Communications.* 2011;406(4):643-8.
82. Hassn Mesrati M, Behrooz AB, Y. Abuhamad A, Syahir A. Understanding Glioblastoma Biomarkers: Knocking a Mountain with a Hammer. *Cells.* 2020;9(5):1236.
83. Tunici P, Bissola L, Lualdi E, Pollo B, Cajola L, Broggi G, et al. Genetic alterations and in vivo tumorigenicity of neurospheres derived from an adult glioblastoma. *Molecular Cancer.* 2004;3(1):25.
84. LAURA ANNOVAZZI, MARTA MELLAI, VALENTINA CALDERA, VALENTE G, SCHIFFER D. SOX2 Expression and Amplification in Gliomas and Glioma Cell Lines. *Cancer Genomics and Proteomics* 2011;8:139-48.
85. Singh SK, Hawkins C, Clarke ID, Squire JA, Bayani J, Hide T, et al. Identification of human brain tumour initiating cells. *Nature.* 2004;432(7015):396-401.
86. Tang X, Zuo C, Fang P, Liu G, Qiu Y, Huang Y, et al. Targeting Glioblastoma Stem Cells: A Review on Biomarkers, Signal Pathways and Targeted Therapy. *Front Oncol.* 2021;11:701291.
87. Jacob J. Mandel, Michael Youssef, Ethan Ludmir, Shlomit Yust-Katz, Akash J. Patel, Groot JFD. Highlighting the need for reliable clinical trials in glioblastoma. *Expert Review of Anticancer Therapy.* 2018;18(10):1031-40.
88. Bagley SJ, Kothari S, Rahman R, Lee EQ, Dunn GP, Galanis E, et al. Glioblastoma Clinical Trials: Current Landscape and Opportunities for Improvement. *Clin Cancer Res.* 2022;28(4):594-602.
89. Catarina Fernandes, Andreia Costa, Lígia Osório, Rita Costa Lago, Paulo Linhares, Bruno Carvalho, et al. Current Standards of Care in Glioblastoma Therapy. 2017. In: *Glioblastoma [Internet].* Codon Publications; [197-243].

90. Muller DMJ, De Swart ME, Ardon H, Barkhof F, Bello L, Berger MS, et al. Timing of glioblastoma surgery and patient outcomes: a multicenter cohort study. *Neurooncol Adv.* 2021;3(1):vdab053.
91. Zhang JJY, Lee KS, Voisin MR, Hervey-Jumper SL, Berger MS, Zadeh G. Awake craniotomy for resection of supratentorial glioblastoma: a systematic review and meta-analysis. *Neurooncol Adv.* 2020;2(1):vdaa111.
92. Hadjipanayis CG, Stummer W. 5-ALA and FDA approval for glioma surgery. *Journal of Neuro-Oncology.* 2019;141(3):479-86.
93. Stummer W, Pichlmeier U, Meinel T, Wiestler OD, Zanella F, Reulen H-J. Fluorescence-guided surgery with 5-aminolevulinic acid for resection of malignant glioma: a randomised controlled multicentre phase III trial. *The Lancet Oncology.* 2006;7(5):392-401.
94. Michael E. Berens, Giese A. "...those left behind". *Biology and Oncology of Invasive Glioma Cells. Neoplasia.* 1999;1(3):206-19.
95. Pala A, Karpel-Massler G, Kast RE, Wirtz CR, Halatsch ME. Epidermal to Mesenchymal Transition and Failure of EGFR-Targeted Therapy in Glioblastoma. *Cancers (Basel).* 2012;4(2):523-30.
96. Strobel H, Baisch T, Fitzel R, Schilberg K, Siegelin MD, Karpel-Massler G, et al. Temozolomide and Other Alkylating Agents in Glioblastoma Therapy. *Biomedicines.* 2019;7(3):69.
97. Sharyn D. Baker, Mark Wirth, Paul Statkevich, Pascale Reidenberg, Kevin Alton, Susan E. Sartorius, et al. Absorption, Metabolism, and Excretion of ¹⁴C-Temozolomide following Oral Administration to Patients with Advanced Cancer. *Clinical Cancer Research.* 1999;5:309-17.
98. Fan CH, Liu WL, Cao H, Wen C, Chen L, Jiang G. O6-methylguanine DNA methyltransferase as a promising target for the treatment of temozolomide-resistant gliomas. *Cell Death Dis.* 2013;4:e876.
99. Thomas A, Tanaka M, Trepel J, Reinhold WC, Rajapakse VN, Pommier Y. Temozolomide in the Era of Precision Medicine. *Cancer Res.* 2017;77(4):823-6.
100. Jiapaer S, Furuta T, Tanaka S, Kitabayashi T, Nakada M. Potential Strategies Overcoming the Temozolomide Resistance for Glioblastoma. *Neurol Med Chir (Tokyo).* 2018;58(10):405-21.

101. Erasimus H, Gobin M, Niclou S, Van Dyck E. DNA repair mechanisms and their clinical impact in glioblastoma. *Mutat Res Rev Mutat Res*. 2016;769:19-35.
102. Rivera AL, Pelloski CE, Gilbert MR, Colman H, De La Cruz C, Sulman EP, et al. MGMT promoter methylation is predictive of response to radiotherapy and prognostic in the absence of adjuvant alkylating chemotherapy for glioblastoma. *Neuro Oncol*. 2010;12(2):116-21.
103. Sciuscio D, Diserens AC, van Dommelen K, Martinet D, Jones G, Janzer RC, et al. Extent and patterns of MGMT promoter methylation in glioblastoma- and respective glioblastoma-derived spheres. *Clin Cancer Res*. 2011;17(2):255-66.
104. Hegi ME, Diserens A-C, Gorlia T, Hamou M-F, Tribolet Nd, Weller M, et al. MGMT Gene Silencing and Benefit from Temozolomide in Glioblastoma. *The New England Journal of Medicine*. 2005;335:997-1003.
105. Binabaj MM, Bahrami A, ShahidSales S, Joodi M, Joudi Mashhad M, Hassanian SM, et al. The prognostic value of MGMT promoter methylation in glioblastoma: A meta-analysis of clinical trials. *J Cell Physiol*. 2018;233(1):378-86.
106. Weller M, Stupp R, Reifenberger G, Brandes AA, van den Bent MJ, Wick W, et al. MGMT promoter methylation in malignant gliomas: ready for personalized medicine? *Nat Rev Neurol*. 2010;6(1):39-51.
107. Morris KV, Mattick JS. The rise of regulatory RNA. *Nat Rev Genet*. 2014;15(6):423-37.
108. Djebali S, Davis CA, Merkel A, Dobin A, Lassmann T, Mortazavi A, et al. Landscape of transcription in human cells. *Nature*. 2012;489(7414):101-8.
109. Li X, Wang CY. From bulk, single-cell to spatial RNA sequencing. *Int J Oral Sci*. 2021;13(1):36.
110. Hong M, Tao S, Zhang L, Diao LT, Huang X, Huang S, et al. RNA sequencing: new technologies and applications in cancer research. *J Hematol Oncol*. 2020;13(1):166.
111. Stark R, Grzelak M, Hadfield J. RNA sequencing: the teenage years. *Nat Rev Genet*. 2019;20(11):631-56.
112. Hegenbarth J-C, Lezzoche G, De Windt LJ, Stoll M. Perspectives on Bulk-Tissue RNA Sequencing and Single-Cell RNA Sequencing for Cardiac Transcriptomics. *Frontiers in Molecular Medicine*. 2022;2.

113. Hedlund E, Deng Q. Single-cell RNA sequencing: Technical advancements and biological applications. *Mol Aspects Med.* 2018;59:36-46.
114. McDermaid A, Monier B, Zhao J, Liu B, Ma Q. Interpretation of differential gene expression results of RNA-seq data: review and integration. *Brief Bioinform.* 2019;20(6):2044-54.
115. Consortium G. Glioma through the looking GLASS: molecular evolution of diffuse gliomas and the Glioma Longitudinal Analysis Consortium. *Neuro Oncol.* 2018;20(7):873-84.
116. Costa-Silva J, Domingues D, Lopes FM. RNA-Seq differential expression analysis: An extended review and a software tool. *PLoS One.* 2017;12(12):e0190152.
117. Conesa A, Madrigal P, Tarazona S, Gomez-Cabrero D, Cervera A, McPherson A, et al. A survey of best practices for RNA-seq data analysis. *Genome Biol.* 2016;17:13.
118. Dazhi W, Jing D, Chunling R, Mi Z, Zhixuan X. Elevated SLC6A6 expression drives tumorigenesis and affects clinical outcomes in gastric cancer. *Biomarkers in Medicine.* 2019;13(02):95-104.
119. Yasunaga M, Matsumura Y. Role of SLC6A6 in promoting the survival and multidrug resistance of colorectal cancer. *Sci Rep.* 2014;4:4852.
120. Bowman R, Wang Q, Carro A, Verhaak R, Squatrito M. GlioVis data portal for visualization and analysis of brain tumor expression datasets. *Oncotarget.* 2016;7(31):139-41.
121. P31641 · SC6A6_HUMAN UniProt [Available from: <https://www.uniprot.org/uniprotkb/P31641/entry>].
122. SLC6A6 solute carrier family 6 member 6 [Homo sapiens (human)] National Library of Medicine [Available from: <https://www.ncbi.nlm.nih.gov/gene?Db=gene&Cmd=DetailsSearch&Term=6533>]
123. Hernandez-Benitez R, Ramos-Mandujano G, Pasantes-Morales H. Taurine stimulates proliferation and promotes neurogenesis of mouse adult cultured neural stem/progenitor cells. *Stem Cell Res.* 2012;9(1):24-34.
124. Lin L, Yee SW, Kim RB, Giacomini KM. SLC transporters as therapeutic targets: emerging opportunities. *Nature Reviews Drug Discovery.* 2015;14(8):543-60.
125. Colas C, Ung PM-U, Schlessinger A. SLC transporters: structure, function, and drug discovery. *MedChemComm.* 2016;7(6):1069-81.

126. Wang WW, Gallo L, Jadhav A, Hawkins R, Parker CG. The Druggability of Solute Carriers. *J Med Chem.* 2020;63(8):3834-67.
127. Rudnick G, Krämer R, Blakely RD, Murphy DL, Verrey F. The SLC6 transporters: perspectives on structure, functions, regulation, and models for transporter dysfunction. *Pflügers Archiv - European Journal of Physiology.* 2014;466(1):25-42.
128. Colas C. Toward a Systematic Structural and Functional Annotation of Solute Carriers Transporters-Example of the SLC6 and SLC7 Families. *Front Pharmacol.* 2020;11:1229.
129. Yasunaga M, Matsumura Y. Role of SLC6A6 in promoting the survival and multidrug resistance of colorectal cancer. *Scientific Reports.* 2015;4(1).
130. Wang Dazhi, Du Jing, Ren Chunling, Zhou Mi, Zhixuan X. Elevated SLC6A6 expression drives tumorigenesis and affects clinical outcomes in gastric cancer. *Biomarkers in medicine.* 2019;13(2).
131. Grażyna Janikowska, Tomasz Janikowski, Alina Pyka-Pająk, Urszula Mazurek, Marcin Janikowski, Maciej Gonciarz, et al. Potential biomarkers for the early diagnosis of colorectal adenocarcinoma – transcriptomic analysis of four clinical stages. *Cancer Biomarkers.* 2018;2(1):89–99.
132. Garnier S, Harakalova M, Weiss S, Mokry M, Regitz-Zagrosek V, Hengstenberg C, et al. Genome-wide association analysis in dilated cardiomyopathy reveals two new players in systolic heart failure on chromosomes 3p25.1 and 22q11.23. *Eur Heart J.* 2021;42(20):2000-11.
133. Ansar M, Ranza E, Shetty M, Paracha SA, Azam M, Kern I, et al. Taurine treatment of retinal degeneration and cardiomyopathy in a consanguineous family with SLC6A6 taurine transporter deficiency. *Hum Mol Genet.* 2020;29(4):618-23.
134. Siefken W, Carstensen S, Springmann G, Wittern K-P, Wenck H, Stüb F, et al. Role of Taurine Accumulation in Keratinocyte Hydration. *Journal of Investigative Dermatology.* 2003;121(2):354-61.
135. Voss JW, Pedersen SF, Christensen ST, Lambert IH. Regulation of the expression and subcellular localization of the taurine transporter TauT in mouse NIH3T3 fibroblasts. *European Journal of Biochemistry.* 2004;271(23-24):4646-58.

136. Pramod AB, Foster J, Carvelli L, Henry LK. SLC6 transporters: Structure, function, regulation, disease association and therapeutics. *Molecular Aspects of Medicine*. 2013;34(2-3):197-219.
137. Goncalves LS, Kratz C, Santos L, Carvalho VH, Sales LP, Nemezio K, et al. Insulin does not stimulate beta-alanine transport into human skeletal muscle. *Am J Physiol Cell Physiol*. 2020;318(4):C777-C86.
138. Nishimura T, Higuchi K, Yoshida Y, Sugita-Fujisawa Y, Kojima K, Sugimoto M, et al. Hypotaurine Is a Substrate of GABA Transporter Family Members GAT2/Slc6a13 and TAUT/Slc6a6. *Biological and Pharmaceutical Bulletin*. 2018;41(10):1523-9.
139. Shen D, Tian L, Yang F, Li J, Li X, Yao Y, et al. ADO/hypotaurine: a novel metabolic pathway contributing to glioblastoma development. *Cell Death Discovery*. 2021;7(1).
140. Han X, Budreau AM, Chesney RW. Role of conserved peptide in taurine transporter inactivation modulated by protein kinase C. *Journal of the American Society of Nephrology*. 1996;7(10):2088-96.
141. W.Q. Chen, H. Jin, M. Nguyen, J. Carr, Y.J. Lee, C.C. Hsu, et al. Role of Taurine in Regulation of Intracellular Calcium Level and Neuroprotective Function in Cultured Neurons. *Journal of Neuroscience Research*. 2001;66:612-9.
142. Information NCfB. PubChem Compound Summary for CID 1123, Taurine [Available from: <https://pubchem.ncbi.nlm.nih.gov/compound/Taurine>].
143. Harris Ripps, Shen W. Review- Taurine- A “very essential” amino acid. *Molecular Vision*. 2012;18:2673-86.
144. Wojcik OP, Koenig KL, Zeleniuch-Jacquotte A, Costa M, Chen Y. The potential protective effects of taurine on coronary heart disease. *Atherosclerosis*. 2010;208(1):19-25.
145. Scimemi A. Structure, function, and plasticity of GABA transporters. *Front Cell Neurosci*. 2014;8:161.
146. Iori Ueki, Stipanuk MH. Enzymes of the Taurine Biosynthetic Pathway Are Expressed in Rat Mammary Gland. *The Journal of Nutrition*. 2008;137(8):1887–94.
147. Baliou S, Kyriakopoulos A, Goulielmaki M, Panayiotidis M, Spandidos D, Zoumpourlis V. Significance of taurine transporter (TauT) in homeostasis and its layers of regulation (Review). *Molecular Medicine Reports*. 2020;22(3):2163-73.

148. K C Hayes, R E Carey, Schmidt SY. Retinal Degeneration Associated with Taurine Deficiency in the Cat. *Science*. 1975;188:949-51.
149. Keiko Yamauchi-Takahara, Junichi Azuma, Kishimoto S. Taurine protection against experimental arterial calcinosis in mice *Biochemical and Biophysical Research Communications*. 1986;140(2):679-83.
150. Herbert F. Pierson, Joyce M. Fisher, Rabinovitz M. Modulation by Taurine of the Toxicity of Taumustine, a Compound With Antitumor Activity. *Journal of the National Cancer Institute*. 1985;75(5).
151. Bae M, Ahmed K, Yim JE. Beneficial Effects of Taurine on Metabolic Parameters in Animals and Humans. *J Obes Metab Syndr*. 2022;31(2):134-46.
152. Hernandez-Benitez R, Vangipuram SD, Ramos-Mandujano G, Lyman WD, Pasantes-Morales H. Taurine enhances the growth of neural precursors derived from fetal human brain and promotes neuronal specification. *Dev Neurosci*. 2013;35(1):40-9.
153. Baliou S, Adamaki M, Ioannou P, Pappa A, Panayiotidis MI, Spandidos DA, et al. Protective role of taurine against oxidative stress (Review). *Mol Med Rep*. 2021;24(2).
154. Palackal T, Moretz R, Wisniewski H, Sturman JA. Abnormal visual cortex development in the kitten associated with maternal dietary taurine deprivation. *Journal of Neuroscience Research*. 1986;15(2):223-39.
155. Sturman JA, Moretz RC, French JH, Wisniewski HM. Postnatal taurine deficiency in the kitten results in a persistence of the cerebellar external granule cell layer: Correction by taurine feeding. *Journal of Neuroscience Research*. 1985;13(4):521-8.
156. Thomas Maar, Julio Morán, rne Schousboe, Pasantes-Morales H. Taurine deficiency in dissociated mouse cerebellar cultures affects neuronal migration. *International journal of developmental neuroscience*. 1995;13(5):491-502.
157. Sturman JA, Moretz RC, French JH, Wisniewski HM. Taurine deficiency in the developing cat: Persistence of the cerebellar external granule cell layer. *Journal of Neuroscience Research*. 1985;13(3):405-16.
158. Cubillos S, Obregón F, Vargas MaF, Salazar LA, Lima L. Taurine concentrations in human gliomas and meningiomas: tumoral, peritumoral, and extratumoral tissue. *Advances in experimental medicine and biology*. 2006:419-22.

159. Surarak T, Chantree P, Sangpairoj K. Synergistic Effects of Taurine and Temozolomide Via Cell Proliferation Inhibition and Apoptotic Induction on U-251 MG Human Glioblastoma Cells. *Asian Pacific Journal of Cancer Prevention*. 2021;22(12):4001-9.
160. Caragher S, Chalmers AJ, Gomez-Roman N. Glioblastoma's Next Top Model: Novel Culture Systems for Brain Cancer Radiotherapy Research. *Cancers (Basel)*. 2019;11(1).
161. Joseph JV, Roosmalen IAMV, Busschers E, Tomar T, Conroy S, Eggens-Meijer E, et al. Serum-Induced Differentiation of Glioblastoma Neurospheres Leads to Enhanced Migration/Invasion Capacity That Is Associated with Increased MMP9. *PLOS ONE*. 2015;10(12):e0145393.
162. Ledur PF, Onzi GR, Zong H, Lenz G. Culture conditions defining glioblastoma cells behavior- what is the impact for novel discoveries. *Oncogene*. 2017;8(40):69185-97.
163. Lee J, Kotliarova S, Kotliarov Y, Li A, Su Q, Donin NM, et al. Tumor stem cells derived from glioblastomas cultured in bFGF and EGF more closely mirror the phenotype and genotype of primary tumors than do serum-cultured cell lines. *Cancer Cell*. 2006;9(5):391-403.
164. Fiscon G, Conte F, Licursi V, Nasi S, Paci P. Computational identification of specific genes for glioblastoma stem-like cells identity. *Sci Rep*. 2018;8(1):7769.
165. Leek R, Grimes DR, Harris AL, McIntyre A. Methods: Using Three-Dimensional Culture (Spheroids) as an In Vitro Model of Tumour Hypoxia. *Adv Exp Med Biol*. 2016;899:167-96.
166. Ong CS, XunZhou, Han J, Huang CY, Nashed A, Khatri S, et al. In vivo therapeutic applications of cell spheroids. *Biotechnology Advances*. 2018;36(2):494-505.
167. Riffle S, Hegde RS. Modeling tumor cell adaptations to hypoxia in multicellular tumor spheroids. *J Exp Clin Cancer Res*. 2017;36(1):102.
168. Mehta G, Hsiao AY, Ingram M, Luker GD, Takayama S. Opportunities and challenges for use of tumor spheroids as models to test drug delivery and efficacy. *J Control Release*. 2012;164(2):192-204.
169. Clevers H. Modeling Development and Disease with Organoids. *Cell*. 2016;165(7):1586-97.

170. Sthijns M, LaPointe VLS, van Blitterswijk CA. Building Complex Life Through Self-Organization. *Tissue Eng Part A*. 2019;25(19-20):1341-6.
171. Chen Y-W, Huang SX, De Carvalho ALRT, Ho S-H, Islam MN, Volpi S, et al. A three-dimensional model of human lung development and disease from pluripotent stem cells. *Nature Cell Biology*. 2017;19(5):542-9.
172. Eiraku M, Watanabe K, Matsuo-Takasaki M, Kawada M, Yonemura S, Matsumura M, et al. Self-Organized Formation of Polarized Cortical Tissues from ESCs and Its Active Manipulation by Extrinsic Signals. *Cell Stem Cell*. 2008;3(5):519-32.
173. Takebe T, Sekine K, Enomura M, Koike H, Kimura M, Ogaeri T, et al. Vascularized and functional human liver from an iPSC-derived organ bud transplant. *Nature*. 2013;499(7459):481-4.
174. Takasato M, Er PX, Chiu HS, Maier B, Baillie GJ, Ferguson C, et al. Kidney organoids from human iPS cells contain multiple lineages and model human nephrogenesis. *Nature*. 2015;526(7574):564-8.
175. Giandomenico SL, Sutcliffe M, Lancaster MA. Generation and long-term culture of advanced cerebral organoids for studying later stages of neural development. *Nature Protocols*. 2021;16(2):579-602.
176. Vandamme TF. Use of rodents as models of human diseases. *Journal of Pharmacy and Bioallied Sciences*. 2014;6(1).
177. Yoshida GJ. Applications of patient-derived tumor xenograft models and tumor organoids. *Journal of Hematology & Oncology*. 2020;13(1).
178. Noorani I. Genetically Engineered Mouse Models of Gliomas: Technological Developments for Translational Discoveries. *Cancers*. 2019;11(9):1335.
179. Haddad AF, Young JS, Amara D, Berger MS, Raleigh DR, Aghi MK, et al. Mouse models of glioblastoma for the evaluation of novel therapeutic strategies. *Neurooncol Adv*. 2021;3(1):vdab100.
180. Cheon DJ, Orsulic S. Mouse models of cancer. *Annu Rev Pathol*. 2011;6:95-119.
181. Rhiannon Barrow, Joseph N. Wilkinson, Yichen He, Martin Callaghan, Anke Brüning-Richardson, Mark Dunning, et al. SpheroidAnalyseR – an online platform for analysing data from 3D spheroids or organoids grown in 96-well plates. *bioRxiv*. 2022.

182. Martin M. Cutadapt removes adapter sequences from high-throughput sequencing reads. *EMBnet Journal*. 2011;17(1):10-2.
183. Love MI, Huber W, Anders S. Moderated estimation of fold change and dispersion for RNA-seq data with DESeq2. *Genome Biol*. 2014;15(12):550.
184. Ge SX, Jung D, Yao R. ShinyGO: a graphical gene-set enrichment tool for animals and plants. *Bioinformatics*. 2020;36(8):2628-9.
185. Diego US, institute B. Molecular signatures database. Hallmark gene sets Gene Set Enrichment Analysis [Available from: <http://www.gsea-msigdb.org/gsea/msigdb/genesets.jsp?collection=H>].
186. Liao Y, Wang J, Jaehnig EJ, Shi Z, Zhang B. WebGestalt 2019: gene set analysis toolkit with revamped UIs and APIs. *Nucleic Acids Res*. 2019;47(W1):W199-W205.
187. Sato S, Rancourt A, Sato Y, Satoh MS. Single-cell lineage tracking analysis reveals that an established cell line comprises putative cancer stem cells and their heterogeneous progeny. *Sci Rep*. 2016;6:23328.
188. Ravi M, Paramesh V, Kaviya SR, Anuradha E, Solomon FD. 3D cell culture systems: advantages and applications. *J Cell Physiol*. 2015;230(1):16-26.
189. Jacobs VL, Valdes PA, Hickey WF, De Leo JA. Current review of in vivo GBM rodent models: emphasis on the CNS-1 tumour model. *ASN Neuro*. 2011;3(3):e00063.
190. Stringer BW, Day BW, D'Souza RCJ, Jamieson PR, Ensbey KS, Bruce ZC, et al. A reference collection of patient-derived cell line and xenograft models of proneural, classical and mesenchymal glioblastoma. *Sci Rep*. 2019;9(1):4902.
191. Pollard SM, Yoshikawa K, Clarke ID, Danovi D, Stricker S, Russell R, et al. Glioma stem cell lines expanded in adherent culture have tumor-specific phenotypes and are suitable for chemical and genetic screens. *Cell Stem Cell*. 2009;4(6):568-80.
192. De Witt Hamer PC, Van Tilborg AA, Eijk PP, Sminia P, Troost D, Van Noorden CJ, et al. The genomic profile of human malignant glioma is altered early in primary cell culture and preserved in spheroids. *Oncogene*. 2008;27(14):2091-6.
193. Xie ZR, Chen J, Wu Y. Linking 3D and 2D binding kinetics of membrane proteins by multiscale simulations. *Protein Sci*. 2014;23(12):1789-99.

194. Kapalczynska M, Kolenda T, Przybyla W, Zajaczkowska M, Teresiak A, Filas V, et al. 2D and 3D cell cultures - a comparison of different types of cancer cell cultures. *Arch Med Sci.* 2018;14(4):910-9.
195. Bresciani G, Hofland LJ, Dogan F, Giamas G, Gagliano T, Zatelli MC. Evaluation of Spheroid 3D Culture Methods to Study a Pancreatic Neuroendocrine Neoplasm Cell Line. *Front Endocrinol (Lausanne).* 2019;10:682.
196. Ryu NE, Lee SH, Park H. Spheroid Culture System Methods and Applications for Mesenchymal Stem Cells. *Cells.* 2019;8(12).
197. O Y, S S. Is 'Hanging Drop' a Useful Method to Form Spheroids of Jimt, Mcf-7, T-47d, Bt-474 That are Breast Cancer Cell Lines. *Single Cell Biology.* 2018;07(01).
198. Katt ME, Placone AL, Wong AD, Xu ZS, Searson PC. In Vitro Tumor Models: Advantages, Disadvantages, Variables, and Selecting the Right Platform. *Front Bioeng Biotechnol.* 2016;4:12.
199. Schneider CA, Rasband WS, Eliceiri KW. NIH Image to ImageJ: 25 years of image analysis. *Nat Methods.* 2012;9(7):671-5.
200. Jakaria M, Azam S, Haque ME, Jo SH, Uddin MS, Kim IS, et al. Taurine and its analogs in neurological disorders: Focus on therapeutic potential and molecular mechanisms. *Redox Biol.* 2019;24:101223.
201. Mario Galarreta, Jukn Bustamante, Rafael Martin del Rio, Solisls JM. Taurine Induces a Long-Lasting Increase of Synaptic Efficacy and Axon Excitability in the Hippocampus. *The Journal of Neuroscience.* 1996;16(1):92-102.
202. Lu W, Yang Y, Gao S, Wu J, Sun X. Taurine protects R28 cells from hypoxia/re-oxygenation-induced damage via regulation of mitochondrial energy metabolism. *Amino Acids.* 2022.
203. Ma Z, Niu B, Phan TA, Stensjoen AL, Ene C, Woodiwiss T, et al. Stochastic growth pattern of untreated human glioblastomas predicts the survival time for patients. *Sci Rep.* 2020;10(1):6642.
204. Aasland D, Reich TR, Tomicic MT, Switzeny OJ, Kaina B, Christmann M. Repair gene O(6) -methylguanine-DNA methyltransferase is controlled by SP1 and up-regulated by glucocorticoids, but not by temozolomide and radiation. *J Neurochem.* 2018;144(2):139-51.

205. Moen EL, Stark AL, Zhang W, Dolan ME, Godley LA. The role of gene body cytosine modifications in MGMT expression and sensitivity to temozolomide. *Mol Cancer Ther.* 2014;13(5):1334-44.
206. Chen W, Wong C, Vosburgh E, Levine AJ, Foran DJ, Xu EY. High-throughput image analysis of tumor spheroids: a user-friendly software application to measure the size of spheroids automatically and accurately. *J Vis Exp.* 2014(89).
207. Malo N, Hanley JA, Cerquozzi S, Pelletier J, Nadon R. Statistical practice in high-throughput screening data analysis. *Nat Biotechnol.* 2006;24(2):167-75.
208. Graham K, Unger E. Overcoming tumor hypoxia as a barrier to radiotherapy, chemotherapy and immunotherapy in cancer treatment. *Int J Nanomedicine.* 2018;13:6049-58.
209. Portnow J, Badie B, Chen M, Liu A, Blanchard S, Synold TW. The neuropharmacokinetics of temozolomide in patients with resectable brain tumors: potential implications for the current approach to chemoradiation. *Clin Cancer Res.* 2009;15(22):7092-8.
210. Zhang X, Tu S, Wang Y, Xu B, Wan F. Mechanism of taurine-induced apoptosis in human colon cancer cells. *Acta Biochim Biophys Sin (Shanghai).* 2014;46(4):261-72.
211. Tu S, Zhang XL, Wan HF, Xia YQ, Liu ZQ, Yang XH, et al. Effect of taurine on cell proliferation and apoptosis human lung cancer A549 cells. *Oncology Letters.* 2018.
212. Chen Z, Hambardzumyan D. Immune Microenvironment in Glioblastoma Subtypes. *Front Immunol.* 2018;9:1004.
213. Galli F, Aguilera JV, Palermo B, Markovic SN, Nistico P, Signore A. Relevance of immune cell and tumor microenvironment imaging in the new era of immunotherapy. *J Exp Clin Cancer Res.* 2020;39(1):89.
214. DeCordova S, Shastri A, Tsolaki AG, Yasmin H, Klein L, Singh SK, et al. Molecular Heterogeneity and Immunosuppressive Microenvironment in Glioblastoma. *Front Immunol.* 2020;11:1402.
215. Kim J, Koo BK, Knoblich JA. Human organoids: model systems for human biology and medicine. *Nat Rev Mol Cell Biol.* 2020;21(10):571-84.
216. Antoni D, Burckel H, Josset E, Noel G. Three-dimensional cell culture: a breakthrough in vivo. *Int J Mol Sci.* 2015;16(3):5517-27.

217. da Hora CC, Schweiger MW, Wurdinger T, Tannous BA. Patient-Derived Glioma Models: From Patients to Dish to Animals. *Cells*. 2019;8(10).
218. Gunti S, Hoke ATK, Vu KP, London NR, Jr. Organoid and Spheroid Tumor Models: Techniques and Applications. *Cancers (Basel)*. 2021;13(4).
219. Investigating new diagnostic biomarkers of glioblastoma Yorkshire Brain tumour Charity website 2021 [Available from:
<https://www.yorksbtcc.org.uk/Loving-Research/Research/Current-Research/Investigating-new-diagnostic-biomarkers>].
220. Kumar P, Nagarajan A, Uchil PD. Analysis of Cell Viability by the Lactate Dehydrogenase Assay. *Cold Spring Harb Protoc*. 2018;2018(6).
221. Terry L Riss, Richard A Moravec, Andrew L Niles, Sarah Duellman, Hélène A Benink, Worzella TJ, et al. Cell Viability Assays. 2013. In: *The Assay Guidance Manual* [Internet]. Eli Lilly & Company and the National Center for Advancing Translational Sciences. Available from:
<https://www.ncbi.nlm.nih.gov/books/>.
222. Monika Kijanska, Kelm J. In vitro 3D Spheroids and Microtissues- ATP-based Cell Viability and Toxicity Assays. 2016. In: *The Assay Guidance Manual* [Internet]. Eli Lilly & Company and the National Center for Advancing Translational Sciences. Available from: Bookshelf URL:
<https://www.ncbi.nlm.nih.gov/books/>.
223. CellTiter-Glo® Luminescent Cell Viability Assay [Available from:
https://www.promega.co.uk/products/cell-health-assays/cell-viability-and-cytotoxicity-assays/celltiter_glo-luminescent-cell-viability-assay/?catNum=G7570].
224. Han H. RNA Interference to Knock Down Gene Expression. *Methods Mol Biol*. 2018;1706:293-302.
225. Argani H. Genome Engineering for Stem Cell Transplantation. *Exp Clin Transplant*. 2019;17(Suppl 1):31-7.
226. Sun N, Petiwala S, Wang R, Lu C, Hu M, Ghosh S, et al. Development of drug-inducible CRISPR-Cas9 systems for large-scale functional screening. *BMC Genomics*. 2019;20(1):225.
227. Frank SB, Schulz VV, Miranti CK. A streamlined method for the design and cloning of shRNAs into an optimized Dox-inducible lentiviral vector. *BMC Biotechnol*. 2017;17(1):24.

228. Rao DD, Vorhies JS, Senzer N, Nemunaitis J. siRNA vs. shRNA: similarities and differences. *Adv Drug Deliv Rev.* 2009;61(9):746-59.
229. Moore CB, Guthrie EH, Huang MT, Taxman DJ. Short hairpin RNA (shRNA): design, delivery, and assessment of gene knockdown. *Methods Mol Biol.* 2010;629:141-58.
230. Raja MAG, Katas H, Amjad MW. Design, mechanism, delivery and therapeutics of canonical and Dicer-substrate siRNA. *Asian J Pharm Sci.* 2019;14(5):497-510.
231. HAMILTON AJ, BAULCOMBE DC. A Species of Small AntisenseRNA in Posttranscriptional Gene Silencing in Plants. *Science.* 1999;286(5441):950-2.
232. Elbashir SM, Harborth J, Lendeckel W, Yalcin A, Weber K, Tuschl T. Duplexes of 21±nucleotide RNAs mediate RNA interference in cultured mammalian cells. *Nature.* 2001;411.
233. Dana H, Chalbatani GM, Mahmoodzadeh H, Karimloo R, Rezaiean O, Moradzadeh A, et al. Molecular Mechanisms and Biological Functions of siRNA. *International Journal of Biological Science.* 2017;12(2):48-57.
234. Hu B, Zhong L, Weng Y, Peng L, Huang Y, Zhao Y, et al. Therapeutic siRNA: state of the art. *Signal Transduct Target Ther.* 2020;5(1):101.
235. Huang Y. Approval of the first-ever rnaI therapeutics and its technological development history. *Progress in Biochemistry and Biophysics.* 2019;46(3):313-22.
236. Agarwal S, Simon AR, Goel V, Habtemariam BA, Clausen VA, Kim JB, et al. Pharmacokinetics and Pharmacodynamics of the Small Interfering Ribonucleic Acid, Givosiran, in Patients With Acute Hepatic Porphyria. *Clin Pharmacol Ther.* 2020;108(1):63-72.
237. Singh A, Trivedi P, Jain NK. Advances in siRNA delivery in cancer therapy. *Artif Cells Nanomed Biotechnol.* 2018;46(2):274-83.
238. Dong Y, Siegwart DJ, Anderson DG. Strategies, design, and chemistry in siRNA delivery systems. *Adv Drug Deliv Rev.* 2019;144:133-47.
239. Cell Transfection 2021 [Available from: <http://www.cell-transfection.com/cell-transfection-wiki/sirna-transfection/>].
240. Lambeth LS, Smith CA. Short hairpin RNA-mediated gene silencing. *Methods Mol Biol.* 2013;942:205-32.
241. Siolas D, Lerner C, Burchard J, Ge W, Linsley PS, Paddison PJ, et al. Synthetic shRNAs as potent RNAi triggers. *Nat Biotechnol.* 2005;23(2):227-31.

242. McAnuff MA, Rettig GR, Rice KG. Potency of siRNA versus shRNA mediated knockdown in vivo. *J Pharm Sci.* 2007;96(11):2922-30.
243. Song H, Yang P-C. Construction of shRNA lentiviral vector. *North American Journal of Medical Sciences.* 2012;2(12):598-601.
244. Potter H, Heller R. Transfection by electroporation. *Curr Protoc Mol Biol.* 2003;Chapter 9:Unit 9 3.
245. Carter M, Shieh J. *Gene Delivery Strategies. Guide to Research Techniques in Neuroscience*2015. p. 239-52.
246. Zhu L, Mahato RI. Lipid and polymeric carrier-mediated nucleic acid delivery. *Expert Opin Drug Deliv.* 2010;7(10):1209-26.
247. Wang J, Lu Z, Wientjes MG, Au JL. Delivery of siRNA therapeutics: barriers and carriers. *AAPS J.* 2010;12(4):492-503.
248. Song H, Hart SL, Du Z. Assembly strategy of liposome and polymer systems for siRNA delivery. *Int J Pharm.* 2021;592:120033.
249. Kleefeldt JM, Pozarska A, Nardiello C, Pfeffer T, Vadasz I, Herold S, et al. Commercially available transfection reagents and negative control siRNA are not inert. *Anal Biochem.* 2020;606:113828.
250. Chong ZX, Yeap SK, Ho WY. Transfection types, methods and strategies: a technical review. *PeerJ.* 2021;9:e11165.
251. How electroporation works Thermofisher: Thermofisher; 2021 [Available from: <https://www.thermofisher.com/uk/en/home/references/gibco-cell-culture-basics/transfection-basics/transfection-methods/electroporation.html>].
252. siRNA applications Horizon Discovery: Horizon Discovery; 2021 [Available from: <https://horizondiscovery.com/en/applications/rnai/sirna-applications>]
253. Savic N, Schwank G. Advances in therapeutic CRISPR/Cas9 genome editing. *Transl Res.* 2016;168:15-21.
254. Zhang F, Wen Y, Guo X. CRISPR/Cas9 for genome editing: progress, implications and challenges. *Hum Mol Genet.* 2014;23(R1):R40-6.
255. Redman M, King A, Watson C, King D. What is CRISPR/Cas9? *Arch Dis Child Educ Pract Ed.* 2016;101(4):213-5.
256. Liu M, Zhang W, Xin C, Yin J, Shang Y, Ai C, et al. Global detection of DNA repair outcomes induced by CRISPR-Cas9. *Nucleic Acids Res.* 2021;49(15):8732-42.

257. Makarova KS, Koonin EV. Annotation and Classification of CRISPR-Cas Systems. *Methods Mol Biol.* 2015;1311:47-75.
258. Ran FA, Hsu PD, Wright J, Agarwala V, Scott DA, Zhang F. Genome engineering using the CRISPR-Cas9 system. *Nat Protoc.* 2013;8(11):2281-308.
259. Tang L. PAM-less is more. *Nat Methods.* 2020;17(6):559.
260. Mir A, Edraki A, Lee J, Sontheimer EJ. Type II-C CRISPR-Cas9 Biology, Mechanism, and Application. *ACS Chem Biol.* 2018;13(2):357-65.
261. Adli M. The CRISPR tool kit for genome editing and beyond. *Nat Commun.* 2018;9(1):1911.
262. F, Patrick, Lin C-Y, Jonathan, Konermann S, Trevino AE, et al. Double Nicking by RNA-Guided CRISPR Cas9 for Enhanced Genome Editing Specificity. *Cell.* 2013;154(6):1380-9.
263. E.Trevino A, Zhang F. Chapter Eight - Genome Editing Using Cas9 Nickases. 2014. In: *Methods in Enzymology* [Internet]. [161-74].
264. Shin JW, Kim KH, Chao MJ, Atwal RS, Gillis T, MacDonald ME, et al. Permanent inactivation of Huntington's disease mutation by personalized allele-specific CRISPR/Cas9. *Hum Mol Genet.* 2016;25(20):4566-76.
265. Li Y, Zang H, Qian G, Owonikoko TK, Ramalingam SR, Sun SY. ERK inhibition effectively overcomes acquired resistance of epidermal growth factor receptor-mutant non-small cell lung cancer cells to osimertinib. *Cancer.* 2020;126(6):1339-50.
266. Taylor SC, Nadeau K, Abbasi M, Lachance C, Nguyen M, Fenrich J. The Ultimate qPCR Experiment: Producing Publication Quality, Reproducible Data the First Time. *Trends Biotechnol.* 2019;37(7):761-74.
267. Basic Principles of RT-qPCR ThermoFisher Scientific2021 [Available from: <https://www.thermofisher.com/uk/en/home/brands/thermo-scientific/molecular-biology/molecular-biology-learning-center/molecular-biology-resource-library/spotlight-articles/basic-principles-rt-qpcr.html>].
268. Kralik P, Ricchi M. A Basic Guide to Real Time PCR in Microbial Diagnostics: Definitions, Parameters, and Everything. *Front Microbiol.* 2017;8:108.
269. How does qPCR work (technology basics)? BioSistemika [Available from: <https://biosistemika.com/blog/qpcr-technology-basics/>].
270. Stahlberg A, Kubista M. Technical aspects and recommendations for single-cell qPCR. *Mol Aspects Med.* 2018;59:28-35.

271. Taylor SC, Posch A. The design of a quantitative western blot experiment. *Biomed Res Int.* 2014;2014:361590.
272. Weiss WA, Taylor SS, Shokat KM. Recognizing and exploiting differences between RNAi and small-molecule inhibitors. *Nat Chem Biol.* 2007;3(12):739-44.
273. Liang C, Tian D, Ren X, Ding S, Jia M, Xin M, et al. The development of Bruton's tyrosine kinase (BTK) inhibitors from 2012 to 2017: A mini-review. *Eur J Med Chem.* 2018;151:315-26.
274. Raghavendra NM, Pingili D, Kadasi S, Mettu A, Prasad S. Dual or multi-targeting inhibitors: The next generation anticancer agents. *Eur J Med Chem.* 2018;143:1277-300.
275. Valembois S, Krall J, Frolund B, Steffansen B. Imidazole-4-acetic acid, a new lead structure for interaction with the taurine transporter in outer blood-retinal barrier cells. *Eur J Pharm Sci.* 2017;103:77-84.
276. Mortensen M, Kristiansen U, Ebert B, Frolund B, Krogsgaard-Larsen P, Smart TG. Activation of single heteromeric GABA(A) receptor ion channels by full and partial agonists. *J Physiol.* 2004;557(Pt 2):389-413.
277. Lewin L, Rassin DK, Sellstrom A. Net taurine transport and its inhibition by a taurine antagonist. *Neurochemical research.* 1994;19(3):347-52.
278. Barakat L, Wang D, Bordey A. Carrier-mediated uptake and release of taurine from Bergmann glia in rat cerebellar slices. *J Physiol.* 2002;541(Pt 3):753-67.
279. Suarez LM, Munoz MD, Gonzalez JC, Bustamante J, Del Rio RM, Solis JM. The taurine transporter substrate guanidinoethyl sulfonate mimics the action of taurine on long-term synaptic potentiation. *Amino Acids.* 2016;48(11):2647-56.
280. Sergeeva OA, Chepkova AN, Haas HL. Guanidinoethyl sulphonate is a glycine receptor antagonist in striatum. *Br J Pharmacol.* 2002;137(6):855-60.
281. Jia YF, Li YC, Tang YP, Cao J, Wang LP, Yang YX, et al. Interference of TRPV1 function altered the susceptibility of PTZ-induced seizures. *Front Cell Neurosci.* 2015;9:20.
282. Hao Guo, Jing Zhou, Yanjun Zhang, Zhi Wang, Likun Liu, Zhang W. Identification of Hypoxia-Related Differentially Expressed Genes and Construction of the Clinical Prognostic Predictor in Hepatocellular Carcinoma by Bioinformatic Analysis. *BioMed Research International.* 2021;2021.

283. Tasca CI, Dal-Cim T, Cimarosti H. In vitro oxygen-glucose deprivation to study ischemic cell death. *Methods Mol Biol.* 2015;1254:197-210.
284. Munoz-Sanchez J, Chanez-Cardenas ME. The use of cobalt chloride as a chemical hypoxia model. *J Appl Toxicol.* 2019;39(4):556-70.
285. Kimberly A. Butash, Pachai Natarajan, Alice Young, Fox DK. Reexamination of the Effect of Endotoxin on Cell Proliferation and Transfection Efficiency. *BioTechniques.* 2000;29:610-9.
286. Pítia Flores Ledur, Giovana Ravizzoni Onzi, Hui Zong, Lenz G. Culture conditions defining glioblastoma cells behavior- what is the impact for novel discoveries. *Oncotarget.* 2017;8(40):69185-97.
287. Pítia F. Ledur, Chong Liu, Hua He, Alexandra R. Harris, Darlan C. Minussi, Hai-Yan Zhou, et al. Culture conditions defining glioblastoma cells behavior- what is the impact for novel discoveries. *Neuro-Oncology.* 2016;18(10):1413-242.
288. Huang, Wang Y, Thompson JW, Yin T, Alexander PB, Qin D, et al. Cancer-cell-derived GABA promotes beta-catenin-mediated tumour growth and immunosuppression. *Nat Cell Biol.* 2022;24(2):230-41.
289. Abdul M, McCray SD, Hoosein NM. Expression of gamma-aminobutyric acid receptor (subtype A) in prostate cancer. *Acta Oncologica.* 2008;47(8):1546-50.
290. Takehara A, Hosokawa M, Eguchi H, Ohigashi H, Ishikawa O, Nakamura Y, et al. Gamma-aminobutyric acid (GABA) stimulates pancreatic cancer growth through overexpressing GABAA receptor pi subunit. *Cancer Res.* 2007;67(20):9704-12.
291. Jiang SH, Hu LP, Wang X, Li J, Zhang ZG. Neurotransmitters: emerging targets in cancer. *Oncogene.* 2020;39(3):503-15.
292. Ngo DH, Vo TS. An Updated Review on Pharmaceutical Properties of Gamma-Aminobutyric Acid. *Molecules.* 2019;24(15).
293. D Purves, GJ Augustine DF, et al. Neurotransmitter Synthesis. *Neuroscience: Sunderland* 2001.
294. Briguglio M, Dell'Osso B, Panzica G, Malgaroli A, Banfi G, Zanaboni Dina C, et al. Dietary Neurotransmitters: A Narrative Review on Current Knowledge. *Nutrients.* 2018;10(5).
295. Jorgensen EM. Gaba. *WormBook.* 2005:1-13.

296. Wang DD, Kriegstein AR. Defining the role of GABA in cortical development. *J Physiol*. 2009;587(Pt 9):1873-9.
297. Petroff OA. GABA and glutamate in the human brain. *Neuroscientist*. 2002;8(6):562-73.
298. Jung E, Alfonso J, Osswald M, Monyer H, Wick W, Winkler F. Emerging intersections between neuroscience and glioma biology. *Nat Neurosci*. 2019;22(12):1951-60.
299. Varn FS, Johnson KC, Martinek J, Huse JT, Nasrallah MP, Wesseling P, et al. Glioma progression is shaped by genetic evolution and microenvironment interactions. *Cell*. 2022;185(12):2184-99 e16.
300. Andrews S. FastQC Babraham Bioinformatics: Babraham Institute [17.8.22]. FastQC]. Available from: <https://www.bioinformatics.babraham.ac.uk/projects/fastqc/>.
301. Martin M. Cutadapt removes adapter sequences from high throughput sequencing reads. *EMBnet Journal* 17(1):10-2.
302. Krueger F. Trim Galore Babraham Bioinformatics: Babraham Institute; [Available from: https://www.bioinformatics.babraham.ac.uk/projects/trim_galore/].
303. Srivastava A, Malik L, Sarkar H, Zakeri M, Almodaresi F, Sonesson C, et al. Alignment and mapping methodology influence transcript abundance estimation. *Genome Biol*. 2020;21(1):239.
304. Langmead B, Salzberg SL. Fast gapped-read alignment with Bowtie 2. *Nat Methods*. 2012;9(4):357-9.
305. Deschamps-Francoeur G, Simoneau J, Scott MS. Handling multi-mapped reads in RNA-seq. *Comput Struct Biotechnol J*. 2020;18:1569-76.
306. Hadley Wickham, Winston Chang, Lionel Henry, Thomas Lin Pedersen, Kohske Takahashi, Claus Wilke, et al. ggplot2 [Available from: <https://ggplot2.tidyverse.org/>].
307. McCarthy DJ, Chen Y, Smyth GK. Differential expression analysis of multifactor RNA-Seq experiments with respect to biological variation. *Nucleic Acids Res*. 2012;40(10):4288-97.
308. Garofano L, Migliozi S, Oh YT, D'Angelo F, Najac RD, Ko A, et al. Pathway-based classification of glioblastoma uncovers a mitochondrial subtype with therapeutic vulnerabilities. *Nat Cancer*. 2021;2(2):141-56.

309. Mao B, Zhang Z, Wang G. BTG2: a rising star of tumor suppressors (review). *Int J Oncol*. 2015;46(2):459-64.
310. Iwadate Y. Epithelial-mesenchymal transition in glioblastoma progression. *Oncol Lett*. 2016;11(3):1615-20.
311. Murat A, Migliavacca E, Gorlia T, Lambiv WL, Shay T, Hamou MF, et al. Stem cell-related "self-renewal" signature and high epidermal growth factor receptor expression associated with resistance to concomitant chemoradiotherapy in glioblastoma. *J Clin Oncol*. 2008;26(18):3015-24.
312. Bhat KPL, Balasubramanian V, Vaillant B, Ezhilarasan R, Hummelink K, Hollingsworth F, et al. Mesenchymal differentiation mediated by NF-kappaB promotes radiation resistance in glioblastoma. *Cancer Cell*. 2013;24(3):331-46.
313. Rispoli R, Conti C, Celli P, Caroli E, Carletti S. Neural Stem Cells and Glioblastoma. *The Neuroradiology Journal*. 2014;27(2):169-74.
314. Bazzoni R, Bentivegna A. Role of Notch Signaling Pathway in Glioblastoma Pathogenesis. *Cancers (Basel)*. 2019;11(3).
315. Nik Nabil WN, Xi Z, Song Z, Jin L, Zhang XD, Zhou H, et al. Towards a Framework for Better Understanding of Quiescent Cancer Cells. *Cells*. 2021;10(3).
316. Marescal O, Cheeseman IM. Cellular Mechanisms and Regulation of Quiescence. *Dev Cell*. 2020;55(3):259-71.
317. Recasens A, Munoz L. Targeting Cancer Cell Dormancy. *Trends Pharmacol Sci*. 2019;40(2):128-41.
318. Bollard J, Miguela V, Ruiz de Galarreta M, Venkatesh A, Bian CB, Roberto MP, et al. Palbociclib (PD-0332991), a selective CDK4/6 inhibitor, restricts tumour growth in preclinical models of hepatocellular carcinoma. *Gut*. 2017;66(7):1286-96.
319. Wiedemeyer WR, Dunn IF, Quayle SN, Zhang J, Chheda MG, Dunn GP, et al. Pattern of retinoblastoma pathway inactivation dictates response to CDK4/6 inhibition in GBM. *Proc Natl Acad Sci U S A*. 2010;107(25):11501-6.
320. Waszczak BL, Hruska RE, Walters JR. Gabaergic actions of THIP in vivo and in vitro: a comparison with muscimol and GABA. *European Journal of Pharmacology*. 1980;65:21-9.
321. M Tatsuta., H Iishi., M Baba., Taniguchi H. Attenuation by the GABA Receptor Agonist Baclofen of Experimental Carcinogenesis in Rat Colon by Azoxymethane. *Oncology*. 1992;49:241-5.

322. Blanchart A, Fernando R, Haring M, Assaife-Lopes N, Romanov RA, Andang M, et al. Endogenous GABAA receptor activity suppresses glioma growth. *Oncogene*. 2017;36(6):777-86.
323. D'Urso PI, D'Urso OF, Storelli C, Mallardo M, Gianfreda CD, Montinaro A, et al. miR-155 is up-regulated in primary and secondary glioblastoma and promotes tumour growth by inhibiting GABA receptors. *Int J Oncol*. 2012;41(1):228-34.
324. Charalampos Labrakakis, Stephan Patt, Jana Hartmann, Kettenmann H. Functional GABA receptors on human glioma cells. *European Journal of Neuroscience*. 1998;10:231-8.
325. Hujber Z, Horvath G, Petovari G, Krencz I, Danko T, Meszaros K, et al. GABA, glutamine, glutamate oxidation and succinic semialdehyde dehydrogenase expression in human gliomas. *J Exp Clin Cancer Res*. 2018;37(1):271.
326. Bhattacharya D, Gawali VS, Kallay L, Toukam DK, Koehler A, Stambrook P, et al. Therapeutically leveraging GABAA receptors in cancer. *Exp Biol Med (Maywood)*. 2021;246(19):2128-35.
327. Taylor RA, Watt MJ. Unsuspected Protumorigenic Signaling Role for the Oncometabolite GABA in Advanced Prostate Cancer. *Cancer Res*. 2019;79(18):4580-1.
328. Johnson AL, Lattera J, Lopez-Bertoni H. Exploring glioblastoma stem cell heterogeneity: Immune microenvironment modulation and therapeutic opportunities. *Front Oncol*. 2022;12:995498.
329. Daubon T, Hemadou A, Romero Garmendia I, Saleh M. Glioblastoma Immune Landscape and the Potential of New Immunotherapies. *Front Immunol*. 2020;11:585616.
330. Pombo Antunes AR, Scheyltjens I, Duerinck J, Neyns B, Movahedi K, Van Ginderachter JA. Understanding the glioblastoma immune microenvironment as basis for the development of new immunotherapeutic strategies. *eLife*. 2020;9.
331. Alves AH, Nucci MP, Mamani JB, Valle NME, Ribeiro EF, Rego GNA, et al. The Advances in Glioblastoma On-a-Chip for Therapy Approaches. *Cancers*. 2022;14(4):869.
332. Yi H-G, Jeong YH, Kim Y, Choi Y-J, Moon HE, Park SH, et al. A bioprinted human-glioblastoma-on-a-chip for the identification of patient-specific

responses to chemoradiotherapy. *Nature Biomedical Engineering*. 2019;3(7):509-19.

333. Tsai H-F, Trubelja A, Shen AQ, Bao G. Tumour-on-a-chip: microfluidic models of tumour morphology, growth and microenvironment. *Journal of The Royal Society Interface*. 2017;14(131):20170137.

334. Shimada T, Yamagata K. Pentylene-tetrazole-Induced Kindling Mouse Model. *Journal of Visualized Experiments*. 2018(136).